AEROSOL LIMB IMAGER

USER REQUIREMENTS DOCUMENT

Authors

Adam Bourassa, Landon Rieger, Doug Degenstein, Jeff Langille, Jean-Pierre Blanchette, Yann Blanchard

Contributing Scientists

Chris McLinden, Jason Cole, Matthew Toohey, Kaley Walker, Michael Höpfner, Alexei Rozanov

Review Editors

Thomas Piekutowski, Ali Ziad, David Golla, Michael Maszkiewicz

Version 1.0

March 30, 2020

This page intentionally left blank

Revision History

Initial Draft	Draft issue for revision	2020/31/01
Draft v0.1	Corrections for internal review	2020/28/02
Draft v0.2	Distribution to NASA SIT-A	2020/27/03
Version 1.0	Submission to CSA	2020/30/03

Table of Contents

Executive Summary

Aerosol in the stratosphere and upper troposphere is an important driver of climate, scattering radiation that leads to a cooling effect near the surface. Additionally, these aerosols can interact with high altitude cirrus clouds, changing the optical properties, and cloud frequency. Uncertainty in both the aerosol measurements and high altitude cloud feedbacks are important factors in climate modelling and have been identified as important topics by both the Canadian and international science communities.

While the need for improved knowledge is clear, high quality, high resolution measurements of aerosol and clouds in the upper troposphere and stratosphere (UTS) from remote sensing platforms has been difficult. The Aerosol Limb Imager (ALI) is a proposed instrument that will take hyper-spectral images of the Earth's limb and provide global, vertically resolved measurements of aerosol extinction, particle size and information on thin, high altitude clouds in the UTS. ALI will address the following scientific issues:

1. Continued monitoring of the variable aerosol background layer.
2. Climate and air quality impacts of extreme events.
3. High altitude cloud-aerosol interactions and feedbacks

ALI has the potential to complement the Canadian instruments SHOW and TICFIRE, as well as baseline instruments planned for the NASA Aerosol Cloud, Convection and Precipitation observing platform. ALI brings higher sensitivity to thin optical depths, a large spectral range, and wide cross crack coverage facilitating more detailed studies of aerosol-cloud and water vapour interactions, polar stratospheric clouds, and volcanic plumes than individual instruments would allow. ALI, both alone and in conjunction with these other instruments, addresses several priorities laid out by the Canadian Government and Environment Canada:

1. New monitoring and modelling systems.
2. Understanding tracking and predicting emissions and processes.
3. Providing foundational knowledge on climate change.

ALI, in particular in cooperation with other instruments, represents an excellent opportunity to advance our knowledge of aerosol and clouds in the UTS and reduce uncertainty in stratospheric aerosol forcing and high-altitude cloud feedbacks.

1 Introduction

1.1 Purpose and Scope

This document describes the user and scientific objectives, justification and requirements for the ALI mission. Section 1 focuses on the ALI instrument, outlining the mission statement and main objectives, and current status of the hardware. The mission objectives presented here are the main scientific goals of the instrument, and inform the choices that follow. Section 2 discusses the rationale for these goals and why ALI is the correct instrument to meet them. This includes how the goals align with government priorities and the NASA decadal survey. Section 3 explores the ALI observables, and how they will effectuate these goals through specific products and applications. Sections 4, 5 and 6 investigate the specific platform and instrument requirements that are needed to produce the observables in Section 4. The description of the user and science requirements provided in this document has the objective of allowing their flow-down to the Mission Requirements and System Requirements Documents.

Figure 1: Information flow through ALI requirement documents

1.2 Applicable and Reference Documents

Atmospheric Limb Sounding Satellite (ALISS) User Requirement Document, Final Release, September 30, 2014.

Microsatellite CATS User Requirements Document, Final Release, April 20, 2015.

SHOW User Requirements Document, Under Revision

TICFIRE User Requirements Document, Under Revision

1.3 Mission Statement

The Aerosol Limb Imager (ALI) is a science payload that will provide high quality atmospheric profiles of aerosol and cloud information from a low Earth orbit satellite platform. ALI responds to the strongly expressed need, nationally and internationally, for

improved measurements of clouds, aerosols and their interactions. These measurements are crucial to improve understanding of cloud feedbacks and aerosol indirect effects, a leading cause of uncertainty in global warming projections. Additionally, current high resolution monitoring of aerosols after events such as extreme wildfires and volcanic eruptions remains limited, but it is vital to understand our current climate and predict the human health implications of these events. ALI builds on the decades of Canadian experience in using limb scattering observations to measure key observables that address these goals, while enhancing measurements from coordinated systems.

1.4 Objectives

ALI has five primary scientific objectives:

1. Extend long-term records of stratospheric aerosols and improve optical properties used for historical simulations of climate.
2. Facilitate the study of aerosol microphysical processes after volcanic eruptions and forest fires that impact particle size and lifetime; improving the modelling, and forecasting of impacts of aerosol injections into the stratosphere.
3. Contribute to the knowledge of cloud, aerosol and water-vapour interaction processes including:
    a. Understanding of cloud-aerosol feedbacks that influence the frequency of high altitude and thin cirrus clouds
    b. Facilitate studies of aerosol, cloud and water vapour interaction in the tropical tropopause layer and extratropical UTLS.
    c. Cloud interaction in the Arctic (high-altitude thin cloud coverage especially at high resolution)
4. Improve air quality forecasting after large events such as forest fires through improved plume knowledge.
5. Improve understanding of climate engineering scenarios and feedbacks

Section 2.2 explains the need to address these objectives with sections 2.3 and 2.4 discussing how they fit into the larger picture of government priorities and international initiatives respectively.

1.5 Instrument Design and Progress

The ALI instrument is an original instrument concept, designed and developed at the University of Saskatchewan largely with previous Canadian Space Agency FAST funding. Fundamentally, ALI is a hyperspectral polarization imager covering the visible and near infrared spectral range, utilizing a new acousto-optic tunable filter and liquid crystal

polarization rotator technology. The instrument is optimized for high spatial resolution stratospheric aerosol, volcanic plume, forest fire smoke, and thin cirrus cloud measurements in the upper troposphere and stratosphere with a wide-angle two-dimensional field-of-view to provide cross track horizontal coverage. Two successively advanced prototypes of the instrument have already successfully flown on stratospheric balloons: ALI-v1 from Timmins in 2015 (Elash et al., 2016), and ALI-v2 from Timmins in 2018. Samples of these observations are shown in Figure 1. These sub-orbital flights have allowed us to identify limiting elements of the instruments that require future work and improvements.

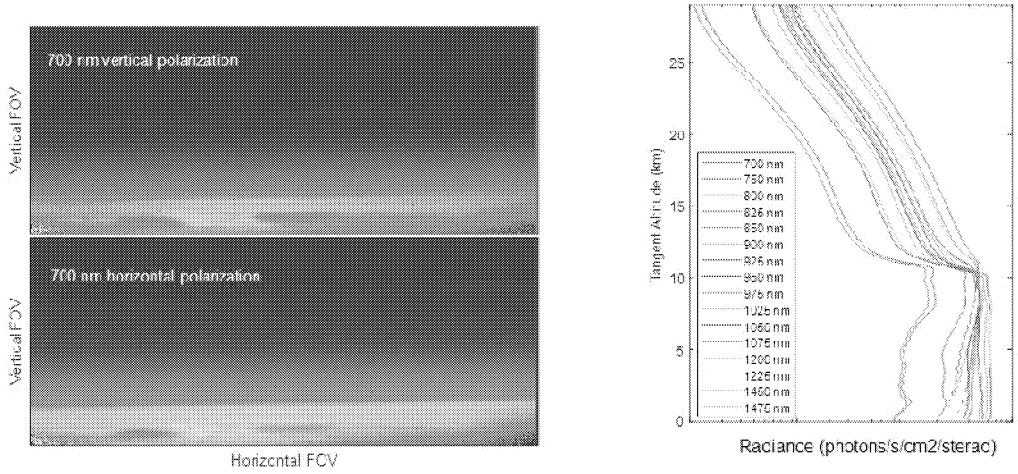

Figure 1: Limb radiance images (left) at 700 nm for vertical and horizontal linear polarization taken from stratospheric balloon in 2019 using the ALI-v2 prototype. Vertical profiles of limb radiance (right) at several multi-spectral channels.

1.6 Canadian Heritage

Canada has been an innovator in the use of limb-scattering measurements for observing atmospheric composition dating back a half century, using stratospheric balloons (Kerr and McElroy, 1976), the space shuttle (Evans et al., 1985), and high-altitude aircraft (McLinden et al., 1999). In space-based limb observing, Canada remains a leader with over 20 years of experience developing and managing OSIRIS on Odin (Llewellyn et al., 2004). Since its launch in 2001, OSIRIS measurements have been used by Canadian teams to pioneer limb-scattering retrievals of ozone (Degenstein et al., 2009), nitrogen dioxide (Bourassa et al., 2011), bromine monoxide (McLinden et al., 2010), and aerosol (Bourassa et al., 2007), with several other trace constituent retrieval products investigated (McLinden et al., 2012). The complexities of the limb-scattering measurements has also driven the advancement of SASKTRAN, a fast and accurate radiative transfer modelling

infrastructure used in the retrievals and developed at the University of Saskatchewan (Bourassa et al., 2008; Zawada et al., 2015).

The OSIRIS data products have been used in many scientific advancements. Process studies of reactive nitrogen from lightning (Sioris et al., 2007), impact of volcanic particles on lower stratospheric photochemistry (Adams et al., 2017), and volcanic plume evolution from high latitude eruptions (Bourassa et al., 2010) have been published. The data products have also been used in large international collaborations. The ozone climatology has been used for long-term trend analysis (Bourassa et al., 2018) in the WMO ozone assessment and LOTUS effort (Petropavlovskikh et al., 2018) that aims to better understand ozone recovery, while the aerosol record has been used to construct input forcings for the Coupled Model Intercomparison Project 6 (Thomason et al., 2018).

2 Science Objectives

2.1 Background

Measurements of atmospheric composition are invaluable for understanding the dynamical, chemical and radiative processes that dictate weather (including air quality), and contribute to climate change. While greenhouse gases are the main forcings causing climate change, aerosols in the form of clouds and particulates also play a major role. Gases such as CO_2 absorb upwelling infrared radiation, reradiating some back towards the ground, acting as a blanket that warms the surface and troposphere. Aerosols absorb and emit infrared radiation as well, but they also scatter solar radiation. This reduces the amount of sunlight absorbed by the surface and lower atmosphere, resulting in a cooling that can offset warming due to greenhouse gases. Aerosol at all altitudes can have this effect, but at high altitudes, in the stratosphere where the air is stable and dry, their lifetime is very long, magnifying their potential impacts. For example, in 1991 Mount Pinatubo erupted, spewing ash and sulfur as high as 35 km, producing aerosols which remained detectable in the stratosphere until 1995, and caused global near-surface temperatures to drop by almost 0.5°C (Thompson et al., 2009).

Although this magnitude of eruption occurs only once every 30-50 years on average (Masson-Delmotte et al., 2013, Deligne et al., 2010), small-to-moderate volcanic eruptions can also have important climate impacts, in particular due to their greater frequency, which can drive sustained enhancements to stratospheric aerosol levels (Solomon et al., 2011). The climate influence of these smaller eruptions has been under intense scrutiny in the last decade in efforts to explain a possible discrepancy between climate models and measurements (Fyfe et al., 2013, Solomon et al., 2011, Santer et al., 2017). However, many uncertainties remain, in part due to a lack of aerosol size measurements that increase uncertainty in both the measured extinction, and the radiative impacts. The size of the aerosol particles plays a major role in the climate effect, since the magnitude of scattering by aerosols is strongly dependent on the distribution of aerosol sizes (Pinto et al., 1989, Lacis et al., 1992). Direct measurements of aerosol sizes are sparse at best, and while retrieval of aerosol size information from satellite instruments is emerging as a valuable contribution, the products still lack information on particle size during both background conditions and after injection events from volcanoes and wildfires. For example, the Ångström exponent retrieved by Rieger et al., (2014) does not extend into the UTLS due to instrument limitations, while the particle size parameters retrieved by Malinina et al., (2018) are available only in the tropics. Particle size retrievals from occultation instruments provide more complete coverage in terms of altitude and latitude (Bingen et

al., 2004); however, the sampling is poorer with global coverage on a monthly timescale. This results in undersampling the rapidly evolving plumes of volcanic eruptions and wildfires.

While volcanic eruptions can be a large source of stratospheric aerosols, they are not the sole driver of periodic enhancements. The recent forest fire seasons in Canada have garnered considerable attention due to their magnitude and impact on the lives of Canadians, but have had global impacts as well. The British Columbian wildfires of 2017 burned large and hot enough for smoke to reach the stratosphere, spreading smoke and ash across continents (Thomas et al., 2017). The updrafts were strong enough to inject aerosols into the stratosphere, leading to elevated aerosol for months following the eruption, and climate impact comparable to that of volcanic eruptions (Bourassa et al., 2018). This is not unique to Canada, with other countries also experiencing intense fires that have reached the stratosphere (Fromm et al., 2000, 2007). More recently, the devastating 2019/2020 Australian bushfires have led to the worst air quality recorded in Australian cities, with smoke plumes observed to be circulating around the Southern Hemisphere. As the intensity of wildfires is expected to increase both in Canada (Wotton et al., 2017) and globally (Liu et al., 2010), measurements of smoke will become increasingly valuable from both a human health and climate perspective. While human health is impacted by smoke in the boundary layer, long-range transport occurs at higher altitudes, making measurements of high-altitude plumes important to forecasting as well.

In addition to the "direct" effect of aerosols on radiation, aerosols have many "indirect" effects. Aerosol particles can act as nucleation sites for clouds and change the temperature of surrounding air, influencing the growth of new particles and changing their optical properties. While this phenomenon is often referenced in regards to the low-altitude clouds, limb-scattering measurements are well suited to explore the interactions at higher altitudes. These mid-to-high altitude clouds are also an important driver of Earth's climate, so even small changes to their properties can have a large impact on temperatures and precipitation patterns. Understanding and predicting changes in Earth's climate therefore requires accurate knowledge of both aerosol and cloud properties as well as their interactions. However, these effects have been difficult to fully quantify, and clouds, aerosol, and their interactions remain one of the largest contributions to climate uncertainty (Boucher et al., 2013, Zelinka et al., 2016, 2020).

Measurements of these local and global quantities from satellites are achieved through a wide variety of means, but for passive instruments, high resolution profiles require the limb geometry where the instrument line of sight intersects the Earth's horizon. This provides long paths through the atmosphere at the tangent point, amplifying the aerosol signal and yielding good sensitivity and vertical resolution. Limb instruments can be

broadly grouped into three categories: occultation, where a source such as the sun is viewed directly through the atmosphere; limb-emission, where radiation emitted by the atmosphere is measured; and limb-scattering, where light from the sun is scattered into the instrument. The first satellite-based limb-viewer used to measure the vertical distribution of an atmospheric state parameter was launched in 1962 (Rawcliffe et al., 1963) and measured mesospheric ozone using its absorption in the visible in solar occultation mode. It wasn't until 20 years later that the Solar Mesosphere Explorer first measured an atmospheric profile using the limb-scattering technique (Thomas et al., 1983), retrieving profiles of stratospheric aerosol. Since then limb scattering has evolved considerably, with multiple satellite instruments expanding the number of measured species and quality and coverage of the measurements.

2.2 Rationale

As Earth's climate changes, there is a growing need for high quality projections that can inform policy decisions to reduce anthropogenic impacts and mitigate the consequences of global warming. The IPCC AR5 report (Pachauri et al., 2014, Ch. SPM 2.3) predicts a high risk of increased damages from wildfires, heat-related human mortality, and increased damage from river and coastal floods in North America over the near term (2030-2040), assuming current levels of adaptation. Regions at higher latitudes are also expected to warm faster than lower latitudes, seeing an additional 1-2°C increase from the global average (Zhang et al., 2019). Climate projections require reasonable estimates of future radiative forcings, including stratospheric aerosols, which can be developed using high quality measurements of historical variations. These measurements also provide guidance to the development and evaluation of process parameterizations. While substantial advancements have been made in the last decade, further improvements require ongoing reductions in observational uncertainty.

2.2.1 Continued monitoring of 'variable' background layer

Global measurements have been crucial in understanding the sources and climate effects of stratospheric aerosols. Consistent, decadal increases in stratospheric aerosol levels were originally speculated to be from anthropogenic emissions (Hofmann et al., 2009), and it wasn't until the global picture provided by long-running satellites became available that this was correctly attributed to a series of smaller volcanic eruptions (Vernier et al., 2011). These global measurements have also helped to establish the presence of an Asian tropopause aerosol layer, or ATAL (Vernier et al., 2011b, Thomason et al., 2013). Diabatic ascent in the Asian summer monsoon and large convective systems over India create a transport pathway from the troposphere to the stratosphere (Randel and Park 2010, Garny et al., 2016) that creates a sustained aerosol layer during the summer months. As emissions from China and India change, continued monitoring of the ATAL and

monsoon region will be important to understand impacts on UTLS composition and climate.

Aerosol in the UTLS is a major component of total stratospheric aerosol loading, but uncertainty here remains high (Andersson et al., 2015). This is due largely to the limitations of the current generation of instruments. Limb and occultation systems have good sensitivity to aerosol, but without polarization information are unable to reliably distinguish between aerosol and clouds. Conversely, while lidars have good cloud discrimination, the short path lengths make them less sensitive to aerosol at background levels (Vernier et al., 2009). By incorporating both the limb geometry and polarization information ALI has the potential to greatly reduce these uncertainties.

These more accurate measurements of stratospheric aerosols will improve understanding of its current state as well as potential future perturbations including those due to climate engineering through injection of sulfur into the stratosphere (Rasch et al., 2008, Ricke et al., 2010, Kravitz et al., 2011). Ongoing monitoring of stratospheric aerosols in the absence of manmade sulfur injections combined with the ability to monitor aerosol formation and evolution after small-scale experiments, such as those proposed by *Dykema et al.,* (2014), or much larger injections, will be crucial in determining both the impacts and effectiveness of these interventions.

2.2.2 Climatic and air quality impacts of extreme events

Small to moderate eruptions have a non-negligible impact on climate (Solomon et al., 2012), although with considerable uncertainty about the precise magnitude of the forcing due to lack of complete records of stratospheric aerosol amount, size distributions and optical properties. The difficulties of measuring in the UTLS mentioned in the previous section are exacerbated during a volcanic eruption when an even larger fraction of the total aerosol can reside here (Ridley et al., 2014). Additionally, a chronic lack of particle size measurements leads to uncertainty when calculating scattering and absorption properties needed for radiative forcing calculations, and is suggested as a cause of recent differences in measured and modelled tropospheric temperatures (Santer et al., 2017). Improved stratospheric aerosol records are crucial for reducing the uncertainty related to future volcanic eruptions.

The problem of understanding stratospheric aerosol particle size has been long-standing. In situ measurements have provided a snapshot of aerosol size at specific times and locations, and have painted a complex picture of multi-modal size distributions requiring six or more parameters to quantify (Deshler et al., 2003). Unfortunately, satellites can typically only measure two to three aerosol parameters; usually extinction, and some parameterization of size properties (Thomason et al., 2003, Rieger et al., 2014, Malinina et

al., 2018), leaving many assumptions when computing optical properties. This is further complicated by the difficulty in accurately parameterizing particle size after eruptions: while large eruptions such as Pinatubo resulted in a clear increase in particle size (Bingen et al., 2005), smaller eruptions have had converse effects (Rieger et al., 2014). Aerosols injected into the stratosphere by forest fires have a different microphysical signature, with depolarization ratios that evolve differently from volcanic aerosols (Christian et al., 2019). Polarized limb-scattering measurements from ALI will improve measurement of particle size by providing information in the crucial near-infrared region of the spectrum (Rieger et al., 2014). Retrieved properties from these measurements such as the particle effective radius will help in understanding the drivers of the microphysical processes after an eruption and improve modelling of eruption events.

Accurate prediction of the climate impact of any future volcanic eruption or wildfire relies upon numerical simulation of the global spread and physical evolution of stratospheric aerosols. Interactive stratospheric aerosol models have had some success simulating the stratospheric aerosols from volcanic eruptions and their global radiative impacts (Mills et al., 2016; Timmreck et al., 2018). However, there remain significant differences between models in coordinated experiments using consistent injection locations and sulfur magnitudes (Zanchettin et al., 2018) , which point to fundamental uncertainties in model parameterizations of microphysical and radiative processes. Efforts to improve the accuracy of these aerosol models rely upon measurements of stratospheric aerosol, including information on the aerosol size distribution wherever possible. While occultation instruments can provide size information, the plumes can be highly inhomogeneous in the early days and weeks after an eruption and this is not well captured by the coarse sampling (Bourassa et al., 2018).

Small eruptions and forest fires can exhibit complex dynamics, sometimes becoming entrained in the Asian monsoon, and lofted into the stratosphere (as with the ATAL), even when the initial plume altitudes may not have been at sufficient altitudes to achieve this (Bourassa et al., 2012). Multiple events, either volcanic or fire related may also overlap, with plumes splitting and merging. Untangling the sources and movement of these highly dynamic events requires high sampling rates to track the plumes while they evolve. The excellent along, and horizontal track resolution of ALI will provide a much clearer picture of these events than occultation instruments, increasing the detail of plumes in their early stages of development and improving understanding of the evolution of simultaneous plumes with different sources.

2.2.3 Cloud feedbacks

Clouds feedbacks in general represent a substantial uncertainty in the global climate projections (Stephens et al., 2005, Dolinar et al., 2015), and according to the IPCC Fifth

Assessment Report, the role of thin cirrus feedbacks in particular are not constrained, representing a significant feedback uncertainty (Boucher et al., 2013 Ch. 7). Cirrus clouds have a radiative forcing of approximately 5-6 W/m^2 (Hong et al., 2016; Gasparini et al., 2016), more than double that of CO_2 (Stocker et al., 2013), so small changes to their properties have a large potential to affect global climate. As stratospheric aerosols sediment out of the atmosphere, they can interact with cirrus formation, potentially impacting the lifetime, frequency and microphysical characteristics of high altitude clouds. Studies on stratospheric aerosol and cirrus feedbacks show effects comparable in magnitude to the direct aerosol forcing (Kuebbler et al., 2012), but the results are uncertain.

Thin cirrus in the tropical tropopause layer play not only a radiative role (McFarquhar et al., 2000, Hartmann et al., 2001) but also serve to dehydrate the air entering the stratosphere (Jensen et al., 2004, Luo et al., 2003). As rising air cools, ice droplets form and sediment out, removing water vapour from the TTL. However, measurements of thin cirrus clouds in the TTL (McFarquhar et al., 1999, Peter et al., 2003), remain uncertain due to the difficulty of in situ measurements at such high altitudes, and the inability of satellite lidar instruments to measure thin cirrus clouds with optical depths below approximately 0.01 (Dessler et al., 2006, Haladay et al., 2009). Limb scattering measurements with polarization information have not previously been performed from satellites, yielding a unique opportunity to measure the thin cirrus clouds not typically distinguishable from aerosols with other techniques. ALI will therefore fill an important role in reducing uncertainty in thin cirrus clouds and feedbacks.

2.2.4 Air Quality

Extreme forest fires play a dual role in the environment, causing both large scale climate effects when they reach the stratosphere (Yu et al., 2018), and substantial human health consequences (Rittmaster et al., 2008). As climate change occurs and heat waves and droughts become more commonplace the impact of forest fires is expected to accelerate (Girardin et al., 2008, Wotton et al., 2017); with events on-par with the Fort McMurray or the recent BC fires more likely. . Particulate matter, in part from these wildfire events, is a significant environmental and health concern, associated with nearly 9M premature deaths globally per year (Burnett et al., 2018). In Canada, 21,000 deaths result annually from the effects of air pollution. Some of the most intense air quality events are a result of large wildfires or volcanic eruptions in which aerosol plumes are lofted into the middle troposphere or above. At these heights, transport long distances downwind are common and generally difficult to forecast. One reason for this is uncertainty in the height and vertical extent of the plumes. Current passive satellite instruments provide, at best, a single height with large uncertainty, which require oversimplification of the plume (Griffin et al., 2020).

2.3 Alignment with Government of Canada Priorities

The Environment Canada science strategy focuses on four main categories which include the following goals[1]

1. Environment Canada will focus its science on developing new monitoring and modelling systems and tools, and improving existing systems.
2. Environment Canada will focus its science on understanding, tracking and predicting the emissions and atmospheric processes that affect climate change.
3. Environment Canada will also focus its science on providing the foundational knowledge to understand anticipated climate change to help Canadians plan and adapt to future change.

The objectives of the ALI mission relate directly to these priorities.

2.3.1 New monitoring and modelling systems

ALI will provide a novel platform for measuring stratospheric and upper tropospheric composition; imaging the limb to produce high resolution information in both the along- and cross-track dimensions. This builds on limb scattering heritage of the Canadian instruments OSIRIS, that viewed the limb using a single line of sight, and μCATS, that used seven. ALI extends this by approximately two orders of magnitude, measuring hundreds of lines of sight simultaneously. Fully utilizing these measurements will require advancing the current generation of aerosol retrievals to incorporate the additional wavelength information as was done by Rieger et al., (2019) and extending the tomographic techniques used by Zawada et al., (2018) to exploit the cross-track information.

2.3.2 Understanding, tracking and predicting emissions and processes

The ALI measurements will support the continued monitoring of stratospheric aerosols due to volcanic eruptions, a critical factor in modelling the climate (Santer et al., 2017). Measurements at wavelengths up to 1500nm will enable retrieval of aerosol information in the upper troposphere, filling important gaps in the forcing record (Ridley et al., 2014, Andersson et al., 2015). This will extend to monitoring and tracking of the vertical distribution of high-altitude smoke plumes from wildfires. These measurements will be used to improve the air quality model, and the numerical forecasting of smoke trajectories that influence air quality estimates. In addition to the science priorities of EC,

[1] "Environment Canada's Science Strategy 2014 to 2019" 6 Mar. 2018, Environment Canada's Science Strategy 2014 to 2019. Accessed 28 Jan. 2020.

this furthers Minister of Health's mandate to "better protect people and the environment from toxins and other pollution, including by strengthening the Canadian Environmental Protection Act, 1999."[2]

2.3.3 Providing foundational knowledge on climate change

Clouds and aerosols continue to be a major source of uncertainty in model predictions, due to uncertainties in cloud feedbacks (eg. Webb et al., 2017), aerosol-cloud interactions (Carslaw et al., 2013) and radiative forcings (Thomason et al., 2018). Estimates of subvisual cirrus are difficult with the current generation of instruments due to detection limits or cloud-aerosol discrimination. The combination of limb scattering and polarization measurements to provide coincident, high vertical resolution measurements of thin clouds, with cross-track information, in aerosol conditions will improve understanding of how aerosol affects the lifetime and frequency of subvisual cirrus clouds. These measurements can be used to improve forcing estimates of thin clouds and improve parameterizations of clouds in climate models.

2.4 Alignment with NASA Decadal Survey and ACCP

The objectives of the ALI mission overlap with many of the most pressing science questions as determined by the NASA decadal survey.[3] The decadal survey identified five key areas of research for the next decade, including two focused on aerosol related observables:[4]

1. Climate variability and change
2. Weather and air quality

To measure these observables NASA is designing the Aerosol Cloud, Convection and Precipitation (ACCP) observing system. The goal of ACCP is to observe parameters that fall into five main categories[5] as shown in the table below:

[2] "Minister of Environment and Climate Change Mandate Letter 2019" Minister of Environment and Climate Change Mandate Letter. Accessed 28 Jan. 2020.
[3] "Decadal Survey | Science Mission Directorate - Science@NASA." Decadal Survey. Accessed 29 Jan. 2020.
[4] "Aerosol and Cloud, Convection and Precipitation (ACCP)" Aerosol and Cloud, Convection and Precipitation (ACCP). Accessed 29 Jan. 2020.
[5] "Science and Applications Traceability Matrix" Traceability Matrix Public Release Candidate E. Accessed 29 Jan. 2020

Cloud Feedbacks	Reduce the uncertainty in low- and high-cloud climate feedbacks by advancing our ability to predict the properties of low and high clouds.
Storm Dynamics	Improve our physical understanding and model representations of cloud, precipitation and dynamical processes within deep convective storms.
Cold Cloud and Precipitation	Improve understanding of cold (supercooled liquid, ice, and mixed phase) cloud processes and associated precipitation and their coupling to the surface at mid to high latitudes and to the cryosphere.
Aerosol Processes	Reduce uncertainty in key processes that link aerosols to weather, climate and air quality related impacts.
Aerosol Impacts on Radiation	Reduce the uncertainty in Direct and Indirect aerosol-related radiative forcing of the climate system.

Table 1: ACCP goals and objectives

These science questions and objectives in the decadal report drive the need for a host of observables, several of which can be measured using ALI measurements. The table below indicates in more detail the decadal survey goal, the specific objective, the desired observable that ALI can contribute to, and the specific ALI measurement that will make the contribution.

Science Goal	Mission Objective	ACCP Observable[6]	ALI Contribution and Enhancement
W-2 Larger Range Environmental Predictions	**W-2a** Improve the observed and modeled representation of natural, low-frequency modes of weather and climate variability.	Vertical profiles of aerosols and clouds in the middle atmosphere and lower stratosphere.	Excellent sensitivity allows extending Lidar measurements into upper troposphere and stratosphere
W-10 Clouds and Radiative Forcing	**W-10a** Quantify the effects of clouds of all scales on radiative Fluxes. Determine the structure, evolution and physical/dynamical properties of clouds on all scales.	3D aerosols.	Cross track information and high along-track sampling allows for a more complete picture of vertical distribution than lidar and nadir imagers alone can produce.
C-2 Climate Feedback and Sensitivity	**C-2a** Reduce uncertainty in low and high cloud feedback by a factor of 2.	Cloud fraction	Improved sensitivity to thin cirrus clouds for more complete maps.

[6] Only ACCP observables related to ALI measurements are listed here

	C-2g Quantify the contribution of the upper troposphere and stratosphere (UTS) to climate feedbacks and change.	Vertical profiles of UTS aerosol radiative properties, for quantifying radiative forcing.	Vertical profiles of radiance at multiple wavelengths from 500 to 1500 nm with high sensitivity in the UTS provides information on particle size as well as extinction.
	C-2h Reduce the IPCC AR5 total aerosol radiative forcing uncertainty.	Vertical profiles of aerosol effective radius.	Broad wavelength range allows retrieval of aerosol properties from the upper troposphere to 30km at 0.5km resolution
		Nearby (to aerosol fields) and simultaneous measurements of cloud properties.	Sensitivity to thin subvisual cirrus clouds and low levels of aerosol allow for improved masking and aerosol/cloud co-location flagging.
	C-5a Improve estimates of the emissions of natural and anthropogenic aerosols.	Vertical profiles of particle effective radius.	Broad wavelength range coupled with polarization information provides effective radius as well as distinction between liquid and solid particles to discriminate aerosol sources.
C-5 Aerosols and Aerosol Cloud Interactions	**C-5b** Characterize the properties and distribution in the atmosphere of natural and anthropogenic aerosols.	Aerosol extinction, AOD, (spectrally resolved), polarization, and size with vertical and horizontal distribution.	Spectrally resolved, vertical profiles of aerosol extinction allow the ability to remove stratospheric contribution from nadir measurements of AOD.
	C-5c Quantify the effect that aerosol has on cloud formation, cloud height, and cloud properties.	Vertical and horizontal distribution of clouds.	Improved sensitivity to thin cirrus clouds and low levels of aerosol for more complete maps when combined with baseline instruments.
C-7 How are decadal-scale global atmospheric and ocean circulation patterns changing?	**C-7b** Quantify the linkage between natural and anthropogenic forcing.	Vertical distribution of stratospheric and tropospheric aerosols.	Continuation of vertical aerosol profile measurements to provide long-term global records back to 1980 that can be used in climate models. Polarization information improves cloud discrimination to enhance measurements in regions
	C-7e Provide observational verification of models used for climate projections. Are the models simulating the observed evolution of the large-scale patterns in the	Vertical distribution of stratospheric and tropospheric aerosols.	

	atmosphere and ocean circulation.		of large-scale convective patterns such as the ATAL.
C-8 Causes and Effects of Polar Amplification	**C-8g** Determine the amount of pollutants (e.g., black carbon, soot from fires, and other aerosols and dust) transported into polar regions.	Aerosol optical depth.	Cross track information allows for particularly high resolution mapping in the Arctic, improving tracing of aerosols after large-scale volcanic eruptions and forest fires that inject aerosol to the UTLS.
C-9 Ozone and Other Trace Gases in the Stratosphere and Troposphere	**C-9a** Quantify the amount of UV-B reaching the surface, and relate to changes in stratospheric ozone and atmospheric aerosols.	Vertical profiles of UTS aerosol radiative properties.	Vertical profiles of both extinction and particle size properties such as surface area density that are important for ozone chemistry.
		Volcanic and biomass burning emissions.	Separation of soot and ash from sulfur aerosols using multi-wavelength polarization capabilities.
S-2 How do geological disasters directly impact the Earth system and society following an event?	**S-2a** Rapidly capture the transient processes following disasters for improved predictive modeling.	All high-resolution visible to thermal IR imagery.	Spectrally resolved limb images of radiance from 500 to 1500 nm to capture volcanic plume or pyro-cumulus extent in the UTLS in the days and weeks following an event.

Table 2: ALI contribution to ACCP goals and objectives

2.5 Synergy between ALI and ACCP Instruments

This section outlines basic retrieval elements that may be improved through instrument synergy, but technical details and feasibility will be explored more fully in upcoming simulation studies.

While many parameters required to meet the decadal survey objectives can be retrieved directly from ALI or lidar measurements, retrieval of many geophysical parameters needed for objectives are greatly improved through synergy with potential instruments in the ACCP architecture.

2.5.1 Improved Lidar measurements

While lidar measurements provide excellent high resolutions profiles of backscattering ratios, the conversion to extinction in the stratosphere relies heavily on assumptions of optical properties, typically assuming a constant conversion of 50sr (Kar et al., 2019). Particle size information allows for improved conversion of backscatter to extinction by reducing uncertainty in particle size.

In addition to conversion uncertainty the short path lengths of lidars can struggle with signal to noise problems and high altitude normalization in the stratosphere when aerosol levels are low. This can be mitigated by binning measurements as done by Kar et al., (2019), but this eliminates many of the benefits of the high resolution lidar measurements. The long ALI path lengths provide much higher sensitivity in the stratosphere, providing the ability to complement the tropospheric and UTLS lidar measurements at higher altitudes without relying on spatial and temporal binning.

2.5.2 Aerosol and Cloud Interactions

Provide information on the vertical structure of thin and subvisual cirrus clouds

2.5.3 Improved ALI retrievals

ACCP baseline instruments can also be used to improve ALI retrievals. Limb scattering aerosol retrievals rely on albedo retrieved from looking at high tangent altitudes. This has limitations on accuracy and information content due to the indirect nature of the measurement. Information provided by nadir sensors could potentially provide information on the type of scene below the limb measurement, improving estimation of upwelling radiation.

The polarization measurements provided by ALI allow for cloud aerosol discrimation, but the long path lengths of approximately 200km mean measurements may contain both cloudy and cloud-free regions. The high horizontal resolution of the lidar measurements will allow for additional screening of measurements that have a smaller fraction of clouds along the line sight.

2.5.4 Linking Processes to Global Scales

ALI's wider swath and global coverage provides a link between process driven studies and global scale phenomena, showing the context in which the process events occur. Cross track aerosol information can help place lidar profiles in the context of large and potentially inhomogeneous aerosol plumes. This is particularly relevant for conditions after forest fire and volcanic events when conditions can change rapidly.

2.6 Synergy between ALI, TICFIRE and SHOW

In addition to the synergy with baseline instruments onboard the ACCP payload. ALI also provides excellent integration with proposed Canadian instruments. ALI, SHOW and TICFIRE will provide a complementary suite of measurements that allow for much more complete investigation of cloud properties than each instrument alone. A schematic of the measurement configuration for these three instruments is shown in the figure 2.

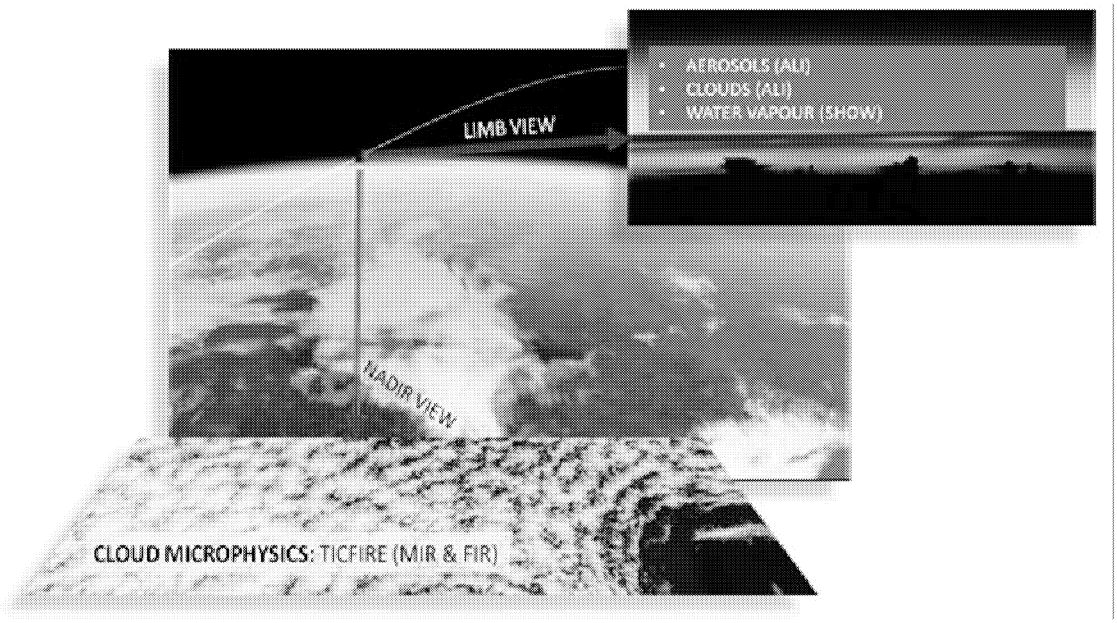

Figure 2: Synergistic measurement configuration between the three Canadian instruments.

The **SHOW** high-resolution water vapor measurements strengthen our understanding of the moisture variability in the critical and under-sampled upper troposphere and lower stratosphere (UTLS), and to link this variability to changes in surface weather and climate conditions. It is designed to provide the best along-track sampling of any existing limb sounder to capture the high variability of water vapor in the global UTLS. The novel SHOW design measures absorption features in limb scattered sunlight and has been tested through suborbital demonstrations, including a test flight of an advanced prototype on the NASA ER-2.

The **TICFIRE-FIRR** (Far IR Radiometer) measures thin cloud composition and microphysical properties from fine to large crystals leading to estimation of the extensive light precipitation common to cold climates and global scale UTLS regions, like initiation of precipitation soon after ice crystal nucleation in convective cloud anvils for instance. Complementing microwave radiometers, it accurately measures the radiance in 8 spectral bands from 8 to 100 μm, which is a range sensitive to cloud microphysics and low water

concentration. This is the only instrument to measure directly the cloud radiative forcing spectrally resolved and over the wide infrared domain. In other words, it probes directly the effect of cloud changes on the atmospheric energy balance, a key quantity on the role of clouds and many important related processes on the climate system.

2.6.1 Improvement to SHOW retrievals

Synergistic measurements with ALI and TICFIRE will be used to improve the SHOW water vapour retrievals. Co-located measurements of aerosol with ALI will be used to improve the information content in the forward model utilized in the SHOW water vapour retrievals. Sensitivity studies performed in support of the sub-orbital demonstration campaign show that knowledge of the aerosol profile can improve the accuracy of the SHOW measurements on the order of 0.1-0.5 ppm [Langille et al., 2018]. In addition, ALI and TICFIRE observations will aid in the determination of the lower boundary cut-off of the SHOW retrievals where the optical depth becomes too large to see the tangent point. The impact of this knowledge on SHOW water vapour retrievals needs to be evaluated through detailed simulation studies.

2.6.2 Process studies

It is well known that cloud tops play a key role in the fate of the cloud radiative properties and precipitation. Observations with all three instruments, ALI, TICFIRE and SHOW will be combined to close the feedback loop between aerosol (including ice forming nuclei), cloud, optical depth, temperature, moisture and their alteration of the water vapour concentration respectively. Furthermore, direct radiance measurements from TICFIRE provide information on radiative forcing which can be used to evaluate the atmospheric perturbation and its impact on the energy cycle. On their own, the three Canadian instruments provide us the ability to do a near closure experiment, a challenging goal for future missions. This closure is reinforced locally by the active instruments (lidar and radar) collocated on board the ACCP mission. Although radar and lidar see only a small sample of the scene, the combined ALI-SHOW-TICFIRE observations will widen the scene view, providing a rich perspective and strongly enhancing the whole mission.

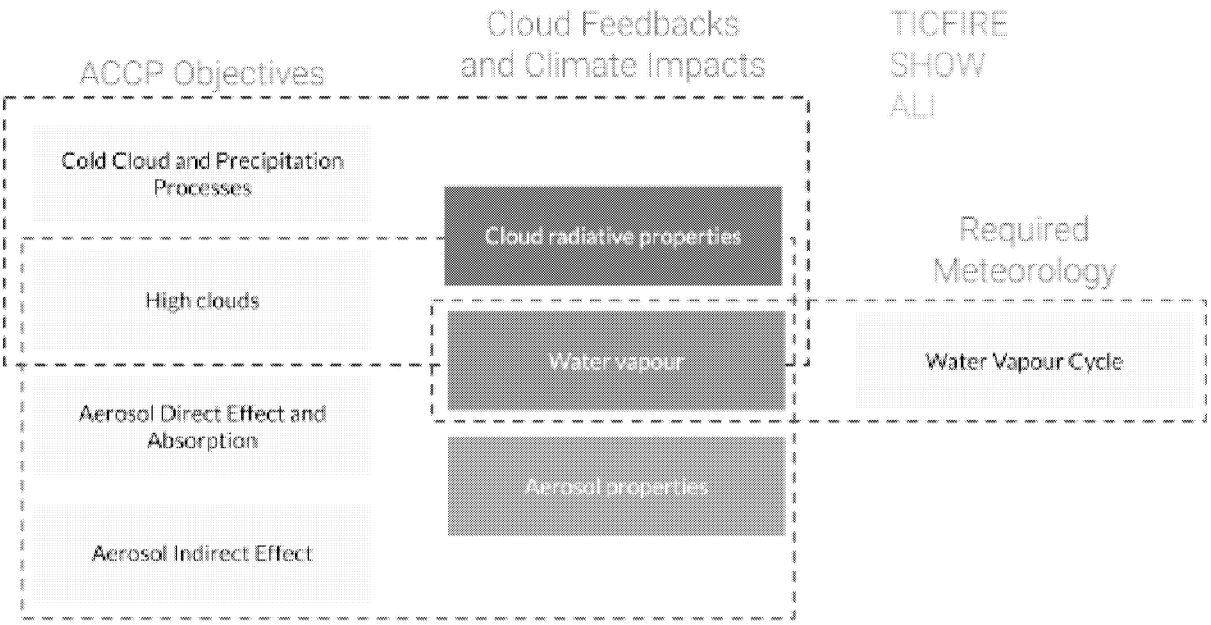

Figure 3: Synergistic measurements between the three Canadian instruments – SHOW, ALI and TICFIRE. Each measures an important component of high cloud feedbacks relevant to climate.

Overall, the ensemble is a unique system for high resolution of aerosols, water and cloud, a key to the study of their interaction, and an extended source of genuine new information in data assimilation systems for weather forecasting. Synergistic measurements with these three instruments will allow for:

- Improving measurements of water-vapor concentration in the low limit where cold regions are most sensitive.
- Determining the contribution of Thin Ice Clouds (TIC) to the energy balance and the role of their microphysical properties on atmospheric cooling.
- Bridging the observational gap in the far IR spectral region between the atmospheric window in the mid-IR and the passive microwave region.
- Providing a wealth of new and unique FIR data for assimilation in the weather forecast models, which will help improve the range and the reliability of operational meteorology
- Strengthening our understanding of the variability in the critical and under-sampled upper troposphere and lower stratosphere and to link this variability to changes in surface weather and climate.
- Providing a high-quality extension of the stratospheric aerosol record for understanding the radiative and hence climate impacts of volcanic eruptions, wildfire and anthropogenic perturbations.

Several studies have highlighted the role of aerosol composition on cloud nucleation, their development, their radiative properties and initiation of precipitation (Jouan et al, 2012; 2014). Figure ??? illustrates the effect of volcanic aerosol on cloud formation and precipitation as a common phenomenon in cold atmospheres, yet these processes are very complex to reproduce in atmospheric models, not to mention their omission in today's data assimilation system. However, this will change in the current decade with ACCP and consequent model improvements.

As an example, the ISDAC airborne campaign of April 2008 (Figure ???) has provided a rare dataset for studying the interaction between aerosol composition and clouds microphysics. From a limited number of successful flights in ice clouds, detailed studies (Jouan et al., 2012; 2014) have quantified in situ the critical links between aerosol acid concentration from 5 volcanic plumes and the enhanced formation of large precipitating ice crystals that were theorized (Blanchet and Girard, 1994) and previously verified in laboratory controlled experiments (Eastwood et al, 2009). These results have permitted the development of a new parameterization of ice nucleation processes based on aerosol chemical composition in atmospheric weather and climate models using WRF-Chem (Keita et al.; 2016; 2019; 2020). Clearly, much more observations on global scale are needed to refine and generalize such parameterization based solely on limited number available measurements. This central objective of ACCP is where the tandem ALI, SHOW and TICFIRE and their synergies aim to contribute.

3 Data Products and Applications

This section outlines the retrieval products, and how they will enable the science objectives discussed in the preceding sections. Additionally, how these products will integrate with measurements from other ACCP and Canadian instruments to enhance the science return.

3.1 Retrieval Products

Since the advent of occultation limb profilers, vertical profiles of extinction in the visible and near infrared have formed the backbone of our global picture of stratospheric aerosol loading (Thomason and Peter, 2006). The measurements provide information on the distribution, amount and movement of aerosol and have been foundational for the aerosol climatologies needed for understanding climatic effects of stratospheric aerosols (Thomason et al., 2018). To meet the needs of the climate community for continued forcing datasets ALI will provide several fundamental aerosol and cloud quantities. The table below shows the four primary ALI retrieval products and their properties.

Product	Accuracy	Vertical Range	Vertical resolution	Horizontal resolution	
				Along track	Cross track
Aerosol Extinction	10% (Tropopause to 10^{-5} km^{-1} @ 750nm)	8 to 35 km	0.5 km	250 km	20 km
Effective Radius	20% (Tropopause to 10^{-5} km^{-1}@ 1000nm)	10 to 30 km	0.5 km	250 km	20 km
Angstrom Coefficient	20% (Tropopause to 10^{-5} km^{-1}@ 1000nm)	10 to 30 km	0.5 km	250 km	20 km
Cirrus Detection		8 to 22 km	0.5 km	250 km	20 km

Table 3: ALI retrieval product requirements. *This table is a work in progress, and numbers will be updated as results of simulation work informs the required uncertainties.*

3.1.1 Multi-wavelength aerosol extinction profiles in the visible and near infrared

The 2-dimensional images of the limb provided by ALI will be used to retrieve aerosol extinction profiles using similar techniques employed by Bourassa et al., (2012), Rieger et al., (2019), and Zawada et al., (2018). The central profile will be used in a tomographic retrieval to maximize along-track resolution, while off-center profiles will be retrieved using horizontal homogeneity assumptions. The 5° field of view will provide global coverage over the course of several days at a cross-track resolution of approximately 20km, along track resolution of 250km, and vertical resolution of 500m. These measurements will feed directly into aerosol climatologies such as GloSSAC to improve and extend climate forcing records.

3.1.2 Vertical profiles of particle size information

Particle size retrievals from limb scattering observations have been performed with measurements from OSIRIS (Bourassa et al., 2007, Rieger et al., 2014) and SCIAMACHY (Malinina et al., 2018). Information in the near infrared is crucial for deriving particle size. With ALI's wavelength range of 500 to 1500nm, it is well suited to provide both extinction and effective radius for input to climate forcing analyses. These quantities directly improve the optical property parameterizations used in climate models to calculate aerosol forcing. The addition of polarization information also adds an exciting component for particle size retrievals to distinguish smoke and ash from sulphates after volcanic eruptions and wildfires (Vernier et al., 2016). These particles have very different optical properties than sulphate aerosols, so distinguishing them will improve the extinction retrievals, and estimates of radiative forcing.

3.1.3 Vertical profiles of Ångström coefficient

The spectral dependence of extinction is often modeled as linear relationship in log-wavelength log-extinction space, with the slope of this dependence referred to as the Ångström coefficient, or exponent. The Ångström coefficient is commonly used as a proxy for particle size or backscattering efficiency. While there is not an exact mapping between these quantities, it has been a staple measurement for decades from occultation instruments, in part because it does not rely on a priori assumptions of size distribution. The ability to continue these measurements into the future will help extend occultation measurements, and provide extended records to the studies that use the Ångström coefficient.

3.1.4 Clouds

Feedbacks involving clouds pose one of the largest unknowns in forecasting the future climate (Boucher et al., 2013). Long term records of cloud properties provide an excellent method to evaluate climate models and can provide guidance when developing model parameterizations. A lidar-based product widely used for climate model evaluation is the GCM Oriented Cloud Calipso Product (GOCCP) (Chepfer et al., 2010) which is often compared with simulated clouds. However, this limits the comparisons to clouds with sufficient optical depth to be measured with space-based lidars, missing the thinner subvisual cirrus clouds (Sassen et al., 2008, 2009).

The long path lengths and high sensitivity of limb scattering measurements allows retrieval of subvisual cirrus below the detection threshold of lidar instruments (Bourassa et al., 2005). ALI will be able to measure thin clouds with sufficient discrimination of aerosol using polarizaiton information to produce cirrus frequency climatolagies for comparison with climate models. The retrieval of cirrus size parameters has also been performed with limb scattering instruments (Wiensz et al., 2013), however these were not performed operationally. Estimates of cirrus crystal size could help improve estimates of cirrus radiative forcing, with changes to these quantities indicators of feedbacks between cloud and aerosol.

3.2 Science Studies

Large, temporary perturbations to the aerosol loading can cause significant climate effects, but the violent processes of volcanic eruptions and forest fires that generate these events lead to inhomogeneous and rapidly changing aerosol distributions. While satellite lidars can provide excellent along track resolution, the horizontal swath is narrow, measuring only a curtain of aerosol under the the satellite orbit. ALI will fill this gap by providing the ability to measure at high resolution in the along track plane through use of tomographic retrievals as pioneered by Zawada et al., (2015), but also measure a substantial cross-track component. This will provide unprecedented information on the extent of aerosol plumes in the stratosphere and upper troposphere. This is particularly true in the Arctic, where overlapping satellite tracks combined with ALI's imaging capabilities yield measurements of stratospheric aerosols at multiple angles over a short period of time. These dense measurements will support process studies to elucidate pressing climate questions in the UTLS.

3.2.1 Forest Fires

Limb scattering observations have been used to track the evolution of high altitude smoke plumes after large fires (Bourassa et al., 2018). However, limitations in cloud filtering and low altitude sensitivity limit the ability to observe smoke lower into the troposphere. The longer wavelength range and cloud discrimination enabled by polarization information will enable ALI to see plumes at lower altitudes and at lower thresholds than previously possible, extending well into the mid and upper troposphere. For extreme events, this is low enough to measure plume altitude, which can be assimilated by numerical prediction centers to improve air quality estimates.

ALI observations can also improve analyses of these extreme fires on climate. While climate models with interactive aerosol and chemistry components can simulate the plume evolution it is difficult to compare all aspects with observations (Yu et al., 2018). Occultation measurements are too sparse to map the early plume, and lidar measurements are insensitive to the lower extinction values as the plume evolves. ALI will fill this gap by providing much higher spatial detail of the aerosol distribution, while being able to monitor the lofting to higher altitudes as the plume thins, due to the higher sensitivity than lidar instruments.

3.2.2 Volcanic Eruptions

Determining the climate ramifications from volcanic eruptions relies on accurate knowledge of the aerosol plume and dispersion. Relatively similar eruptions can have vastly different effects depending on the latitude, eruption altitude, SO_2 and ash composition of the plume, and timing of the eruption with respect to large scale dynamical cycles (Marshall et al., 2019). ALI will provide extinction measurements on spatial scales of hundreds of kilometers, with near global coverage, improving the ability to track the evolution of aerosol plumes from the origin to eventual dispersal and removal from the stratosphere. This will reduce uncertainty in important dynamical interactions that influence lifetime and climate impact. For instance, the interaction with the Asian Monsoon is very sensitive to the timing and altitude of the plume, with small changes greatly affecting the amount of aerosol that is transported to the stratosphere. The high resolution ALI measurements will reduce uncertainty in the injection mechanisms of aerosols into the stratosphere.

Aerosol lifetimes in the stratosphere depend strongly on particle size, as larger particles sediment faster. Estimates on particle size and determination of ash vs sulphate is crucial in estimating the lifetime, and therefore climatic impact of an eruption (Vernier et al., 2016). While current measurements from lidars can distinguish ash from sulphate the

single wavelength backscatter measurements do not provide information on particle size. Conversely, occultation measurements do not provide polarization to distinguish particle shape. ALI is in a unique position to provide both size and classification information of volcanic plumes to improve understanding of particle evolution in both ash and ash-free conditions.

Interactive aerosols in climate models remain computationally taxing, with reliance on bulk schemes a common practice. These require parameterization of aerosol evolution and removal processes. However, the effect of eruptions on particle microphysics is not well constrained by current observations. ALI measurements will improve the relationships between aerosol loading and microphysical properties after an eruption through retrieval of particle size. Similarly, models that use interactive aerosols to fully simulate particle evolution show large inter-model spread (Timmreck, et al, 2018), highlighting the need for measurements that can help constrain model results.

3.2.3 Tropical Tropopause layer

The Tropical Tropopause Layer (TTL) is a layer near 14 to 18 km in the tropics that marks the transition between convective and radiative regimes. Strong circulation in this region driven by wave activity drives the upwelling branch Brewer Dobson circulation, feeding the stratosphere with tropospheric air and largely dictating the composition of the stratosphere (Fueglistaler et al., 2009). As the climate warms and the Brewer Dobson circulation increases in strength, changes to the temperatures and chemical composition of the TTL are expected, affecting cirrus composition (Randel and Jensen, 2013). The presence of aerosol in the TTL also changes cirrus properties, with sulfuric acid coating ice particles. When particles are small this can produce substantial radiative changes (Räisänen et al., 2006). The ability to measure thin cirrus in the presence of background and volcanically active aerosol levels will provide an excellent opportunity to monitor this crucial region during a period of changing climate. The vertical resolution of ALI is sufficient to resolve cirrus clouds above convective cells at extinction levels as low as 10^{-5} km^{-1}. This will provide a much more complete map of thin cirrus clouds in the TTL, improving radiative forcing estimates, but also the understanding of atmospheric composition and water vapour, as these clouds serve to dehydrate the stratosphere.

4 Discussion on Priority Trade-Offs

The ALI instrument is designed to measure two dimensional images of the atmospheric limb radiance in a series of multi-spectral bands with a selectable polarization state. The nature of the instrument means that several priority trade-offs exist in the modes of operation, the primary being the trade between signal-to-noise ratio (SNR) and the number of multi-spectral/polarization channels per observation set.. A multi-spectral, dual polarization observation set has essentially four dimensions: two spatial (tangent altitude and cross track distance), one spectral, and one polarization. The instrument obtains the spatial dimension with a single exposure time, and the spectral and polarization samples are obtained by scanning in time. This means that the more rapidly these are scanned to improve the spatial sampling between observation sets, the lower the signal-to-noise of each radiance measurement. The current requirement calls for 11+3 channels (horizontal+vertical) across the spectral range with a minimum SNR of 200 for the horizontal polarization (used for extinction coefficient retrievals) and 50 for the vertical polarization (used for cloud discrimination). This observation cadence should be captured within 30 seconds to meet the sampling requirements along the satellite track. The compatibility of these two requirements must be confirmed with simulation; retrieval algorithms must be used to test the need for the 11+3 channels to confirm if this the minimal set required in terms of information content to obtain the particle size distribution information and perform the cloud/aerosol discrimination.

The other priority trade-off in the ALI instrument operation is in nature of the binning of the limb images into vertical columns for profile retrieval. The cross track field-of-view on the instrument is 5 degrees, which is approximately 300 km at the tangent point. This image will be nominally binned into 10 vertical columns for downlink, for an effective cross track sampling of 30 km. This must be done so as not to degrade the vertical sampling of 0.25 km due to the curvature of the Earth across the image. Preliminary calculations show this is feasible; however, a trade study should be performed to optimize the spatial sampling while maintaining the spectral signal to noise ratio.

5 Requirement Format

5.1 Conventions

The wording of statements in this section determines the disposition of requirements:
"**SHALL**" and "**SHALL NOT**" indicate a (mandatory) requirement.
"**SHOULD**" and "**SHOULD NOT**" indicate a recommendation, which is not mandatory.
"**MAY**" and "**NEED NOT**" indicate a permission or option.
"**WILL**" indicates a statement of fact or intention.

5.2 Requirement Format and Numbering

The standard for numbering is ALI-CAT-###-V.V where CAT is a three letter keyword for the category as provided in the table below. ### is a sequential number where a 0 digit has been added to allow for later insertions and V.V is the version of the associated User Requirement Document (e.g. 1.0).

Requirements are stated, followed by a brief rationale including assumptions. Both the goal and threshold requirement values are specified if applicable. Comments do not form part of the requirement and are provided for information only.

Category	Description	Examples
MIS	Mission level requirements	Viewing geometry, mission lifetime, tasking and data latency, etc.
INT	Instrument level requirements	Spectral, spatial radiometric resolution
DAT	Data requirements	Bias, precision, sampling, etc.

Table 4: Requirement name formats

The threshold values represent the minimum required performance. When a threshold is not met, at least one of the mission objectives cannot be met. The goal values represent the ideal performance. Performance beyond these values provides limited additional benefit towards achieving the mission objectives. The goal is an ideal value for the most demanding mission objective.

5.3 Data Processing Levels

The data obtained from the ALI instrument will go through multiple levels of processing to obtain geophysical variables used for scientific analysis. The table below describes the various data processing levels used in this report.

Data Level	Description
Level 0	Reconstructed, unprocessed instrument and payload data at full resolution, with any and all communications artifacts (e.g., synchronization frames, communications headers, duplicate data) removed.
Level 1A	Reconstructed, unprocessed instrument data at full resolution, time-referenced, and annotated with ancillary information, including radiometric and geometric calibration coefficients and georeferencing parameters (e.g., platform ephemeris) computed and appended but not applied to Level 0 data.
Level 1B	Level 1A data that have been processed to sensor units.
Level 2	Derived geophysical variables from the Level 1 source data along the satellite orbit.
Level 3	Level 2 variables averaged onto uniform space-time grid scales.
Level 4	Results from analyses of lower-level data (e.g., variables derived from multiple measurements or combined with model output).

Table 5: Description of data processing levels[7]

[7] Adapted from "Data Processing Levels - Science@NASA." Data Processing Levels. Accessed 27 Mar. 2020.

6 Mission Coverage Requirements

6.1 Position and Orientation Knowledge Requirements

6.1.1 [ALI-MIS-001-0.2]-Sun-Synchronous Orbit

Description: Low earth orbit. The orbit shall be sun-synchronous..

Assumptions and Rationale: Sun-synchronous orbit provides stability in solar viewing geometry for limb scattering observations and addresses the need for daily global (all longitudes) coverage, i.e. enable measurements for all portions of the orbit and covering both hemispheres, reaching as far north and south as possible (where solar illumination conditions allow).

Comments: Measurements can be made from either polar or highly inclined asynchronous orbit with impact only on the global coverage. Design shall not preclude either scenario.

6.1.2 [ALI-MIS-002-0.2]-Spacecraft Pointing Control

Description: The satellite pitch angle shall be controlled to better than ±5 arcmin, the yaw angle shall be controlled to better than ±1 degree of the orbit plane, and the spacecraft roll angle shall be controlled to better than ±5 arcmin (TBC).

Assumptions and rationale: Pitch control ensures the vertical iFOV of the instrument is mapped to the target range of tangent altitudes on the atmospheric limb. Control in the roll direction minimizes the range of tangent height spanned by one iFOV, for example. Controlling roll and yaw ensures the measured profile is within the orbit plane and thus is important for tomographic inversion and coordination with potential nadir observations on the same platform.

Comments: The pitch angle control translates to tangent height control of 4-5 km. The yaw control requirement translates to 50 km of across-track displacement of the tangent point. The movement of the tangent point is a function of the tangent height during roll anomaly with a worst case for the extremes of the instantaneously sampled tangent height range.

6.1.3 [ALI-MIS-003-0.2]-Spacecraft Pointing Knowledge

Description: During a hyperspectral measurement cycle, the yaw angle (relative to the orbit plane) shall be known to 5 arcmin, the roll angle shall be known to 1 arcmin (TBC).

Assumptions and Rationale: Required for geo-locating cross track measurements (yaw) and for limiting impact on altitude coverage and resolution of cross track profiles (roll).

Comments: The pointing knowledge on yaw and roll are post-processed.

6.1.4 [ALI-MIS-004-0.2]-Spacecraft Altitude Tolerance

Description: The satellite altitude shall be controlled to +/- 10 km of the nominal orbit altitude.

Assumptions and rationale: The ALI instrument design can accommodate a wide range of potential platform altitudes; however, pitch offset is highly sensitive to platform altitude and variations in platform altitude throughout the mission duration (in the absence of pitch correction) shall be maintained within relatively tight constraints.

Comments: This will ensure the same approximate altitude range is sampled over the duration of the mission.

6.1.5 [ALI-MIS-005-0.2]-Spacecraft Altitude Knowledge

Description: The satellite altitude shall be known to within 0.15 km.

Assumptions and rationale: The ALI instrument design can accommodate a wide range of potential platform altitudes; however, pitch offset is highly sensitive to platform altitude and variations in platform altitude throughout the mission duration (in the absence of pitch correction) and shall be maintained within relatively tight constraints.

Comments: Knowledge of this parameter is essential for instrument specific tangent altitude knowledge.

6.1.6 [ALI-MIS-006-0.2]-Design Lifetime

Description: The design lifetime threshold shall be 3 years (goal of 5 years).

Assumptions and rationale: Alignment with A-CCP mission lifetime..

Comments: N/A.

6.2 Solar Geometry Requirements

6.2.1 [ALI-MIS-006-0.2]-Solar Zenith Angle

Description: The mission shall measure limb-scattered sunlight with the ALI payload whenever the Solar Zenith Angle at the measurement tangent point is less than 92 degrees and be capable of making measurements at less than 95 degrees.

Assumptions and rationale: Ensures maximum latitudinal coverage of the sunlit portion of Earth.

Comments: N/A

6.2.2 [ALI-MIS-007-0.2]-Solar Scattering Angle

Description: The mission shall measure limb-scattered sunlight with the ALI payload whenever the Solar Scattering Angle (SSA) at the measurement tangent point is 30° < SSA < 150° and be capable of making measurements at 20° < SSA < 180°.

Assumptions and rationale: Ensures maximum latitudinal coverage of the sunlit portion of Earth.

Comments: N/A

6.3 Viewing Requirements

6.3.1 [ALI-MIS-008-0.2]-Limb Viewing in the Orbit Plane

Description: The spacecraft shall enable unobstructed atmospheric limb measurements with the cross-track swath centered on the orbit plane.

Assumptions and Rationale: Within the pointing control accuracy defined in the Pointing Control requirement.

Comments: Observations in the orbit plane are essential for tomographic retrievals.

6.4 Latency Requirements

6.4.1 [ALI-MIS-009-0.2]-ALI Data Latency

Description: The mission shall be capable of providing Level 2 data from ALI, from acquisition on-orbit to product delivery to the end-user, within 2 days.

Assumptions and Rationale: The latency requirement stems from the need for aerosol observations to be available for forest fire and volcanic plume monitoring/forecasting.

Comments: To be confirmed with ECCC.

6.5 Other Mission Coverage Requirements

6.5.1 [ALI-MIS-010-0.2]-Synergy with other instrumentation

Description: Co-alignment with SHOW, and common air mass view with TICFIRE and lidar given the inherent time delay from moutning on a common platform.

Assumptions and Rationale: The 5 degree field of view of ALI is sufficient to provide overlap to account for the Earth rotation and sample the same airmass as nadir-viewing instruments on a typical low Earth observing platform.

Comments: TBC

7 Instrument Requirements

7.1 Spectral Requirements

7.1.1 [ALI-INT-001-0.2]- Wavelength Range

Description: ALI shall provide measurements in the wavelength range of 550 nm to 1500 nm

Assumptions and Rationale: Provides enough spectral range for aerosol particle size retrieval and ozone correction.

Comments: N/A

7.1.2 [ALI-INT-002-0.2]- Spectral Resolution

Description: The spectral resolution of ALI shall be better than 10 nm for the spectral range 550-900 nm, and better than 20 nm for the spectral range 900-1500 nm.

Assumptions and Rationale: This is evaluated as the FWHM. The contribution from regions outside +/- 3 FWHM from the passband sidelobes or from internal stray light shall be less than 1 % (TBC).

Comments: This resolution is sufficient for retrieval of aerosol properties from the atmospheric limb measurements due to the broadband nature of aerosol scattering. The spectral resolution is driven by the nature of the AOTF interaction and SNR. Other optical components shall not reduce the spectral resolution beyond this limit.

7.1.3 [ALI-INT-003-0.2]- Spectral Gradient across FOV

Description: For any individual spectral image, the variation of the central wavelength of the passband across the Field of View shall be less than 0.8% of the central wavelength.

Assumptions and Rationale: A wavelength variation across the field of view is tolerable within the aerosol retrieval process. The described variation is sufficiently small when compared to the broad spectral scattering signature of

aerosol. The variation is driven by the nature of the acousto-optic interaction with collimated light. Other optical components shall not increase the wavelength variation.

Comments: This is potentially on the high side and needs confirmation with instrument modelling and lab measurements.[LR5]

7.2 Spatial Requirements

7.2.1 [ALI-INT-004-0.2]- Instrument Pointing Knowledge

Description: The mission shall be provided measurement tangent altitude registration within ±0.25 km (TBC) (threshold), and should be able to register measurement tangent altitudes within ±0.1 km (goal). These do not need to be provided in real time, but should be made available for the ground segment.

Assumptions and Rationale: This includes all contributing effects such as those related to pointing and position knowledge (time-tagging, position knowledge, orientation knowledge, misalignment/co-registration with star-trackers, thermo-elastic distortions, atmospheric refraction, geoid, etc.) and refers to post-processed spatial location knowledge of the acquired data.

Comments: The description above does not distinguish between pointing knowledge precision, bias, and long-term stability. Long-term stability of Level 2 data products is important for trend studies.

7.2.2 [ALI-INT-005-0.2]- Vertical (Tangent Altitude) Range

Description: ALI shall provide spectral images of the atmospheric limb on the sunlit portion of the orbit track extending from the surface to 45 km tangent altitude.

Assumptions and Rationale: This ensures coverage of the UTLS region and allows for calibration using spectral and radiometric measurements from tangent altitudes above 35 km. Depending on spacecraft altitude, this is approximately 1 degree FOV.

Comments: N/A

7.2.3 [ALI-INT-006-0.2]- Vertical (Tangent altitude) Resolution

Description: ALI shall provide spectral radiance images at a vertical resolution equal to or less than 0.25 km on the atmospheric limb.

Assumptions and Rationale: The vertical resolution includes contributions from the optical performance, pixilation, and the line-of-sight (LOS) motion during exposures. The vertical resolution is evaluated as the FWHM.

Comments: N/A

7.2.4 [ALI-INT-007-0.2]- Vertical (Tangent Altitude) Sampling

Description: ALI shall provide spectral radiance images with vertical sampling at the pixel level equal to two samples per vertical resolution element.

Assumptions and Rationale: Sampling twice as fine as the vertical resolution is sufficient according to the Nyquist limit.

Comments: N/A

7.2.5 [ALI-INT-008-0.2]- Cross-Track Range

Description: ALI shall provide spectral images of the atmospheric limb on the sunlit portion of the orbit track with a 5 degree cross-track FOV, centered on the orbit plane. This translates to a cross track field of view of approximately 250km at the tangent point.

Assumptions and Rationale: This provides sampling between the orbital tracks and greatly increases daily, global coverage and revisit times.

Comments: 8 degrees is desired, but this seems to be too difficult technically.

7.2.6 [ALI-INT-009-0.2]- Cross-Track Sampling

Description: The cross-track sampling shall be less than or equal to 40 arcseconds.

Assumptions and Rationale: The across-track sampling will be sufficient to reach SNR requirements through across-track binning to approximately 10 vertical profiles per image. This sampling requirement should also ensure that the curvature of the Earth can be compensated when binning so as not to degrade the vertical resolution.

Comments:

7.2.7 [ALI-INT-010-0.2]- Along-Track Sampling

Description: ALI shall provide one full along-track hyperspectral observation every 30 s.

Assumptions and Rationale: Feasibility with SNR requirements must be confirmed.

Comments: N/A

7.3 Radiometric Requirements

7.3.1 [ALI-INT-011-0.2]- Accuracy

Description: ALI shall be capable of measuring calibrated radiances to within 5% across the spectral and spatial range of the target observations.

Assumptions and Rationale: Accuracy is driven by the requirement to use high tangent altitude observations to retrieve effective Earth surface reflectance.

Comments: N/A

7.3.2 [ALI-INT-012-0.2]- Signal to Noise Ratio

Description: The Signal to Noise Ratio (SNR) of ALI shall be greater than 200 for horizontally polarized light and greater than 50 for vertically polarized light across all wavelengths and tangent altitudes up to 35 km.

Assumptions and Rationale: Accuracy is driven by the requirement to use high tangent altitude observations to retrieve effective Earth surface reflectance.

Comments: SNR requirement based on radiative transfer model simulations at typical viewing geometry. This requirement maps to science requirements for the level 2 data product.

7.3.3 [ALI-INT-013-0.2]- Stray Light Suppression

Description: The design of ALI shall incorporate stray light control features to address stray light sources including out-of-field and 0th order in-field signals, as well as ghosts from internal reflections.

Assumptions and Rationale: Out of field stray light from the Earth surface is a known issue for limb imaging and substantial effort should be made at the design level to minimize this effect. Quantitative requirements need confirmation from simulation.

Comments: N/A

7.3.4 [ALI-INT-014-0.2]- Dynamic Range

Description: ALI shall be capable of measuring limb radiances from 10^{11} to 10^{15} photons/cm2/steradian/second/nm.

Assumptions and Rationale: Based on radiative transfer forward model simulations at typical viewing geometry.

Comments: N/A

7.3.5 [ALI-INT-015-0.2]- Polarization

Description: ALI shall be capable of measuring two orthogonal polarizations of the limb radiance. The accuracy of the polarization state shall be (TBC with simulation).

Assumptions and Rationale: Based on radiative transfer forward model simulations at typical viewing geometry.

Comments: N/A

7.4 Operational Mode Requirement

7.4.1 [ALI-INT-016-0.2]- Hyperspectral Mode Observation Acquisition

Description: ALI shall perform measurements at a minimum of 11 wavelengths {551, 601, 676, 755, 869, 950, 1022, 1100, 1200, 1450, 1500 nm}, for horizontally polarized input, and 3 wavelengths {755, 1022, 1500 nm} for vertically polarized input, within the specified along-track sampling rate. The cadence shall also

include one sample with the RF driver disabled to sample the stray light contribution from the undiffracted (0th order) beam.

Assumptions and Rationale: Wavelength selection to match NASA SAGE heritage observations.

Comments: The vertical polarization state measurement is a science requirement primarily for cloud/aerosol discrimination. Fewer samples spaced across the spectral range are sufficient for the discrimination algorithm.

7.4.2 [ALI-INT-017-0.2]- Event Mode Observation Acquisition

Description: ALI shall perform measurements at a single wavelength, nominally 1020 nm, for both polarizations and with the RF driver in a repeated cadence.

Assumptions and Rationale: Allows for high spatial resolution observation for tracking smoke/aerosol plume from forest fires and volcanic eruptions.

Comments: N/A.

7.4.3 [ALI-INT-018-0.2]- Dark Signal Characterization

Description: ALI shall be capable of performing measurements on the night side of the orbit with the RF driver disabled with variable exposure time so as to characterize the detector dark signal.

Assumptions and Rationale: No shutter is required.

Comments: N/A.

7.4.4 [ALI-INT-019-0.2] Lunar/Stellar Observation

Description: ALI shall be capable of performing hyperspectral observations of the moon or stars during the night side of the orbit at opportunistic times when these targets are within the field of view.

Assumptions and Rationale: Provides spectral, radiative and pointing calibration opportunities.

Comments: N/A.

8 Level 2 Data Requirements

8.1 Aerosol Extinction Profiles

8.1.1 [ALI-DAT-001-0.2] Wavelength Sampling

Description: ALI extinction profiles shall be retrieved at 551, 675, 755, 1022, and 1500nm.

Assumptions and Rationale: Extinction retrievals at these wavelengths provide continuity with current limb scattering and solar occultation instruments. The 551nm extinction retrieval will also help enhance synergy with the ACCP lidar, which is expected to have a channel in the 525nm range (TBC).

Comments: N/A.

8.1.2 [ALI-DAT-002-0.2] Vertical Range

Description: ALI extinction profiles shall retrieve extinction from the tropopause (assuming a 2°C lapse rate definition) or the lowest altitude where extinction at 755nm is below 10^{-2} km^{-1}, whichever is higher, up to the lowest altitude where extinction at 755nm exceeds 10^{-5} km^{-1} (TBC). The retrieval should extend down to 8km when clouds do not obstruct the field of view.

Assumptions and Rationale: This range covers the majority of stratospheric aerosol, and allows normalization at altitudes with sufficiently low levels of aerosol loading. Retrieval below the tropopause is desirable to better quantify transport, but is not required as ACCP baseline instruments will cover this range.

Comments: Extinction levels exceeding 10^{-2} km^{-1} at 755nm may be measurable at longer wavelengths, but cannot be guaranteed.

8.1.3 [ALI-DAT-003-0.2] Vertical Resolution

Description: Vertical resolution shall meet or exceed 0.5km.

Assumptions and Rationale: Vertically inhomogeneous plumes from volcanic eruptions require high vertical resolutions to resolve. High resolution also helps

reduce cloud contamination and improve filtering in the UTLS where aerosol levels are crucial for understanding total loading.

Comments: N/A.

8.1.4 [ALI-DAT-004-0.2] Horizontal Resolution

Description: Horizontal resolution shall meet or exceed 250km.

Assumptions and Rationale: 250km is sufficient to resolve most volcanic and wildfire plumes shortly after the initial injection, and provides comparable resolution to cross-track measurements.

Comments: N/A.

8.1.5 [ALI-DAT-005-0.2] Accuracy

Description: Horizontal resolution shall meet or exceed 250km.

Assumptions and Rationale: 250km is sufficient to resolve most volcanic and wildfire plumes shortly after the initial injection, and provides comparable resolution to cross-track measurements.

Comments: N/A.

Bibliography

Adams, C., Bourassa, A. E., McLinden, C. A., Sioris, C. E., Von Clarmann, T., Funke, B., ... & Degenstein, D. A. (2017). Effect of volcanic aerosol on stratospheric NO2 and N2O5 from 2002-2014 as measured by Odin-OSIRIS and Envisat-MIPAS.

Andersson, S. M., Martinsson, B. G., Vernier, J. P., Friberg, J., Brenninkmeijer, C. A., Hermann, M., ... & Zahn, A. (2015). Significant radiative impact of volcanic aerosol in the lowermost stratosphere. Nature communications, 6, 7692.

Barth, C. A., Rusch, D. W., Thomas, R. J., Mount, G. H., Rottman, G. J., Thomas, G. E., ... & Lawrence, G. M. (1983). Solar mesosphere explorer: Scientific objectives and results. Geophysical research letters, 10(4), 237-240.

Bingen, C., Fussen, D., & Vanhellemont, F. (2004). A global climatology of stratospheric aerosol size distribution parameters derived from SAGE II data over the period 1984–2000: 2. Reference data. Journal of Geophysical Research: Atmospheres, 109(D6).

Boucher, O., Randall, D., Artaxo, P., Bretherton, C., Feingold, G., Forster, P., ... & Rasch, P. (2013). Clouds and aerosols. In Climate change 2013: the physical science basis. Contribution of Working Group I to the Fifth Assessment Report of the Intergovernmental Panel on Climate Change (pp. 571-657). Cambridge University Press.

Bourassa, A. E., Degenstein, D. A., & Llewellyn, E. J. (2005). Climatology of the subvisual cirrus clouds as seen by OSIRIS on Odin. Advances in Space Research, 36(5), 807-812.

Bourassa, A. E., Degenstein, D. A., Gattinger, R. L., & Llewellyn, E. J. (2007). Stratospheric aerosol retrieval with optical spectrograph and infrared imaging system limb scatter measurements. Journal of Geophysical Research: Atmospheres, 112(D10).

Bourassa, A. E., Degenstein, D. A., & Llewellyn, E. J. (2008). SASKTRAN: A spherical geometry radiative transfer code for efficient estimation of limb scattered sunlight. Journal of Quantitative Spectroscopy and Radiative Transfer, 109(1), 52-73.

Bourassa, A. E., Degenstein, D. A., Elash, B. J., & Llewellyn, E. J. (2010). Evolution of the stratospheric aerosol enhancement following the eruptions of Okmok and Kasatochi: Odin-OSIRIS measurements. Journal of Geophysical Research: Atmospheres, 115(D2).

Bourassa, A. E., McLinden, C. A., Sioris, C. E., Brohede, S., Bathgate, A. F., Llewellyn, E. J., & Degenstein, D. A. (2011). Fast NO2 retrievals from Odin-OSIRIS limb scatter measurements. Atmospheric Measurement Techniques, 4(5), 965-972.

Bourassa, A. E., Roth, C. Z., Zawada, D. J., Rieger, L. A., McLinden, C. A., & Degenstein, D. A. (2018). Drift-corrected Odin-OSIRIS ozone product: algorithm and updated stratospheric ozone trends. Atmospheric Measurement Techniques, 11(1), 489-498.

Bourassa, A. E., Rieger, L. A., Zawada, D. J., Khaykin, S., Thomason, L. W., & Degenstein, D. A. (2019). Satellite Limb Observations of Unprecedented Forest Fire Aerosol in the Stratosphere. Journal of Geophysical Research: Atmospheres, 124(16), 9510-9519.

Carslaw, K. S., Lee, L. A., Reddington, C. L., Pringle, K. J., Rap, A., Forster, P. M., ... & Pierce, J. R. (2013). Large contribution of natural aerosols to uncertainty in indirect forcing. Nature, 503(7474), 67-71.

Chepfer, H., Bony, S., Winker, D., Cesana, G., Dufresne, J. L., Minnis, P., ... & Zeng, S. (2010). The GCM-oriented calipso cloud product (CALIPSO-GOCCP). Journal of Geophysical Research: Atmospheres, 115(D4).

Christian, K., Yorks, J., Colarco, P., Aquila, V., & Das, S. (2019). Differences in the Vertical and Microphysical Evolution of Volcanic and Pyrocumulonimbus Stratospheric Aerosol Plumes as Observed by CALIOP and CATS Satellite Lidar.

Degenstein, D. A., Bourassa, A. E., Roth, C. Z., & Llewellyn, E. J. (2009). Limb scatter ozone retrieval from 10 to 60 km using a multiplicative algebraic reconstruction technique. Atmospheric Chemistry & Physics, 9(17).

Deligne, N. I., Coles, S. G., & Sparks, R. S. J. (2010). Recurrence rates of large explosive volcanic eruptions. Journal of Geophysical Research: Solid Earth, 115(B6).

Deshler, T., Hervig, M. E., Hofmann, D. J., Rosen, J. M., & Liley, J. B. (2003). Thirty years of in situ stratospheric aerosol size distribution measurements from Laramie, Wyoming (41 N), using balloon-borne instruments. Journal of Geophysical Research: Atmospheres, 108(D5).

Dessler, A. E., Palm, S. P., Hart, W. D., & Spinhirne, J. D. (2006). Tropopause-level thin cirrus coverage revealed by ICESat/Geoscience Laser Altimeter System. Journal of Geophysical Research: Atmospheres, 111(D8).

Dykema, J. A., Keith, D. W., Anderson, J. G., & Weisenstein, D. (2014). Stratospheric controlled perturbation experiment: a small-scale experiment to improve understanding of the risks of solar geoengineering. *Philosophical Transactions of the Royal Society A: Mathematical, Physical and Engineering Sciences*, *372*(2031), 20140059.

English, J. M., Toon, O. B., & Mills, M. J. (2012). Microphysical simulations of sulfur burdens from stratospheric sulfur geoengineering. Atmospheric Chemistry and Physics, 12(10), 4775-4793.

Garny, H., & Randel, W. J. (2016). Transport pathways from the Asian monsoon anticyclone to the stratosphere. Atmos. Chem. Phys, 16, 2703-2718.

Gasparini, B., & Lohmann, U. (2016). Why cirrus cloud seeding cannot substantially cool the planet. Journal of Geophysical Research: Atmospheres, 121(9), 4877-4893.

Fromm, M., Alfred, J., Hoppel, K., Hornstein, J., Bevilacqua, R., Shettle, E., ... & Stocks, B. (2000). Observations of boreal forest fire smoke in the stratosphere by POAM III, SAGE II, and lidar in 1998. Geophysical Research Letters, 27(9), 1407-1410.

Fromm, M., Tupper, A., Rosenfeld, D., Servranckx, R., & McRae, R. (2006). Violent pyro-convective storm devastates Australia's capital and pollutes the stratosphere. Geophysical Research Letters, 33(5).

Fueglistaler, S., Dessler, A. E., Dunkerton, T. J., Folkins, I., Fu, Q., & Mote, P. W. (2009). Tropical tropopause layer. Reviews of Geophysics, 47(1).

Fyfe, J. C., Von Salzen, K., Cole, J. N. S., Gillett, N. P., & Vernier, J. P. (2013). Surface response to stratospheric aerosol changes in a coupled atmosphere–ocean model. Geophysical Research Letters, 40(3), 584-588.

Gasparini, B., & Lohmann, U. (2016). Why cirrus cloud seeding cannot substantially cool the planet. Journal of Geophysical Research: Atmospheres, 121(9), 4877-4893.

Girardin, M. P., & Mudelsee, M. (2008). Past and future changes in Canadian boreal wildfire activity. Ecological Applications, 18(2), 391-406.

Griffin, D., C. Sioris, J. Chen, N. Dickson, A. Kovachik, M. de Graaf, S. Nanda, P. Veefkind, E. Dammers, C. A. McLinden, P A. Makar, & A. Akingunola. (2020). The 2018 fire season in North America as seen by TROPOMI: aerosol layer height validation and evaluation of model-derived plume heights, Atmospheric Measurement Techniques, revised.

Haladay, T., & Stephens, G. (2009). Characteristics of tropical thin cirrus clouds deduced from joint CloudSat and CALIPSO observations. Journal of Geophysical Research: Atmospheres, 114(D8).

Hartmann, D. L., Holton, J. R., & Fu, Q. (2001). The heat balance of the tropical tropopause, cirrus, and stratospheric dehydration. Geophysical research letters, 28(10), 1969-1972.

Haywood, J. M., Jones, A., & Jones, G. S. (2014). The impact of volcanic eruptions in the period 2000–2013 on global mean temperature trends evaluated in the HadGEM2-ES climate model. Atmospheric Science Letters, 15(2), 92-96.

Heckendorn, P., Weisenstein, D., Fueglistaler, S., Luo, B. P., Rozanov, E., Schraner, M., ... & Peter, T. (2009). The impact of geoengineering aerosols on stratospheric temperature and ozone. *Environmental research letters*, *4*(4), 045108.

Henderson, S. B., Burkholder, B., Jackson, P. L., Brauer, M., & Ichoku, C. (2008). Use of MODIS products to simplify and evaluate a forest fire plume dispersion model for PM10 exposure assessment. *Atmospheric Environment*, *42*(36), 8524-8532.

Hofmann, D., Barnes, J., O'Neill, M., Trudeau, M., & Neely, R. (2009). Increase in background stratospheric aerosol observed with lidar at Mauna Loa Observatory and Boulder, Colorado. Geophysical Research Letters, 36(15).

Hong, Y., Liu, G., & Li, J. L. (2016). Assessing the radiative effects of global ice clouds based on CloudSat and CALIPSO measurements. Journal of Climate, 29(21), 7651-7674.

Homeyer, C. R., McAuliffe, J. D., & Bedka, K. M. (2017). On the development of above-anvil cirrus plumes in extratropical convection. Journal of the Atmospheric Sciences, 74(5), 1617-1633.

Jensen, E., & Pfister, L. (2004). Transport and freeze-drying in the tropical tropopause layer. Journal of Geophysical Research: Atmospheres, 109(D2).

Kar, J., Lee, K. P., Vaughan, M. A., Tackett, J. L., Trepte, C. R., Winker, D. M., ... & Getzewich, B. J. (2019). CALIPSO level 3 stratospheric aerosol profile product: version 1.00 algorithm description and initial assessment. *Atmospheric Measurement Techniques*, *12*(11).

Kravitz, B., Robock, A., Boucher, O., Schmidt, H., Taylor, K. E., Stenchikov, G., & Schulz, M. (2011). The geoengineering model intercomparison project (GeoMIP). Atmospheric Science Letters, 12(2), 162-167.

Kremser, S., Thomason, L. W., von Hobe, M., Hermann, M., Deshler, T., Timmreck, C., ... & Fueglistaler, S. (2016). Stratospheric aerosol—Observations, processes, and impact on climate. Reviews of Geophysics, 54(2), 278-335.

Kuebbeler, M., Lohmann, U., & Feichter, J. (2012). Effects of stratospheric sulfate aerosol geo-engineering on cirrus clouds. Geophysical Research Letters, 39(23).

Lacis, A., Hansen, J., & Sato, M. (1992). Climate forcing by stratospheric aerosols. *Geophysical Research Letters*, *19*(15), 1607-1610.

Lau, W. K., Yuan, C., & Li, Z. (2018). Origin, maintenance and variability of the Asian tropopause aerosol layer (ATAL): the roles of monsoon dynamics. Scientific reports, 8(1), 1-14.

Liu, Y., Stanturf, J., & Goodrick, S. (2010). Trends in global wildfire potential in a changing climate. Forest ecology and management, 259(4), 685-697.

Llewellyn, E. J., Lloyd, N. D., Degenstein, D. A., Gattinger, R. L., Petelina, S. V., Bourassa, A. E., ... & McConnell, J. C. (2004). The OSIRIS instrument on the Odin spacecraft. Canadian Journal of Physics, 82(6), 411-422.

Malinina, E., Rozanov, A., Rozanov, V., Liebing, P., Bovensmann, H., & Burrows, J. P. (2018). Aerosol particle size distribution in the stratosphere retrieved from SCIAMACHY limb measurements. Atmospheric Measurement Techniques, 11(4).

Marshall, L., Johnson, J. S., Mann, G. W., Lee, L., Dhomse, S. S., Regayre, L., ... & Schmidt, A. (2019). Exploring how eruption source parameters affect volcanic radiative forcing using statistical emulation. *Journal of Geophysical Research: Atmospheres*, *124*(2), 964-985.

Masson-Delmotte, V., Schulz, M., Abe-Ouchi, A., Beer, J., Ganopolski, A., Gonzalez Rouco, J. F., ... & Osboorn, T. (2013). X., and Timmermann, A.: Information from paleoclimate archives. Climate change.

McFarquhar, G. M., Heymsfield, A. J., Spinhirne, J., & Hart, B. (2000). Thin and subvisual tropopause tropical cirrus: Observations and radiative impacts. Journal of the atmospheric sciences, 57(12), 1841-1853.

Mills, M. J., Schmidt, A., Easter, R., Solomon, S., Kinnison, D. E., Ghan, S. J., ... & Gettelman, A. (2016). Global volcanic aerosol properties derived from emissions, 1990–2014, using CESM1 (WACCM). *Journal of Geophysical Research: Atmospheres*, *121*(5), 2332-2348.

Pachauri, R. K., Allen, M. R., Barros, V. R., Broome, J., Cramer, W., Christ, R., ... & Dubash, N. K. (2014). *Climate change 2014: synthesis report. Contribution of Working Groups I, II and III to the fifth assessment report of the Intergovernmental Panel on Climate Change* (p. 151). IPCC.

Petropavlovskikh, I., Godin-Beekmann, S., Hubert, D., Damadeo, R., Hassler, B., Sofieva, V., ... & Tourpali, K. (2018). Sparc/io3c/gaw report on long-term ozone trends and uncertainties in the stratosphere. 39th session of the WCRP Joint Scientific Committee, 8.

Pinto, J. P., Turco, R. P., & Toon, O. B. (1989). Self-limiting physical and chemical effects in volcanic eruption clouds. *Journal of Geophysical Research: Atmospheres*, *94*(D8), 11165-11174.

Räisänen, P., Bogdan, A., Sassen, K., Kulmala, M., & Molina, M. J. (2006). Impact of H2SO4/H2O coating and ice crystal size on radiative properties of sub-visible cirrus.

Randall, D. A., Wood, R. A., Bony, S., Colman, R., Fichefet, T., Fyfe, J., ... & Stouffer, R. J. (2007). Climate models and their evaluation. In Climate change 2007: The physical science basis. Contribution of Working Group I to the Fourth Assessment Report of the IPCC (FAR) (pp. 589-662). Cambridge University Press.

Randel, W. J., Park, M., Emmons, L., Kinnison, D., Bernath, P., Walker, K. A., ... & Pumphrey, H. (2010). Asian monsoon transport of pollution to the stratosphere. Science, 328(5978), 611-613.

Randel, W. J., & Jensen, E. J. (2013). Physical processes in the tropical tropopause layer and their roles in a changing climate. Nature Geoscience, 6(3), 169-176.

Rasch, P. J., Crutzen, P. J., & Coleman, D. B. (2008). Exploring the geoengineering of climate using stratospheric sulfate aerosols: The role of particle size. Geophysical Research Letters, 35(2).

Rawcliffe, R. D., Meloy, G. E., Friedman, R. M., & Rogers, E. H. (1963). Measurement of vertical distribution of ozone from a polar orbiting satellite. Journal of Geophysical Research, 68(24), 6425-6429.

Ricke, K. L., Morgan, M. G., & Allen, M. R. (2010). Regional climate response to solar-radiation management. Nature Geoscience, 3(8), 537-541.

Ridley, D. A., Solomon, S., Barnes, J. E., Burlakov, V. D., Deshler, T., Dolgii, S. I., ... & Ritter, C. (2014). Total volcanic stratospheric aerosol optical depths and implications for global climate change. Geophysical Research Letters, 41(22), 7763-7769.

Rieger, L. A., Bourassa, A. E., & Degenstein, D. A. (2014). Stratospheric aerosol particle size information in Odin-OSIRIS limb scatter spectra. Atmospheric Measurement Techniques, 7(2), 507.

Rieger, L. A., Zawada, D. J., Bourassa, A. E., & Degenstein, D. A. (2019). A Multiwavelength Retrieval Approach for Improved OSIRIS Aerosol Extinction Retrievals. Journal of Geophysical Research: Atmospheres, 124(13), 7286-7307.

Rittmaster, R., Adamowicz, W. L., Amiro, B., & Pelletier, R. T. (2006). Economic analysis of health effects from forest fires. Canadian Journal of Forest Research, 36(4), 868-877.

Santer, B. D., Fyfe, J. C., Pallotta, G., Flato, G. M., Meehl, G. A., England, M. H., ... & Cvijanovic, I. (2017). Causes of differences in model and satellite tropospheric warming rates. Nature Geoscience, 10(7), 478-485.

Sassen, K., Wang, Z., & Liu, D. (2008). Global distribution of cirrus clouds from CloudSat/Cloud-Aerosol lidar and infrared pathfinder satellite observations (CALIPSO) measurements. Journal of Geophysical Research: Atmospheres, 113(D8).

Sassen, K., Wang, Z., & Liu, D. (2009). Cirrus clouds and deep convection in the tropics: Insights from CALIPSO and CloudSat. Journal of Geophysical Research: Atmospheres, 114(D4).

Sellitto, P., Sèze, G., & Legras, B. (2017). Secondary sulphate aerosols and cirrus clouds detection with SEVIRI during Nabro volcano eruption. International Journal of Remote Sensing, 38(20), 5657-5672.

Sioris, C. E., McLinden, C. A., Martin, R. V., Sauvage, B., Haley, C. S., Lloyd, N. D., ... & McElroy, C. T. (2007). Vertical profiles of lightning-produced NO 2 enhancements in the upper troposphere observed by OSIRIS.

Solomon, S., Daniel, J. S., Neely, R. R., Vernier, J. P., Dutton, E. G., & Thomason, L. W. (2011). The persistently variable "background" stratospheric aerosol layer and global climate change. Science, 333(6044), 866-870.

Stanfield, R. E., Dong, X., Xi, B., Kennedy, A., Del Genio, A. D., Minnis, P., & Jiang, J. H. (2014). Assessment of NASA GISS CMIP5 and post-CMIP5 simulated clouds and TOA radiation budgets using satellite observations. Part I: Cloud fraction and properties. Journal of climate, 27(11), 4189-4208.

Stephens, G. L. (2005). Cloud feedbacks in the climate system: A critical review. Journal of climate, 18(2), 237-273.

Stocker, T. F., Qin, D., Plattner, G. K., Tignor, M., Allen, S. K., Boschung, J., ... & Midgley, P. M. (2013). Climate change 2013: The physical science basis. Contribution of working group I to the fifth assessment report of the intergovernmental panel on climate change, 1535.

Tackett, J. L., Winker, D. M., Getzewich, B. J., Vaughan, M. A., Young, S. A., & Kar, J. (2018). CALIPSO lidar level 3 aerosol profile product: version 3 algorithm design.

Timmreck, C., Lorenz, S. J., Crowley, T. J., Kinne, S., Raddatz, T. J., Thomas, M. A., & Jungclaus, J. H. (2009). Limited temperature response to the very large AD 1258 volcanic eruption. Geophysical Research Letters, 36(21).

Timmreck, C., Mann, G. W., Aquila, V., Hommel, R., Lee, L. A., Schmidt, A., ... & Diehl, T. (2018). The Interactive Stratospheric Aerosol Model Intercomparison Project (ISA-MIP): motivation and experimental design. *Geoscientific Model Development Discussions*, *11*(7), 2581-2608.

Thomas, G. E., Jakosky, B. M., West, R. A., & Sanders, R. W. (1983). Satellite limb-scanning thermal infrared observations of the El Chichon stratospheric aerosol: First results. Geophysical research letters, 10(11), 997-1000.

Thomas, J. L., Polashenski, C. M., Soja, A. J., Marelle, L., Casey, K. A., Choi, H. D., ... & Pelon, J. (2017). Quantifying black carbon deposition over the Greenland ice sheet from forest fires in Canada. Geophysical Research Letters, 44(15), 7965-7974.

Thomason, L. and Th. Peter (2006) SPARC, 2006: SPARC Assessment of Stratospheric Aerosol Properties (ASAP). L. Thomason and Th. Peter (Eds.), SPARC Report No. 4, WCRP-124, WMO/TD – No. 1295, available at www.sparc-climate.org/publications/sparc-reports/

Thomason, L. W., & Vernier, J. P. (2013). Improved SAGE II cloud/aerosol categorization and observations of the Asian tropopause aerosol layer: 1989-2005. Atmospheric Chemistry and Physics, 13(9), 4605.

Thomason, L. W., Ernest, N., Millán, L., Rieger, L., Bourassa, A., Vernier, J. P., ... & Peter, T. (2018). A global space-based stratospheric aerosol climatology: 1979-2016. Earth System Science Data, 10(1), 469-492.

Thompson, D. W., & Solomon, S. (2009). Understanding recent stratospheric climate change. Journal of Climate, 22(8), 1934-1943.

Vernier, J. P., Pommereau, J. P., Garnier, A., Pelon, J., Larsen, N., Nielsen, J., ... & McDermid, I. S. (2009). Tropical stratospheric aerosol layer from CALIPSO lidar observations. Journal of Geophysical Research: Atmospheres, 114(D4).

Vernier, J. P., Thomason, L. W., Pommereau, J. P., Bourassa, A., Pelon, J., Garnier, A., ... & Vargas, F. (2011). Major influence of tropical volcanic eruptions on the stratospheric aerosol layer during the last decade. Geophysical Research Letters, 38(12).

Vernier, J. P., Thomason, L. W., & Kar, J. (2011b). CALIPSO detection of an Asian tropopause aerosol layer. Geophysical Research Letters, 38(7).

Vernier, J. P., Fairlie, T. D., Natarajan, M., Wienhold, F. G., Bian, J., Martinsson, B. G., ... & Bedka, K. M. (2015). Increase in upper tropospheric and lower stratospheric aerosol levels and its potential connection with Asian pollution. Journal of Geophysical Research: Atmospheres, 120(4), 1608-1619.

Vernier, J. P., Fairlie, T. D., Deshler, T., Natarajan, M., Knepp, T., Foster, K., ... & Trepte, C. (2016). In situ and space-based observations of the Kelud volcanic plume: The persistence of ash in the lower stratosphere. Journal of Geophysical Research: Atmospheres, 121(18), 11-104.

Webb, M. J., Andrews, T., Bodas-Salcedo, A., Bony, S., Bretherton, C. S., Chadwick, R., ... & Klein, S. A. (2017). The cloud feedback model intercomparison project (CFMIP) contribution to CMIP6. Geoscientific Model Development, 2017, 359-384.

Wiensz, J. T., Degenstein, D. A., Lloyd, N. D., & Bourassa, A. E. (2013). Retrieval of subvisual cirrus cloud optical thickness from limb-scatter measurements. Atmospheric Measurement Techniques, 6(1), 105.

Wotton, B. M., Flannigan, M. D., & Marshall, G. A. (2017). Potential climate change impacts on fire intensity and key wildfire suppression thresholds in Canada. Environmental Research Letters, 12(9), 095003.

Yu, P., Toon, O. B., Bardeen, C. G., Zhu, Y., Rosenlof, K. H., Portmann, R. W., ... & de Gouw, J. (2019). Black carbon lofts wildfire smoke high into the stratosphere to form a persistent plume. Science, 365(6453), 587-590.

Zanchettin, D., Timmreck, C., Toohey, M., Jungclaus, J. H., Bittner, M., Lorenz, S. J., & Rubino, A. (2019). Clarifying the relative role of forcing uncertainties and initial-condition unknowns in spreading the climate response to volcanic eruptions. *Geophysical Research Letters, 46*(3), 1602-1611.

Zawada, D. J., Dueck, S. R., Rieger, L. A., Bourassa, A. E., Lloyd, N. D., & Degenstein, D. A. (2015). High resolution and Monte Carlo additions to the SASKTRAN radiative transfer model. Atmospheric Measurement Techniques Discussions, 8(3).

Zawada, D. J., Rieger, L. A., Bourassa, A. E., & Degenstein, D. A. (2018). Tomographic retrievals of ozone with the OMPS Limb Profiler: algorithm description and preliminary results. Atmospheric Measurement Techniques, 11(4), 2375-2393.

Zelinka, M. D., Zhou, C., & Klein, S. A. (2016). Insights from a refined decomposition of cloud feedbacks. *Geophysical Research Letters, 43*(17), 9259-9269.

Zelinka, M. D., Myers, T. A., McCoy, D. T., Po-Chedley, S., Caldwell, P. M., Ceppi, P., et al. (2020). Causes of higher climate sensitivity in CMIP6 models. Geophysical Research Letters, 47, e2019GL085782.

Zhang, X., Flato, G., Kirchmeier-Young, M., Vincent, L., Wan, H., Wang, X., Rong, R., Fyfe, J., Li, G., Kharin, V.V. (2019): Changes in Temperature and Precipitation Across Canada; Chapter 4 *in* Bush, E. and Lemmen, D.S. (Eds.) Canada's Changing Climate Report. Government of Canada, Ottawa, Ontario, pp 112-193.

Abbreviations and Acronyms

ACCP	Aerosol Cloud Convection and Precipitation
ALI	Aerosol Limb Imager
ATAL	Asian Tropopause Aerosol Layer
AOTF	Acoustic Optical Tunable Filter
CALIPSO	Cloud-Aerosol Lidar and Infrared Pathfinder Satellite Observation
CSA	Canadian Space Agency
EC	Environment Canada
ECCC	Environment and Climate Change Canada
FOV	Field of View
FWHM	Full Width at Half Maximum
GCM	Global Climate Model
ICCP	International Climate Change Partnership
LOS	Line of Sight
NASA	National Aeronautic and Space Administration
OSIRIS	Optical Spectrograph and InfraRed Imaging System
SAGE	Stratospheric Aerosol and Gas Experiment
SCIAMACHY	SCanning Imaging Absorption SpectroMeter for Atmospheric CHartographY
SHOW	Spatial-Heterodyne Observations of Water Vapour
SNR	Signal to Noise Ratio
SSA	Solar Scattering Angle
SZA	Solar Zenith Angle
TICFIRE	Thin Ice Clouds in Far Infrared Experiment
TTL	Tropical Tropopause Layer
μCATS	Microsatellite Canadian Atmospheric Tomography System
URD	User Requirements Document
UTLS	Upper Troposphere and Lower Stratosphere
UTS	Upper Troposphere and Stratosphere
WMO	World Meteorological Organization

AEROSOL LIMB IMAGER

USER REQUIREMENTS DOCUMENT

Authors

Adam Bourassa, Landon Rieger, Doug Degenstein, Jeff Langille, Jean-Pierre Blanchette, Yann Blanchard

Contributing Scientists

Chris McLinden, Jason Cole, Matthew Toohey, Kaley Walker, Michael Höpfner, Alexei Rozanov

Review Editors

Thomas Piekutowski, Ali Ziad, David Golla, Michael Maszkiewicz

Draft v0.2

March 27th, 2020

This page intentionally left blank

Revision History

Initial Draft	Draft issue for revision	2020/31/01
Draft v0.1	Corrections for internal review	2020/28/02
Draft v0.2	Distribution to NASA SIT-A	2020/27/03

Table of Contents

Executive Summary

Aerosol in the stratosphere and upper troposphere is an important driver of climate, scattering radiation that leads to a cooling effect near the surface. Additionally, these aerosols can interact with high altitude cirrus clouds, changing the optical properties, and cloud frequency. Uncertainty in both the aerosol measurements and high altitude cloud feedbacks are important factors in climate modelling and have been identified as important topics by both the Canadian and international science communities.

While the need for improved knowledge is clear, high quality, high resolution measurements of aerosol and clouds in the upper troposphere and stratosphere (UTS) from remote sensing platforms has been difficult. The Aerosol Limb Imager (ALI) is a proposed instrument that will take hyper-spectral images of the Earth's limb and provide global, vertically resolved measurements of aerosol extinction, particle size and information on thin, high altitude clouds in the UTS. ALI will address the following scientific issues:

1. Continued monitoring of the variable aerosol background layer.
2. Climate and air quality impacts of extreme events.
3. High altitude cloud-aerosol interactions and feedbacks

ALI has the potential to complement the Canadian instruments SHOW and TICFIRE, as well as baseline instruments planned for the NASA Aerosol Cloud, Convection and Precipitation observing platform. ALI brings higher sensitivity to thin optical depths, a large spectral range, and wide cross crack coverage facilitating more detailed studies of aerosol-cloud and water vapour interactions, polar stratospheric clouds, and volcanic plumes than individual instruments would allow. ALI, both alone and in conjunction with these other instruments, addresses several priorities laid out by the Canadian Government and Environment Canada:

1. New monitoring and modelling systems.
2. Understanding tracking and predicting emissions and processes.
3. Providing foundational knowledge on climate change.

ALI, in particular in cooperation with other instruments, represents an excellent opportunity to advance our knowledge of aerosol and clouds in the UTS and reduce uncertainty in stratospheric aerosol forcing and high-altitude cloud feedbacks.

1 Introduction

1.1 Purpose and Scope

This document describes the user and scientific objectives, justification and requirements for the ALI mission. Section 1 focuses on the ALI instrument, outlining the mission statement and main objectives, and current status of the hardware. The mission objectives presented here are the main scientific goals of the instrument, and inform the choices that follow. Section 2 discusses the rationale for these goals and why ALI is the correct instrument to meet them. This includes how the goals align with government priorities and the NASA decadal survey. Section 3 explores the ALI observables, and how they will effectuate these goals through specific products and applications. Sections 4, 5 and 6 investigate the specific platform and instrument requirements that are needed to produce the observables in Section 4. The description of the user and science requirements provided in this document has the objective of allowing their flow-down to the Mission Requirements and System Requirements Documents.

Figure 1: Information flow through ALI requirement documents

1.2 Applicable and Reference Documents

Atmospheric Limb Sounding Satellite (ALISS) User Requirement Document, Final Release, September 30, 2014.

Microsatellite CATS User Requirements Document, Final Release, April 20, 2015.

SHOW User Requirements Document, Under Revision

TICFIRE User Requirements Document, Under Revision

1.3 Mission Statement

The Aerosol Limb Imager (ALI) is a science payload that will provide high quality atmospheric profiles of aerosol and cloud information from a low Earth orbit satellite platform. ALI responds to the strongly expressed need, nationally and internationally, for

improved measurements of clouds, aerosols and their interactions. These measurements are crucial to improve understanding of cloud feedbacks and aerosol indirect effects, a leading cause of uncertainty in global warming projections. Additionally, current high resolution monitoring of aerosols after events such as extreme wildfires and volcanic eruptions remains limited, but it is vital to understand our current climate and predict the human health implications of these events. ALI builds on the decades of Canadian experience in using limb scattering observations to measure key observables that address these goals, while enhancing measurements from coordinated systems.

1.4 Objectives

ALI has five primary scientific objectives:

1. Extend long-term records of stratospheric aerosols and improve optical properties used for historical simulations of climate.
2. Facilitate the study of aerosol microphysical processes after volcanic eruptions and forest fires that impact particle size and lifetime; improving the modelling, and forecasting of impacts of aerosol injections into the stratosphere.
3. Contribute to the knowledge of cloud, aerosol and water-vapour interaction processes including:
    a. Understanding of cloud-aerosol feedbacks that influence the frequency of high altitude and thin cirrus clouds
    b. Facilitate studies of aerosol, cloud and water vapour interaction in the tropical tropopause layer and extratropical UTLS.
    c. Cloud interaction in the Arctic (high-altitude thin cloud coverage especially at high resolution)
4. Improve air quality forecasting after large events such as forest fires through improved plume knowledge.
5. Improve understanding of climate engineering scenarios and feedbacks

Section 2.2 explains the need to address these objectives with sections 2.3 and 2.4 discussing how they fit into the larger picture of government priorities and international initiatives respectively.

1.5 Instrument Design and Progress

The ALI instrument is an original instrument concept, designed and developed at the University of Saskatchewan largely with previous CSA FAST funding. Fundamentally, ALI is a hyperspectral polarization imager covering the visible and near infrared spectral range, utilizing a new acousto-optic tunable filter and liquid crystal polarization rotator

technology. The instrument is optimized for high spatial resolution stratospheric aerosol, volcanic plume, forest fire smoke, and thin cirrus cloud measurements in the upper troposphere and stratosphere with a wide-angle two-dimensional field-of-view to provide cross track horizontal coverage. Two successively advanced prototypes of the instrument have already successfully flown on stratospheric balloons: ALI-v1 from Timmins in 2015 (Elash et al., 2016), and ALI-v2 from Timmins in 2018. These flights have allowed us to identify limiting elements of the instruments that require future work and improvements.

1.6 Canadian Heritage

Canada has been an innovator in the use of limb-scattering measurements for observing atmospheric composition dating back a half century, using stratospheric balloons (Kerr and McElroy, 1976), the space shuttle (Evans et al., 1985), and high-altitude aircraft (McLinden et al., 1999). In space-based limb observing, Canada remains a leader with over 20 years of experience developing and managing OSIRIS on Odin (Llewellyn et al., 2004). Since its launch in 2001, OSIRIS measurements have been used by Canadian teams to pioneer limb-scattering retrievals of ozone (Degenstein et al., 2009), nitrogen dioxide (Bourassa et al., 2011), bromine monoxide (McLinden et al., 2010), and aerosol (Bourassa et al., 2007), with several other trace constituent retrieval products investigated (McLinden et al., 2012). The complexities of the limb-scattering measurements has also driven the advancement of SASKTRAN, a fast and accurate radiative transfer modelling infrastructure used in the retrievals and developed at the University of Saskatchewan (Bourassa et al., 2008; Zawada et al., 2015).

The OSIRIS data products have been used in many scientific advancements. Process studies of reactive nitrogen from lightning (Sioris et al., 2007), impact of volcanic particles on lower stratospheric photochemistry (Adams et al., 2017), and volcanic plume evolution from high latitude eruptions (Bourassa et al., 2010) have been published. The data products have also been used in large international collaborations. The ozone climatology has been used for long-term trend analysis (Bourassa et al., 2018) in the WMO ozone assessment and LOTUS effort (Petropavlovskikh et al., 2018) that aims to better understand ozone recovery, while the aerosol record has been used to construct input forcings for the Coupled Model Intercomparison Project 6 (Thomason et al., 2018).

2 Science Objectives

2.1 Background

Measurements of atmospheric composition are invaluable for understanding the dynamical, chemical and radiative processes that dictate weather (including air quality), and contribute to climate change. While greenhouse gases are the main forcings causing climate change, aerosols in the form of clouds and particulates also play a major role. Gases such as CO_2 absorb upwelling infrared radiation, reradiating some back towards the ground, acting as a blanket that warms the surface and troposphere. Aerosols absorb and emit infrared radiation as well, but they also scatter solar radiation. This reduces the amount of sunlight absorbed by the surface and lower atmosphere, resulting in a cooling that can offset warming due to greenhouse gases. Aerosol at all altitudes can have this effect, but at high altitudes, in the stratosphere where the air is stable and dry, their lifetime is very long, magnifying their potential impacts. For example, in 1991 Mount Pinatubo erupted, spewing ash and sulfur as high as 35 km, producing aerosols which remained detectable in the stratosphere until 1995, and caused global near-surface temperatures to drop by almost 0.5°C (Thompson et al., 2009).

Although this magnitude of eruption occurs only once every 30-50 years on average (Masson-Delmotte et al., 2013, Deligne et al., 2010), small-to-moderate volcanic eruptions can also have important climate impacts, in particular due to their greater frequency, which can drive sustained enhancements to stratospheric aerosol levels (Solomon et al., 2011). The climate influence of these smaller eruptions has been under intense scrutiny in the last decade in efforts to explain a possible discrepancy between climate models and measurements (Fyfe et al., 2013, Solomon et al., 2011, Santer et al., 2017). However, many uncertainties remain, in part due to a lack of aerosol size measurements that increase uncertainty in both the measured extinction, and the radiative impacts. The size of the aerosol particles plays a major role in the climate effect, since the magnitude of scattering by aerosols is strongly dependent on the distribution of aerosol sizes (Pinto et al., 1989, Lacis et al., 1992). Direct measurements of aerosol sizes are sparse at best, and while retrieval of aerosol size information from satellite instruments is emerging as a valuable contribution, the products still lack information on particle size during both background conditions and after injection events from volcanoes and wildfires. For example, the Ångström exponent retrieved by Rieger et al., (2014) does not extend into the UTLS due to instrument limitations, while the particle size parameters retrieved by Malinina et al., (2018) are available only in the tropics. Particle size retrievals from occultation instruments provide more complete coverage in terms of altitude and latitude (Bingen et

al., 2004); however, the sampling is poorer with global coverage on a monthly timescale. This results in undersampling the rapidly evolving plumes of volcanic eruptions and wildfires.

While volcanic eruptions can be a large source of stratospheric aerosols, they are not the sole driver of periodic enhancements. The recent forest fire seasons in Canada have garnered considerable attention due to their magnitude and impact on the lives of Canadians, but have had global impacts as well. The British Columbian wildfires of 2017 burned large and hot enough for smoke to reach the stratosphere, spreading smoke and ash across continents (Thomas et al., 2017). The updrafts were strong enough to inject aerosols into the stratosphere, leading to elevated aerosol for months following the eruption, and climate impact comparable to that of volcanic eruptions (Bourassa et al., 2018). This is not unique to Canada, with other countries also experiencing intense fires that have reached the stratosphere (Fromm et al., 2000, 2007). More recently, the devastating 2019/2020 Australian bushfires have led to the worst air quality recorded in Australian cities, with smoke plumes observed to be circulating around the Southern Hemisphere. As the intensity of wildfires is expected to increase both in Canada (Wotton et al., 2017) and globally (Liu et al., 2010), measurements of smoke will become increasingly valuable from both a human health and climate perspective. While human health is impacted by smoke in the boundary layer, long-range transport occurs at higher altitudes, making measurements of high-altitude plumes important to forecasting as well.

In addition to the "direct" effect of aerosols on radiation, aerosols have many "indirect" effects. Aerosol particles can act as nucleation sites for clouds and change the temperature of surrounding air, influencing the growth of new particles and changing their optical properties. While this phenomenon is often referenced in regards to the low-altitude clouds, limb-scattering measurements are well suited to explore the interactions at higher altitudes. These mid-to-high altitude clouds are also an important driver of Earth's climate, so even small changes to their properties can have a large impact on temperatures and precipitation patterns. Understanding and predicting changes in Earth's climate therefore requires accurate knowledge of both aerosol and cloud properties as well as their interactions. However, these effects have been difficult to fully quantify, and clouds, aerosol, and their interactions remain one of the largest contributions to climate uncertainty (Boucher et al., 2013, Zelinka et al., 2016, 2020).

Measurements of these local and global quantities from satellites are achieved through a wide variety of means, but for passive instruments, high resolution profiles require the limb geometry where the instrument line of sight intersects the Earth's horizon. This provides long paths through the atmosphere at the tangent point, amplifying the aerosol signal and yielding good sensitivity and vertical resolution. Limb instruments can be

broadly grouped into three categories: occultation, where a source such as the sun is viewed directly through the atmosphere; limb-emission, where radiation emitted by the atmosphere is measured; and limb-scattering, where light from the sun is scattered into the instrument. The first satellite-based limb-viewer used to measure the vertical distribution of an atmospheric state parameter was launched in 1962 (Rawcliffe et al., 1963) and measured mesospheric ozone using its absorption in the visible in solar occultation mode. It wasn't until 20 years later that the Solar Mesosphere Explorer first measured an atmospheric profile using the limb-scattering technique (Thomas et al., 1983), retrieving profiles of stratospheric aerosol. Since then limb scattering has evolved considerably, with multiple satellite instruments expanding the number of measured species and quality and coverage of the measurements.

2.2 Rationale

As Earth's climate changes, there is a growing need for high quality projections that can inform policy decisions to reduce anthropogenic impacts and mitigate the consequences of global warming. The IPCC AR5 report (Pachauri et al., 2014, Ch. SPM 2.3) predicts a high risk of increased damages from wildfires, heat-related human mortality, and increased damage from river and coastal floods in North America over the near term (2030-2040), assuming current levels of adaptation. Regions at higher latitudes are also expected to warm faster than lower latitudes, seeing an additional 1-2°C increase from the global average (Zhang et al., 2019). Climate projections require reasonable estimates of future radiative forcings, including stratospheric aerosols, which can be developed using high quality measurements of historical variations. These measurements also provide guidance to the development and evaluation of process parameterizations. While substantial advancements have been made in the last decade, further improvements require ongoing reductions in observational uncertainty.

2.2.1 Continued monitoring of 'variable' background layer

Global measurements have been crucial in understanding the sources and climate effects of stratospheric aerosols. Consistent, decadal increases in stratospheric aerosol levels were originally speculated to be from anthropogenic emissions (Hofmann et al., 2009), and it wasn't until the global picture provided by long-running satellites became available that this was correctly attributed to a series of smaller volcanic eruptions (Vernier et al., 2011). These global measurements have also helped to establish the presence of an Asian tropopause aerosol layer, or ATAL (Vernier et al., 2011b, Thomason et al., 2013). Diabatic ascent in the Asian summer monsoon and large convective systems over India create a transport pathway from the troposphere to the stratosphere (Randel and Park 2010, Garny et al., 2016) that creates a sustained aerosol layer during the summer months. As emissions from China and India change, continued monitoring of the ATAL and

monsoon region will be important to understand impacts on UTLS composition and climate.

Aerosol in the UTLS is a major component of total stratospheric aerosol loading, but uncertainty here remains high (Andersson et al., 2015). This is due largely to the limitations of the current generation of instruments. Limb and occultation systems have good sensitivity to aerosol, but without polarization information are unable to reliably distinguish between aerosol and clouds. Conversely, while lidars have good cloud discrimination, the short path lengths make them less sensitive to aerosol at background levels (Vernier et al., 2009). By incorporating both the limb geometry and polarization information ALI has the potential to greatly reduce these uncertainties.

These more accurate measurements of stratospheric aerosols will improve understanding of its current state as well as potential future perturbations including those due to climate engineering through injection of sulfur into the stratosphere (Rasch et al., 2008, Ricke et al., 2010, Kravitz et al., 2011). Ongoing monitoring of stratospheric aerosols in the absence of manmade sulfur injections combined with the ability to monitor aerosol formation and evolution after small-scale experiments, such as those proposed by *Dykema et al.,* (2014), or much larger injections, will be crucial in determining both the impacts and effectiveness of these interventions.

2.2.2 Climatic and air quality impacts of extreme events

Small to moderate eruptions have a non-negligible impact on climate (Solomon et al., 2012), although with considerable uncertainty about the precise magnitude of the forcing due to lack of complete records of stratospheric aerosol amount, size distributions and optical properties. The difficulties of measuring in the UTLS mentioned in the previous section are exacerbated during a volcanic eruption when an even larger fraction of the total aerosol can reside here (Ridley et al., 2014). Additionally, a chronic lack of particle size measurements leads to uncertainty when calculating scattering and absorption properties needed for radiative forcing calculations, and is suggested as a cause of recent differences in measured and modelled tropospheric temperatures (Santer et al., 2017). Improved stratospheric aerosol records are crucial for reducing the uncertainty related to future volcanic eruptions.

The problem of understanding stratospheric aerosol particle size has been long-standing. In situ measurements have provided a snapshot of aerosol size at specific times and locations, and have painted a complex picture of multi-modal size distributions requiring six or more parameters to quantify (Deshler et al., 2003). Unfortunately, satellites can typically only measure two to three aerosol parameters; usually extinction, and some parameterization of size properties (Thomason et al., 2003, Rieger et al., 2014, Malinina et

al., 2018), leaving many assumptions when computing optical properties. This is further complicated by the difficulty in accurately parameterizing particle size after eruptions: while large eruptions such as Pinatubo resulted in a clear increase in particle size (Bingen et al., 2005), smaller eruptions have had converse effects (Rieger et al., 2014). Aerosols injected into the stratosphere by forest fires have a different microphysical signature, with depolarization ratios that evolve differently from volcanic aerosols (Christian et al., 2019). Polarized limb-scattering measurements from ALI will improve measurement of particle size by providing information in the crucial near-infrared region of the spectrum (Rieger et al., 2014). Retrieved properties from these measurements such as the particle effective radius will help in understanding the drivers of the microphysical processes after an eruption and improve modelling of eruption events.

Accurate prediction of the climate impact of any future volcanic eruption or wildfire relies upon numerical simulation of the global spread and physical evolution of stratospheric aerosols. Interactive stratospheric aerosol models have had some success simulating the stratospheric aerosols from volcanic eruptions and their global radiative impacts (Mills et al., 2016; Timmreck et al., 2018). However, there remain significant differences between models in coordinated experiments using consistent injection locations and sulfur magnitudes (Zanchettin et al., 2018) , which point to fundamental uncertainties in model parameterizations of microphysical and radiative processes. Efforts to improve the accuracy of these aerosol models rely upon measurements of stratospheric aerosol, including information on the aerosol size distribution wherever possible. While occultation instruments can provide size information, the plumes can be highly inhomogeneous in the early days and weeks after an eruption and this is not well captured by the coarse sampling (Bourassa et al., 2018).

Small eruptions and forest fires can exhibit complex dynamics, sometimes becoming entrained in the Asian monsoon, and lofted into the stratosphere (as with the ATAL), even when the initial plume altitudes may not have been at sufficient altitudes to achieve this (Bourassa et al., 2012). Multiple events, either volcanic or fire related may also overlap, with plumes splitting and merging. Untangling the sources and movement of these highly dynamic events requires high sampling rates to track the plumes while they evolve. The excellent along, and horizontal track resolution of ALI will provide a much clearer picture of these events than occultation instruments, increasing the detail of plumes in their early stages of development and improving understanding of the evolution of simultaneous plumes with different sources.

2.2.3 Cloud feedbacks

Clouds feedbacks in general represent a substantial uncertainty in the global climate projections (Stephens et al., 2005, Dolinar et al., 2015), and according to the IPCC Fifth

Assessment Report, the role of thin cirrus feedbacks in particular are not constrained, representing a significant feedback uncertainty (Boucher et al., 2013 Ch. 7). Cirrus clouds have a radiative forcing of approximately 5-6 W/m^2 (Hong et al., 2016; Gasparini et al., 2016), more than double that of CO_2 (Stocker et al., 2013), so small changes to their properties have a large potential to affect global climate. As stratospheric aerosols sediment out of the atmosphere, they can interact with cirrus formation, potentially impacting the lifetime, frequency and microphysical characteristics of high altitude clouds. Studies on stratospheric aerosol and cirrus feedbacks show effects comparable in magnitude to the direct aerosol forcing (Kuebbler et al., 2012), but the results are uncertain.

Thin cirrus in the tropical tropopause layer play not only a radiative role (McFarquhar et al., 2000, Hartmann et al., 2001) but also serve to dehydrate the air entering the stratosphere (Jensen et al., 2004, Luo et al., 2003). As rising air cools, ice droplets form and sediment out, removing water vapour from the TTL. However, measurements of thin cirrus clouds in the TTL (McFarquhar et al., 1999, Peter et al., 2003), remain uncertain due to the difficulty of in situ measurements at such high altitudes, and the inability of satellite lidar instruments to measure thin cirrus clouds with optical depths below approximately 0.01 (Dessler et al., 2006, Haladay et al., 2009). Limb scattering measurements with polarization information have not previously been performed from satellites, yielding a unique opportunity to measure the thin cirrus clouds not typically distinguishable from aerosols with other techniques. ALI will therefore fill an important role in reducing uncertainty in thin cirrus clouds and feedbacks.

2.2.4 Air Quality

Extreme forest fires play a dual role in the environment, causing both large scale climate effects when they reach the stratosphere (Yu et al., 2018), and substantial human health consequences (Rittmaster et al., 2008). As climate change occurs and heat waves and droughts become more commonplace the impact of forest fires is expected to accelerate (Girardin et al., 2008, Wotton et al., 2017); with events on-par with the Fort McMurray or the recent BC fires more likely. . Particulate matter, in part from these wildfire events, is a significant environmental and health concern, associated with nearly 9M premature deaths globally per year (Burnett et al., 2018). In Canada, 21,000 deaths result annually from the effects of air pollution. Some of the most intense air quality events are a result of large wildfires or volcanic eruptions in which aerosol plumes are lofted into the middle troposphere or above. At these heights, transport long distances downwind are common and generally difficult to forecast. One reason for this is uncertainty in the height and vertical extent of the plumes. Current passive satellite instruments provide, at best, a single height with large uncertainty, which require oversimplification of the plume (Griffin et al., 2020).

2.3 Alignment with Government of Canada Priorities

The Environment Canada science strategy focuses on four main categories which include the following goals[1]

1. Environment Canada will focus its science on developing new monitoring and modelling systems and tools, and improving existing systems.
2. Environment Canada will focus its science on understanding, tracking and predicting the emissions and atmospheric processes that affect climate change.
3. Environment Canada will also focus its science on providing the foundational knowledge to understand anticipated climate change to help Canadians plan and adapt to future change.

The objectives of the ALI mission relate directly to these priorities.

2.3.1 New monitoring and modelling systems

ALI will provide a novel platform for measuring stratospheric and upper tropospheric composition; imaging the limb to produce high resolution information in both the along- and cross-track dimensions. This builds on limb scattering heritage of the Canadian instruments OSIRIS, that viewed the limb using a single line of sight, and μCATS, that used seven. ALI extends this by approximately two orders of magnitude, measuring hundreds of lines of sight simultaneously. Fully utilizing these measurements will require advancing the current generation of aerosol retrievals to incorporate the additional wavelength information as was done by Rieger et al., (2019) and extending the tomographic techniques used by Zawada et al., (2018) to exploit the cross-track information.

2.3.2 Understanding, tracking and predicting emissions and processes

The ALI measurements will support the continued monitoring of stratospheric aerosols due to volcanic eruptions, a critical factor in modelling the climate (Santer et al., 2017). Measurements at wavelengths up to 1500nm will enable retrieval of aerosol information in the upper troposphere, filling important gaps in the forcing record (Ridley et al., 2014, Andersson et al., 2015). This will extend to monitoring and tracking of the vertical distribution of high-altitude smoke plumes from wildfires. These measurements will be used to improve the air quality model, and the numerical forecasting of smoke trajectories that influence air quality estimates. In addition to the science priorities of EC,

[1] "Environment Canada's Science Strategy 2014 to 2019" 6 Mar. 2018, Environment Canada's Science Strategy 2014 to 2019. Accessed 28 Jan. 2020.

this furthers Minister of Health's mandate to "better protect people and the environment from toxins and other pollution, including by strengthening the Canadian Environmental Protection Act, 1999."[2]

2.3.3 Providing foundational knowledge on climate change

Clouds and aerosols continue to be a major source of uncertainty in model predictions, due to uncertainties in cloud feedbacks (eg. Webb et al., 2017), aerosol-cloud interactions (Carslaw et al., 2013) and radiative forcings (Thomason et al., 2018). Estimates of subvisual cirrus are difficult with the current generation of instruments due to detection limits or cloud-aerosol discrimination. The combination of limb scattering and polarization measurements to provide coincident, high vertical resolution measurements of thin clouds, with cross-track information, in aerosol conditions will improve understanding of how aerosol affects the lifetime and frequency of subvisual cirrus clouds. These measurements can be used to improve forcing estimates of thin clouds and improve parameterizations of clouds in climate models.

2.4 Alignment with NASA Decadal Survey and ACCP

The objectives of the ALI mission overlap with many of the most pressing science questions as determined by the NASA decadal survey.[3] The decadal survey identified five key areas of research for the next decade, including two focused on aerosol related observables:[4]

1. Climate variability and change
2. Weather and air quality

To measure these observables NASA is designing the Aerosol Cloud, Convection and Precipitation (ACCP) observing system. The goal of ACCP is to observe parameters that fall into five main categories[5] as shown in the table below:

[2] "Minister of Environment and Climate Change Mandate Letter 2019" Minister of Environment and Climate Change Mandate Letter. Accessed 28 Jan. 2020.
[3] "Decadal Survey | Science Mission Directorate - Science@NASA." Decadal Survey. Accessed 29 Jan. 2020.
[4] "Aerosol and Cloud, Convection and Precipitation (ACCP)" Aerosol and Cloud, Convection and Precipitation (ACCP). Accessed 29 Jan. 2020.
[5] "Science and Applications Traceability Matrix" Traceability Matrix Public Release Candidate E. Accessed 29 Jan. 2020

Cloud Feedbacks	Reduce the uncertainty in low- and high-cloud climate feedbacks by advancing our ability to predict the properties of low and high clouds.
Storm Dynamics	Improve our physical understanding and model representations of cloud, precipitation and dynamical processes within deep convective storms.
Cold Cloud and Precipitation	Improve understanding of cold (supercooled liquid, ice, and mixed phase) cloud processes and associated precipitation and their coupling to the surface at mid to high latitudes and to the cryosphere.
Aerosol Processes	Reduce uncertainty in key processes that link aerosols to weather, climate and air quality related impacts.
Aerosol Impacts on Radiation	Reduce the uncertainty in Direct and Indirect aerosol-related radiative forcing of the climate system.

Table 1: ACCP goals and objectives

These science questions and objectives in the decadal report drive the need for a host of observables, several of which can be measured using ALI measurements. The table below indicates in more detail the decadal survey goal, the specific objective, the desired observable that ALI can contribute to, and the specific ALI measurement that will make the contribution.

Science Goal	Mission Objective	ACCP Observable[6]	ALI Contribution and Enhancement
W-2 Larger Range Environmental Predictions	**W-2a** Improve the observed and modeled representation of natural, low-frequency modes of weather and climate variability.	Vertical profiles of aerosols and clouds in the middle atmosphere and lower stratosphere.	Excellent sensitivity allows extending Lidar measurements into upper troposphere and stratosphere
W-10 Clouds and Radiative Forcing	**W-10a** Quantify the effects of clouds of all scales on radiative Fluxes. Determine the structure, evolution and physical/dynamical properties of clouds on all scales.	3D aerosols.	Cross track information and high along-track sampling allows for a more complete picture of vertical distribution than lidar and nadir imagers alone can produce.
C-2 Climate Feedback and Sensitivity	**C-2a** Reduce uncertainty in low and high cloud feedback by a factor of 2.	Cloud fraction	Improved sensitivity to thin cirrus clouds for more complete maps.

[6] Only ACCP observables related to ALI measurements are listed here

	C-2g Quantify the contribution of the upper troposphere and stratosphere (UTS) to climate feedbacks and change.	Vertical profiles of UTS aerosol radiative properties, for quantifying radiative forcing.	Vertical profiles of radiance at multiple wavelengths from 500 to 1500 nm with high sensitivity in the UTS provides information on particle size as well as extinction.
	C-2h Reduce the IPCC AR5 total aerosol radiative forcing uncertainty.	Vertical profiles of aerosol effective radius.	Broad wavelength range allows retrieval of aerosol properties from the upper troposphere to 30km at 0.5km resolution
		Nearby (to aerosol fields) and simultaneous measurements of cloud properties.	Sensitivity to thin subvisual cirrus clouds and low levels of aerosol allow for improved masking and aerosol/cloud co-location flagging.
	C-5a Improve estimates of the emissions of natural and anthropogenic aerosols.	Vertical profiles of particle effective radius.	Broad wavelength range coupled with polarization information provides effective radius as well as distinction between liquid and solid particles to discriminate aerosol sources.
C-5 Aerosols and Aerosol Cloud Interactions	**C-5b** Characterize the properties and distribution in the atmosphere of natural and anthropogenic aerosols.	Aerosol extinction, AOD, (spectrally resolved), polarization, and size with vertical and horizontal distribution.	Spectrally resolved, vertical profiles of aerosol extinction allow the ability to remove stratospheric contribution from nadir measurements of AOD.
	C-5c Quantify the effect that aerosol has on cloud formation, cloud height, and cloud properties.	Vertical and horizontal distribution of clouds.	Improved sensitivity to thin cirrus clouds and low levels of aerosol for more complete maps when combined with baseline instruments.
C-7 How are decadal-scale global atmospheric and ocean circulation patterns changing?	**C-7b** Quantify the linkage between natural and anthropogenic forcing.	Vertical distribution of stratospheric and tropospheric aerosols.	Continuation of vertical aerosol profile measurements to provide long-term global records back to 1980 that can be used in climate models. Polarization information improves cloud discrimination to enhance measurements in regions
	C-7e Provide observational verification of models used for climate projections. Are the models simulating the observed evolution of the large-scale patterns in the	Vertical distribution of stratospheric and tropospheric aerosols.	

	atmosphere and ocean circulation.		of large-scale convective patterns such as the ATAL.
C-8 Causes and Effects of Polar Amplification	**C-8g** Determine the amount of pollutants (e.g., black carbon, soot from fires, and other aerosols and dust) transported into polar regions.	Aerosol optical depth.	Cross track information allows for particularly high resolution mapping in the Arctic, improving tracing of aerosols after large-scale volcanic eruptions and forest fires that inject aerosol to the UTLS.
C-9 Ozone and Other Trace Gases in the Stratosphere and Troposphere	**C-9a** Quantify the amount of UV-B reaching the surface, and relate to changes in stratospheric ozone and atmospheric aerosols.	Vertical profiles of UTS aerosol radiative properties.	Vertical profiles of both extinction and particle size properties such as surface area density that are important for ozone chemistry.
		Volcanic and biomass burning emissions.	Separation of soot and ash from sulfur aerosols using multi-wavelength polarization capabilities.
S-2 How do geological disasters directly impact the Earth system and society following an event?	**S-2a** Rapidly capture the transient processes following disasters for improved predictive modeling.	All high-resolution visible to thermal IR imagery.	Spectrally resolved limb images of radiance from 500 to 1500 nm to capture volcanic plume or pyro-cumulus extent in the UTLS in the days and weeks following an event.

Table 2: ALI contribution to ACCP goals and objectives

2.5 Synergy between ALI and ACCP Instruments

This section outlines basic retrieval elements that may be improved through instrument synergy, but technical details and feasibility will be explored more fully in upcoming simulation studies.

While many parameters required to meet the decadal survey objectives can be retrieved directly from ALI or lidar measurements, retrieval of many geophysical parameters needed for objectives are greatly improved through synergy with potential instruments in the ACCP architecture.

2.5.1 Improved Lidar measurements

While lidar measurements provide excellent high resolutions profiles of backscattering ratios, the conversion to extinction in the stratosphere relies heavily on assumptions of optical properties, typically assuming a constant conversion of 50sr (Kar et al., 2019). Particle size information allows for improved conversion of backscatter to extinction by reducing uncertainty in particle size.

In addition to conversion uncertainty the short path lengths of lidars can struggle with signal to noise problems and high altitude normalization in the stratosphere when aerosol levels are low. This can be mitigated by binning measurements as done by Kar et al., (2019), but this eliminates many of the benefits of the high resolution lidar measurements. The long ALI path lengths provide much higher sensitivity in the stratosphere, providing the ability to complement the tropospheric and UTLS lidar measurements at higher altitudes without relying on spatial and temporal binning.

2.5.2 Aerosol and Cloud Interactions

Provide information on the vertical structure of thin and subvisual cirrus clouds

2.5.3 Improved ALI retrievals

ACCP baseline instruments can also be used to improve ALI retrievals. Limb scattering aerosol retrievals rely on albedo retrieved from looking at high tangent altitudes. This has limitations on accuracy and information content due to the indirect nature of the measurement. Information provided by nadir sensors could potentially provide information on the type of scene below the limb measurement, improving estimation of upwelling radiation.

The polarization measurements provided by ALI allow for cloud aerosol discrimation, but the long path lengths of approximately 200km mean measurements may contain both cloudy and cloud-free regions. The high horizontal resolution of the lidar measurements will allow for additional screening of measurements that have a smaller fraction of clouds along the line sight.

2.5.4 Linking Processes to Global Scales

ALI's wider swath and global coverage provides a link between process driven studies and global scale phenomena, showing the context in which the process events occur. Cross track aerosol information can help place lidar profiles in the context of large and potentially inhomogeneous aerosol plumes. This is particularly relevant for conditions after forest fire and volcanic events when conditions can change rapidly.

2.6 Synergy between ALI, TICFIRE and SHOW

In addition to the synergy with baseline instruments onboard the ACCP payload. ALI also provides excellent integration with proposed Canadian instruments. ALI, SHOW and TICFIRE will provide a complementary suite of measurements that allow for much more complete investigation of cloud properties than each instrument alone. A schematic of the measurement configuration for these three instruments is shown in the figure 2.

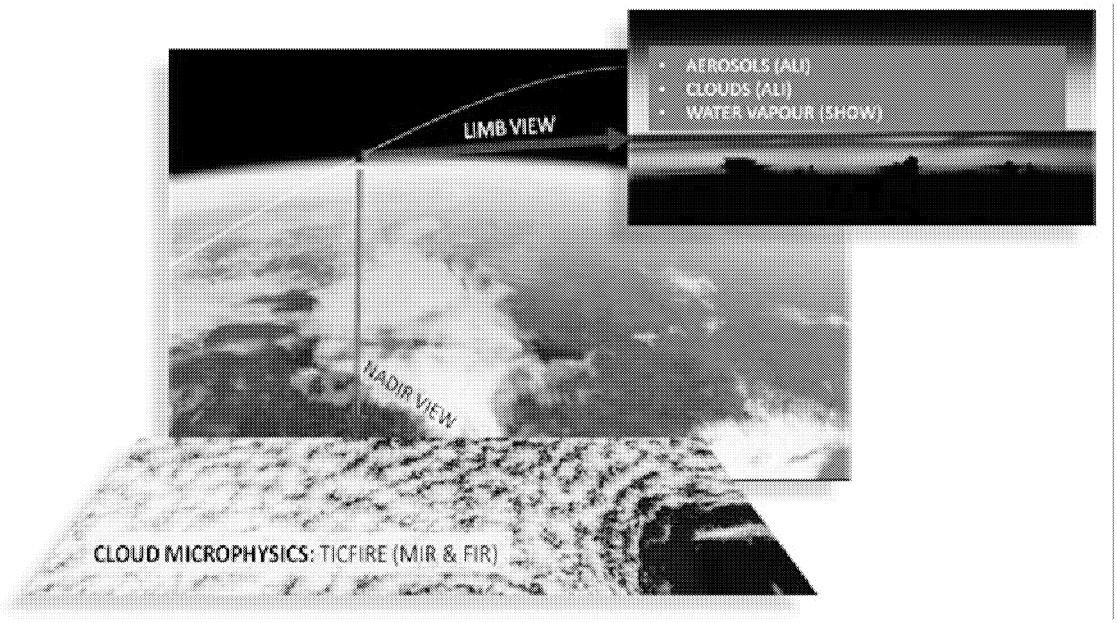

Figure 2: Synergistic measurement configuration between the three Canadian instruments.

The **SHOW** high-resolution water vapor measurements strengthen our understanding of the moisture variability in the critical and under-sampled upper troposphere and lower stratosphere (UTLS), and to link this variability to changes in surface weather and climate conditions. It is designed to provide the best along-track sampling of any existing limb sounder to capture the high variability of water vapor in the global UTLS. The novel SHOW design measures absorption features in limb scattered sunlight and has been tested through suborbital demonstrations, including a test flight of an advanced prototype on the NASA ER-2.

The **TICFIRE-FIRR** (Far IR Radiometer) measures thin cloud composition and microphysical properties from fine to large crystals leading to estimation of the extensive light precipitation common to cold climates and global scale UTLS regions, like initiation of precipitation soon after ice crystal nucleation in convective cloud anvils for instance. Complementing microwave radiometers, it accurately measures the radiance in 8 spectral bands from 8 to 100 μm, which is a range sensitive to cloud microphysics and low water

concentration. This is the only instrument to measure directly the cloud radiative forcing spectrally resolved and over the wide infrared domain. In other words, it probes directly the effect of cloud changes on the atmospheric energy balance, a key quantity on the role of clouds and many important related processes on the climate system.

2.6.1 Improvement to SHOW retrievals

Synergistic measurements with ALI and TICFIRE will be used to improve the SHOW water vapour retrievals. Co-located measurements of aerosol with ALI will be used to improve the information content in the forward model utilized in the SHOW water vapour retrievals. Sensitivity studies performed in support of the sub-orbital demonstration campaign show that knowledge of the aerosol profile can improve the accuracy of the SHOW measurements on the order of 0.1-0.5 ppm [Langille et al., 2018]. In addition, ALI and TICFIRE observations will aid in the determination of the lower boundary cut-off of the SHOW retrievals where the optical depth becomes too large to see the tangent point. The impact of this knowledge on SHOW water vapour retrievals needs to be evaluated through detailed simulation studies.

2.6.2 Process studies

It is well known that cloud tops play a key role in the fate of the cloud radiative properties and precipitation. Observations with all three instruments, ALI, TICFIRE and SHOW will be combined to close the feedback loop between aerosol (including ice forming nuclei), cloud, optical depth, temperature, moisture and their alteration of the water vapour concentration respectively. Furthermore, direct radiance measurements from TICFIRE provide information on radiative forcing which can be used to evaluate the atmospheric perturbation and its impact on the energy cycle. On their own, the three Canadian instruments provide us the ability to do a near closure experiment, a challenging goal for future missions. This closure is reinforced locally by the active instruments (lidar and radar) collocated on board the ACCP mission. Although radar and lidar see only a small sample of the scene, the combined ALI-SHOW-TICFIRE observations will widen the scene view, providing a rich perspective and strongly enhancing the whole mission.

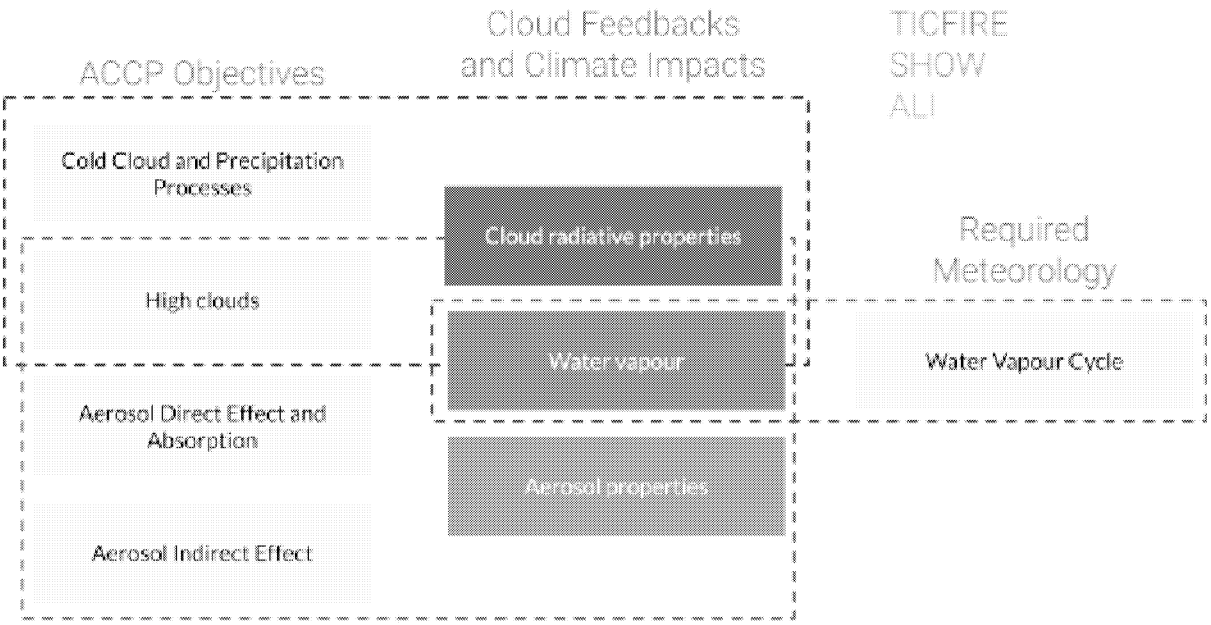

Figure 3: Synergistic measurements between the three Canadian instruments – SHOW, ALI and TICFIRE. Each measures an important component of high cloud feedbacks relevant to climate.

Overall, the ensemble is a unique system for high resolution of aerosols, water and cloud, a key to the study of their interaction, and an extended source of genuine new information in data assimilation systems for weather forecasting. Synergistic measurements with these three instruments will allow for:

- Improving measurements of water-vapor concentration in the low limit where cold regions are most sensitive.
- Determining the contribution of Thin Ice Clouds (TIC) to the energy balance and the role of their microphysical properties on atmospheric cooling.
- Bridging the observational gap in the far IR spectral region between the atmospheric window in the mid-IR and the passive microwave region.
- Providing a wealth of new and unique FIR data for assimilation in the weather forecast models, which will help improve the range and the reliability of operational meteorology
- Strengthening our understanding of the variability in the critical and under-sampled upper troposphere and lower stratosphere and to link this variability to changes in surface weather and climate.
- Providing a high-quality extension of the stratospheric aerosol record for understanding the radiative and hence climate impacts of volcanic eruptions, wildfire and anthropogenic perturbations.

Several studies have highlighted the role of aerosol composition on cloud nucleation, their development, their radiative properties and initiation of precipitation (Jouan et al, 2012; 2014). Figure ??? illustrates the effect of volcanic aerosol on cloud formation and precipitation as a common phenomenon in cold atmospheres, yet these processes are very complex to reproduce in atmospheric models, not to mention their omission in today's data assimilation system. However, this will change in the current decade with ACCP and consequent model improvements.

As an example, the ISDAC airborne campaign of April 2008 (Figure ???) has provided a rare dataset for studying the interaction between aerosol composition and clouds microphysics. From a limited number of successful flights in ice clouds, detailed studies (Jouan et al., 2012; 2014) have quantified in situ the critical links between aerosol acid concentration from 5 volcanic plumes and the enhanced formation of large precipitating ice crystals that were theorized (Blanchet and Girard, 1994) and previously verified in laboratory controlled experiments (Eastwood et al, 2009). These results have permitted the development of a new parameterization of ice nucleation processes based on aerosol chemical composition in atmospheric weather and climate models using WRF-Chem (Keita et al.; 2016; 2019; 2020). Clearly, much more observations on global scale are needed to refine and generalize such parameterization based solely on limited number available measurements. This central objective of ACCP is where the tandem ALI, SHOW and TICFIRE and their synergies aim to contribute.

3 Data Products and Applications

This section outlines the retrieval products, and how they will enable the science objectives discussed in the preceding sections. Additionally, how these products will integrate with measurements from other ACCP and Canadian instruments to enhance the science return.

3.1 Retrieval Products

Since the advent of occultation limb profilers, vertical profiles of extinction in the visible and near infrared have formed the backbone of our global picture of stratospheric aerosol loading (Thomason and Peter, 2006). The measurements provide information on the distribution, amount and movement of aerosol and have been foundational for the aerosol climatologies needed for understanding climatic effects of stratospheric aerosols (Thomason et al., 2018). To meet the needs of the climate community for continued forcing datasets ALI will provide several fundamental aerosol and cloud quantities. The table below shows the four primary ALI retrieval products and their properties.

Product	Accuracy	Vertical Range	Vertical resolution	Horizontal resolution	
				Along track	Cross track
Aerosol Extinction	10% (Tropopause to 10^{-5} km^{-1} @ 750nm)	8 to 35 km	0.5 km	250 km	20 km
Effective Radius	20% (Tropopause to 10^{-5} km^{-1}@ 1000nm)	10 to 30 km	0.5 km	250 km	20 km
Angstrom Coefficient	20% (Tropopause to 10^{-5} km^{-1}@ 1000nm)	10 to 30 km	0.5 km	250 km	20 km
Cirrus Detection		8 to 22 km	0.5 km	250 km	20 km

Table 3: ALI retrieval product requirements. *This table is a work in progress, and numbers will be updated as results of simulation work informs the required uncertainties.*

3.1.1 Multi-wavelength aerosol extinction profiles in the visible and near infrared

The 2-dimensional images of the limb provided by ALI will be used to retrieve aerosol extinction profiles using similar techniques employed by Bourassa et al., (2012), Rieger et al., (2019), and Zawada et al., (2018). The central profile will be used in a tomographic retrieval to maximize along-track resolution, while off-center profiles will be retrieved using horizontal homogeneity assumptions. The 5° field of view will provide global coverage over the course of several days at a cross-track resolution of approximately 20km, along track resolution of 250km, and vertical resolution of 500m. These measurements will feed directly into aerosol climatologies such as GloSSAC to improve and extend climate forcing records.

3.1.2 Vertical profiles of particle size information

Particle size retrievals from limb scattering observations have been performed with measurements from OSIRIS (Bourassa et al., 2007, Rieger et al., 2014) and SCIAMACHY (Malinina et al., 2018). Information in the near infrared is crucial for deriving particle size. With ALI's wavelength range of 500 to 1500nm, it is well suited to provide both extinction and effective radius for input to climate forcing analyses. These quantities directly improve the optical property parameterizations used in climate models to calculate aerosol forcing. The addition of polarization information also adds an exciting component for particle size retrievals to distinguish smoke and ash from sulphates after volcanic eruptions and wildfires (Vernier et al., 2016). These particles have very different optical properties than sulphate aerosols, so distinguishing them will improve the extinction retrievals, and estimates of radiative forcing.

3.1.3 Vertical profiles of Ångström coefficient

The spectral dependence of extinction is often modeled as linear relationship in log-wavelength log-extinction space, with the slope of this dependence referred to as the Ångström coefficient, or exponent. The Ångström coefficient is commonly used as a proxy for particle size or backscattering efficiency. While there is not an exact mapping between these quantities, it has been a staple measurement for decades from occultation instruments, in part because it does not rely on a priori assumptions of size distribution. The ability to continue these measurements into the future will help extend occultation measurements, and provide extended records to the studies that use the Ångström coefficient.

3.1.4 Clouds

Feedbacks involving clouds pose one of the largest unknowns in forecasting the future climate (Boucher et al., 2013). Long term records of cloud properties provide an excellent method to evaluate climate models and can provide guidance when developing model parameterizations. A lidar-based product widely used for climate model evaluation is the GCM Oriented Cloud Calipso Product (GOCCP) (Chepfer et al., 2010) which is often compared with simulated clouds. However, this limits the comparisons to clouds with sufficient optical depth to be measured with space-based lidars, missing the thinner subvisual cirrus clouds (Sassen et al., 2008, 2009).

The long path lengths and high sensitivity of limb scattering measurements allows retrieval of subvisual cirrus below the detection threshold of lidar instruments (Bourassa et al., 2005). ALI will be able to measure thin clouds with sufficient discrimination of aerosol using polarizaiton information to produce cirrus frequency climatolagies for comparison with climate models. The retrieval of cirrus size parameters has also been performed with limb scattering instruments (Wiensz et al., 2013), however these were not performed operationally. Estimates of cirrus crystal size could help improve estimates of cirrus radiative forcing, with changes to these quantities indicators of feedbacks between cloud and aerosol.

3.2 Science Studies

Large, temporary perturbations to the aerosol loading can cause significant climate effects, but the violent processes of volcanic eruptions and forest fires that generate these events lead to inhomogeneous and rapidly changing aerosol distributions. While satellite lidars can provide excellent along track resolution, the horizontal swath is narrow, measuring only a curtain of aerosol under the the satellite orbit. ALI will fill this gap by providing the ability to measure at high resolution in the along track plane through use of tomographic retrievals as pioneered by Zawada et al., (2015), but also measure a substantial cross-track component. This will provide unprecedented information on the extent of aerosol plumes in the stratosphere and upper troposphere. This is particularly true in the Arctic, where overlapping satellite tracks combined with ALI's imaging capabilities yield measurements of stratospheric aerosols at multiple angles over a short period of time. These dense measurements will support process studies to elucidate pressing climate questions in the UTLS.

3.2.1 Forest Fires

Limb scattering observations have been used to track the evolution of high altitude smoke plumes after large fires (Bourassa et al., 2018). However, limitations in cloud filtering and low altitude sensitivity limit the ability to observe smoke lower into the troposphere. The longer wavelength range and cloud discrimination enabled by polarization information will enable ALI to see plumes at lower altitudes and at lower thresholds than previously possible, extending well into the mid and upper troposphere. For extreme events, this is low enough to measure plume altitude, which can be assimilated by numerical prediction centers to improve air quality estimates.

ALI observations can also improve analyses of these extreme fires on climate. While climate models with interactive aerosol and chemistry components can simulate the plume evolution it is difficult to compare all aspects with observations (Yu et al., 2018). Occultation measurements are too sparse to map the early plume, and lidar measurements are insensitive to the lower extinction values as the plume evolves. ALI will fill this gap by providing much higher spatial detail of the aerosol distribution, while being able to monitor the lofting to higher altitudes as the plume thins, due to the higher sensitivity than lidar instruments.

3.2.2 Volcanic Eruptions

Determining the climate ramifications from volcanic eruptions relies on accurate knowledge of the aerosol plume and dispersion. Relatively similar eruptions can have vastly different effects depending on the latitude, eruption altitude, SO_2 and ash composition of the plume, and timing of the eruption with respect to large scale dynamical cycles (Marshall et al., 2019). ALI will provide extinction measurements on spatial scales of hundreds of kilometers, with near global coverage, improving the ability to track the evolution of aerosol plumes from the origin to eventual dispersal and removal from the stratosphere. This will reduce uncertainty in important dynamical interactions that influence lifetime and climate impact. For instance, the interaction with the Asian Monsoon is very sensitive to the timing and altitude of the plume, with small changes greatly affecting the amount of aerosol that is transported to the stratosphere. The high resolution ALI measurements will reduce uncertainty in the injection mechanisms of aerosols into the stratosphere.

Aerosol lifetimes in the stratosphere depend strongly on particle size, as larger particles sediment faster. Estimates on particle size and determination of ash vs sulphate is crucial in estimating the lifetime, and therefore climatic impact of an eruption (Vernier et al., 2016). While current measurements from lidars can distinguish ash from sulphate the

single wavelength backscatter measurements do not provide information on particle size. Conversely, occultation measurements do not provide polarization to distinguish particle shape. ALI is in a unique position to provide both size and classification information of volcanic plumes to improve understanding of particle evolution in both ash and ash-free conditions.

Interactive aerosols in climate models remain computationally taxing, with reliance on bulk schemes a common practice. These require parameterization of aerosol evolution and removal processes. However, the effect of eruptions on particle microphysics is not well constrained by current observations. ALI measurements will improve the relationships between aerosol loading and microphysical properties after an eruption through retrieval of particle size. Similarly, models that use interactive aerosols to fully simulate particle evolution show large inter-model spread (Timmreck, et al, 2018), highlighting the need for measurements that can help constrain model results.

3.2.3 Tropical Tropopause layer

The Tropical Tropopause Layer (TTL) is a layer near 14 to 18 km in the tropics that marks the transition between convective and radiative regimes. Strong circulation in this region driven by wave activity drives the upwelling branch Brewer Dobson circulation, feeding the stratosphere with tropospheric air and largely dictating the composition of the stratosphere (Fueglistaler et al., 2009). As the climate warms and the Brewer Dobson circulation increases in strength, changes to the temperatures and chemical composition of the TTL are expected, affecting cirrus composition (Randel and Jensen, 2013). The presence of aerosol in the TTL also changes cirrus properties, with sulfuric acid coating ice particles. When particles are small this can produce substantial radiative changes (Räisänen et al., 2006). The ability to measure thin cirrus in the presence of background and volcanically active aerosol levels will provide an excellent opportunity to monitor this crucial region during a period of changing climate. The vertical resolution of ALI is sufficient to resolve cirrus clouds above convective cells at extinction levels as low as 10^{-5} km^{-1}. This will provide a much more complete map of thin cirrus clouds in the TTL, improving radiative forcing estimates, but also the understanding of atmospheric composition and water vapour, as these clouds serve to dehydrate the stratosphere.

4 Discussion on Priority Trade-Offs

SNR vs sampling

Cross track FOV vs vertical resolution

Stray light vs mass/volume

Spectral/spatial

5 Requirement Format

5.1 Conventions

The wording of statements in this section determines the disposition of requirements:
"**SHALL**" and "**SHALL NOT**" indicate a (mandatory) requirement.
"**SHOULD**" and "**SHOULD NOT**" indicate a recommendation, which is not mandatory.
"**MAY**" and "**NEED NOT**" indicate a permission or option.
"**WILL**" indicates a statement of fact or intention.

5.2 Requirement Format and Numbering

The standard for numbering is ALI-CAT-###-V.V where CAT is a three letter keyword for the category as provided in the table below. ### is a sequential number where a 0 digit has been added to allow for later insertions and V.V is the version of the associated User Requirement Document (e.g. 1.0).

Requirements are stated, followed by a brief rationale including assumptions. Both the goal and threshold requirement values are specified if applicable. Comments do not form part of the requirement and are provided for information only.

Category	Description	Examples
MIS	Mission level requirements	Viewing geometry, mission lifetime, tasking and data latency, etc.
INT	Instrument level requirements	Spectral, spatial radiometric resolution
DAT	Data requirements	Bias, precision, sampling, etc.

Table 4: Requirement name formats

The threshold values represent the minimum required performance. When a threshold is not met, at least one of the mission objectives cannot be met. The goal values represent the ideal performance. Performance beyond these values provides limited additional benefit towards achieving the mission objectives. The goal is an ideal value for the most demanding mission objective.

5.3 Data Processing Levels

The data obtained from the ALI instrument will go through multiple levels of processing to obtain geophysical variables used for scientific analysis. The table below describes the various data processing levels used in this report.

Data Level	Description
Level 0	Reconstructed, unprocessed instrument and payload data at full resolution, with any and all communications artifacts (e.g., synchronization frames, communications headers, duplicate data) removed.
Level 1A	Reconstructed, unprocessed instrument data at full resolution, time-referenced, and annotated with ancillary information, including radiometric and geometric calibration coefficients and georeferencing parameters (e.g., platform ephemeris) computed and appended but not applied to Level 0 data.
Level 1B	Level 1A data that have been processed to sensor units.
Level 2	Derived geophysical variables from the Level 1 source data along the satellite orbit.
Level 3	Level 2 variables averaged onto uniform space-time grid scales.
Level 4	Results from analyses of lower-level data (e.g., variables derived from multiple measurements or combined with model output).

Table 5: Description of data processing levels[7]

[7] Adapted from "Data Processing Levels - Science@NASA." Data Processing Levels. Accessed 27 Mar. 2020.

6 Mission Coverage Requirements

6.1 Position and Orientation Knowledge Requirements

6.1.1 [ALI-MIS-001-0.2]-Sun-Synchronous Orbit

Description: Low earth orbit. The orbit should be sun-synchronous or near sun-synchronous.

Assumptions and Rationale: Sun-synchronous orbit provides stability in solar viewing geometry for limb scattering observations and addresses the need for daily global (all longitudes) coverage, i.e. enable measurements for all portions of the orbit and covering both hemispheres, reaching as far north and south as possible (where solar illumination conditions allow).

Comments: Measurements can be made from either polar or highly inclined asynchronous orbit with impact only on the global coverage. Design shall not preclude either scenario.

6.1.2 [ALI-MIS-002-0.2]-Spacecraft Pointing Control

Description: The satellite pitch angle shall be controlled to better than ±5 arcmin, the yaw angle shall be controlled to better than ±1 degree of the orbit plane, and the spacecraft roll angle shall be controlled to better than ±5 arcmin (TBC).

Assumptions and rationale: Pitch control ensures the vertical iFOV of the instrument is mapped to the target range of tangent altitudes on the atmospheric limb. Control in the roll direction minimizes the range of tangent height spanned by one iFOV, for example. Controlling roll and yaw ensures the measured profile is within the orbit plane and thus is important for tomographic inversion and coordination with potential nadir observations on the same platform.

Comments: The pitch angle control translates to tangent height control of 4-5 km. The yaw control requirement translates to 50 km of across-track displacement of the tangent point. The movement of the tangent point is a function of the tangent height during roll anomaly with a worst case for the extremes of the instantaneously sampled tangent height range.

6.1.3 [ALI-MIS-003-0.2]-Spacecraft Pointing Knowledge

Description: During a hyperspectral measurement cycle, the yaw angle (relative to the orbit plane) shall be known to 5 arcmin, the roll angle shall be known to 1 arcmin (TBC).

Assumptions and Rationale: Required for geo-locating cross track measurements (yaw) and for limiting impact on altitude coverage and resolution of cross track profiles (roll).

Comments: The pointing knowledge on yaw and roll are post-processed.

6.1.4 [ALI-MIS-004-0.2]-Spacecraft Altitude Tolerance

Description: The satellite altitude shall be controlled to +/- 10 km of the nominal orbit altitude.

Assumptions and rationale: The ALI instrument design can accommodate a wide range of potential platform altitudes; however, pitch offset is highly sensitive to platform altitude and variations in platform altitude throughout the mission duration (in the absence of pitch correction) shall be maintained within relatively tight constraints.

Comments: This will ensure the same approximate altitude range is sampled over the duration of the mission.

6.1.5 [ALI-MIS-005-0.2]-Spacecraft Altitude Knowledge

Description: The satellite altitude shall be known to within 0.15 km.

Assumptions and rationale: The ALI instrument design can accommodate a wide range of potential platform altitudes; however, pitch offset is highly sensitive to platform altitude and variations in platform altitude throughout the mission duration (in the absence of pitch correction) and shall be maintained within relatively tight constraints.

Comments: Knowledge of this parameter is essential for instrument specific tangent altitude knowledge.

6.2 Solar Geometry Requirements

6.2.1 [ALI-MIS-006-0.2]-Solar Zenith Angle

Description: The mission shall measure limb-scattered sunlight with the ALI payload whenever the Solar Zenith Angle at the measurement tangent point is less than 92 degrees and be capable of making measurements at less than 95 degrees.

Assumptions and rationale: Ensures maximum latitudinal coverage of the sunlit portion of Earth.

Comments: N/A

6.2.2 [ALI-MIS-007-0.2]-Solar Scattering Angle

Description: The mission shall measure limb-scattered sunlight with the ALI payload whenever the Solar Scattering Angle (SSA) at the measurement tangent point is 30° < SSA < 150° and be capable of making measurements at 20° < SSA < 180°.

Assumptions and rationale: Ensures maximum latitudinal coverage of the sunlit portion of Earth.

Comments: N/A

6.3 Viewing Requirements

6.3.1 [ALI-MIS-008-0.2]-Limb Viewing in the Orbit Plane

Description: The spacecraft shall enable unobstructed atmospheric limb measurements with the cross-track swath centered on the orbit plane.

Assumptions and Rationale: Within the pointing control accuracy defined in the Pointing Control requirement.

Comments: Observations in the orbit plane are essential for tomographic retrievals.

6.4 Latency Requirements

6.4.1 [ALI-MIS-009-0.2]-ALI Data Latency

Description: The mission shall be capable of providing Level 2 data from ALI, from acquisition on-orbit to product delivery to the end-user, within 2 days.

Assumptions and Rationale: The latency requirement stems from the need for aerosol observations to be available for forest fire and volcanic plume monitoring/forecasting.

Comments: To be confirmed with ECCC.

6.5 Other Mission Coverage Requirements

6.5.1 [ALI-MIS-010-0.2]-Synergy with other instrumentation

Description: Co-alignment with SHOW, and common air mass view with TICFIRE and lidar. The 5 degree field of view of ALI is sufficient to sample the same airmass as nadir-viewing instruments on a typical low Earth observing platform.

Assumptions and Rationale: TBC.

Comments: TBC

7 Instrument Requirements

7.1 Spectral Requirements

7.1.1 [ALI-INT-001-0.2]- Wavelength Range

Description: ALI shall provide measurements in the wavelength range of 550 nm to 1500 nm

Assumptions and Rationale: Provides enough spectral range for aerosol particle size retrieval and ozone correction.

Comments: N/A

7.1.2 [ALI-INT-002-0.2]- Spectral Resolution

Description: The spectral resolution of ALI shall be better than 10 nm for the spectral range 550-900 nm, and better than 20 nm for the spectral range 900-1500 nm.

Assumptions and Rationale: This is evaluated as the FWHM. The contribution from regions outside +/- 3 FWHM from the passband sidelobes or from internal stray light shall be less than 1 % (TBC).

Comments: This resolution is sufficient for retrieval of aerosol properties from the atmospheric limb measurements due to the broadband nature of aerosol scattering. The spectral resolution is driven by the nature of the AOTF interaction and SNR. Other optical components shall not reduce the spectral resolution beyond this limit.

7.1.3 [ALI-INT-003-0.2]- Spectral Gradient across FOV

Description: For any individual spectral image, the variation of the central wavelength of the passband across the Field of View shall be less than 0.8% of the central wavelength.

Assumptions and Rationale: A wavelength variation across the field of view is tolerable within the aerosol retrieval process. The described variation is sufficiently small when compared to the broad spectral scattering signature of

aerosol. The variation is driven by the nature of the acousto-optic interaction with collimated light. Other optical components shall not increase the wavelength variation.

Comments: This is potentially on the high side and needs confirmation with instrument modelling and lab measurements.[LR5]

7.2 Spatial Requirements

7.2.1 [ALI-INT-004-0.2]- Instrument Pointing Knowledge

Description: The mission shall be provided measurement tangent altitude registration within ±0.25 km (TBC) (threshold), and should be able to register measurement tangent altitudes within ±0.1 km (goal). These do not need to be provided in real time, but should be made available

Assumptions and Rationale: This includes all contributing effects such as those related to pointing and position knowledge (time-tagging, position knowledge, orientation knowledge, misalignment/co-registration with star-trackers, thermo-elastic distortions, atmospheric refraction, geoid, etc.) and refers to post-processed spatial location knowledge of the acquired data.

Comments: The description above does not distinguish between pointing knowledge precision, bias, and long-term stability. Long-term stability of Level 2 data products is important for trend studies.

7.2.2 [ALI-INT-005-0.2]- Vertical (Tangent Altitude) Range

Description: ALI shall provide spectral images of the atmospheric limb on the sunlit portion of the orbit track extending from the surface to 45 km tangent altitude.

Assumptions and Rationale: This ensures coverage of the UTLS region and allows for calibration using spectral and radiometric measurements from tangent altitudes above 35 km. Depending on spacecraft altitude, this is approximately 1 degree FOV.

Comments: N/A

7.2.3 [ALI-INT-006-0.2]- Vertical (Tangent altitude) Resolution

Description: ALI shall provide spectral radiance images at a vertical resolution equal to or less than 0.25 km on the atmospheric limb.

Assumptions and Rationale: The vertical resolution includes contributions from the optical performance, pixilation, and the line-of-sight (LOS) motion during exposures. The vertical resolution is evaluated as the FWHM.

Comments: N/A

7.2.4 [ALI-INT-007-0.2]- Vertical (Tangent Altitude) Sampling

Description: ALI shall provide spectral radiance images with vertical sampling at the pixel level equal to two samples per vertical resolution element.

Assumptions and Rationale: Sampling twice as fine as the vertical resolution is sufficient according to the Nyquist limit.

Comments: N/A

7.2.5 [ALI-INT-008-0.2]- Cross-Track Range

Description: ALI shall provide spectral images of the atmospheric limb on the sunlit portion of the orbit track with a 5 degree cross-track FOV, centered on the orbit plane. This translates to a cross track field of view of approximately 250km at the tangent point.

Assumptions and Rationale: This provides sampling between the orbital tracks and greatly increases daily, global coverage and revisit times.

Comments: 8 degrees is desired, but this seems to be too difficult technically.

7.2.6 [ALI-INT-009-0.2]- Cross-Track Sampling

Description: The cross-track sampling shall be less than or equal to 40 arcseconds.

Assumptions and Rationale: The across-track sampling will be sufficient to reach SNR requirements through across-track binning to approximately 10 vertical profiles per image. This sampling requirement should also ensure that the curvature of the Earth can be compensated when binning so as not to degrade the vertical resolution.

Comments:

7.2.7 [ALI-INT-010-0.2]- Along-Track Sampling

Description: ALI shall provide one full along-track hyperspectral observation every 30 s.

Assumptions and Rationale: Feasibility with SNR requirements must be confirmed.

Comments: N/A

7.3 Radiometric Requirements

7.3.1 [ALI-INT-011-0.2]- Accuracy

Description: ALI shall be capable of measuring calibrated radiances to within 5% across the spectral and spatial range of the target observations.

Assumptions and Rationale: Accuracy is driven by the requirement to use high tangent altitude observations to retrieve effective Earth surface reflectance.

Comments: N/A

7.3.2 [ALI-INT-012-0.2]- Signal to Noise Ratio

Description: The Signal to Noise Ratio (SNR) of ALI shall be greater than 200 for horizontally polarized light and greater than 50 for vertically polarized light across all wavelengths and tangent altitudes up to 35 km.

Assumptions and Rationale: Accuracy is driven by the requirement to use high tangent altitude observations to retrieve effective Earth surface reflectance.

Comments: SNR requirement based on radiative transfer model simulations at typical viewing geometry. This requirement maps to science requirements for the level 2 data product.

7.3.3 [ALI-INT-013-0.2]- Stray Light Suppression

Description: The design of ALI shall incorporate stray light control features to address all first-order stray light sources including out-of-field and 0th order in-field signals, as well as ghosts from internal reflections.

Assumptions and Rationale: Out of field stray light from the Earth surface is a known issue for limb imaging and substantial effort should be made at the design level to minimize this effect.

Comments: N/A

7.3.4 [ALI-INT-014-0.2]- Dynamic Range

Description: ALI shall be capable of measuring limb radiances from 10^{11} to 10^{15} photons/cm2/steradian/second/nm.

Assumptions and Rationale: Based on radiative transfer forward model simulations at typical viewing geometry.

Comments: N/A

7.3.5 [ALI-INT-015-0.2]- Polarization

Description: ALI shall be capable of measuring two orthogonal polarizations of the limb radiance. The accuracy of the polarization state shall be (TBC)

Assumptions and Rationale: Based on radiative transfer forward model simulations at typical viewing geometry.

Comments: N/A

7.4 Operational Mode Requirement

7.4.1 [ALI-INT-016-0.2]- Hyperspectral Mode Observation Acquisition

Description: ALI shall perform measurements at a minimum of 11 wavelengths {551, 601, 676, 755, 869, 950, 1022, 1100, 1200, 1450, 1500 nm}, for horizontally polarized input, and 3 wavelengths {755, 1022, 1500 nm} for vertically polarized input, within the specified along-track sampling rate. The cadence shall also

include one sample at a representative exposure time with the RF driver disabled to sample the stray light contribution from the undiffracted (0th order) beam.

Assumptions and Rationale: Wavelength selection to match NASA SAGE heritage observations.

Comments: The vertical polarization state measurement is a science requirement primarily for cloud/aerosol discrimination. Fewer samples spaced across the spectral range are sufficient for the discrimination algorithm.

7.4.2 [ALI-INT-017-0.2]- Event Mode Observation Acquisition

Description: ALI shall perform measurements at a single wavelength, nominally 1020 nm, for both polarizations and with the RF driver in a repeated cadence.

Assumptions and Rationale: Allows for high spatial resolution observation for tracking smoke/aerosol plume from forest fires and volcanic eruptions.

Comments: N/A.

7.4.3 [ALI-INT-018-0.2]- Dark Signal Characterization

Description: ALI shall be capable of performing measurements on the night side of the orbit with the RF driver disabled with variable exposure time so as to characterize the detector dark signal.

Assumptions and Rationale: No shutter is required.

Comments: N/A.

7.4.4 [ALI-INT-019-0.2] Lunar/Stellar Observation

Description: ALI shall be capable of performing hyperspectral observations of the moon or stars during the night side of the orbit at opportunistic times when these targets are within the field of view.

Assumptions and Rationale: Provides spectral, radiative and pointing calibration opportunities.

Comments: N/A.

8 Level 2 Data Requirements

8.1 Aerosol Extinction Profiles

8.1.1 [ALI-DAT-001-0.2] Wavelength Sampling

Description: ALI extinction profiles shall be retrieved at 551, 675, 755, 1022, and 1500nm.

Assumptions and Rationale: Extinction retrievals at these wavelengths provide continuity with current limb scattering and solar occultation instruments. The 551nm extinction retrieval will also help enhance synergy with the ACCP lidar, which is expected to have a channel in the 525nm range (TBC).

Comments: N/A.

8.1.2 [ALI-DAT-002-0.2] Vertical Range

Description: ALI extinction profiles shall retrieve extinction from the tropopause (assuming a 2°C lapse rate definition) or the lowest altitude where extinction at 755nm is below 10^{-2} km^{-1}, whichever is higher, up to the lowest altitude where extinction at 755nm exceeds 10^{-5} km^{-1} (TBC). The retrieval should extend down to 8km when clouds do not obstruct the field of view.

Assumptions and Rationale: This range covers the majority of stratospheric aerosol, and allows normalization at altitudes with sufficiently low levels of aerosol loading. Retrieval below the tropopause is desirable to better quantify transport, but is not required as ACCP baseline instruments will cover this range.

Comments: Extinction levels exceeding 10^{-2} km^{-1} at 755nm may be measurable at longer wavelengths, but cannot be guaranteed.

8.1.3 [ALI-DAT-003-0.2] Vertical Resolution

Description: Vertical resolution shall meet or exceed 0.5km.

Assumptions and Rationale: Vertically inhomogeneous plumes from volcanic eruptions require high vertical resolutions to resolve. High resolution also helps

reduce cloud contamination and improve filtering in the UTLS where aerosol levels are crucial for understanding total loading.

Comments: N/A.

8.1.4 [ALI-DAT-004-0.2] Horizontal Resolution

Description: Horizontal resolution shall meet or exceed 250km.

Assumptions and Rationale: 250km is sufficient to resolve most volcanic and wildfire plumes shortly after the initial injection, and provides comparable resolution to cross-track measurements.

Comments: N/A.

8.1.5 [ALI-DAT-005-0.2] Accuracy

Description: Horizontal resolution shall meet or exceed 250km.

Assumptions and Rationale: 250km is sufficient to resolve most volcanic and wildfire plumes shortly after the initial injection, and provides comparable resolution to cross-track measurements.

Comments: N/A.

Bibliography

Adams, C., Bourassa, A. E., McLinden, C. A., Sioris, C. E., Von Clarmann, T., Funke, B., ... & Degenstein, D. A. (2017). Effect of volcanic aerosol on stratospheric NO2 and N2O5 from 2002-2014 as measured by Odin-OSIRIS and Envisat-MIPAS.

Andersson, S. M., Martinsson, B. G., Vernier, J. P., Friberg, J., Brenninkmeijer, C. A., Hermann, M., ... & Zahn, A. (2015). Significant radiative impact of volcanic aerosol in the lowermost stratosphere. Nature communications, 6, 7692.

Barth, C. A., Rusch, D. W., Thomas, R. J., Mount, G. H., Rottman, G. J., Thomas, G. E., ... & Lawrence, G. M. (1983). Solar mesosphere explorer: Scientific objectives and results. Geophysical research letters, 10(4), 237-240.

Bingen, C., Fussen, D., & Vanhellemont, F. (2004). A global climatology of stratospheric aerosol size distribution parameters derived from SAGE II data over the period 1984–2000: 2. Reference data. Journal of Geophysical Research: Atmospheres, 109(D6).

Boucher, O., Randall, D., Artaxo, P., Bretherton, C., Feingold, G., Forster, P., ... & Rasch, P. (2013). Clouds and aerosols. In Climate change 2013: the physical science basis. Contribution of Working Group I to the Fifth Assessment Report of the Intergovernmental Panel on Climate Change (pp. 571-657). Cambridge University Press.

Bourassa, A. E., Degenstein, D. A., & Llewellyn, E. J. (2005). Climatology of the subvisual cirrus clouds as seen by OSIRIS on Odin. Advances in Space Research, 36(5), 807-812.

Bourassa, A. E., Degenstein, D. A., Gattinger, R. L., & Llewellyn, E. J. (2007). Stratospheric aerosol retrieval with optical spectrograph and infrared imaging system limb scatter measurements. Journal of Geophysical Research: Atmospheres, 112(D10).

Bourassa, A. E., Degenstein, D. A., & Llewellyn, E. J. (2008). SASKTRAN: A spherical geometry radiative transfer code for efficient estimation of limb scattered sunlight. Journal of Quantitative Spectroscopy and Radiative Transfer, 109(1), 52-73.

Bourassa, A. E., Degenstein, D. A., Elash, B. J., & Llewellyn, E. J. (2010). Evolution of the stratospheric aerosol enhancement following the eruptions of Okmok and Kasatochi: Odin-OSIRIS measurements. Journal of Geophysical Research: Atmospheres, 115(D2).

Bourassa, A. E., McLinden, C. A., Sioris, C. E., Brohede, S., Bathgate, A. F., Llewellyn, E. J., & Degenstein, D. A. (2011). Fast NO2 retrievals from Odin-OSIRIS limb scatter measurements. Atmospheric Measurement Techniques, 4(5), 965-972.

Bourassa, A. E., Roth, C. Z., Zawada, D. J., Rieger, L. A., McLinden, C. A., & Degenstein, D. A. (2018). Drift-corrected Odin-OSIRIS ozone product: algorithm and updated stratospheric ozone trends. Atmospheric Measurement Techniques, 11(1), 489-498.

Bourassa, A. E., Rieger, L. A., Zawada, D. J., Khaykin, S., Thomason, L. W., & Degenstein, D. A. (2019). Satellite Limb Observations of Unprecedented Forest Fire Aerosol in the Stratosphere. Journal of Geophysical Research: Atmospheres, 124(16), 9510-9519.

Carslaw, K. S., Lee, L. A., Reddington, C. L., Pringle, K. J., Rap, A., Forster, P. M., ... & Pierce, J. R. (2013). Large contribution of natural aerosols to uncertainty in indirect forcing. Nature, 503(7474), 67-71.

Chepfer, H., Bony, S., Winker, D., Cesana, G., Dufresne, J. L., Minnis, P., ... & Zeng, S. (2010). The GCM-oriented calipso cloud product (CALIPSO-GOCCP). Journal of Geophysical Research: Atmospheres, 115(D4).

Christian, K., Yorks, J., Colarco, P., Aquila, V., & Das, S. (2019). Differences in the Vertical and Microphysical Evolution of Volcanic and Pyrocumulonimbus Stratospheric Aerosol Plumes as Observed by CALIOP and CATS Satellite Lidar.

Degenstein, D. A., Bourassa, A. E., Roth, C. Z., & Llewellyn, E. J. (2009). Limb scatter ozone retrieval from 10 to 60 km using a multiplicative algebraic reconstruction technique. Atmospheric Chemistry & Physics, 9(17).

Deligne, N. I., Coles, S. G., & Sparks, R. S. J. (2010). Recurrence rates of large explosive volcanic eruptions. Journal of Geophysical Research: Solid Earth, 115(B6).

Deshler, T., Hervig, M. E., Hofmann, D. J., Rosen, J. M., & Liley, J. B. (2003). Thirty years of in situ stratospheric aerosol size distribution measurements from Laramie, Wyoming (41 N), using balloon-borne instruments. Journal of Geophysical Research: Atmospheres, 108(D5).

Dessler, A. E., Palm, S. P., Hart, W. D., & Spinhirne, J. D. (2006). Tropopause-level thin cirrus coverage revealed by ICESat/Geoscience Laser Altimeter System. Journal of Geophysical Research: Atmospheres, 111(D8).

Dykema, J. A., Keith, D. W., Anderson, J. G., & Weisenstein, D. (2014). Stratospheric controlled perturbation experiment: a small-scale experiment to improve understanding of the risks of solar geoengineering. *Philosophical Transactions of the Royal Society A: Mathematical, Physical and Engineering Sciences*, *372*(2031), 20140059.

English, J. M., Toon, O. B., & Mills, M. J. (2012). Microphysical simulations of sulfur burdens from stratospheric sulfur geoengineering. Atmospheric Chemistry and Physics, 12(10), 4775-4793.

Garny, H., & Randel, W. J. (2016). Transport pathways from the Asian monsoon anticyclone to the stratosphere. Atmos. Chem. Phys, 16, 2703-2718.

Gasparini, B., & Lohmann, U. (2016). Why cirrus cloud seeding cannot substantially cool the planet. Journal of Geophysical Research: Atmospheres, 121(9), 4877-4893.

Fromm, M., Alfred, J., Hoppel, K., Hornstein, J., Bevilacqua, R., Shettle, E., ... & Stocks, B. (2000). Observations of boreal forest fire smoke in the stratosphere by POAM III, SAGE II, and lidar in 1998. Geophysical Research Letters, 27(9), 1407-1410.

Fromm, M., Tupper, A., Rosenfeld, D., Servranckx, R., & McRae, R. (2006). Violent pyro-convective storm devastates Australia's capital and pollutes the stratosphere. Geophysical Research Letters, 33(5).

Fueglistaler, S., Dessler, A. E., Dunkerton, T. J., Folkins, I., Fu, Q., & Mote, P. W. (2009). Tropical tropopause layer. Reviews of Geophysics, 47(1).

Fyfe, J. C., Von Salzen, K., Cole, J. N. S., Gillett, N. P., & Vernier, J. P. (2013). Surface response to stratospheric aerosol changes in a coupled atmosphere–ocean model. Geophysical Research Letters, 40(3), 584-588.

Gasparini, B., & Lohmann, U. (2016). Why cirrus cloud seeding cannot substantially cool the planet. Journal of Geophysical Research: Atmospheres, 121(9), 4877-4893.

Girardin, M. P., & Mudelsee, M. (2008). Past and future changes in Canadian boreal wildfire activity. Ecological Applications, 18(2), 391-406.

Griffin, D., C. Sioris, J. Chen, N. Dickson, A. Kovachik, M. de Graaf, S. Nanda, P. Veefkind, E. Dammers, C. A. McLinden, P A. Makar, & A. Akingunola. (2020). The 2018 fire season in North America as seen by TROPOMI: aerosol layer height validation and evaluation of model-derived plume heights, Atmospheric Measurement Techniques, revised.

Haladay, T., & Stephens, G. (2009). Characteristics of tropical thin cirrus clouds deduced from joint CloudSat and CALIPSO observations. Journal of Geophysical Research: Atmospheres, 114(D8).

Hartmann, D. L., Holton, J. R., & Fu, Q. (2001). The heat balance of the tropical tropopause, cirrus, and stratospheric dehydration. Geophysical research letters, 28(10), 1969-1972.

Haywood, J. M., Jones, A., & Jones, G. S. (2014). The impact of volcanic eruptions in the period 2000–2013 on global mean temperature trends evaluated in the HadGEM2-ES climate model. Atmospheric Science Letters, 15(2), 92-96.

Heckendorn, P., Weisenstein, D., Fueglistaler, S., Luo, B. P., Rozanov, E., Schraner, M., ... & Peter, T. (2009). The impact of geoengineering aerosols on stratospheric temperature and ozone. *Environmental research letters*, *4*(4), 045108.

Henderson, S. B., Burkholder, B., Jackson, P. L., Brauer, M., & Ichoku, C. (2008). Use of MODIS products to simplify and evaluate a forest fire plume dispersion model for PM10 exposure assessment. *Atmospheric Environment*, *42*(36), 8524-8532.

Hofmann, D., Barnes, J., O'Neill, M., Trudeau, M., & Neely, R. (2009). Increase in background stratospheric aerosol observed with lidar at Mauna Loa Observatory and Boulder, Colorado. Geophysical Research Letters, 36(15).

Hong, Y., Liu, G., & Li, J. L. (2016). Assessing the radiative effects of global ice clouds based on CloudSat and CALIPSO measurements. Journal of Climate, 29(21), 7651-7674.

Homeyer, C. R., McAuliffe, J. D., & Bedka, K. M. (2017). On the development of above-anvil cirrus plumes in extratropical convection. Journal of the Atmospheric Sciences, 74(5), 1617-1633.

Jensen, E., & Pfister, L. (2004). Transport and freeze-drying in the tropical tropopause layer. Journal of Geophysical Research: Atmospheres, 109(D2).

Kar, J., Lee, K. P., Vaughan, M. A., Tackett, J. L., Trepte, C. R., Winker, D. M., ... & Getzewich, B. J. (2019). CALIPSO level 3 stratospheric aerosol profile product: version 1.00 algorithm description and initial assessment. *Atmospheric Measurement Techniques*, *12*(11).

Kravitz, B., Robock, A., Boucher, O., Schmidt, H., Taylor, K. E., Stenchikov, G., & Schulz, M. (2011). The geoengineering model intercomparison project (GeoMIP). Atmospheric Science Letters, 12(2), 162-167.

Kremser, S., Thomason, L. W., von Hobe, M., Hermann, M., Deshler, T., Timmreck, C., ... & Fueglistaler, S. (2016). Stratospheric aerosol—Observations, processes, and impact on climate. Reviews of Geophysics, 54(2), 278-335.

Kuebbeler, M., Lohmann, U., & Feichter, J. (2012). Effects of stratospheric sulfate aerosol geo-engineering on cirrus clouds. Geophysical Research Letters, 39(23).

Lacis, A., Hansen, J., & Sato, M. (1992). Climate forcing by stratospheric aerosols. *Geophysical Research Letters*, *19*(15), 1607-1610.

Lau, W. K., Yuan, C., & Li, Z. (2018). Origin, maintenance and variability of the Asian tropopause aerosol layer (ATAL): the roles of monsoon dynamics. Scientific reports, 8(1), 1-14.

Liu, Y., Stanturf, J., & Goodrick, S. (2010). Trends in global wildfire potential in a changing climate. Forest ecology and management, 259(4), 685-697.

Llewellyn, E. J., Lloyd, N. D., Degenstein, D. A., Gattinger, R. L., Petelina, S. V., Bourassa, A. E., ... & McConnell, J. C. (2004). The OSIRIS instrument on the Odin spacecraft. Canadian Journal of Physics, 82(6), 411-422.

Malinina, E., Rozanov, A., Rozanov, V., Liebing, P., Bovensmann, H., & Burrows, J. P. (2018). Aerosol particle size distribution in the stratosphere retrieved from SCIAMACHY limb measurements. Atmospheric Measurement Techniques, 11(4).

Marshall, L., Johnson, J. S., Mann, G. W., Lee, L., Dhomse, S. S., Regayre, L., ... & Schmidt, A. (2019). Exploring how eruption source parameters affect volcanic radiative forcing using statistical emulation. *Journal of Geophysical Research: Atmospheres*, *124*(2), 964-985.

Masson-Delmotte, V., Schulz, M., Abe-Ouchi, A., Beer, J., Ganopolski, A., Gonzalez Rouco, J. F., ... & Osboorn, T. (2013). X., and Timmermann, A.: Information from paleoclimate archives. Climate change.

McFarquhar, G. M., Heymsfield, A. J., Spinhirne, J., & Hart, B. (2000). Thin and subvisual tropopause tropical cirrus: Observations and radiative impacts. Journal of the atmospheric sciences, 57(12), 1841-1853.

Mills, M. J., Schmidt, A., Easter, R., Solomon, S., Kinnison, D. E., Ghan, S. J., ... & Gettelman, A. (2016). Global volcanic aerosol properties derived from emissions, 1990–2014, using CESM1 (WACCM). *Journal of Geophysical Research: Atmospheres*, *121*(5), 2332-2348.

Pachauri, R. K., Allen, M. R., Barros, V. R., Broome, J., Cramer, W., Christ, R., ... & Dubash, N. K. (2014). *Climate change 2014: synthesis report. Contribution of Working Groups I, II and III to the fifth assessment report of the Intergovernmental Panel on Climate Change* (p. 151). IPCC.

Petropavlovskikh, I., Godin-Beekmann, S., Hubert, D., Damadeo, R., Hassler, B., Sofieva, V., ... & Tourpali, K. (2018). Sparc/io3c/gaw report on long-term ozone trends and uncertainties in the stratosphere. 39th session of the WCRP Joint Scientific Committee, 8.

Pinto, J. P., Turco, R. P., & Toon, O. B. (1989). Self-limiting physical and chemical effects in volcanic eruption clouds. *Journal of Geophysical Research: Atmospheres*, *94*(D8), 11165-11174.

Räisänen, P., Bogdan, A., Sassen, K., Kulmala, M., & Molina, M. J. (2006). Impact of H2SO4/H2O coating and ice crystal size on radiative properties of sub-visible cirrus.

Randall, D. A., Wood, R. A., Bony, S., Colman, R., Fichefet, T., Fyfe, J., ... & Stouffer, R. J. (2007). Climate models and their evaluation. In Climate change 2007: The physical science basis. Contribution of Working Group I to the Fourth Assessment Report of the IPCC (FAR) (pp. 589-662). Cambridge University Press.

Randel, W. J., Park, M., Emmons, L., Kinnison, D., Bernath, P., Walker, K. A., ... & Pumphrey, H. (2010). Asian monsoon transport of pollution to the stratosphere. Science, 328(5978), 611-613.

Randel, W. J., & Jensen, E. J. (2013). Physical processes in the tropical tropopause layer and their roles in a changing climate. Nature Geoscience, 6(3), 169-176.

Rasch, P. J., Crutzen, P. J., & Coleman, D. B. (2008). Exploring the geoengineering of climate using stratospheric sulfate aerosols: The role of particle size. Geophysical Research Letters, 35(2).

Rawcliffe, R. D., Meloy, G. E., Friedman, R. M., & Rogers, E. H. (1963). Measurement of vertical distribution of ozone from a polar orbiting satellite. Journal of Geophysical Research, 68(24), 6425-6429.

Ricke, K. L., Morgan, M. G., & Allen, M. R. (2010). Regional climate response to solar-radiation management. Nature Geoscience, 3(8), 537-541.

Ridley, D. A., Solomon, S., Barnes, J. E., Burlakov, V. D., Deshler, T., Dolgii, S. I., ... & Ritter, C. (2014). Total volcanic stratospheric aerosol optical depths and implications for global climate change. Geophysical Research Letters, 41(22), 7763-7769.

Rieger, L. A., Bourassa, A. E., & Degenstein, D. A. (2014). Stratospheric aerosol particle size information in Odin-OSIRIS limb scatter spectra. Atmospheric Measurement Techniques, 7(2), 507.

Rieger, L. A., Zawada, D. J., Bourassa, A. E., & Degenstein, D. A. (2019). A Multiwavelength Retrieval Approach for Improved OSIRIS Aerosol Extinction Retrievals. Journal of Geophysical Research: Atmospheres, 124(13), 7286-7307.

Rittmaster, R., Adamowicz, W. L., Amiro, B., & Pelletier, R. T. (2006). Economic analysis of health effects from forest fires. Canadian Journal of Forest Research, 36(4), 868-877.

Santer, B. D., Fyfe, J. C., Pallotta, G., Flato, G. M., Meehl, G. A., England, M. H., ... & Cvijanovic, I. (2017). Causes of differences in model and satellite tropospheric warming rates. Nature Geoscience, 10(7), 478-485.

Sassen, K., Wang, Z., & Liu, D. (2008). Global distribution of cirrus clouds from CloudSat/Cloud-Aerosol lidar and infrared pathfinder satellite observations (CALIPSO) measurements. Journal of Geophysical Research: Atmospheres, 113(D8).

Sassen, K., Wang, Z., & Liu, D. (2009). Cirrus clouds and deep convection in the tropics: Insights from CALIPSO and CloudSat. Journal of Geophysical Research: Atmospheres, 114(D4).

Sellitto, P., Sèze, G., & Legras, B. (2017). Secondary sulphate aerosols and cirrus clouds detection with SEVIRI during Nabro volcano eruption. International Journal of Remote Sensing, 38(20), 5657-5672.

Sioris, C. E., McLinden, C. A., Martin, R. V., Sauvage, B., Haley, C. S., Lloyd, N. D., ... & McElroy, C. T. (2007). Vertical profiles of lightning-produced NO 2 enhancements in the upper troposphere observed by OSIRIS.

Solomon, S., Daniel, J. S., Neely, R. R., Vernier, J. P., Dutton, E. G., & Thomason, L. W. (2011). The persistently variable "background" stratospheric aerosol layer and global climate change. Science, 333(6044), 866-870.

Stanfield, R. E., Dong, X., Xi, B., Kennedy, A., Del Genio, A. D., Minnis, P., & Jiang, J. H. (2014). Assessment of NASA GISS CMIP5 and post-CMIP5 simulated clouds and TOA radiation budgets using satellite observations. Part I: Cloud fraction and properties. Journal of climate, 27(11), 4189-4208.

Stephens, G. L. (2005). Cloud feedbacks in the climate system: A critical review. Journal of climate, 18(2), 237-273.

Stocker, T. F., Qin, D., Plattner, G. K., Tignor, M., Allen, S. K., Boschung, J., ... & Midgley, P. M. (2013). Climate change 2013: The physical science basis. Contribution of working group I to the fifth assessment report of the intergovernmental panel on climate change, 1535.

Tackett, J. L., Winker, D. M., Getzewich, B. J., Vaughan, M. A., Young, S. A., & Kar, J. (2018). CALIPSO lidar level 3 aerosol profile product: version 3 algorithm design.

Timmreck, C., Lorenz, S. J., Crowley, T. J., Kinne, S., Raddatz, T. J., Thomas, M. A., & Jungclaus, J. H. (2009). Limited temperature response to the very large AD 1258 volcanic eruption. Geophysical Research Letters, 36(21).

Timmreck, C., Mann, G. W., Aquila, V., Hommel, R., Lee, L. A., Schmidt, A., ... & Diehl, T. (2018). The Interactive Stratospheric Aerosol Model Intercomparison Project (ISA-MIP): motivation and experimental design. *Geoscientific Model Development Discussions*, *11*(7), 2581-2608.

Thomas, G. E., Jakosky, B. M., West, R. A., & Sanders, R. W. (1983). Satellite limb-scanning thermal infrared observations of the El Chichon stratospheric aerosol: First results. Geophysical research letters, 10(11), 997-1000.

Thomas, J. L., Polashenski, C. M., Soja, A. J., Marelle, L., Casey, K. A., Choi, H. D., ... & Pelon, J. (2017). Quantifying black carbon deposition over the Greenland ice sheet from forest fires in Canada. Geophysical Research Letters, 44(15), 7965-7974.

Thomason, L. and Th. Peter (2006) SPARC, 2006: SPARC Assessment of Stratospheric Aerosol Properties (ASAP). L. Thomason and Th. Peter (Eds.), SPARC Report No. 4, WCRP-124, WMO/TD – No. 1295, available at www.sparc-climate.org/publications/sparc-reports/

Thomason, L. W., & Vernier, J. P. (2013). Improved SAGE II cloud/aerosol categorization and observations of the Asian tropopause aerosol layer: 1989-2005. Atmospheric Chemistry and Physics, 13(9), 4605.

Thomason, L. W., Ernest, N., Millán, L., Rieger, L., Bourassa, A., Vernier, J. P., ... & Peter, T. (2018). A global space-based stratospheric aerosol climatology: 1979-2016. Earth System Science Data, 10(1), 469-492.

Thompson, D. W., & Solomon, S. (2009). Understanding recent stratospheric climate change. Journal of Climate, 22(8), 1934-1943.

Vernier, J. P., Pommereau, J. P., Garnier, A., Pelon, J., Larsen, N., Nielsen, J., ... & McDermid, I. S. (2009). Tropical stratospheric aerosol layer from CALIPSO lidar observations. Journal of Geophysical Research: Atmospheres, 114(D4).

Vernier, J. P., Thomason, L. W., Pommereau, J. P., Bourassa, A., Pelon, J., Garnier, A., ... & Vargas, F. (2011). Major influence of tropical volcanic eruptions on the stratospheric aerosol layer during the last decade. Geophysical Research Letters, 38(12).

Vernier, J. P., Thomason, L. W., & Kar, J. (2011b). CALIPSO detection of an Asian tropopause aerosol layer. Geophysical Research Letters, 38(7).

Vernier, J. P., Fairlie, T. D., Natarajan, M., Wienhold, F. G., Bian, J., Martinsson, B. G., ... & Bedka, K. M. (2015). Increase in upper tropospheric and lower stratospheric aerosol levels and its potential connection with Asian pollution. Journal of Geophysical Research: Atmospheres, 120(4), 1608-1619.

Vernier, J. P., Fairlie, T. D., Deshler, T., Natarajan, M., Knepp, T., Foster, K., ... & Trepte, C. (2016). In situ and space-based observations of the Kelud volcanic plume: The persistence of ash in the lower stratosphere. Journal of Geophysical Research: Atmospheres, 121(18), 11-104.

Webb, M. J., Andrews, T., Bodas-Salcedo, A., Bony, S., Bretherton, C. S., Chadwick, R., ... & Klein, S. A. (2017). The cloud feedback model intercomparison project (CFMIP) contribution to CMIP6. Geoscientific Model Development, 2017, 359-384.

Wiensz, J. T., Degenstein, D. A., Lloyd, N. D., & Bourassa, A. E. (2013). Retrieval of subvisual cirrus cloud optical thickness from limb-scatter measurements. Atmospheric Measurement Techniques, 6(1), 105.

Wotton, B. M., Flannigan, M. D., & Marshall, G. A. (2017). Potential climate change impacts on fire intensity and key wildfire suppression thresholds in Canada. Environmental Research Letters, 12(9), 095003.

Yu, P., Toon, O. B., Bardeen, C. G., Zhu, Y., Rosenlof, K. H., Portmann, R. W., ... & de Gouw, J. (2019). Black carbon lofts wildfire smoke high into the stratosphere to form a persistent plume. Science, 365(6453), 587-590.

Zanchettin, D., Timmreck, C., Toohey, M., Jungclaus, J. H., Bittner, M., Lorenz, S. J., & Rubino, A. (2019). Clarifying the relative role of forcing uncertainties and initial-condition unknowns in spreading the climate response to volcanic eruptions. *Geophysical Research Letters, 46*(3), 1602-1611.

Zawada, D. J., Dueck, S. R., Rieger, L. A., Bourassa, A. E., Lloyd, N. D., & Degenstein, D. A. (2015). High resolution and Monte Carlo additions to the SASKTRAN radiative transfer model. Atmospheric Measurement Techniques Discussions, 8(3).

Zawada, D. J., Rieger, L. A., Bourassa, A. E., & Degenstein, D. A. (2018). Tomographic retrievals of ozone with the OMPS Limb Profiler: algorithm description and preliminary results. Atmospheric Measurement Techniques, 11(4), 2375-2393.

Zelinka, M. D., Zhou, C., & Klein, S. A. (2016). Insights from a refined decomposition of cloud feedbacks. *Geophysical Research Letters, 43*(17), 9259-9269.

Zelinka, M. D., Myers, T. A., McCoy, D. T., Po-Chedley, S., Caldwell, P. M., Ceppi, P., et al. (2020). Causes of higher climate sensitivity in CMIP6 models. Geophysical Research Letters, 47, e2019GL085782.

Zhang, X., Flato, G., Kirchmeier-Young, M., Vincent, L., Wan, H., Wang, X., Rong, R., Fyfe, J., Li, G., Kharin, V.V. (2019): Changes in Temperature and Precipitation Across Canada; Chapter 4 *in* Bush, E. and Lemmen, D.S. (Eds.) Canada's Changing Climate Report. Government of Canada, Ottawa, Ontario, pp 112-193.

Abbreviations and Acronyms

ACCP	Aerosol Cloud Convection and Precipitation
ALI	Aerosol Limb Imager
ATAL	Asian Tropopause Aerosol Layer
AOTF	Acoustic Optical Tunable Filter
CALIPSO	Cloud-Aerosol Lidar and Infrared Pathfinder Satellite Observation
CSA	Canadian Space Agency
EC	Environment Canada
ECCC	Environment and Climate Change Canada
FOV	Field of View
FWHM	Full Width at Half Maximum
GCM	Global Climate Model
ICCP	International Climate Change Partnership
LOS	Line of Sight
NASA	National Aeronautic and Space Administration
OSIRIS	Optical Spectrograph and InfraRed Imaging System
SAGE	Stratospheric Aerosol and Gas Experiment
SCIAMACHY	SCanning Imaging Absorption SpectroMeter for Atmospheric CHartographY
SHOW	Spatial-Heterodyne Observations of Water Vapour
SNR	Signal to Noise Ratio
SSA	Solar Scattering Angle
SZA	Solar Zenith Angle
TICFIRE	Thin Ice Clouds in Far Infrared Experiment
TTL	Tropical Tropopause Layer
μCATS	Microsatellite Canadian Atmospheric Tomography System
URD	User Requirements Document
UTLS	Upper Troposphere and Lower Stratosphere
UTS	Upper Troposphere and Stratosphere
WMO	World Meteorological Organization

Earth System Model Scientific Software Engineer

Keywords: Climate engineering, Earth System Model, solar radiation modification, feedback control

Reaching climate targets through mitigation is a preferred pathway but parallel research continues into reaching climate targets using climate intervention, through Carbon Dioxide Removal (CDR) and through solar radiation modification (SRM). While it is recognized that SRM can have unintended consequences, it has been proposed as a method to maintain particular climate targets either long term or temporarily to "buy time" for implementation of mitigation policies. The main method to research SRM is Earth System Models (ESMs). The Canadian ESM (CanESM) developed at CCCma is used to perform SRM research and to contribute to international projects, e.g., GeoMIP.

Performing simulations CanESM of SRM scenarios, even idealized ones with a single forcing (incoming solar radiation) and single target (1850 global mean temperature), have highlighted the complexity of these experiments. The main complication, and cost for person-hours, is manual adjustments of the forcing during the CanESM simulation to maintain the target. As the forcings and targets become more complex, including using multiple forcings and multiple simultaneous targets, the cost in person-hours of these simulations becomes significant. Maintenance of select targets using forcings is broadly studied and applied in engineering, e.g., controlling the temperature in your house using a thermostat. This project uses similar feedback algorithms to maintain climate targets using SRM in CanESM.

While the use of feedback algorithms for SRM experiments in ESMs is not widely used, there are peer-reviewed literature that clearly explain methodologies implemented at some large climate centres, including NCAR. This project will have two goals,

1. Develop software to implement an existing feedback algorithm documented in the literature.
2. Incorporate software into CanESM
3. Perform tests to verify that software performs correctly by reproducing existing SRM experiments performed with CanESM (single forcing and single target).

If time remains after achieving the two goals, new SRM experiments will be performed that exploit the capability provided by the feedback algorithm, e.g., time-varying targets.

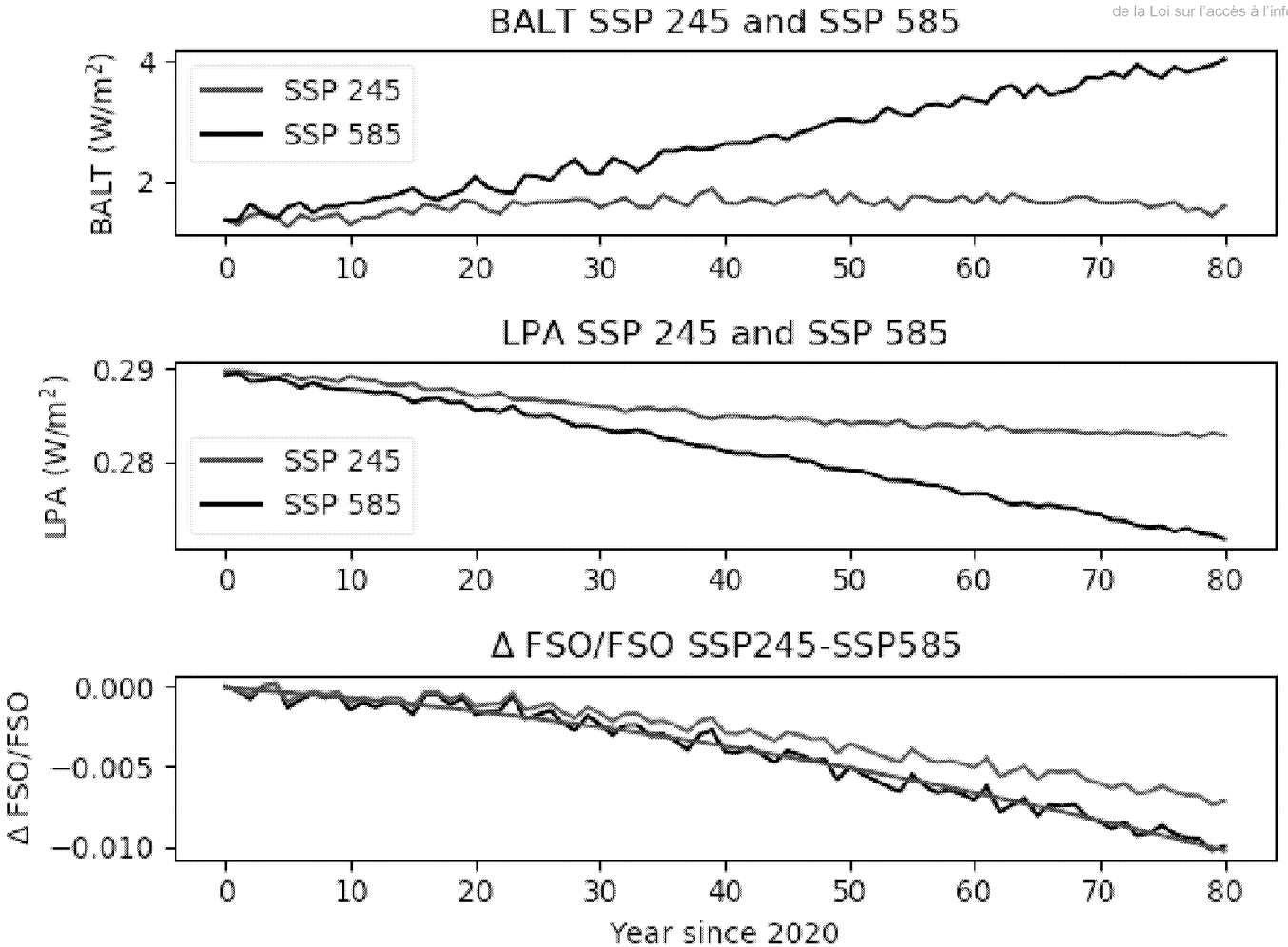

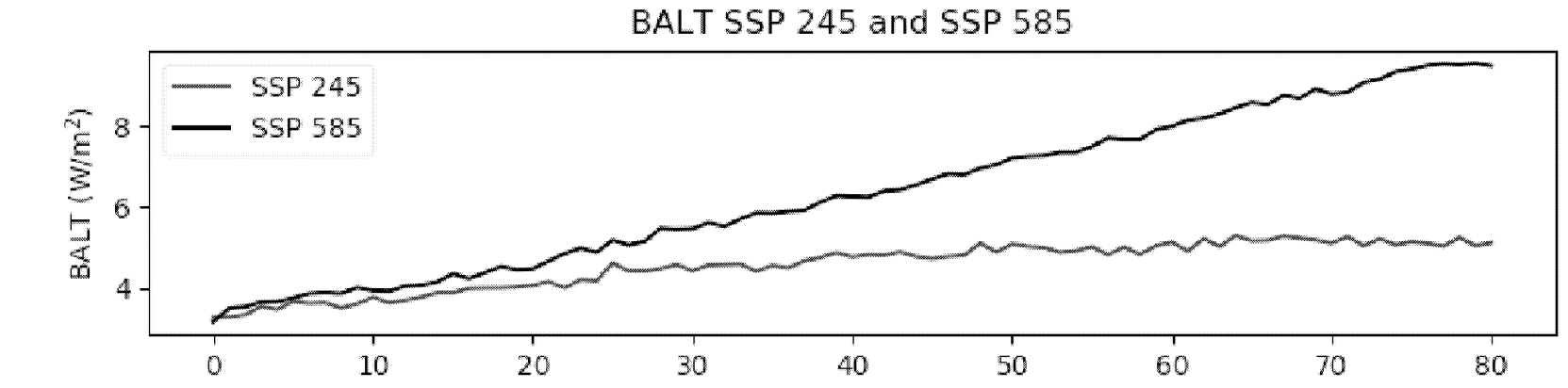

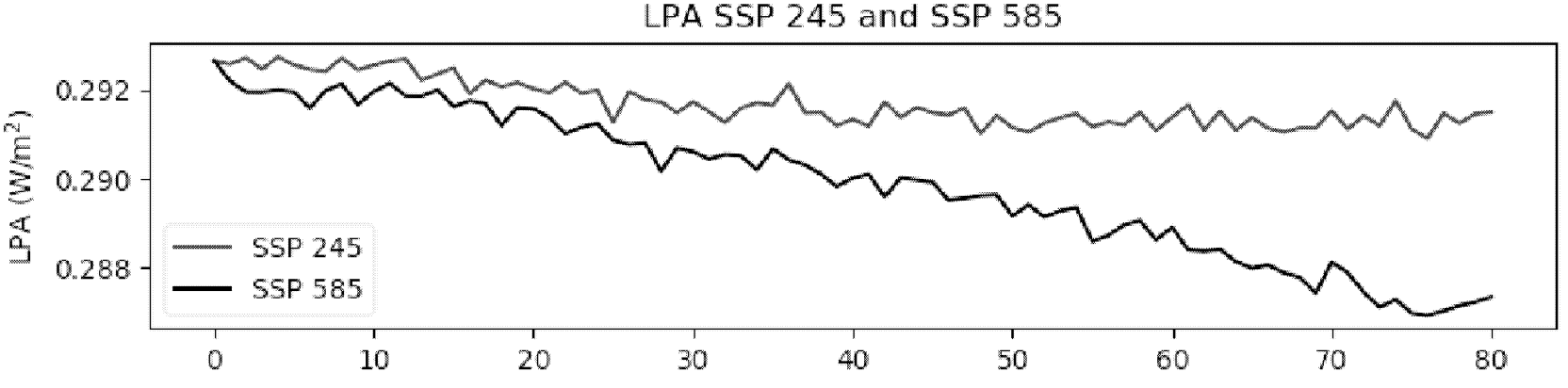

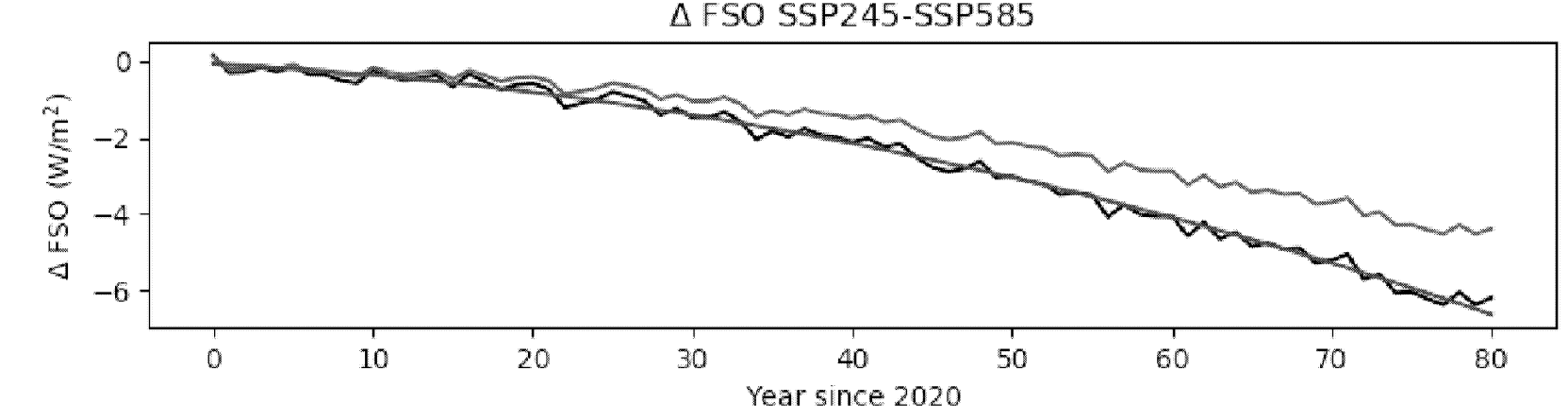

Comparing different generations of idealized solar geoengineering simulations in the Geoengineering Model Intercomparison Project (GeoMIP)

Ben Kravitz[1,2], Douglas G. MacMartin[3], Daniele Visioni[3], Olivier Boucher[4], Jason N. S. Cole[5], Jim Haywood[6,7], Andy Jones[7], Thibaut Lurton[4], Pierre Nabat[8], Ulrike Niemeier[9], Alan Robock[10], Roland Séférian[8], and Simone Tilmes[11]

[1]Department of Earth and Atmospheric Sciences, Indiana University, Bloomington, IN, USA
[2]Atmospheric Sciences and Global Change Division, Pacific Northwest National Laboratory, Richland, WA, USA
[3]Sibley School of Mechanical and Aerospace Engineering, Cornell University, Ithaca, NY, USA
[4]Institut Pierre-Simon Laplace (IPSL), Sorbonne Université/CNRS, Paris, France
[5]Environment and Climate Change Canada, Toronto, Ontario, Canada
[6]College of Engineering, Mathematics and Physical Sciences, University of Exeter, Exeter, United Kingdom
[7]UK Met Office Hadley Centre, Exeter, United Kingdom
[8]CNRM, Université de Toulouse, Météo-France, CNRS, Météo-France, Toulouse, France
[9]Max Planck Institute for Meteorology, Hamburg, Germany
[10]Department of Environmental Sciences, Rutgers University, New Brunswick, NJ, USA
[11]Atmospheric Chemistry Observations and Modeling Laboratory, National Center for Atmospheric Research, Boulder, CO, USA

Correspondence: Ben Kravitz, 1001 E. 10th Street, Bloomington, IN 47405-1405, USA. (bkravitz@iu.edu)

Abstract. Solar geoengineering has been receiving increased attention in recent years as a potential temporary solution to offset global warming. One method of approximating global-scale solar geoengineering in climate models is via solar reduction experiments. Two generations of models in the Geoengineering Model Intercomparison Project (GeoMIP) have now simulated offsetting a quadrupling of the CO_2 concentration with solar reduction. This simulation is ~~artificial~~ idealized and designed to elicit large responses in the models. Here we show that energetics, temperature, and hydrological cycle changes in this experiment are statistically indistinguishable between the two ensembles. Of the variables analyzed here, the only major differences involve highly parameterized and uncertain processes, such as cloud forcing or terrestrial net primary productivity. We conclude that despite numerous structural differences and uncertainties in models over the past 20 years, including an increase in climate sensitivity in the latest generation of models, broad conclusions about the climate response to global solar dimming remain robust.

1 Introduction

Solar geoengineering describes a set of technologies designed to (ideally) temporarily, deliberately reduce some of the effects of climate change by changing the radiative balance of the planet, often by reflecting sunlight back to space (NRC, 2015). Numerous methods have been proposed, but the most studied is stratospheric sulfate aerosol injection (Budyko, 1977; Crutzen, 2006). This method involves substantially increasing the stratospheric sulfate aerosol burden, replicating the mechanisms that cause cooling after large volcanic eruptions (Robock, 2000). Climate models ~~remain the most promising~~ are currently the only tools for understanding the climatic consequences of solar geoengineering. In model simulations of solar geoengineering, insolation reduction is often used as a proxy for actual stratospheric sulfate aerosols, as it captures many of the broad radiative effects of stratospheric aerosol geoengineering as well as some of the important climate effects like surface cooling and hydrological cycle strength reduction (Niemeier et al., 2013; Kalidindi et al., 2015). However, stratospheric sulfate aerosols also absorb longwave radiative flux, which heats the upper troposphere and lower stratosphere. As such, any implementation of stratospheric geoengineering with sulfate aerosols would produce additional effects, such as changing atmospheric circulation in response to stratospheric heating and heating gradients (e.g., Richter et al., 2017; Tilmes et al., 2018; Simpson et al., 2019) and stratospheric ozone changes (e.g., Pitari et al., 2014), as well as changes in ultraviolet radiative flux and enhanced diffuse radiation at the surface (Madronich et al., 2018). However, here we consider the major, large-scale effect of reflecting sunlight to cool Earth.

Simulations of solar geoengineering with solar reduction have long shown that solar geoengineering would cool the planet, offsetting global warming (e.g., Govindasamy and Caldeira, 2000; NRC, 2015; Irvine et al., 2016). Idealized simulations of solar reduction have also been simulated in a multi-model context under the Geoengineering Model Intercomparison Project (GeoMIP; Kravitz et al., 2011), to understand the robust model responses to various standardized solar geoengineering simulation designs. Multi-model conclusions from these studies indicate that solar geoengineering would be effective at partially offsetting greenhouse gas-induced temperature changes (Kravitz et al., 2013), as well as changes in the hydrological cycle (Tilmes et al., 2013), the cryosphere (Moore et al., 2014), extreme events (Curry et al., 2014; Aswathy et al., 2015), vegetation (Glienke et al., 2015), circulation (Guo et al., 2018; Gertler et al., 2020), ~~agriculture~~ agricultural yield potential (Xia et al., 2014), and numerous other areas. However, the offset is not ~~perfect~~ exact (Moreno-Cruz et al., 2012), particularly on a regional basis or when considering multiple simultaneous metrics of climate change (Kravitz et al., 2014; Irvine et al., 2019), leading to concerns about winners and losers from geoengineering (Ricke et al., 2010). To some extent, the effects of solar geoengineering may be tailored or designed (MacMartin et al., 2013; Kravitz et al., 2016, 2017, 2019), but solar geoengineering will still not be able to ~~perfectly~~ completely offset climate change from greenhouse gases.

The previous phase of GeoMIP was associated with the Coupled Model Intercomparison Project Phase 5 (CMIP5; Taylor et al., 2012), an international collaboration of climate models to attempt to understand robust model responses to various forcings. GeoMIP has now entered a new phase, concurrent with the Coupled Model Intercomparison Project Phase 6 (CMIP6; Eyring et al., 2016), and with it are new solar geoengineering simulations with new and updated versions of the participating Earth System Models (Kravitz et al., 2015). As such, this is an opportunity to revisit some central questions in solar geo-

engineering. Many of the CMIP5 results regarding solar geoengineering showed substantial agreement across the participating GeoMIP models. In this newest iteration of GeoMIP, do the same science conclusions still hold, and do the models still generally agree on the resulting climate effects? Here we address these questions by evaluating and comparing general climate model response to GeoMIP experiment G1 (described in the next section) from both CMIP5 and CMIP6.

2 Simulations and Participating Models

In this study, we evaluate GeoMIP experiment G1, in which, starting from a preindustrial control (piControl) baseline, the atmospheric CO_2 concentration is instantaneously quadrupled (the standard CMIP experiment abrupt4xCO2), and insolation is simultaneously reduced such that net top-of-atmosphere (TOA) radiative flux is ~~approximately unchanged from the baseline~~ within ± 0.1 W m^{-2} of the baseline value in the first decade of simulation (Kravitz et al., 2011, 2015). This experiment was part of the original suite of GeoMIP experiments and was repeated and extended in the newest suite in an effort to understand the role of model structural uncertainty in broad conclusions about solar geoengineering. Participating models are listed in Table 1. We include 13 models from CMIP5 and 7 models from CMIP6. Experiment G1 is an idealized experiment aimed at understanding physical climate response, with limited policy relevance.

The original G1 experiment was 50 years in length, whereas the CMIP6 version is 100 years in length to allow for better analyses of rare events ~~or~~ and to capture very slow responses. Comparison between the two ensembles necessitates only using the first 50 years, but we need to verify that this can be done without losing important longer-term evolution in features. Figures 1 and 2 look at G1 behavior over the entire 100-year period of the CMIP6 simulations to determine whether there is any drift or trend that would not be revealed by only analyzing the first 50 years. ~~With the exception of~~ (Also see Table 2 for quantitative information.) CNRM-ESM2.1 and IPSL-CM6A-LR ~~, no model shows any long-term behavior in temperature. Two models (IPSL-CM6A-LR~~ show appreciable (greater than 0.1 K/decade in magnitude) negative trends in temperature, and ~~GISS-E2~~CESM2(WACCM) and UKESM1.0-LL show appreciable positive trends. This is despite no model showing a trend in net TOA radiative flux greater in magnitude than 0.02 W m^{-2}/decade. Beyond an initial transient period, CESM2(WACCM), CNRM-ESM2.1 ~~G)show a slight trend~~ , and IPSL-CM6A-LR show appreciable (approximately 0.06%/decade) trends in precipitation and evaporation ~~, with a change of <1% over the first 50 years of simulation~~of the same sign as the temperature trends. Nevertheless, these trends are orders of magnitude lower than the changes in these variables in experiment G1 as compared to piControl (Figure 1). As such, we conclude that our choice to focus on the first 50 years of simulation does not appreciably affect our results.

Figure 2 ~~indicates that the temperature trend in IPSL-CM6A-LR is due to temperature changes~~ shows relatively flat lines for the 90°S-30°S and 30°S-30°N regions, whereas this is not the case for the region north of 30°N. In this region, CESM2(WACCM), CNRM-ESM2.1, IPSL-CM6A-LR, and UKESM1.0-LL have some time-varying behavior, indicating that the temperature changes are possibly related to a slight trend in sea ice coverage (Boucher et al., 2020). ~~This model~~

IPSL-CM6A-LR is also known to have a bicentennial oscillation, which could affect G1–piControl differences, depending on the baseline period used for subtraction. To verify that this oscillation is not impacting our results, we divided that model's

1200-year piControl run into 50-year chunks and computed the surface air temperature average for each of those chunks. The largest temperature found was 286.0339 K, and the smallest was 285.6384 K. The average over the entire ensemble was 285.8604 K. As such, using the mean of the entire ensemble versus matching the appropriate period in the bicentennial oscillation would have an impact on G1–piControl temperature by at most 0.22 K. Only averaging the first 100 years of the piControl run (which may be the best match to the period covered by G1) yields a temperature of 285.9084 K, which is 0.048 K different from the mean of the entire piControl run. As such, we conclude that this bicentennial oscillation is unlikely to have substantially influenced our findings.

Per the results in Figure 1, IPSL-CM6A-LR and GISS-E2.1-G appear to have a different responsiveness of the hydrological cycle to the combined CO_2-solar forcing than the other models. We are reluctant to attribute this feature to any potential shortcomings or lack of fidelity to observations because there are no observations of this type of experiment. Although these models are outliers, there is no evidential basis on which to assume they are more or less valid than the other models for this study.

Because the main focus of this paper is a comparison between the CMIP5 and CMIP6 generations of model results, we have opted for the following to aid comparisons:

- Since we are not evaluating any features that require 100 years of statistics, and the results do not show any appreciable time evolution of behavior after the first couple of years (see discussion above), we only evaluate the first 50 years of all simulations. All maps show changes over years 11-50, removing the initial transient period.

- We do not compare previous versions of individual models with current ones, instead only examining ensembles. Even though models may share similar development histories (e.g., atmosphere and ocean dynamical cores, convective parameterizations, radiative transfer modules, terrestrial biosphere and cryosphere; Knutti et al., 2013; Zelinka et al., 2020), there have been numerous developments in models in these areas (and others) between CMIP5 and CMIP6 such that in most cases a direct comparison would not be meaningful.

- We focus extensively on the G1 results and, with few exceptions, do not focus on the corresponding abrupt4xCO2 simulations. It has been well documented that the CMIP6 models tend to have higher climate sensitivities than the CMIP5 models (Flynn and Mauritsen, 2020; Meehl et al., 2020; Zelinka et al., 2020), so we do not wish to make conclusions that might be based on a form of selection bias.

- All lack of stippling on map plots, as in previous GeoMIP studies (e.g., Kravitz et al., 2013), indicates agreement on the sign of the response in at least 75% of models. Because $G1_{CMIP5}$ has more participating models than $G1_{CMIP6}$, this threshold provides some consistency across analyses of the ensembles. When plotting differences between the ensembles ($G1_{CMIP6}$–$G1_{CMIP5}$), there is no stippling, as it is difficult to meaningfully represent such differences between ranges. Aggregate differences between the two ensembles, as calculated using Welch's t-test or differences in stippled area, are discussed in Table 3.

3 Results

3.1 Energetics

Ensemble mean radiative and turbulent flux quantities are plotted in Figure 3, and the ensemble ranges are plotted in Figure 4. An immediate observation is that, in both ensembles, the models were successful at limiting net TOA radiative flux change to within approximately ± 0.1 W m^{-2} of the models' respective preindustrial values. Accomplishing this required an average solar reduction of 4.14% (models range in 3.20–5.00%) in CMIP5 and 4.14% (3.72–4.91%) in CMIP6. As such, despite numerous structural changes between the two generations of models, there is no appreciable change in solar efficacy (Hansen et al., 2005).

None of the radiative flux quantities indicate large transients over 50 years of simulation of G1, other than the initial flux change within the first year or so of simulation. This is consistent with the "perpetual fast response" found by Kravitz et al. (2013b), in which because global mean temperature does not change appreciably over the course of the G1 simulation, climate feedbacks are not excited, and the internal state of the system (as measured by, for example, fluxes and hydrological cycle changes) similarly does not change. Ensemble mean fluxes show few differences (<1 W m^{-2} in magnitude) with the exception of shortwave cloud forcing, defined as all-sky minus clear-sky shortwave flux at the surface. On average, the CMIP6 ensemble has 3–4 W m^{-2} less shortwave cloud forcing than CMIP5. Neglecting some outliers, for each flux except shortwave (and hence total) cloud forcing, the median model in one ensemble is within the inter-quartile range of the other ensemble. This indicates that there are no major differences between the ensembles in how the models handle energy balance and energetics, with the exception of clouds, which is consistent with findings about CMIP6 (Zelinka et al., 2020). Moreover, it appears that most of the major differences in shortwave cloud forcing are due to outliers in each ensemble, positive for CMIP5 and negative for CMIP6. To further explore these potential differences, Figure 5 provides maps of the ensemble means for cloud forcing. In G1, the CMIP5 ensemble showed more positive shortwave cloud forcing and more negative longwave cloud forcing (i.e., more cancellation) than the CMIP6 ensemble. Overall, the CMIP6 ensemble has greatly reduced (in some places by over 10 W m^{-2}) shortwave cloud forcing as compared to CMIP5 under the G1 experiment. This is a widespread result, but the most prominent features are in the tropics, especially over the Amazon, Africa, and the Maritime Continent. These regions encompass tropical forests, indicating a potential for vegetation feedbacks on the temperature reductions. However, the reasons behind these forcing changes are difficult to diagnose, as they could be due to changes in cloud thickness, cloud cover, or cloud level between CMIP5 and CMIP6 models (e.g., Vignesh et al., 2020), differences in how solar geoengineering affects clouds (Russotto and Ackerman, 2018), or artifacts of the analyses (e.g., cloud masking; Andrews et al., 2009; Kravitz et al., 2013b). Moreover, based on the results in Figure 4, it is likely that many of these features are exaggerated by outlier models (also see Vignesh et al., 2020). As such, we reserve such detailed investigations for future work.

3.2 Temperature

These small flux changes also lead to few G1 temperature changes between the two ensembles. Figure 6 shows global, land, and ocean-averaged temperatures for the CMIP5 and CMIP6 ensembles. In general, the abrupt4xCO2 simulation in CMIP6 has higher temperatures than in CMIP5, consistent with the noted increase in climate sensitivity (Vial et al., 2013; Flynn

and Mauritsen, 2020; Meehl et al., 2020; Zelinka et al., 2020). In both ensembles, G1 is effective at offsetting global mean temperature change, in some cases with a slight positive residual temperature change over land. Figure 7 shows three aggregate temperature metrics: global mean temperature (T_0), the interhemispheric temperature gradient (T_1), and the equator-to-pole temperature gradient (T_2) (Ban-Weiss and Caldeira, 2010; Kravitz et al., 2016):

$$T_0 = \frac{1}{A}\int_{-\pi/2}^{\pi/2} T(\psi)\,\mathrm{d}A$$
$$T_1 = \frac{1}{A}\int_{-\pi/2}^{\pi/2} T(\psi)\sin\psi\,\mathrm{d}A \quad (1)$$
$$T_2 = \frac{1}{A}\int_{-\pi/2}^{\pi/2} T(\psi)\frac{1}{2}(3\sin^2\psi - 1)\,\mathrm{d}A$$

where A is area. As for the fluxes, the median model in one ensemble is within the inter-quartile range of the other ensemble. This indicates that no ensemble is on average warmer or cooler than another, has a substantially warmer Northern or Southern Hemisphere than the other, ~~or~~ nor has warmer tropics or poles than the other. We can conclude that spatial patterns of temperature change from G1 are robust across a wide range of structural uncertainty, including an increase in climate sensitivity between the two generations of CMIP.

The spatial structure of temperature change (Figure 8) does have small differences between the two ensembles. G1 in CMIP6 has multiple locations that are warmer than G1 in CMIP5, despite both ensembles achieving net energy balance at TOA and the surface (Figure 3). The majority of the differences are over land and in the tropics, where CMIP6 is slightly warmer than CMIP5 (up to 1°C in some places). Nevertheless, both ensembles show the well noted feature that offsetting a CO_2 increase with globally uniform solar reduction overcools the tropics and undercools the poles (Govindasamy and Caldeira, 2000; Kravitz et al., 2013). CMIP6 shows slightly less high latitude warming than CMIP5, but temperature differences between the two ensembles are largely negligible. However, the warmer temperatures in CMIP6 near Greenland have important implications for ice sheet melt and consequent sea level rise, as well as bottom water formation. We reserve such analyses for future investigations, particularly since the models used here are not capable of simulating the eustatic component of sea level rise. In any case, these ensemble mean differences between CMIP5 and CMIP6 cannot be deemed statistically significant (Table 3 and Figure 7).

3.3 Hydrological and Other Integrative Changes

Figure 9 shows ensemble mean changes in precipitation (P), evaporation (E), and P–E for $\mathrm{G1}_{\mathrm{CMIP5}}$ and $\mathrm{G1}_{\mathrm{CMIP6}}$. Qualitatively, patterns are similar between both ensembles. Precipitation is slightly (<0.3 mm/day in magnitude) different in the tropics between the two ensembles. The majority of those features can be summarized as a more southward Intertropical Convergence Zone (ITCZ), more precipitation in the South Pacific Convergence Zone, and less precipitation over Southeast Asia and the

Maritime Continent in $G1_{CMIP6}$. Evaporation in the two ensembles is nearly identical except for more evaporation in Amazonia and Australia in $G1_{CMIP6}$. As such, the net P–E change between the two ensembles strongly resembles the precipitation changes. Figure 10 shows that, like previous evaluations of ensemble ranges, the median model in one ensemble falls well within the interquartile range of the other ensemble for P, E, and P–E. As such, we cannot conclude any robust hydrological cycle changes between the two ensembles.

Figure 11 shows average (years 11–50) temperature change (with respect to piControl) plotted against average precipitation change for each model, as in Tilmes et al. (2013). Other than a potentially greater climate sensitivity of some CMIP6 models, there is no distinguishable difference in aggregate behavior between the two ensembles. The same conclusion discovered by Tilmes et al. (2013) holds: solar reduction cannot simultaneously offset CO_2-induced changes in both global mean temperature and global mean precipitation.

As an integrator of CO_2, temperature, and precipitation effects over land, Figure 12 shows changes in terrestrial net primary productivity (NPP). Numerous land regions have lower NPP in CMIP6 than in CMIP5. The ensemble average global NPP change (G1–piControl) is 51.2 (4.1–122.1) Pg C y^{-1} in CMIP5 and 38.1 (19.5–77.5) Pg C y^{-1} in CMIP6, representing a 25.6% difference in means. Jones et al. (2013) used NPP to highlight the importance of understanding the influence of structural land model differences on climate results related to geoengineering. While it is beyond the scope of this study to perform a detailed diagnosis of which uncertainties or processes are responsible for this inter-ensemble difference (and indeed the present setup does not allow for a controlled experiment to rigorously test structural uncertainty), we show that the ensemble spread of total terrestrial NPP is smaller in CMIP6 than in CMIP5. This result is consistent with the recent assessment of carbon cycle feedbacks conducted by Arora et al. (2020), ~~which demonstrates~~ who showed that the CMIP6 ensemble has reduced overall uncertainty in the land carbon cycle to rising CO_2 compared to their CMIP5 predecessors.

4 Discussion and Conclusions

Based on the results presented here, model response to G1 has not changed substantially between CMIP5 and CMIP6, despite numerous changes to models between the two generations, including an increase in climate sensitivity. The sign of residual climate impacts (for example in temperature) are in better agreement in CMIP5 than CMIP6 (Table 3 shows a difference in stippled area between the two ensembles), but this could be a function of the smaller ensemble size in CMIP6. Energetics, temperature, and the hydrological cycle are qualitatively and quantitatively similar in both ensemble means and ensemble ranges, although these variables are somewhat related, so we might expect them to all portray a similar picture. Notable differences do exist in shortwave cloud forcing and NPP, particularly in Amazonia, Africa, and Australia, which are also regions of inter-ensemble difference in precipitation.

From these findings, we can conclude that results obtained over the past 20 years of study have not been overturned by the latest round of simulations. All of the major ensemble differences highlighted above deal with clouds and land surface modeling, both of which are difficult to model and are necessarily highly parameterized. The conclusions that are based on more fundamental knowledge, such as column energetics (in the case of the hydrological cycle), are relatively robust to structural

uncertainty, in so far as this study adequately captures representative variations in structural uncertainty. This lends confidence to our conclusions, especially regarding robustness to uncertainty, about the broad climate effects from solar geoengineering methods that can be accurately represented via solar dimming.

We also conclude that the models used in CMIP5 are not obviously biased or inferior as compared to CMIP6. While improvements have been made in the CMIP6 generation of models, and those models are likely better for representing numerous features of the present-day climate that may be important for studies of geoengineering, there are many aspects of climate that are well represented by earlier models. In some cases, more robust analyses may be enabled by augmenting ensemble sizes with archived output from earlier generations of CMIP models.

Many of the broad features of solar geoengineering with sulfate aerosols can be represented by a reduction in solar constant (e.g., Niemeier et al., 2013; Kalidindi et al., 2015). However, the more subtle changes that derive from complex response to stratospheric aerosol heating (for example, consequences of stratospheric heating like the positive wintertime North Atlantic Oscillation; Simpson et al., 2019) require detailed assessments with state-of-the-art aerosol microphysical schemes. This is particularly important for understanding regional and seasonal solar geoengineering (Kravitz et al., 2017; Visioni et al., 2019). Such detailed microphysical calculations can only be simulated in a small number of models. While simple G1-style experiments enable a robust multi-model ensemble analysis, they cannot capture details that depend on microphysics. We emphasize the importance of a variety of modeling approaches to understand solar geoengineering, particularly the role of model uncertainty in conclusions about solar geoengineering.

There are numerous aspects of physical climate that we did not evaluate, nor did we pursue analyses beyond physical climate, including many other aspects of natural science, social science, the humanities, governance, justice, or ethics (to name a few important areas). Moreover, we emphasize that experiment G1 is an idealized experiment aimed at understanding physical climate response to combinations of large forcings and should not be interpreted as a realistic or policy-relevant scenario of geoengineering. A holistic assessment of the consequences of geoengineering, particularly of more policy-relevant scenarios, would certainly need to take these numerous aspects into account. Nevertheless, based on the results presented here, results for geoengineering across several important metrics appear to be robust to some amount of structural uncertainty. This lends confidence to some conclusions drawn from global climate models regarding solar geoengineering.

Data availability. All CMIP5 and CMIP6 output, including the respective GeoMIP simulations, is available via the Earth System Grid Federation (https://esgf-node.llnl.gov/projects/esgf-llnl/) or by contacting the respective modeling groups responsible for the output. For CMIP6 output, seeTable 1 data citations.

Author contributions. BK, OB, JNSC, JH, AJ, TL, PN, UN, RS, and ST contributed model output. BK performed the analysis. BK, DGM, and DV wrote the manuscript with all coauthors.

Competing interests. None.

Acknowledgements. We acknowledge the World Climate Research Programme, which, through its Working Group on Coupled Modelling, coordinated and promoted CMIP. We thank the climate modeling groups for producing and making available their model output, the Earth System Grid Federation (ESGF) for archiving the data and providing access, and the multiple funding agencies who support CMIP6 and ESGF. We also thank all participants of the Geoengineering Model Intercomparison Project and their model development teams. Support for B.K. was provided in part by the National Science Foundation (NSF) through agreement CBET-1931641, the Indiana University Environmental Resilience Institute, and the Prepared for Environmental Change Grand Challenge initiative. The Pacific Northwest National Laboratory is operated for the US Department of Energy by Battelle Memorial Institute under contract DE-AC05-76RL01830. Resources supporting this work were provided by the NASA High-End Computing (HEC) Program through the NASA Center for Climate Simulation (NCCS) at Goddard Space Flight Center. A.R. is supported by NSF grants AGS-1617844 and AGS-2017113. J.H. and A.J. were supported by the Met Office Hadley Centre Climate Programme funded by BEIS and Defra. U.N. is supported by the German DFG-funded Research Unit VolImpact FOR2820 sub project TI344/2-1 and MPIESM simulation have been performed on the computer of Deutsches Klimarechenzentrum (DKRZ). O.B. and T.L. were supported by the IPSL Climate Graduate School EUR (ANR grant ANR-11-IDEX-0004 - 17-EURE-0006). The CMIP6 project at IPSL used the HPC resources of TGCC under the allocations 2016-A0030107732, 2017-R0040110492 and 2018-R0040110492 (project gencmip6) provided by GENCI (Grand Équipement National de Calcul Intensif). R.S. and P.N. were supported by the H2020 CONSTRAIN under the grant agreement No 820829 and the Météo-France/DSI supercomputing center.

References

Alterskjær, K., Kristjánsson, J. E., and Seland, Ø.: Sensitivity to deliberate sea salt seeding of marine clouds – Observations and model simulations, Atmos. Chem. Phys., 12, 2795–2807, https://doi.org/10.5194/acp-12- 2795-2012, 2012.

Andrews, T., Forster, P. M., and Gregory, J. M.: A surface energy perspective on climate change, J. Clim., 22, 2557–2570, https://doi.org/10.1175/2008JCLI2759.1, 2009.

Arora, V. K., Scinocca, J. F., Boer, G. J., Christian, J. R., Denman, K. L., Flato, G. M., Kharin, V. V., Lee, W. G., and Merryfield, W. J.: Carbon emission limits required to satisfy future representative concentration pathways of greenhouse gases, Geophys. Res. Lett., 38, L05 805, https://doi.org/10.1029/2010GL046270, 2011.

Arora, V. K., Katavouta, A., Williams, R. G., Jones, C. D., Brovkin, V., Friedlingstein, P., Schwinger, J., Bopp, L., Boucher, O., Cadule, P., Chamberlain, M. A., Christian, J. R., Delire, C., Fisher, R. A., Hajima, T., Ilyina, T., Joetzjer, E., Kawamiya, M., Koven, C., Krasting, J., Law, R. M., Lawrence, D. M., Lenton, A., Lindsay, K., Pongratz, J., Raddatz, T., Séférian, R., Tachiiri, K., Tjiputra, J. F., Wiltshire, A., Wu, T., and Ziehn, T.: Carbon-concentration and carbon-climate feedbacks in CMIP6 models, and their comparison to CMIP5 models, Biogeosciences, p. in press, 2020.

Aswathy, V. N., Boucher, O., Quaas, M., Niemeier, U., Muri, H., Mülmenstädt, J., and Quaas, J.: Climate extremes in multi-model simulations of stratospheric aerosol and marine cloud brightening climate engineering, Atmospheric Chemistry and Physics, 15, 9593–9610, https://doi.org/10.5194/acp-15-9593-2015, 2015.

Ban-Weiss, G. A. and Caldeira, K.: Geoengineering as an optimization problem, Environ. Res. Lett., 5, 031 001, https://doi.org/10.1088/1748-9326/5/3/034009, 2010.

Boucher, O., Denvil, S., Caubel, A., and Foujols, M. A.: IPSL IPSL-CM6A-LR model output prepared for CMIP6 GeoMIP G1, Earth System Grid Federation, https://doi.org/10.22033/ESGF/CMIP6.5054, 2018a.

Boucher, O., Denvil, S., Caubel, A., and Foujols, M. A.: IPSL IPSL-CM6A-LR model output prepared for CMIP6 CMIP abrupt-4xCO2, Earth System Grid Federation, https://doi.org/10.22033/ESGF/CMIP6.5109, 2018b.

Boucher, O., Denvil, S., Caubel, A., and Foujols, M. A.: IPSL IPSL-CM6A-LR model output prepared for CMIP6 CMIP piControl, Earth System Grid Federation, https://doi.org/10.22033/ESGF/CMIP6.5251, 2018c.

Boucher, O., Servonnat, J., Albright, A. L., Aumont, O., Balkanski, Y., Bastrikov, V., Bekki, S., Bonnet, R., Bony, S., Bopp, L., Braconnot, P., Brockmann, P., Cadule, P., Caubel, A., Cheruy, F., Codron, F., Cozic, A., Cugnet, D., D'Andrea, F., Davini, P., de Lavergne, C., Denvil, S., Deshayes, J., Devilliers, M., Ducharne, A., Dufresne, J.-L., Dupont, E., Éthé, C., Fairhead, L., Falletti, L., Flavoni, S., Foujols, M.-A., Gardoll, S., Gastineau, G., Ghattas, J., Grandpeix, J.-Y., Guenet, B., Guez, L., Guilyardi, E., Guimberteau, M., Hauglustaine, D., Hourdin, F., Idelkadi, A., Joussaume, S., Kageyama, M., Khodri, M., Krinner, G., Lebas, N., Levavasseur, G., Lévy, C., Li, L., Lott, F., Lurton, T., Luyssaert, S., Madec, G., Madeleine, J.-B., Maignan, F., Marchand, M., Marti, O., Mellul, L., Meurdesoif, Y., Mignot, J., Musat, I., Ottlé, C., Peylin, P., Planton, Y., Polcher, J., Rio, C., Rochetin, N., Rousset, C., Sepulchre, P., Sima, A., Swingedouw, D., Thiéblemont, R., Traore, A. K., Vancoppenolle, M., Vial, J., Vialard, J., Viovy, N., and Vuichard, N.: Presentation and evaluation of the IPSL-CM6A-LR climate model, Journal of Advances in Modeling Earth Systems, in press, e2019MS002 010, https://doi.org/10.1029/2019MS002010, 2020.

Budyko, M. I.: Climatic Changes, American Geophysical Union, 1977.

Cole, J. N., Swart, N. C., Kharin, V. V., Lazare, M., Scinocca, J. F., Gillett, N. P., Anstey, J., Arora, V., Christian, J. R., Jiao, Y., Lee, W. G., Majaess, F., Saenko, O. A., Seiler, C., Seinen, C., Shao, A., Solheim, L., von Salzen, K., Yang, D., Winter, B., and Sigmond, M.: CCCma

CanESM5 model output prepared for CMIP6 GeoMIP G1, Earth System Grid Federation, https://doi.org/10.22033/ESGF/CMIP6.3158, 2019.

Collins, W. J., Bellouin, N., Doutriaux-Boucher, M., Gedney, N., Halloran, P., Hinton, T., Hughes, J., Jones, C. D., Joshi, M., Liddicoat, S., Martin, G., O'Connor, F., Rae, J., Senior, C., Sitch, S., Totterdell, I., Wiltshire, A., and Woodward, S.: Development and evaluation of an Earth-System model—HadGEM2, Geosci. Model Dev., 4, 1051–1075, https://doi.org/10.5194/gmd-4-1051-2011, 2011.

Crutzen, P. J.: Albedo enhancement by stratospheric sulfur injections: A contribution to resolve a policy dilemma?, Climatic Change, 77, 211–220, https://doi.org/10.1007/s10584-006-9101-y, 2006.

Curry, C. L., Sillmann, J., Bronaugh, D., Alterskjær, K., Cole, J. N. S., Kravitz., B., Kristjánsson, J. E., Muri, H., Niemeier, U., Robock, A., and Tilmes, S.: A multi-model examination of climate extremes in an idealized geoengineering experiment, J. Geophys. Res., 119, 3900–3923, https://doi.org/10.1002/2013JD020648, 2014.

Danabasoglu, G.: NCAR CESM2-WACCM model output prepared for CMIP6 GeoMIP G1, Earth System Grid Federation, https://doi.org/10.22033/ESGF/CMIP6.10029, 2019a.

Danabasoglu, G.: NCAR CESM2-WACCM model output prepared for CMIP6 CMIP abrupt-4xCO2, Earth System Grid Federation, https://doi.org/10.22033/ESGF/CMIP6.10039, 2019b.

Danabasoglu, G.: NCAR CESM2-WACCM-FV2 model output prepared for CMIP6 CMIP piControl, Earth System Grid Federation, https://doi.org/10.22033/ESGF/CMIP6.11302, 2019c.

Dufresne, J.-L., Foujols, M.-A., Denvil, S., Caubel, A., Marti, O., Aumont, O., Balkanski, Y., Bekki, S., Bellenger, H., Benshila, R., Bony, S., Bopp, L., Braconnot, P., Brockmann, P., Cadule, P., Cheruy, F., Codron, F., Cozic, A., Cugnet, D., de Noblet, N., Duvel, J.-P., Ethé, C., Fairhead, L., Fichefet, T., Flavoni, S., Friedlingstein, P., Grandpeix, J.-Y., Guez, L., Guilyardi, E., Hauglustaine, D., Hourdin, F., Idelkadi, A., Ghattas, J., Joussaume, S., Kageyama, M., Krinner, G., Labetoulle, S., Lahellec, A., Lefebvre, M.-P., Lefevre, F., Levy, C., Li, Z. X., Lloyd, J., Lott, F., Madec, G., Mancip, M., Marchand, M., Masson, S., Meurdesoif, Y., Mignot, J., Musat, I., Parouty, S., Polcher, J., Rio, C., Schulz, M., Swingedouw, D., Szopa, S., Talandier, C., Terray, P., Viovy, N., and Vuichard, N.: Climate change projections using the IPSL-CM5 Earth System Model: From CMIP3 to CMIP5, Clim. Dynam., 40, 2123–2165, https://doi.org/10.1007/s00382-012-1636-1, 2013.

Eyring, V., Bony, S., Meehl, G. A., Senior, C. A., Stevens, B., Stouffer, R. J., and Taylor, K. E.: Overview of the Coupled Model Intercomparison Project Phase 6 (CMIP6) experimental design and organization, Geosci. Model Dev., 9, 1937–1958, https://doi.org/10.5194/gmd-9-1937-2016, 2016.

Flynn, C. M. and Mauritsen, T.: On the climate sensitivity and historical warming evolution in recent coupled model ensembles, Atmospheric Chemistry and Physics, 20, 7829–7842, https://doi.org/10.5194/acp-20-7829-2020, https://www.atmos-chem-phys.net/20/7829/2020/, 2020.

Gent, P. R., Danabasoglu, G., Donner, L. J., Holland, M. M., Hunke, E. C., Jayne, S. R., Lawrence, D. M., Neale, R. B., Rasch, P. J., Vertenstein, M., Worley, P. H., Yang, Z.-L., and Zhang, M.: The Community Climate System Model Version 4, Journal of Climate, 24, 4973–4991, https://doi.org/10.1175/2011JCLI4083.1, 2011.

Gertler, C. G., O'Gorman, P. A., Kravitz, B., Moore, J. C., Phipps, S. J., and Watanabe, S.: Weakening of the extratropical storm tracks in solar geoengineering scenarios, Geophys. Res. Lett., 47, e2020GL087348, https://doi.org/10.1029/2020GL087348, 2020.

Gettelman, A., Mills, M. J., Kinnison, D. E., Garcia, R. R., Smith, A. K., Marsh, D. R., Tilmes, S., Vitt, F., Bardeen, C. G., McInerny, J., Liu, H.-L., Solomon, S. C., Polvani, L. M., Emmons, L. K., Lamarque, J.-F., Richter, J. H., Glanville, A. S., Bacmeister, J. T., Phillips, A. S.,

Neale, R. B., Simpson, I. R., DuVivier, A. K., Hodzic, A., and Randel, W. J.: The Whole Atmosphere Community Climate Model Version 6 (WACCM6), Journal of Geophysical Research: Atmospheres, 124, 12 380–12 403, https://doi.org/10.1029/2019JD030943, 2019.

Giorgetta, M. A., Jungclaus, J., Reick, C. H., Legutke, S., Bader, J., Böttinger, M., Brovkin, V., Crueger, T., Esch, M., Fieg, K., Glushak, K., Gayler, V., Haak, H., Hollweg, H.-D., Ilyina, T., Kinne, S., Kornblueh, L., Matei, D., Mauritsen, T., Mikolajewicz, U., Mueller, W., Notz, D., Pithan, F., Raddatz, T., Rast, S., Redler, R., Roeckner, E., Schmidt, H., Schnur, R., Segschneider, J., Six, K. D., Stockhause, M., Timmreck, C., Wegner, J., Widmann, H., Wieners, K.-H., Claussen, M., Marotzke, J., and Stevens, B.: Climate and carbon cycle changes from 1850 to 2100 in MPI-ESM simulations for the Coupled Model Intercomparison Project Phase 5, J. Adv. Model. Earth Syst., 5, 572–597, https://doi.org/10.1002/jame.20038, 2013.

Glienke, S., Irvine, P. J., and Lawrence, M. G.: The impact of geoengineering on vegetation in experiment G1 of the GeoMIP, J. Geophys. Res., 120, 10 196–10 213, https://doi.org/10.1002/2015JD024202, 2015.

Gordon, C., Cooper, C., Senior, C. A., Banks, H., Gregory, J. M., Johns, T. C., Mitchell, J. F. B., and Wood, R. A.: The simulation of SST, sea ice extents and ocean heat transports in a version of the Hadley Centre coupled model without flux adjustments, Clim. Dyn., 16, 147–168, https://doi.org/10.1007/s003820050010, 2000.

Govindasamy, B. and Caldeira, K.: Geoengineering Earth's radiation balance to mitigate CO_2-induced climate change, Geophys. Res. Lett., 27, 2141–2144, https://doi.org/10.1029/1999GL006086, 2000.

Guo, A., Moore, J. C., and Ji, D.: Tropical atmospheric circulation response to the G1 sunshade geoengineering radiative forcing experiment, Atmospheric Chemistry and Physics, 18, 8689–8706, https://doi.org/10.5194/acp-2018-8689, 2018.

Hansen, J., Sato, M., Ruedy, R., Nazarenko, L., Lacis, A., Schmidt, G. A., Russell, G., Aleinov, I., Bauer, M., Bauer, S., Bell, N., Cairns, B., Canuto, V., Chandler, M., Cheng, Y., Del Genio, A., Faluvegi, G., Fleming, E., Friend, A., Hall, T., Jackman, C., Kelley, M., Kiang, N., Koch, D., Lean, J., Lerner, J., Lo, K., Menon, S., Miller, R., Minnis, P., Novakov, T., Oinas, V., Perlwitz, J., Perlwitz, J., Rind, D., Romanou, A., Shindell, D., Stone, P., Sun, S., Tausnev, N., Thresher, D., Wielicki, B., Wong, T., Yaho, M., and Zhang, S.: Efficacy of Climate Forcings, J. Geophys. Res., 110, D18 104, https://doi.org/10.1029/2005JD005776, 2005.

Hazeleger, W., Wang, X., Severijns, C., Ştefănescu, S., Bintanja, R., Sterl, A., Wyser, K., Semmler, T., Yang, S., van den Hurk, B., van Noije, T., van der Linden, E., and van der Wiel, K.: EC-Earth V2.2: Description and validation of a new seamless Earth system prediction model, Clim. Dynam., 39, 2611–2629, https://doi.org/10.1007/s00382-011-1228-5, 2011.

Hourdin, F., Foujols, M.-A., Codron, F., Guemas, V., Dufresne, J.-L., Bony, S., Denvil, S., Guez, L., Lott, F., Ghattas, J., Braconnot, P., Marti, O., Meurdesoif, Y., and Bopp, L.: Impact of the LMDZ atmospheric grid configuration on the climate and sensitivity of the IPSL-CM5A coupled model, Clim. Dyn., 40, 2167–2192, https://doi.org/10.1007/s00382-012-1411-3, 2012.

Hurrell, J. W., Holland, M. M., Gent, P. R., Ghan, S., Kay, J. E., Kushner, P. J., Lamarque, J.-F., Large, W. G., Lawrence, D., Lindsay, K., Lipscomb, W. H., Long, M. C., Mahowald, N., Marsh, D. R., Neale, R. B., Rasch, P., Vavrus, S., Vertenstein, M., Bader, D., Collins, W. D., Hack, J. J., Kiehl, J., , and Marshall, S.: The Community Earth System Model: A Framework for Collaborative Research, Bull. Amer. Meteor. Soc., 94, 1339–1360, https://doi.org/10.1175/BAMS-D-12-00121.1, 2013.

Irvine, P., Emmanuel, K., He, J., Horowitz, L. W., Vecchi, G., and Keith, D.: Halving warming with idealized solar geoengineering moderates key climate hazards, Nature Climate Change, 9, 295–299, 2019.

Irvine, P. J., Kravitz, B., Lawrence, M. G., and Muri, H.: An overview of the Earth system science of solar geoengineering, WIREs Climate Change, 7, 815–833, https://doi.org/10.1002/wcc.423, 2016.

Ji, D., Wang, L., Feng, J., Wu, Q., Cheng, H., Zhang, Q., Yang, J., Dong, W., Dai, Y., Gong, D., Zhang, R.-H., Wang, X., Liu, J., Moore, J. C., Chen, D., and Zhou, M.: Description and basic evaluation of Beijing Normal University Earth System Model (BNU-ESM) version 1, Geosci. Model. Dev., 7, 2039–2064, https://doi.org/10.5194/gmd-7-2039-2014, 2014.

Jones, A.: MOHC UKESM1.0-LL model output prepared for CMIP6 GeoMIP G1, Earth System Grid Federation, https://doi.org/10.22033/ESGF/CMIP6.5812, 2019.

Jones, A., Haywood, J. M., Alterskjær, K., Boucher, O., Cole, J. N. S., J., C. L. C. P., Irvine, Ji, D., Kravitz, B., Moore, J. E. K. J. C., Niemeier, U., Robock, A., Schmidt, H., Singh, B., Tilmes, S., Watanabe, S., and Yoon, J.-H.: The impact of abrupt suspension of solar radiation management (termination effect) in experiment G2 of the Geoengineering Model Intercomparison Project (GeoMIP), Journal of Geophysical Research: Atmospheres, 118, 9743–9752, https://doi.org/10.1002/jgrd.50762, 2013.

Kalidindi, S., Bala, G., Modak, A., and Caldeira, K.: Modeling of solar radiation management: A comparison of simulations using reduced solar constant and stratospheric sulfate aerosols, Clim. Dynam., 44, 2909–2925, https://doi.org/10.1007/s00382-014-2240-3, 2015.

Kelley, M., Schmidt, G. A., Nazarenko, L. S., Bauer, S. E., Ruedy, R., Russell, G. L., Ackerman, A. S., Aleinov, I., Bauer, M., Bleck, R., Canuto, V., Cesana, G., Cheng, Y., Clune, T. L., Cook, B. I., Cruz, C. A., Del Genio, A. D., Elsaesser, G. S., Faluvegi, G., Kiang, N. Y., Kim, D., Lacis, A. A., Leboissetier, A., LeGrande, A. N., Lo, K. K., Marshall, J., Matthews, E. E., McDermid, S., Mezuman, K., Miller, R. L., Murray, L. T., Oinas, V., Orbe, C., Pérez García-Pando, C., Perlwitz, J. P., Puma, M. J., Rind, D., Romanou, A., Shindell, D. T., Sun, S., Tausnev, N., Tsigaridis, K., Tselioudis, G., Weng, E., Wu, J., and Yao, M.-S.: GISS-E2.1: Configurations and Climatology, Journal of Advances in Modeling Earth Systems, in press, e2019MS002 025, https://doi.org/10.1029/2019MS002025, 2020.

Kirkevåg, A., Iversen, T., Seland, Ø., Hoose, C., Kristjánsson, J. E., Struthers, H., Ekman, A. M. L., Ghan, S., Griesfeller, J., Nilsson, E. D., and Schulz, M.: Aerosol–climate interactions in the Norwegian Earth System Model – NorESM1-M, Geoscientific Model Development, 6, 207–244, https://doi.org/10.5194/gmd-6-207-2013, https://gmd.copernicus.org/articles/6/207/2013/, 2013.

Knutti, R., Masson, D., and Gettelman, A.: Climate model genealogy: Generation CMIP5 and how we got there, Geophys. Res. Lett., 40, 1194–1199, https://doi.org/10.1002/grl.50256, 2013.

Kravitz, B., Robock, A., Boucher, O., Schmidt, H., Taylor, K. E., Stenchikov, G., and Schulz, M.: The Geoengineering Model Intercomparison Project (GeoMIP), Atmos. Sci. Lett., 12, 162–167, https://doi.org/10.1002/asl.316, 2011.

Kravitz, B., Caldeira, K., Boucher, O., Robock, A., Rasch, P. J., Alterskjær, K., Karam, D. B., Cole, J. N. S., Curry, C. L., Haywood, J. M., Irvine, P. J., Ji, D., Jones, A., Kristjánsson, J. E., Lunt, D. J., Moore, J., Niemeier, U., Schmidt, H., Schulz, M., Singh, B., Tilmes, S., Watanabe, S., Yang, S., , and Yoon, J.-H.: Climate model response from the Geoengineering Model Intercomparison Project (GeoMIP), J. Geophys. Res., 118, 8320–8332, https://doi.org/10.1002/jgrd.50646, 2013.

Kravitz, B., Rasch, P. J., Forster, P. M., Andrews, T., Cole, J. N. S., Irvine, P. J., Ji, D., Kristjánsson, J. E., Moore, J. C., Muri, H., Niemeier, U., Robock, A., Singh, B., Tilmes, S., Watanabe, S., , and Yoon, J.-H.: An energetic perspective on hydrological cycle changes in the Geoengineering Model Intercomparison Project (GeoMIP), J. Geophys. Res., 118, 13 087–13 102, https://doi.org/10.1002/2013JD020502, 2013b.

Kravitz, B., MacMartin, D. G., Robock, A., Rasch, P. J., Ricke, K. L., Cole, J. N. S., Curry, C. L., Irvine, P. J., Ji, D., Keith, D. W., Kristjánsson, J. E., Moore, J. C., Muri, H., Singh, B., Tilmes, S., Watanabe, S., Yang, S., and Yoon, J.-H.: A multi-model assessment of regional climate disparities caused by solar geoengineering, Environ. Res. Lett., 9, 074 013, https://doi.org/10.1088/1748-9326/9/7/074013, 2014.

Kravitz, B., Robock, A., Tilmes, S., Boucher, O., English, J. M., Irvine, P. J., Jones, A., Lawrence, M. G., MacCracken, M., Muri, H., Moore, J. C., Niemeier, U., Phipps, S. J., Sillmann, J., Storelvmo, T., Wang, H., and Watanabe, S.: The Geoengineering Model Intercomparison

Project Phase 6 (GeoMIP6): Simulation design and preliminary results, Geosci. Model Dev., 8, 3379–3392, https://doi.org/10.5194/gmd-8-3379-2015, 2015.

Kravitz, B., MacMartin, D. G., Wang, H., and Rasch, P. J.: Geoengineering as a design problem, Earth System Dynamics, 7, 469–497, https://doi.org/10.5194/esd-469-2016, 2016.

Kravitz, B., MacMartin, D. G., Mills, M. J., Richter, J. H., Tilmes, S., Lamarque, J., Tribbia, J. J., and Vitt, F.: First Simulations of Designing Stratospheric Sulfate Aerosol Geoengineering to Meet Multiple Simultaneous Climate Objectives, J. Geophys. Res., 122, 12 616–12 634, https://doi.org/10.1002/2017JD026874, 2017.

Kravitz, B., MacMartin, D. G., Tilmes, S., Richter, J. H., Mills, M. J., Cheng, W., Dagon, K., Glanville, A. S., Lamarque, J.-F., Simpson, I., Tribbia, J., and Vitt, F.: Comparing surface and stratospheric impacts of geoengineering with different SO_2 injection strategies, J. Geophys. Res., 124, 7900–7918, https://doi.org/10.1029/2019JD030329, 2019.

Lurton, T., Balkanski, Y., Bastrikov, V., Bekki, S., Bopp, L., Braconnot, P., Brockmann, P., Cadule, P., Contoux, C., Cozic, A., Cugnet, D., Dufresne, J.-L., Éthé, C., Foujols, M.-A., Ghattas, J., Hauglustaine, D., Hu, R.-M., Kageyama, M., Khodri, M., Lebas, N., Levavasseur, G., Marchand, M., Ottlé, C., Peylin, P., Sima, A., Szopa, S., Thiéblemont, R., Vuichard, N., and Boucher, O.: Implementation of the CMIP6 Forcing Data in the IPSL-CM6A-LR Model, Journal of Advances in Modeling Earth Systems, 12, e2019MS001 940, https://doi.org/10.1029/2019MS001940, 2020.

MacMartin, D. G., Keith, D. W., Kravitz, B., and Caldeira, K.: Management of trade-offs in geoengineering through optimal choice of non-uniform radiative forcing, Nature Climate Change, 3, 365–368, https://doi.org/10.1038/nclimate1722, 2013.

Madronich, S., Tilmes, S., Kravitz, B., MacMartin, D. G., and Richter, J. H.: Response of surface ultraviolet and visible radiation to stratospheric SO_2 injection, Atmosphere, 9, 432, https://doi.org/10.3390/atmos9110432, 2018.

Mauritsen, T., Bader, J., Becker, T., Behrens, J., Bittner, M., Brokopf, R., Brovkin, V., Claussen, M., Crueger, T., Esch, M., Fast, I., Fiedler, S., Fläschner, D., Gayler, V., Giorgetta, M., Goll, D. S., Haak, H., Hagemann, S., Hedemann, C., Hohenegger, C., Ilyina, T., Jahns, T., Jimenéz-de-la Cuesta, D., Jungclaus, J., Kleinen, T., Kloster, S., Kracher, D., Kinne, S., Kleberg, D., Lasslop, G., Kornblueh, L., Marotzke, J., Matei, D., Meraner, K., Mikolajewicz, U., Modali, K., Möbis, B., Müller, W. A., Nabel, J. E. M. S., Nam, C. C. W., Notz, D., Nyawira, S.-S., Paulsen, H., Peters, K., Pincus, R., Pohlmann, H., Pongratz, J., Popp, M., Raddatz, T. J., Rast, S., Redler, R., Reick, C. H., Rohrschneider, T., Schemann, V., Schmidt, H., Schnur, R., Schulzweida, U., Six, K. D., Stein, L., Stemmler, I., Stevens, B., von Storch, J.-S., Tian, F., Voigt, A., Vrese, P., Wieners, K.-H., Wilkenskjeld, S., Winkler, A., and Roeckner, E.: Developments in the MPI-M Earth System Model version 1.2 (MPI-ESM1.2) and Its Response to Increasing CO_2, Journal of Advances in Modeling Earth Systems, 11, 998–1038, https://doi.org/10.1029/2018MS001400, 2019.

Meehl, G. A., Senior, C. A., Eyring, V., Flato, G., Lamarque, J.-F., Stouffer, R. J., Taylor, K. E., and Schlund, M.: Context for interpreting equilibrium climate sensitivity and transient climate response from the CMIP6 Earth system models, Science Advances, 6, eaba1981, https://doi.org/10.1126/sciadv.aba1981, 2020.

Moore, J. C., Rinke, A., Yu, X., Ji, D., Cui, X., Li, Y., Alterskjær, K., Kristjánsson, J. E., Boucher, O., Huneeus, N., Kravitz, B., Robock, A., Niemeier, U., Schmidt, H., Schulz, M., Tilmes, S., and Watanabe, S.: Arctic sea ice and atmospheric circulation under the GeoMIP G1 scenario, J. Geophys. Res., 119, 567–583, https://doi.org/10.1002/2013JD021060, 2014.

Moreno-Cruz, J. B., Ricke, K. L., and Keith, D. W.: A simple model to account for regional inequalities in the effectiveness of solar radiation management, Climatic Change, 110, 649–668, 2012.

NASA Goddard Institute for Space Studies (NASA/GISS): NASA-GISS GISS-E2.1G model output prepared for CMIP6 CMIP abrupt-4xCO2, Earth System Grid Federation, https://doi.org/10.22033/ESGF/CMIP6.6976, 2018.

NASA Goddard Institute for Space Studies (NASA/GISS): NASA-GISS GISS-E2-1-G-CC model output prepared for CMIP6 CMIP piControl, Earth System Grid Federation, https://doi.org/10.22033/ESGF/CMIP6.11856, 2019.

Neale, R. B., Chen, C., Gettelman, A., Lauritzen, P., Park, S., Williamson, D., Conley, A., Garcia, R., Kinnison, D., and Lamarque, J.: Description of the NCAR community atmosphere model (CAM 5.0), Tech. rep., National Center for Atmospheric Research, 2010.

Niemeier, U., Schmidt, H., Alterskjær, K., and Kristjánsson, J. E.: Solar irradiance reduction via climate engineering: Impact of different techniques on the energy balance and the hydrological cycle, J. Geophys. Res., 118, 11 905–11 917, https://doi.org/10.1002/2013JD020445, 2013.

NRC: Climate Intervention: Reflecting Sunlight to Cool Earth, Tech. rep., National Research Council, http://www.nap.edu/catalog/18988/climate-intervention-reflecting-sunlight-to-cool-earth, (last access: 7 May 2015), 2015.

Phipps, S. J., Rotstayn, L. D., Gordon, H. B., Roberts, J. L., Hirst, A. C., , and Budd, W. F.: The CSIRO Mk3L climate system model version 1.0 – Part 1: Description and evaluation, Geosci. Model Dev., 4, 483–509, https://doi.org/10.5194/gmd-4-483-2011, 2011.

Phipps, S. J., Rotstayn, L. D., Gordon, H. B., Roberts, J. L., Hirst, A. C., and Budd, W. F.: The CSIRO Mk3L climate system model version 1.0 – Part 2: Response to external forcings, Geosci. Model Dev., 5, 649–682, https://doi.org/10.5194/gmd-5-649-2012, 2012.

Pitari, G., Aquila, V., Kravitz, B., Robock, A., Watanabe, S., Cionni, I., Luca, N. D., di Genova, G., Mancini, E., and Tilmes, S.: Stratospheric ozone response to sulfate geoengineering: Results from the Geoengineering Model Intercomparison Project (GeoMIP), J. Geophys. Res., 119, 2629–2653, 2014.

Richter, J. H., Tilmes, S., Mills, M. J., Tribbia, J. J., Kravitz, B., MacMartin, D. G., Vitt, F., and Lamarque, J.: Stratospheric Dynamical Response and Ozone Feedbacks in the Presence of SO_2 Injections, J. Geophys. Res., 122, 12 557–12 573, https://doi.org/10.1002/2017JD026912, 2017.

Ricke, K. L., Morgan, M. G., and Allen, M. R.: Regional climate response to solar-radiation management, Nat. Geosci., 3, 537–541, https://doi.org/10.1038/ngeo915, 2010.

Robock, A.: Volcanic eruptions and climate, Rev. Geophys., 38, 191–219, https://doi.org/10.1029/1998RG000054, 2000.

Russotto, R. D. and Ackerman, T. P.: Changes in clouds and thermodynamics under solar geoengineering and implications for required solar reduction, Atmos. Chem. Phys., 18, 11 905–11 925, https://doi.org/10.5194/acp-18-11905-2018, 2018.

Schmidt, G. A., Kelley, M., Nazarenko, L., Ruedy, R., Russell, G. L., Aleinov, I., Bauer, M., Bauer, S. E., Bhat, M. K., Bleck, R., Canuto, V., Chen, Y.-H., Cheng, Y., Clune, T. L., Genio, A. D., de Fainchtein, R., Faluvegi, G., Hansen, J. E., Healy, R. J., Kiang, N. Y., Koch, D., Lacis, A. A., LeGrande, A. N., Lerner, J., Lo, K. K., Matthews, E. E., Menon, S., Miller, R. L., Oinas, V., Oloso, A. O., Perlwitz, J. P., Puma, M. J., Putman, W. M., Rind, D., Romanou, A., Sato, M., Shindell, D. T., Sun, S., Syed, R. A., Tausnev, N., Tsigaridis, K., Under, N., Volugarakis, A., Yao, M.-S., and Zhang, J.: Configuration and assessment of the GISS ModelE2 contributions to the CMIP5 archive, J. Adv. Modell. Earth Syst., 6, 141–184, https://doi.org/10.1002/2013MS000265, 2014.

Séférian, R.: CNRM-CERFACS CNRM-ESM2-1 model output prepared for CMIP6 CMIP abrupt-4xCO2, Earth System Grid Federation, https://doi.org/10.22033/ESGF/CMIP6.3918, 2018a.

Séférian, R.: CNRM-CERFACS CNRM-ESM2-1 model output prepared for CMIP6 CMIP piControl, Earth System Grid Federation, https://doi.org/10.22033/ESGF/CMIP6.4165, 2018b.

Séférian, R.: CNRM-CERFACS CNRM-ESM2-1 model output prepared for CMIP6 CMIP G1, Earth System Grid Federation, https://doi.org/10.22033/ESGF/CMIP6.3902, 2018c.

Séférian, R., Nabat, P., Michou, M., Saint-Martin, D., Voldoire, A., Colin, J., Decharme, B., Delire, C., Berthet, S., Chevallier, M., Sénési, S., Franchisteguy, L., Vial, J., Mallet, M., Joetzjer, E., Geoffroy, O., Guérémy, J.-F., Moine, M.-P., Msadek, R., Ribes, A., Rocher, M.,

Roehrig, R., Salas-y Mélia, D., Sanchez, E., Terray, L., Valcke, S., Waldman, R., Aumont, O., Bopp, L., Deshayes, J., Éthé, C., and Madec, G.: Evaluation of CNRM Earth System Model, CNRM-ESM2-1: Role of Earth System Processes in Present-Day and Future Climate, Journal of Advances in Modeling Earth Systems, 11, 4182–4227, https://doi.org/10.1029/2019MS001791, 2019.

Sellar, A. A., Jones, C. G., Mulcahy, J. P., Tang, Y., Yool, A., Wiltshire, A., O'Connor, F. M., Stringer, M., Hill, R., Palmieri, J., Woodward, S., de Mora, L., Kuhlbrodt, T., Rumbold, S. T., Kelley, D. I., Ellis, R., Johnson, C. E., Walton, J., Abraham, N. L., Andrews, M. B., Andrews, T., Archibald, A. T., Berthou, S., Burke, E., Blockley, E., Carslaw, K., Dalvi, M., Edwards, J., Folberth, G. A., Gedney, N., Griffiths, P. T., Harper, A. B., Hendry, M. A., Hewitt, A. J., Johnson, B., Jones, A., Jones, C. D., Keeble, J., Liddicoat, S., Morgenstern, O., Parker, R. J., Predoi, V., Robertson, E., Siahaan, A., Smith, R. S., Swaminathan, R., Woodhouse, M. T., Zeng, G., and Zerroukat, M.: UKESM1: Description and Evaluation of the U.K. Earth System Model, Journal of Advances in Modeling Earth Systems, 11, 4513–4558, https://doi.org/10.1029/2019MS001739, 2019.

Simpson, I., Tilmes, S., Richter, J., Kravitz, B., MacMartin, D., Mills, M., Fasullo, J., and Pendergrass, A.: The regional hydroclimate response to stratospheric sulfate geoengineering and the role of stratospheric heating, J. Geophys. Res., 124, 12 587–12 616, https://doi.org/10.1029/2019JD031093, 2019.

Stevens, B., Giorgetta, M., Esch, M., Mauritsen, T., Crueger, T., Rast, S., Salzmann, M., Schmidt, H., Bader, J., Block, K., Brokopf, R., Fast, I., Kinne, S., Kornblueh, L., Lohmann, U., Pincus, R., Reichler, T., and Roeckner, E.: Atmospheric component of the MPI-M Earth System Model: ECHAM6, Journal of Advances in Modeling Earth Systems, 5, 146–172, https://doi.org/10.1002/jame.20015, 2013.

Swart, N. C., Cole, J. N., Kharin, V. V., Lazare, M., Scinocca, J. F., Gillett, N. P., Anstey, J., Arora, V., Christian, J. R., Jiao, Y., Lee, W. G., Majaess, F., Saenko, O. A., Seiler, C., Seinen, C., Shao, A., Solheim, L., von Salzen, K., Yang, D., Winter, B., and Sigmond, M.: CCCma CanESM5 model output prepared for CMIP6 CMIP abrupt-4xCO2, Earth System Grid Federation, https://doi.org/10.22033/ESGF/CMIP6.3532, 2019a.

Swart, N. C., Cole, J. N., Kharin, V. V., Lazare, M., Scinocca, J. F., Gillett, N. P., Anstey, J., Arora, V., Christian, J. R., Jiao, Y., Lee, W. G., Majaess, F., Saenko, O. A., Seiler, C., Seinen, C., Shao, A., Solheim, L., von Salzen, K., Yang, D., Winter, B., and Sigmond, M.: CCCma CanESM5 model output prepared for CMIP6 CMIP piControl, Earth System Grid Federation, https://doi.org/10.22033/ESGF/CMIP6.3673, 2019b.

Swart, N. C., Cole, J. N. S., Kharin, V. V., Lazare, M., Scinocca, J. F., Gillett, N. P., Anstey, J., Arora, V., Christian, J. R., Hanna, S., Jiao, Y., Lee, W. G., Majaess, F., Saenko, O. A., Seiler, C., Seinen, C., Shao, A., Sigmond, M., Solheim, L., von Salzen, K., Yang, D., and Winter, B.: The Canadian Earth System Model version 5 (CanESM5.0.3), Geoscientific Model Development, 12, 4823–4873, https://doi.org/10.5194/gmd-12-4823-2019, https://gmd.copernicus.org/articles/12/4823/2019/, 2019c.

Tang, Y., Rumbold, S., Ellis, R., Kelley, D., Mulcahy, J., Sellar, A., Walton, J., and Jones, C.: MOHC UKESM1.0-LL model output prepared for CMIP6 CMIP abrupt-4xCO2, Earth System Grid Federation, https://doi.org/10.22033/ESGF/CMIP6.5843, 2019a.

Tang, Y., Rumbold, S., Ellis, R., Kelley, D., Mulcahy, J., Sellar, A., Walton, J., and Jones, C.: MOHC UKESM1.0-LL model output prepared for CMIP6 CMIP piControl, Earth System Grid Federation, https://doi.org/10.22033/ESGF/CMIP6.6298, 2019b.

Taylor, K. E., Stouffer, R. J., and Meehl, G. A.: An overview of CMIP5 and the experiment design, Bull. Amer. Meteor. Soc., 93, 485–498, https://doi.org/10.1175/BAMS-D-11-00094.1, 2012.

Tilmes, S., Fasullo, J., Lamarque, J.-F., Marsh, D. R., Mills, M., Alterskjær, K., Muri, H., Kristjánsson, J. E., Boucher, O., Schulz, M., Cole, J. N. S., Curry, C. L., Jones, A., Haywood, J., Irvine, P. J., Ji, D., Moore, J. C., Karam, D. B., Kravitz, B., Rasch, P. J., Singh, B., Yoon, J.-H., Niemeier, U., Schmidt, H., Robock, A., Yang, S., and Watanabe, S.: The hydrological impact of geoengineering in the Geoengineering Model Intercomparison Project (GeoMIP), J. Geophys. Res., 118, 11 036–11 058, https://doi.org/10.1002/jgrd.50868, 2013.

Tilmes, S., Richter, J. H., Mills, M. J., Kravitz, B., MacMartin, D. G., Garcia, R. R., Kinnison, D. E., Lamarque, J.-F., Tribbia, J., and Vitt, F.: Effects of Different Stratospheric SO_2 Injection Altitudes on Stratospheric Chemistry and Dynamics, J. Geophys. Res., 123, 4654–4673, https://doi.org/10.1002/2017JD028146, 2018.

Vial, J., Dufresne, J.-L., and Bony, S.: On the interpretation of inter-model spread in CMIP5 climate sensitivity estimates, Climate Dynamics, 41, 3339–3362, https://doi.org/10.1007/s00382-013-1725-9, 2013.

Vignesh, P. P., Jiang, J. H., Kishore, P., Su, H., Smay, T., Brighton, N., and Velicogna, I.: Assessment of CMIP6 cloud fraction and comparison with satellite observations, Earth and Space Science, 7, e2019EA000975, https://doi.org/10.1029/2019EA000975, 2020.

Visioni, D., MacMartin, D. G., Kravitz, B., Tilmes, S., Mills, M. J., Richter, J. H., and Boudreau, M. P.: Seasonal injection strategies for stratospheric aerosol geoengineering, Geophysical Research Letters, 46, 7790–7799, https://doi.org/10.1029/2019GL083680, 2019.

Watanabe, S., Miura, H., Sekiguchi, M., Nagashima, T., Sudo, K., Emori, S., and Kawamiya, M.: Development of an atmospheric general circulation model for integrated Earth system modeling on the Earth Simulator, J. Earth Simulator, 9, 27–35, 2008.

Watanabe, S., Hajima, T., Sudo, K., Nagashima, T., Takemura, T., Okajima, H., Nozawa, T., Kawase, H., Abe, M., Yokohata, T., Ise, T., Sato, H., Kato, E., Takata, K., Emori, S., and Kawamiya, M.: MIROC-ESM 2010: Model description and basic results of CMIP5-20c3m experiments, Geosci. Mod. Dev., 4, 845–872, https://doi.org/10.5194/gmd-4-845-2011, 2011.

Wieners, K.-H., Giorgetta, M., Jungclaus, J., Reick, C., Esch, M., Bittner, M., Legutke, S., Schupfner, M., Wachsmann, F., Gayler, V., Haak, H., de Vrese, P., Raddatz, T., Mauritsen, T., von Storch, J.-S., Behrens, J., Brovkin, V., Claussen, M., Crueger, T., Fast, I., Fiedler, S., Hagemann, S., Hohenegger, C., Jahns, T., Kloster, S., Kinne, S., Lasslop, G., Kornblueh, L., Marotzke, J., Matei, D., Meraner, K., Mikolajewicz, U., Modali, K., Müller, W., Nabel, J., Notz, D., Peters, K., Pincus, R., Pohlmann, H., Pongratz, J., Rast, S., Schmidt, H., Schnur, R., Schulzweida, U., Six, K., Stevens, B., Voigt, A., and Roeckner, E.: MPI-M MPI-ESM1.2-LR model output prepared for CMIP6 CMIP piControl, Earth System Grid Federation, https://doi.org/10.22033/ESGF/CMIP6.6675, 2019a.

Wieners, K.-H., Giorgetta, M., Jungclaus, J., Reick, C., Esch, M., Bittner, M., Legutke, S., Schupfner, M., Wachsmann, F., Gayler, V., Haak, H., de Vrese, P., Raddatz, T., Mauritsen, T., von Storch, J.-S., Behrens, J., Brovkin, V., Claussen, M., Crueger, T., Fast, I., Fiedler, S., Hagemann, S., Hohenegger, C., Jahns, T., Kloster, S., Kinne, S., Lasslop, G., Kornblueh, L., Marotzke, J., Matei, D., Meraner, K., Mikolajewicz, U., Modali, K., Müller, W., Nabel, J., Notz, D., Peters, K., Pincus, R., Pohlmann, H., Pongratz, J., Rast, S., Schmidt, H., Schnur, R., Schulzweida, U., Six, K., Stevens, B., Voigt, A., and Roeckner, E.: MPI-M MPI-ESM1.2-LR model output prepared for CMIP6 CMIP abrupt-4xCO2, Earth System Grid Federation, https://doi.org/10.22033/ESGF/CMIP6.6459, 2019b.

Xia, L., Robock, A., Cole, J. N. S., Curry, C. L., Ji, D., Jones, A., Kravitz, B., Moore, J. C., Muri, H., Niemeier, U., Singh, B., Tilmes, S., Watanabe, S., and Yoon, J.-H.: Solar Radiation Management impacts on agriculture in China: A case study in the Geoengineering Model Intercomparison Project (GeoMIP), J. Geophys. Res., 119, 8695–8711, https://doi.org/10.1002/2013JD020630, 2014.

Zelinka, M. D., Myers, T. A., McCoy, D. T., Po-Chedley, S., Caldwell, P. M., Ceppi, P., Klein, S. A., and Taylor, K. E.: Causes of higher climate sensitivity in CMIP6 models, Geophys. Res. Let., 47, e2019GL085782, https://doi.org/10.1029/2019GL085782, 2020.

Table 1. All participating models in both the CMIP5 and CMIP6 eras of GeoMIP, including references. For G1 solar reduction, the percentage is calculated as the percent change in incident solar irradiance at the top-of-atmosphere between G1 and its respective piControl run. Numbers in the first column correspond to the model numbers in Figure 11.

#	Model	Generation	Reference	G1 Solar Reduction (%)	Data not available	Data Citations (CMIP6 only)
1	BNU-ESM	CMIP5	Ji et al. (2014)	3.80	Cloud forcing	
2	CanESM2	CMIP5	Arora et al. (2011)	4.00		
3	CCSM4	CMIP5	Gent et al. (2011)	4.25	NPP	
4	CESM-CAM5.1-FV	CMIP5	Neale et al. (2010); Hurrell et al. (2013)	4.70		
5	CSIRO-Mk3L-1.2	CMIP5	Phipps et al. (2011, 2012)	3.20	Cloud forcing, NPP	
6	EC-EARTH	CMIP5	Hazeleger et al. (2011)	4.12	Cloud forcing, NPP	
7	GISS-E2-R	CMIP5	Schmidt et al. (2014)	4.47		
8	HadCM3	CMIP5	Gordon et al. (2000)	4.16	Cloud forcing, NPP	
9	HadGEM2-ES	CMIP5	Collins et al. (2011)	3.88		
10	IPSL-CM5A-LR	CMIP5	Dufresne et al. (2013); Hourdin et al. (2012)	3.50	NPP	
11	MIROC-ESM	CMIP5	Watanabe et al. (2008, 2011)	5.00		
12	MPI-ESM-LR	CMIP5	Giorgetta et al. (2013); Stevens et al. (2013)	4.68		
13	NorESM1-M	CMIP5	Alterskjær et al. (2012); Kirkevåg et al. (2013)	4.03		
14	CanESM5	CMIP6	Swart et al. (2019c)	3.72		Swart et al. (2019b, a); Cole et al. (
15	CESM2-WACCM	CMIP6	Gettelman et al. (2019)	4.91		Danabasoglu (2019c, b, a)
16	CNRM-ESM2.1	CMIP6	Séférian et al. (2019)	3.72		Séférian (2018b, a, c)
17	GISS-E2.1-G	CMIP6	Kelley et al. (2020)	4.13		NASA Goddard Institute for Space
18	IPSL-CM6A-LR	CMIP6	Boucher et al. (2020); Lurton et al. (2020)	4.10		Boucher et al. (2018c, b, a)
19	MPI-ESM1.2-LR	CMIP6	Mauritsen et al. (2019)	4.57		Wieners et al. (2019a, b)
20	UKESM1.0-LL	CMIP6	Sellar et al. (2019)	3.80		Tang et al. (2019b, a); Jones (2019)

Table 2. ~~Ensemble differences between~~ Decadal trends in the ~~CMIP5~~ global mean temperature, Net TOA radiative flux, precipitation, and ~~CMIP6 ensembles~~ evaporation values shown in Figure 1 for each ~~variable evaluated in this study (left column)~~model. ~~Column 2 indicates~~ Trends are calculated across the ~~difference between~~ years 11-100 to eliminate any effects due to initial transient adjustment to the ~~ensembles in how much of the Earth's surface is not stippled (more than 75% of models agree on the sign of the response; positive values indicate that CMIP6 has more unstippled area than CMIP5)~~abrupt forcing. ~~Column 3 indicates the fraction of the Earth's surface for which the CMIP5 ensemble is statistically different from the CMIP6 ensemble, based on 95th percentile confidence intervals from Welch's *t* test.~~

Model	Temperature (K/decade)	Rad Flux (W m^{-2}/decade)	Precipitation (%/decade)	Evaporation (%/decade)
CanESM5	0.010	-0.005	0.011	0.011
CESM2(WACCM)	0.023	-0.009	0.067	0.067
CNRM-ESM2.1	-0.033	0.016	-0.058	-0.058
GISS-E2.1-G	-0.005	0.018	-0.006	-0.006
IPSL-CM6A-LR	-0.027	0.015	-0.062	-0.063
MPI-ESM1.2-LR	-0.003	-0.000	-0.015	-0.016
UKESM1.0-LL	0.018	0.008	0.018	0.018
Ensemble Mean	-0.002	0.006	-0.006	-0.007

Table 3. Ensemble differences between the CMIP5 and CMIP6 ensembles for each variable evaluated in this study (left column). Column 2 indicates the difference between the ensembles in how much of the Earth's surface is not stippled (more than 75% of models agree on the sign of the response; positive values indicate that CMIP6 has more unstippled area than CMIP5). Column 3 indicates the percent of the Earth's surface for which the CMIP5 ensemble is statistically different from the CMIP6 ensemble, based on 95th percentile confidence intervals from Welch's *t*-test.

Variable	Stippling (%)	Welch's *t*-test (%)	Notes
Surface air temperature	-25.77	0.87	
Precipitation	-3.56	11.17	
Evaporation	-2.33	6.47	
P–E	-15.23	1.13	
SW Cloud Forcing	-8.02	9.65	
LW Cloud Forcing	11.99	6.57	
Net Primary Productivity	-1.42	1.15	Land surface only

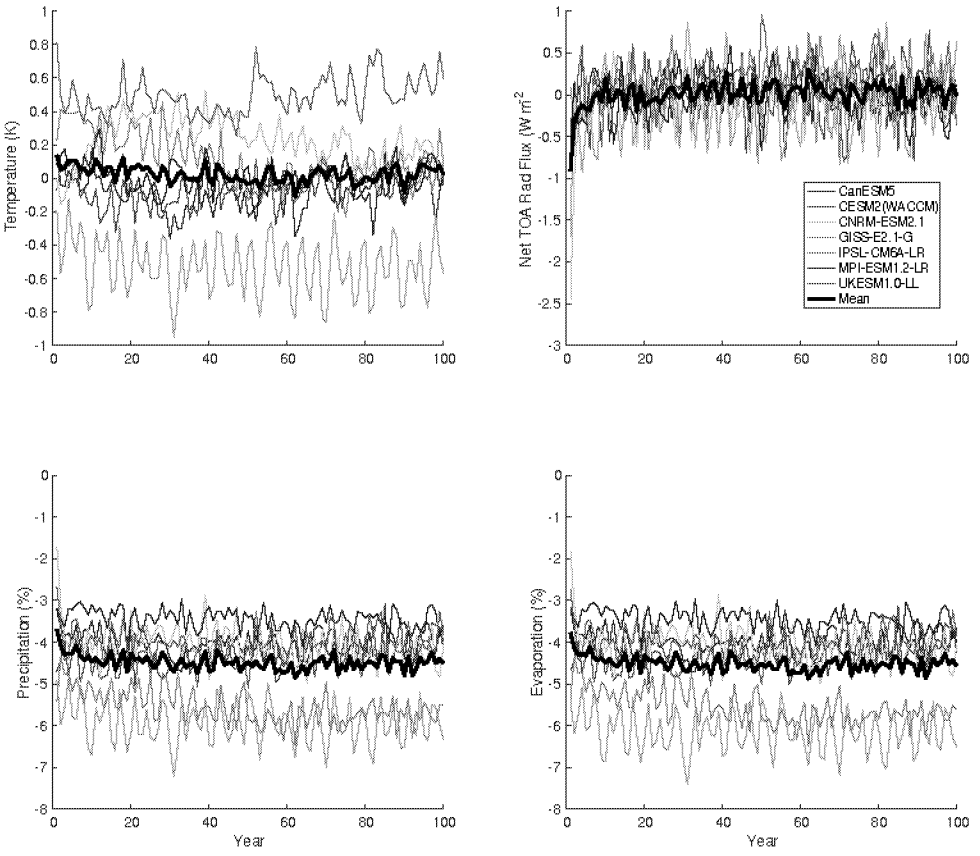

Figure 1. Temperature (top left; K), net top-of-atmosphere radiative flux (top right; W m^{-2}), precipitation (bottom left; %), and evaporation (bottom right; %) change in $G1_{CMIP6}$ compared to piControl over 100 years of simulation. Thin colored lines are individual models, and thick black lines are ensemble means.

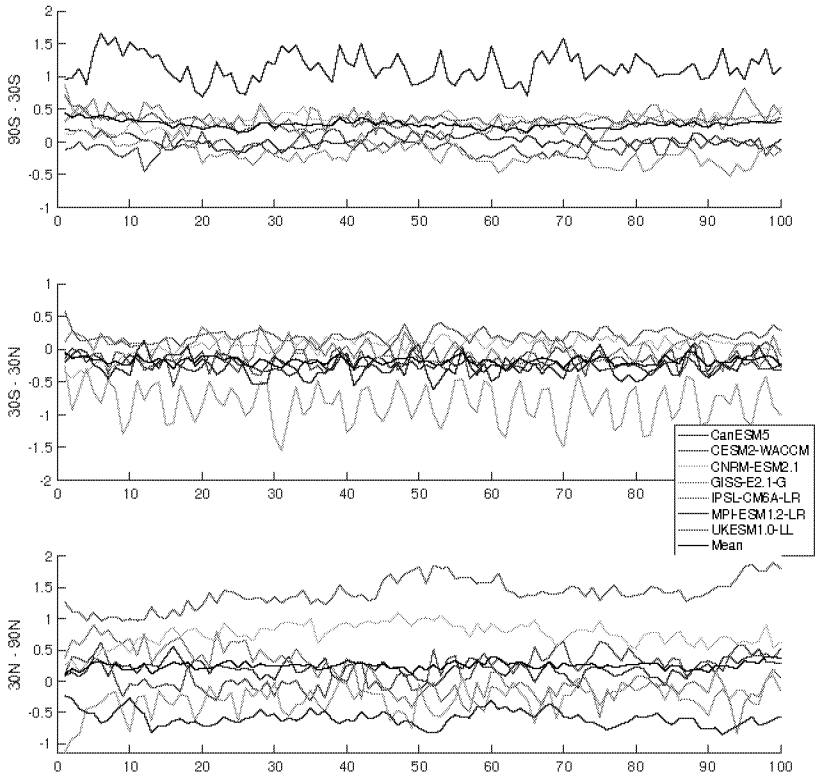

Figure 2. Annual mean surface temperature (K) in each model averaged over 90°S-30°S (top), 30°S-30°N (middle), and 30°N-90°N (bottom). The ensemble mean is plotted as thick black lines.

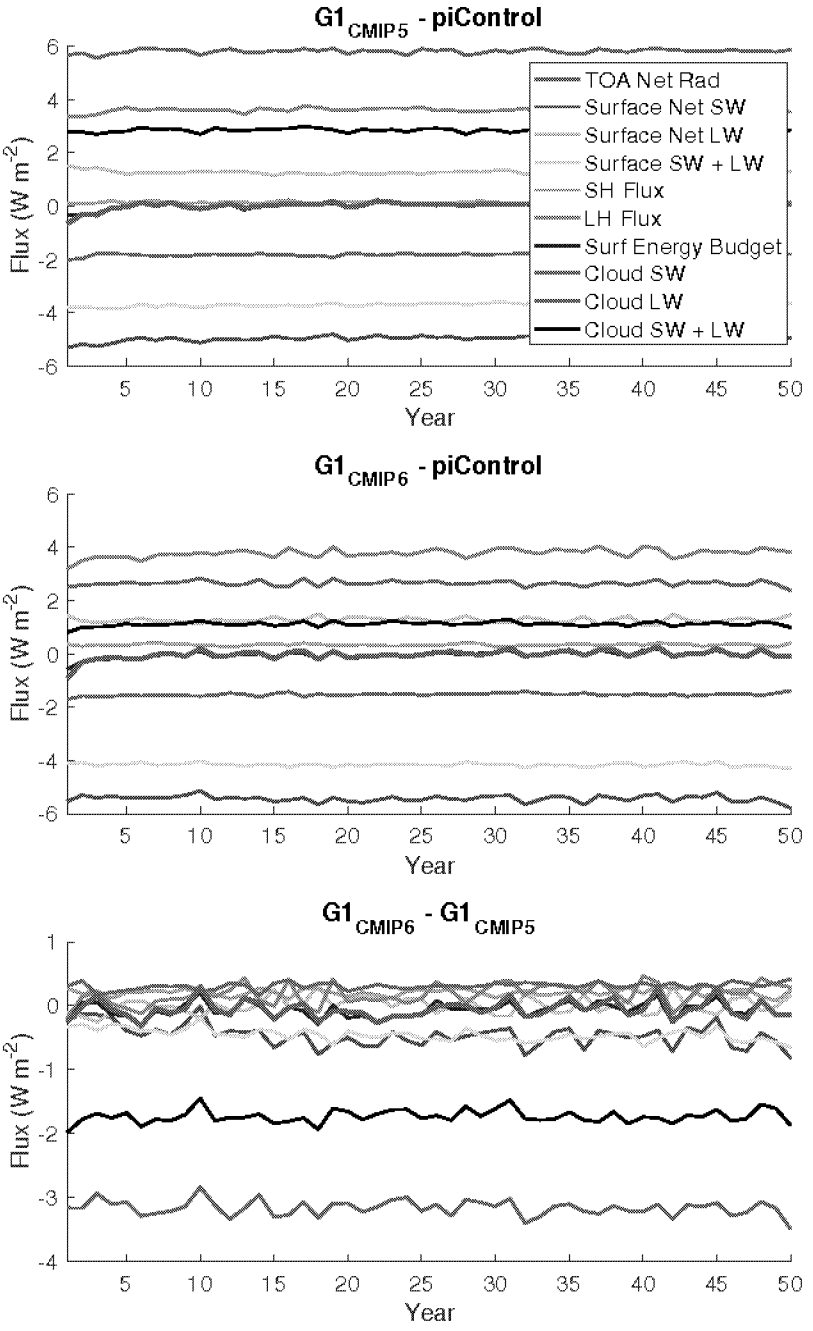

Figure 3. Ensemble mean energetics (W m^{-2}) for various flux quantities in $G1_{CMIP5}$ (top), $G1_{CMIP6}$ (middle), and ~~the~~ their difference (bottom). All fluxes are positive downward, which is counterintuitive for sensible heat (SH) and latent heat (LH). Surf Energy Budget indicates the sum of surface shortwave (SW), surface longwave (LW), SH, and LH. Cloud forcing is calculated as all-sky minus clear-sky.

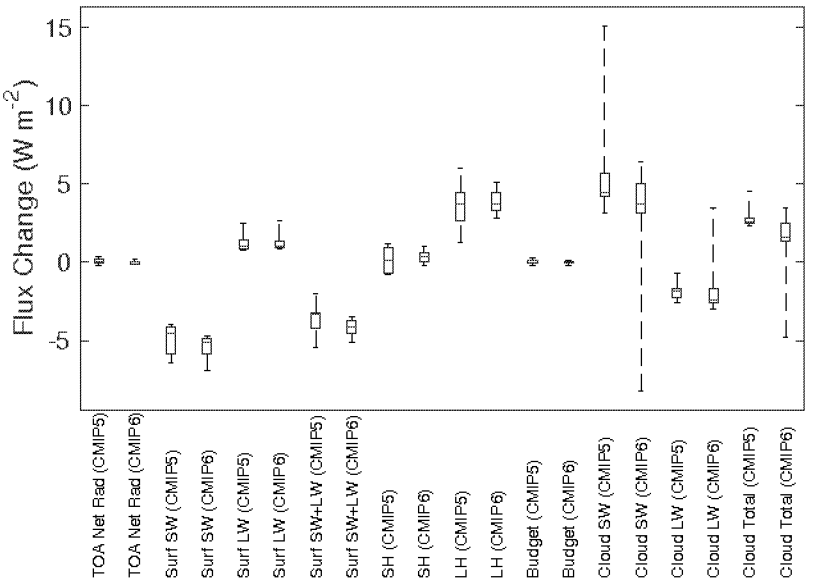

Figure 4. Ensemble median (red lines), inter-quartile (blue boxes), and ranges (black whiskers) for the same global mean energetics quantities as in Figure 3 (G1 minus piControl) for both the CMIP5 and CMIP6 ensembles.

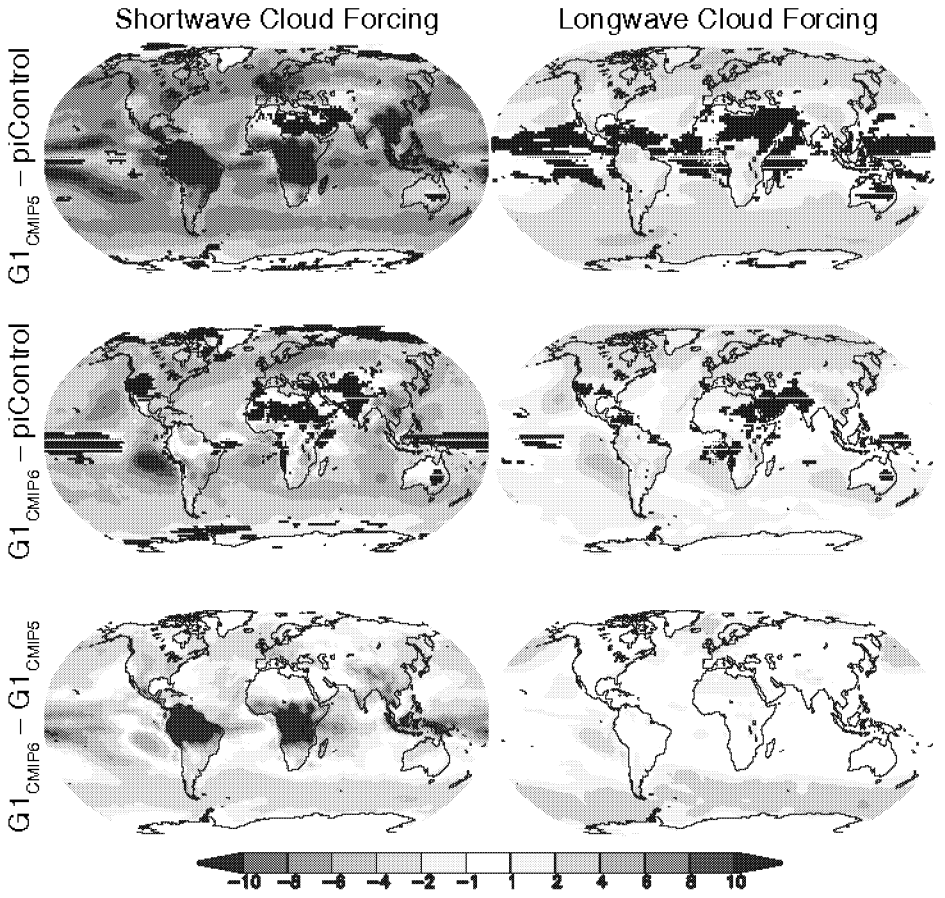

Figure 5. Surface shortwave (left) and longwave (right) cloud forcing (W m^{-2}) change from preindustrial for the CMIP5 (top) and CMIP6 (middle) ensembles, as well as the ensemble differences (bottom). Cloud forcing is measured as all-sky minus clear-sky radiative flux. All shaded values are ensemble means. Lack of stippling indicates agreement on the sign of the values across at least 75% of the models.

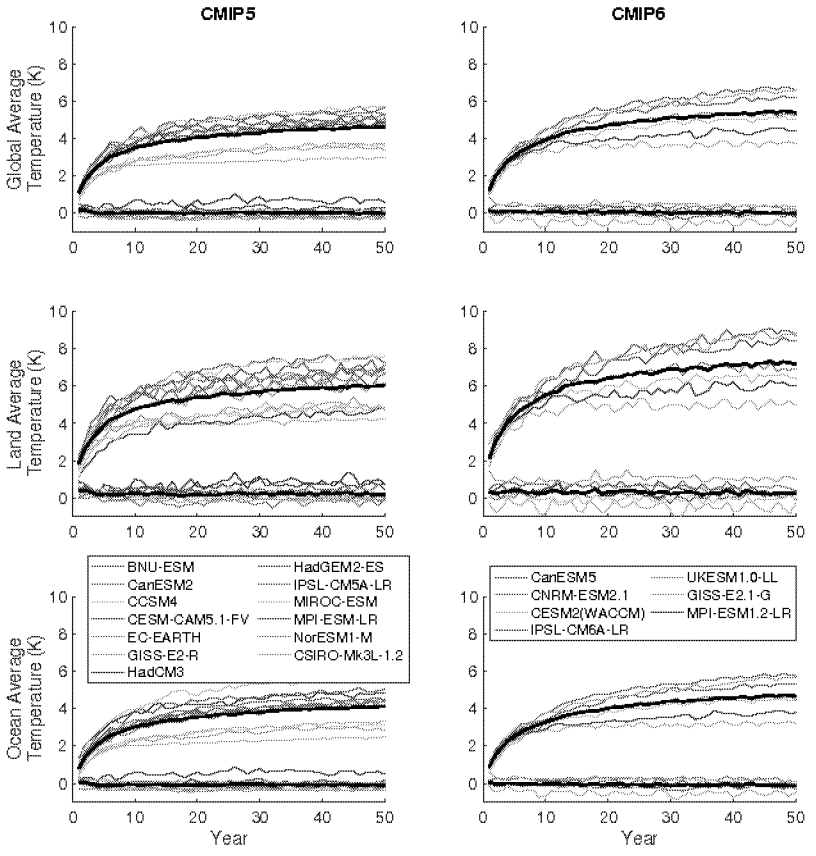

Figure 6. Global mean (top), land mean (middle), and ocean mean (bottom) temperature change (K) for the CMIP5 (left) and CMIP6 (ensembles). Thin colored lines are individual models, and thick black lines are model means. In all panels, the upper cluster of lines is the abrupt4xCO2 simulation, and the lower cluster of lines (approximately zero temperature change for the entire simulation) is experiment G1.

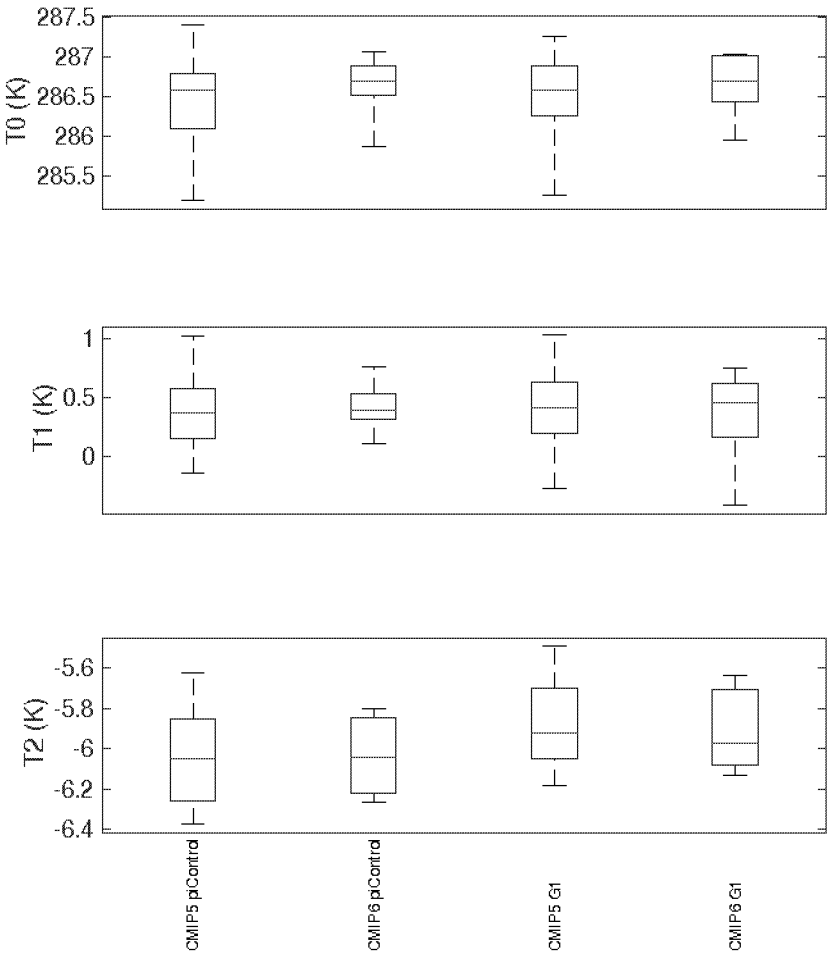

Figure 7. Ensemble ranges for global mean temperature (T_0), the interhemispheric temperature gradient (T_1), and the equator-to-pole temperature gradient (T_2), as defined in Equation 1 (Ban-Weiss and Caldeira, 2010; Kravitz et al., 2016). Red lines indicate ensemble medians, blue boxes are the inter-quartile ranges, and black whiskers indicate total ranges.

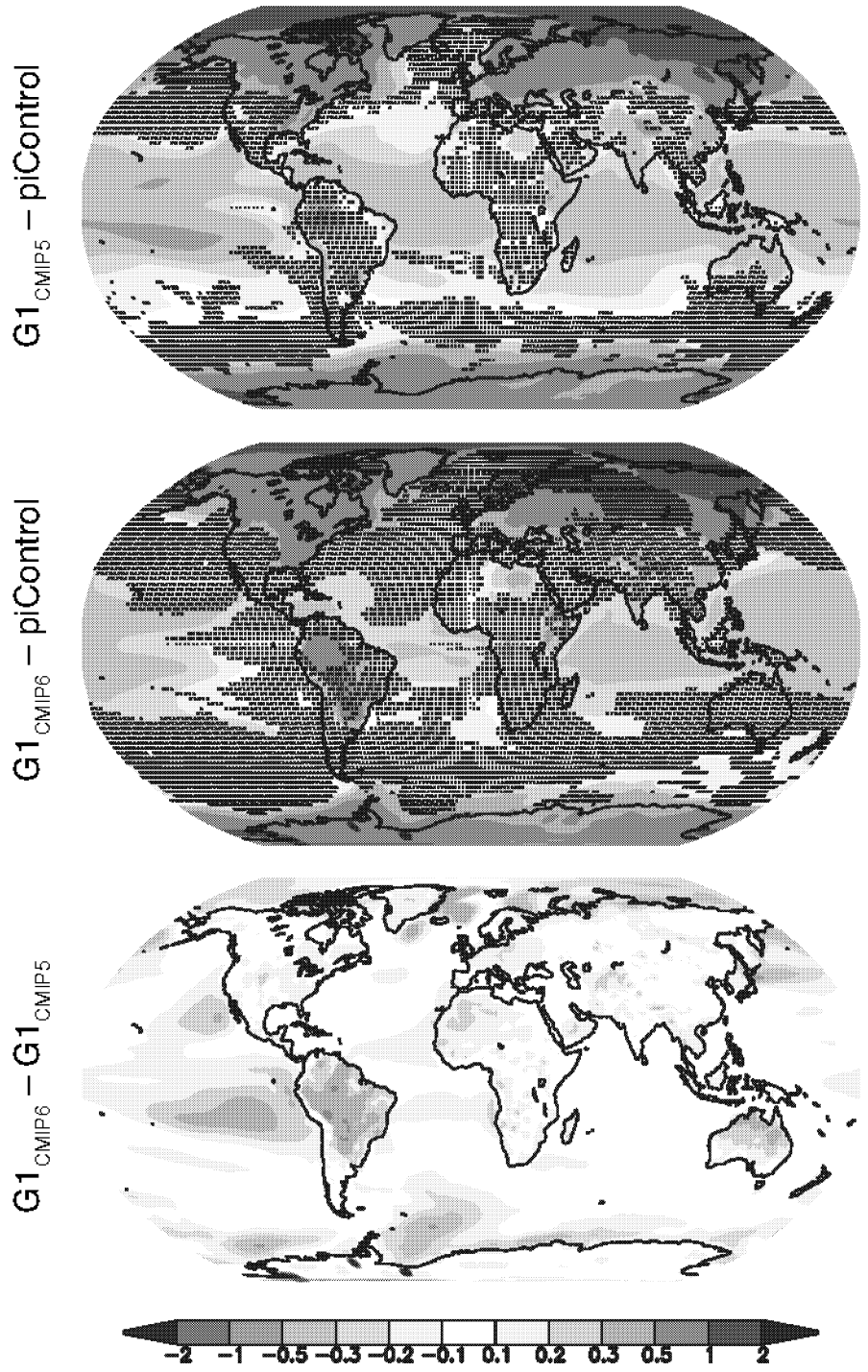

Figure 8. Ensemble average temperature changes (K) for G1 (as compared to the preindustrial control) for CMIP5 (top) and CMIP6 (middle), as well as ~~the~~ their difference ($G1_{CMIP6}$ minus $G1_{CMIP5}$, bottom panel). In the top two panels, stippling indicates regions where fewer than 75% of the models in their respective ensembles agree on the sign of the response.

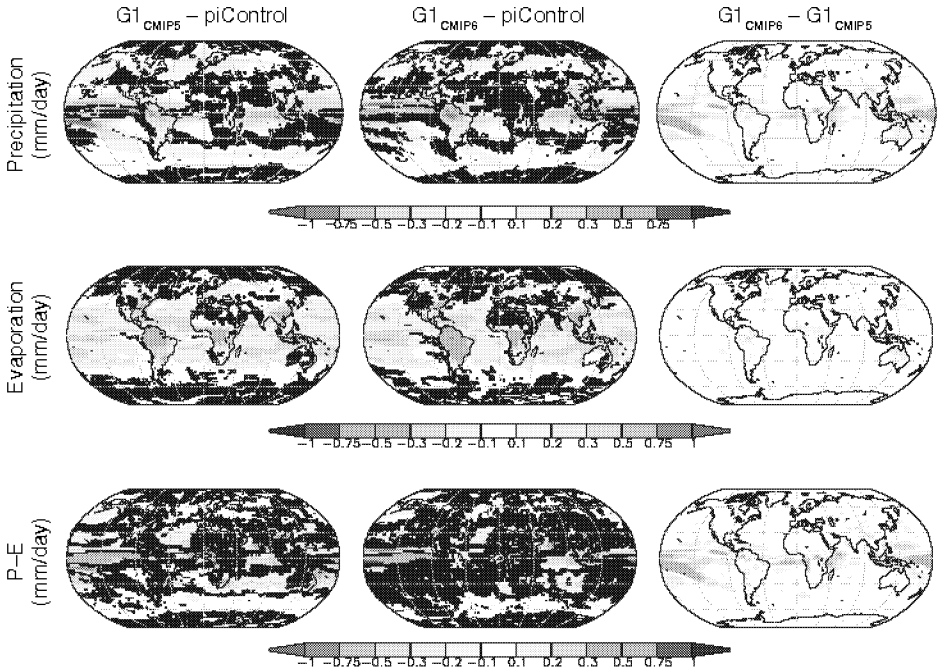

Figure 9. Precipitation (top), evaporation (middle), and precipitation minus evaporation (P–E; bottom) change from preindustrial for the CMIP5 (left) and CMIP6 (middle) ensembles, as well as the ensemble differences (right). All shaded values are ensemble means. Lack of stippling in the left and middle panels indicates agreement on the sign of the values across at least 75% of the models.

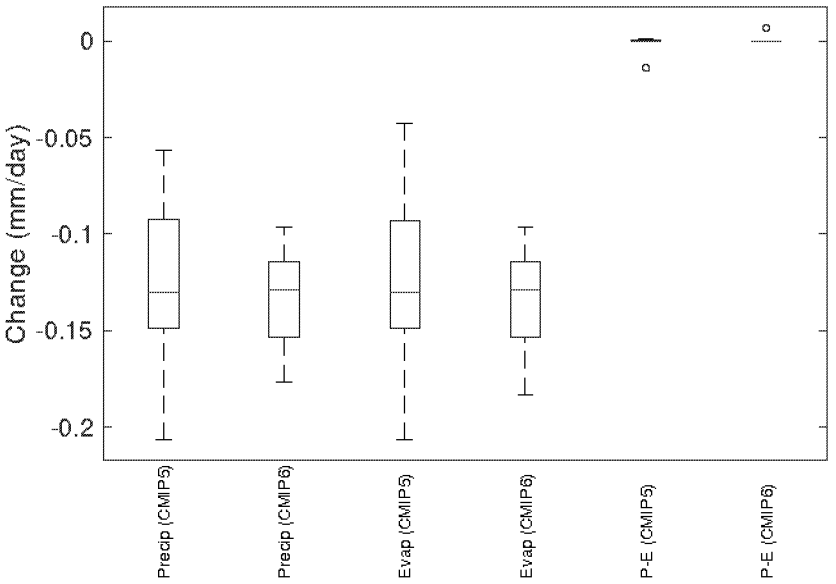

Figure 10. Global mean ensemble median (red lines), inter-quartile (blue boxes), and ranges (black whiskers or, for P–E one blue circle indicating an extreme outlier) for the hydrological quantities shown in Figure 9 for both the CMIP5 and CMIP6 ensembles.

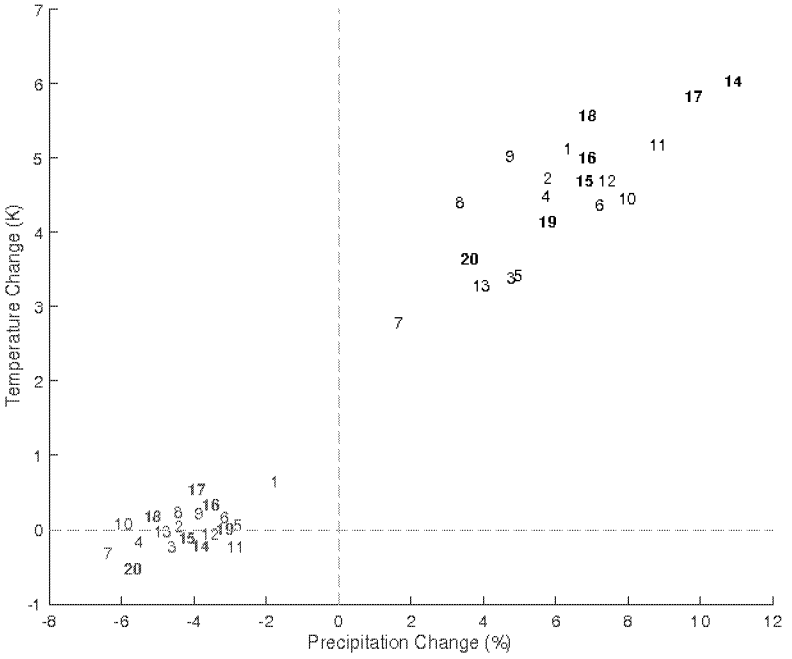

Figure 11. Average (years 11-50) temperature (y-axis; K) and precipitation (x-axis; %) change for each model in this study. Numbers indicate the model number (listed in Table 1, first column). Black numbers are for abrupt4xCO2, and red numbers are for G1. Bolded numbers are for CMIP6

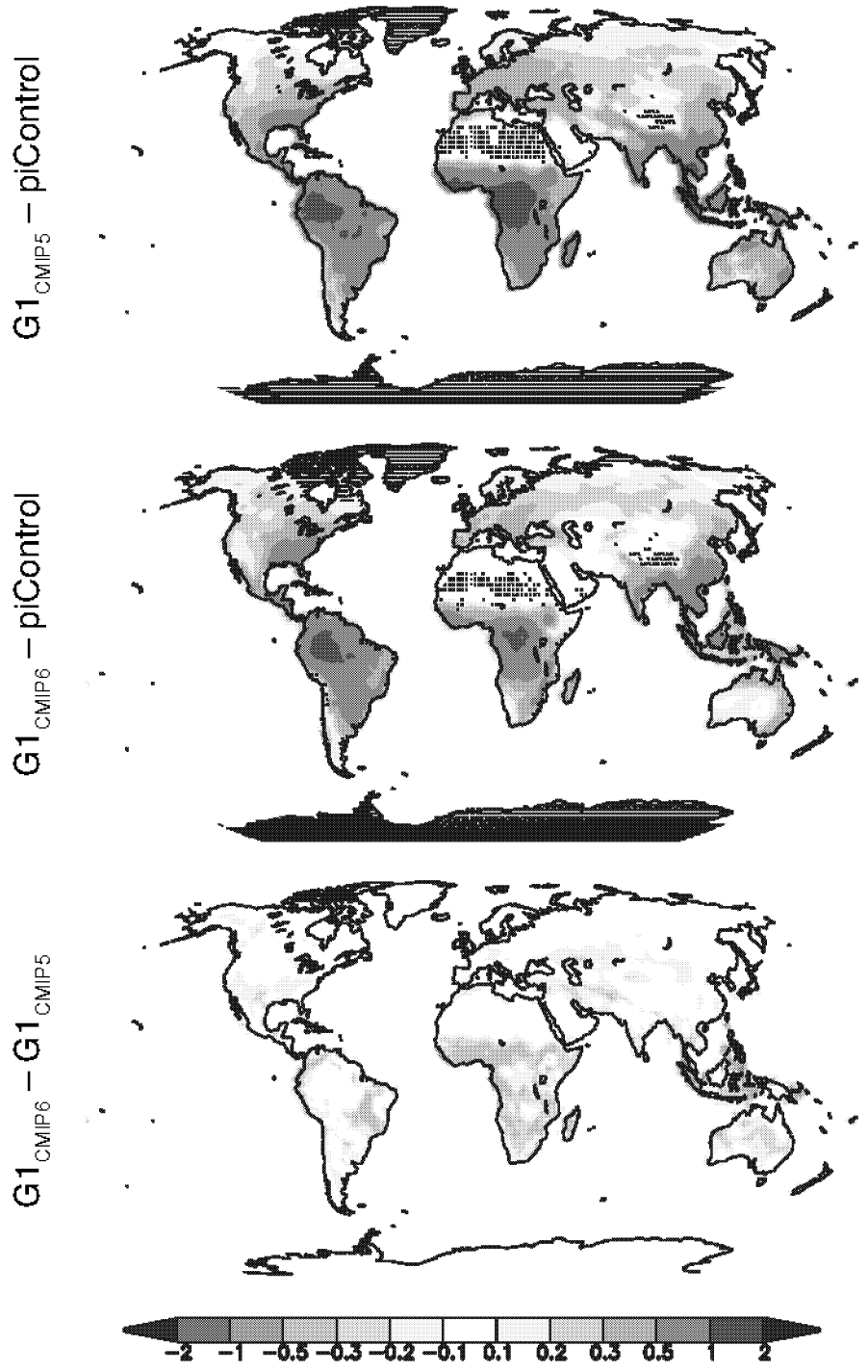

Figure 12. Terrestrial net primary productivity (kg C m^{-2} y^{-1}) for the CMIP5 (top) and CMIP6 (middle) ensembles, as well as the ensemble differences (bottom). All shaded values are ensemble means. Lack of stippling indicates agreement on the sign of the values across at least 75% of the models.

Comparing different generations of idealized solar geoengineering simulations in the Geoengineering Model Intercomparison Project (GeoMIP)

Ben Kravitz,[1,2,*] Douglas G. MacMartin,[3] Daniele Visioni,[3] Olivier Boucher,[4] Jason N. S. Cole,[5] Jim Haywood,[6,7] Andy Jones,[7] Thibaut Lurton,[4] Michael J. Mills,[8] Pierre Nabat,[9] Ulrike Niemeier,[10] Alan Robock,[11] Roland Séférian,[9] and Simone Tilmes[8]

[1]Department of Earth and Atmospheric Sciences, Indiana University, Bloomington, IN, USA
[2]Atmospheric Sciences and Global Change Division, Pacific Northwest National Laboratory, Richland, WA, USA
[3]Sibley School of Mechanical and Aerospace Engineering, Cornell University, Ithaca, NY, USA
[4]Institut Pierre-Simon Laplace (IPSL), Sorbonne Université/CNRS, Paris, France
[5]Environment and Climate Change Canada, Toronto, Ontario, Canada
[6]College of Engineering, Mathematics and Physical Sciences, University of Exeter, Exeter, United Kingdom
[7]UK Met Office Hadley Centre, Exeter, United Kingdom
[8]Atmospheric Chemistry Observations and Modeling Laboratory, National Center for Atmospheric Research, Boulder, CO, USA
[9]Centre National de Recherches Météorologiques, Université de Toulouse, Météo-France, Toulouse, France
[10]Max Planck Institute for Meteorology, Hamburg, Germany.
[11]Department of Environmental Science, Rutgers University, New Brunswick, NJ, USA

Submission to *Environmental Research Letters*

[*]To whom correspondence should be addressed: 1001 E. 10th Street, Bloomington, IN 47405-1405, USA. bkravitz@iu.edu

Abstract

Solar geoengineering has been receiving increased attention in recent years as a potential temporary solution to offset global warming. One method of approximating global-scale solar geoengineering in climate models is via solar reduction experiments. Two generations of models in the Geoengineering Model Intercomparison Project (GeoMIP) have now simulated offsetting a quadrupling of the CO_2 concentration with solar reduction. Here we show that energetics, temperature, and hydrological cycle changes in this experiment are statistically indistinguishable between the two ensembles. Of the variables analyzed here, the only major differences involve highly parameterized and uncertain processes, such as cloud forcing or net primary productivity. We conclude that despite numerous structural differences and uncertainties in models over the past 20 years, broad conclusions about the climate response to global solar dimming remain robust.

Keywords: geoengineering, climate engineering, climate intervention, solar radiation management, climate modeling

Three main points

1. Two solar dimming model ensembles are statistically indistinguishable for many variables
2. Largest ensemble differences are in highly parameterized and uncertain processes
3. Past results about solar dimming are robust to some structural model differences and uncertainties

Suggested reviewers

- Piers Forster
- Don Wuebbles
- Peter Irvine
- Long Cao
- Ken Caldeira
- Govindasamy Bala
- Jim Hurrell

1. Introduction

Solar geoengineering describes a set of technologies designed to (ideally) temporarily, deliberately reduce some of the effects of climate change by changing the radiative balance of the planet, often by reflecting sunlight back to space (NRC, 2015). Numerous methods have been proposed, but arguably the most studied is stratospheric sulfate aerosol injection (Budyko, 1977; Crutzen, 2006). This method involves creating large amounts of highly reflective sulfate aerosols in the stratosphere, replicating the mechanisms that cause cooling after large volcanic eruptions (Robock, 2000). In model simulations of solar geoengineering, solar reduction is often used as a proxy for actual stratospheric sulfate aerosols, as it captures many of the broad radiative effects of stratospheric aerosol geoengineering as well as some of the important climate effects (Niemeier et al., 2013; Kalidindi et al., 2015). Any implementation of stratospheric geoengineering with sulfate aerosols would produce additional effects, such as changing atmospheric circulation in response to stratospheric heating and heating gradients (e.g., Simpson et al., 2019; Jones et al., 2020), ozone depletion (e.g., Pitari et al., 2014), and resultant changes in ultraviolet radiation flux, and enhanced diffuse radiation at the surface, but here we consider the major, large-scale effect of reflecting sunlight to cool Earth.

Simulations of solar geoengineering with solar reduction have long shown that solar geoengineering would cool the planet, offsetting global warming (e.g., Govindasamy and Caldeira, 2000; NRC, 2015; Irvine et al., 2016). Idealized simulations of solar reduction have also been simulated in a multi-model context under the Geoengineering Model Intercomparison Project (GeoMIP; Kravitz et al., 2011), to understand the robust model responses to various standardized solar geoengineering simulation designs. Multi-model conclusions from these studies indicate that solar geoengineering would be effective at partially offsetting greenhouse gas-induced temperature changes (Kravitz et al., 2013a), as well as changes in the hydrological cycle (Tilmes et al., 2013), the cryosphere (Moore et al., 2014), extreme events (Curry et al., 2014; Aswathy et al., 2015), vegetation (Glienke et al., 2015), circulation (Guo et al., 2018; Gertler et al., 2020), agriculture (Xia et al., 2014), and numerous other areas. However, the offset is not perfect (Moreno-Cruz et al., 2012), particularly on a regional basis or when considering multiple simultaneous metrics of climate change (Kravitz et al., 2014; Irvine et al., 2019; Jones et al., 2020), leading to concerns about winners and losers from geoengineering (Ricke et al., 2010). To some extent, the effects of solar geoengineering may be tailored or designed (MacMartin et al., 2013; Kravitz et al., 2016, 2017, 2019), but solar geoengineering will still not be able to perfectly offset climate change from greenhouse gases.

The previous phase of GeoMIP was associated with the Coupled Model Intercomparison Project Phase 5 (CMIP5; Taylor et al., 2012), an international collaboration of climate models to attempt to understand robust model responses to various forcings. GeoMIP has now entered a new phase, concurrent with the Coupled Model Intercomparison Project Phase 6 (CMIP6; Eyring et al., 2016), and with it are new solar geoengineering simulations with new and updated versions of Earth System Models (Kravitz et al., 2015). As such, this is an opportunity to revisit some central questions in solar geoengineering. Many of the CMIP5 results regarding solar geoengineering showed substantial agreement across the participating GeoMIP models. In this

newest iteration of GeoMIP, do the same science conclusions still hold, and do the models still generally agree on the resulting climate effects? Here we address these questions by evaluating and comparing general climate model response to GeoMIP experiment G1 (described in the next section) from both CMIP5 and CMIP6.

2. Simulations and Participating Models

In this study, we evaluate GeoMIP experiment G1, in which, starting from a preindustrial control (piControl) baseline, the atmospheric CO_2 concentration is instantaneously quadrupled (the standard CMIP experiment abrupt4xCO2), and insolation is simultaneously reduced such that net top-of-atmosphere (TOA) radiative flux is approximately unchanged from the baseline in the first decade of simulation (Kravitz et al., 2011, 2015). This experiment was part of the original suite of GeoMIP experiments and was repeated in the newest suite in an effort to understand the role of model structural uncertainty in broad conclusions about solar geoengineering. Participating models are listed in Table 1. We include 13 models from CMIP5 and 7 models from CMIP6.

Because the main focus of this paper is a comparison between the CMIP5 and CMIP6 eras of model results, we have opted for the following to aid comparisons:

- The original G1 experiment was 50 years in length, whereas the CMIP6 version is 100 years in length to allow for better analyses of rare events or to capture very slow responses. Since we are not evaluating any features that require 100 years of statistics, and the results do not show any appreciable time evolution of behavior after the first couple of years (see Supplemental Section 2 and Supplemental Figures 1 and 2), we only evaluate the first 50 years of all simulations. All maps show changes over years 11-50, removing the initial transient period.
- We do not compare previous versions of individual models with current ones, instead only examining ensembles. Even though models may share similar development histories (e.g., atmosphere and ocean dynamical cores, convective parameterizations, radiative transfer modules, terrestrial biosphere and cryosphere, etc.; Knutti et al., 2013; Zelinka et al., 2020), there have been numerous developments in models in these areas (and others) between CMIP5 and CMIP6 such that in most cases a direct comparison would not be meaningful.
- We focus extensively on the G1 results and, with few exceptions, do not focus on the corresponding abrupt4xCO2 simulations. It has been well documented that the CMIP6 models tend to have higher climate sensitivities than the CMIP5 models (Flynn and Mauritsen, 2020; Meehl et al., 2020; Zelinka et al., 2020), so we do not wish to make conclusions that might be based on a form of selection bias.
- All lack of stippling on map plots, as in previous GeoMIP studies (e.g., Kravitz et al., 2013a), indicates agreement on the sign of the response in at least 75% of models. Because $G1_{CMIP5}$ has more participating models than $G1_{CMIP6}$, this threshold provides some consistency across analyses of the ensembles. When plotting differences between the ensembles ($G1_{CMIP6}$-$G1_{CMIP5}$), there is no stippling, as it is difficult to meaningfully represent such differences between ranges. Aggregate differences between the two

ensembles, as calculated using Welch's *t*-test or differences in stippled area, are discussed in Supplemental Table 1.

3. Results

3.1. Energetics

Ensemble mean radiative and turbulent flux quantities are plotted in Figure 1, and the ensemble ranges are plotted in Supplemental Figure 3. An immediate observation is that, in both ensembles, the models were successful at limiting net TOA radiative flux change to within approximately ±0.1 W m^{-2} of the models' respective preindustrial values. Accomplishing this required an average solar reduction of 4.14% (models range in 3.20–5.00%) in CMIP5 and 4.14% (3.72–4.91%) in CMIP6. As such, despite numerous structural changes between the two generations of models, there is no appreciable change in solar efficacy (Hansen et al., 2005).

None of the radiative flux quantities indicate large transients over 50 years of simulation of G1, other than the initial flux change within the first year or so of simulation, which is consistent with the "perpetual fast response" found by Kravitz et al. (2013b). Ensemble mean fluxes show few differences (<1 W m^{-2} in magnitude) with the exception of shortwave cloud forcing, defined as all-sky minus clear-sky shortwave flux at the surface. On average, the CMIP6 ensemble has 3–4 W m^{-2} less shortwave cloud forcing than CMIP5. Neglecting some outliers, for each flux except shortwave (and hence total) cloud forcing, the median model in one ensemble is within the inter-quartile range of the other ensemble. This indicates that there are no major differences between the ensembles in how the models handle energy balance and energetics, with the exception of clouds, which is consistent with findings about CMIP5 (Zelinka et al., 2020). Moreover, it appears that most of the major differences in shortwave cloud forcing are due to outliers in each ensemble, positive for CMIP5 and negative for CMIP6.

To further explore these potential differences, Supplemental Figure 4 provides maps of the ensemble means for cloud forcing. In G1, the CMIP5 ensemble showed more positive shortwave cloud forcing and more negative longwave cloud forcing (i.e., more cancellation) than the CMIP6 ensemble. Overall, the CMIP6 ensemble has greatly reduced (in some places by over 10 W m^{-2}) shortwave cloud forcing as compared to CMIP5 under the G1 experiment. This is a widespread result, but the most prominent features are in the tropics, especially over the Amazon, Africa, and the Maritime Continent. The reasons behind these forcing changes are difficult to diagnose, as they could be due to changes in cloud thickness, cloud cover, or cloud level between CMIP5 and CMIP6 models (e.g., Vignesh et al., 2020), differences in how solar geoengineering affects clouds (Russotto and Ackerman, 2018), or artifacts of the analyses (e.g., cloud masking; Andrews et al., 2009; Kravitz et al., 2013b). Moreover, based on the results in Supplemental Figure 3, it is likely that many of these features are exaggerated by outlier models (also see Vignesh et al., 2020). As such, we reserve such detailed investigations for future work.

3.2. Temperature

These small flux changes also lead to few G1 temperature changes between the two ensembles. Figure 2 shows global, land, and ocean-averaged temperatures for the CMIP5 and CMIP6 ensembles. In general, the abrupt4xCO2 simulation in CMIP6 has higher temperatures than in CMIP5, consistent with the noted increase in climate sensitivity (Flynn and Mauritsen, 2020; Meehl et al., 2020; Zelinka et al., 2020). In both ensembles, G1 is effective at offsetting global mean temperature change, in some cases with a slight positive residual temperature change over land. Supplemental Figure 5 shows three aggregate temperature metrics: global mean temperature, the interhemispheric temperature gradient, and the equator-to-pole temperature gradient (Ban Weiss and Caldeira, 2010; Kravitz et al., 2016). As for the fluxes, the median model in one ensemble is within the inter-quartile range of the other ensemble. This indicates that no ensemble is on average warmer than another, has a substantially warmer Northern or Southern Hemisphere than the other, or has warmer tropics or poles than the other. We can conclude that spatial patterns of temperature change from G1 are robust across a wide range of structural uncertainty.

The spatial structure of temperature change (Figure 3) does have small differences between the two ensembles. G1 in CMIP6 has multiple locations that are warmer than G1 in CMIP5, despite both ensembles achieving net energy balance at TOA and the surface (Figure 1). The majority of the differences are over land and in the tropics, where CMIP6 is slightly warmer than CMIP5 (up to a degree Celsius in some places). Nevertheless, both ensembles show the well noted feature that offsetting a CO_2 increase with solar reduction overcools the tropics and undercools the poles (Govindasamy and Caldeira, 2000; Kravitz et al., 2013a). CMIP6 shows slightly less high latitude warming than CMIP5, but temperature differences between the two ensembles are largely negligible. However, the warmer temperatures in CMIP6 near Greenland have important implications for ice sheet melt and consequent sea level rise, as well as bottom water formation. We reserve such analyses for future investigations, particularly since the models used here are not capable of simulating the eustatic component of sea level rise. In any case, these ensemble mean differences between CMIP5 and CMIP6 cannot be deemed statistically significant (Supplemental Table 1 and Supplemental Figure 4).

3.3. Hydrological and Other Integrative Changes

Figure 4 shows ensemble mean changes in precipitation (P), evaporation (E), and P–E for $G1_{CMIP5}$ and $G1_{CMIP6}$. Qualitatively, patterns are similar between both ensembles. Precipitation is slightly (<0.3 mm/day in magnitude) different in the tropics between the two ensembles. The majority of those features can be summarized as a more southward ~~ITCZ~~Intertropical Convergence Zone, more precipitation in the South Pacific Convergence Zone, and less precipitation over Southeast Asia and the Maritime Continent in CMIP6. Evaporation in the two ensembles is nearly identical except for more evaporation in Amazonia and Australia in CMIP6. As such, the net P–E change between the two ensembles strongly resembles the precipitation changes. Supplemental Figure 6 shows that, like previous evaluations of ensemble ranges, the median model in one ensemble falls well within the interquartile range of the other ensemble for P, E, and P–E. As such, we cannot conclude any robust hydrological cycle changes between the two ensembles.

Figure 5 shows average (years 11–50) temperature change (with respect to piControl) plotted against average precipitation change for each model, as in Tilmes et al. (2013). Other than a potentially greater climate sensitivity of some CMIP6 models, there is no distinguishable difference in aggregate behavior between the two ensembles. The same conclusion discovered by Tilmes et al. (2013) holds: solar reduction cannot simultaneously offset CO_2-induced changes in both global mean temperature and global mean precipitation.

As an integrator of CO_2, temperature, and precipitation effects over land, Figure 6 shows changes in terrestrial net primary productivity (NPP). Numerous land regions, mostly aligned with those showing reduced precipitation in Figure 4, have lower NPP in CMIP6 than in CMIP5. The ensemble average global NPP change (G1–piControl) is 50.9 (4.1–120.9) Pg [C] y^{-1} in CMIP5 and 41.1 (23.0–77.2) Pg [C] y^{-1} in CMIP6, representing a 19.3% difference in means. Jones et al. (2013) used NPP to highlight the importance of understanding the influence of structural land model differences on climate results related to geoengineering. While it is beyond the scope of this study to perform a detailed diagnosis of which uncertainties or processes are responsible for this inter-ensemble difference, we point out that the ensemble spread of total terrestrial NPP is smaller in CMIP6 than in CMIP5, perhaps due to selection bias or perhaps due to some of these uncertainties being addressed in this newest generation of models.

4. Discussion and Conclusions

Based on the results presented here, model response to G1 has not changed substantially between CMIP5 and CMIP6. The sign of residual climate impacts (for example in temperature) are in better agreement in CMIP5 than CMIP6 (see Supplemental Table 1), but this could be a function of the smaller ensemble size in CMIP6. Energetics, temperature, and the hydrological cycle are qualitatively and quantitatively similar in both ensemble means and ensemble ranges, although these variables are somewhat related, so we might expect them to all portray a similar picture. Notable differences do exist in shortwave cloud forcing and NPP, particularly in Amazonia, Africa, and Australia, which are also regions of inter-ensemble difference in precipitation.

From these findings, we can conclude that results obtained over the past 20 years of study have not been overturned by the latest round of simulations. All of the major ensemble differences highlighted above deal with clouds and land surface modeling, both of which are difficult to model and are necessarily highly parameterized. The conclusions that are based on more fundamental knowledge, such as column energetics (in the case of the hydrological cycle), are relatively robust to structural uncertainty, in so far as this study adequately captures representative variations in structural uncertainty. This lends confidence to our conclusions, especially regarding robustness to uncertainty, about the broad climate effects from solar geoengineering methods that can be accurately represented via solar dimming.

We also conclude that the models used in CMIP5 are not obviously biased or inferior as compared to CMIP6. While improvements have been made in the CMIP6 generation of models,

and those models are likely better for representing numerous features of the present-day climate that may be important for studies of geoengineering, there are many aspects of climate that are well represented by earlier models. In some cases, more robust analyses may be enabled by augmenting ensemble sizes with archived output from earlier generations of CMIP models.

There are numerous aspects of physical climate that we did not evaluate, nor did we pursue analyses beyond physical climate, including many other aspects of natural science, social science, the humanities, governance, justice, or ethics (to name a few important areas). A holistic assessment of the consequences of geoengineering would certainly need to take these numerous aspects into account. Nevertheless, based on the results presented here, results for geoengineering across several important metrics appear to be robust to some amount of structural uncertainty. This lends confidence to some conclusions regarding solar geoengineering.

Many of the broad features of solar geoengineering with sulfate aerosols can be represented by a reduction in solar constant (e.g., Kalidindi et al., 2015). However, the more subtle changes that derive from complex response to stratospheric aerosol heating (for example, the positive wintertime North Atlantic Oscillation; Jones et al., 2020) require detailed assessments with state-of-the-art aerosol microphysical schemes. This is particularly important for understanding regional and seasonal solar geoengineering (Kravitz et al., 2017; Visioni et al., 2019). Such detailed microphysical calculations can only be simulated in a small number of models; in the case of Jones et al. (2020), only two models were available. While simple G1-style experiments enable a robust multi-model ensemble analysis, they cannot capture details that depend on microphysics. We emphasize the importance of a variety of modeling approaches to understand solar geoengineering, particularly the role of model uncertainty in conclusions about solar geoengineering.

Acknowledgments. We acknowledge the World Climate Research Programme, which, through its Working Group on Coupled Modelling, coordinated and promoted CMIP. We thank the climate modeling groups for producing and making available their model output, the Earth System Grid Federation (ESGF) for archiving the data and providing access, and the multiple funding agencies who support CMIP6 and ESGF. We also thank all participants of the Geoengineering Model Intercomparison Project and their model development teams. Support for B.K. was provided in part by the National Science Foundation (NSF) through agreement CBET-1931641, the Indiana University Environmental Resilience Institute, and the *Prepared for Environmental Change* Grand Challenge initiative. The Pacific Northwest National Laboratory is operated for the US Department of Energy by Battelle Memorial Institute under contract DE-AC05-76RL01830. Resources supporting this work were provided by the NASA High-End Computing (HEC) Program through the NASA Center for Climate Simulation (NCCS) at Goddard Space Flight Center. A.R. is supported by NSF grants AGS-1617844 and AGS-2017113.

296 **Data Availability.** All CMIP5 and CMIP6 output, including the respective GeoMIP simulations, is
297 available via the Earth System Grid Federation (https://esgf-node.llnl.gov/projects/esgf-llnl/) or
298 by contacting the respective modeling groups responsible for the output.

References

Alterskjær, K., J. E. Kristjansson, and Ø. Seland (2012), Sensitivity to deliberate sea salt seeding of marine clouds – Observations and model simulations, *Atmos. Chem. Phys., 12*, 2,795–2,807, doi:10.5194/acp-12- 2795-2012.

Andrews, T., P. M. Forster, and J. M. Gregory (2009), A surface energy perspective on climate change, *J. Clim., 22*, 2557–2570, doi:10.1175/ 2008JCLI2759.1.

Arora, V. K., and G. J. Boer (2010), Uncertainties in the 20th century carbon budget associated with land use change, *Global Change Biol., 16*, 3327–3348, doi:10.1111/j.1365-2486.2010.02202.x.

Aswathy, V. N., O. Boucher, M. Quaas, U. Niemeier, H. Muri, J. Mülmenstädt, and J. Quaas (2015), Climate extremes in multi-model simulations of stratospheric aerosol and marine cloud brightening climate engineering, *Atmospheric Chemistry and Physics, 15*, 9593-9610, doi:10.5194/acp-15-9593-2015.

Ban-Weiss, G. A., and K. Caldeira (2010), Geoengineering as an optimization problem, *Environ. Res. Lett., 5*, 034009, doi:10.1088/1748-9326/5/ 3/034009.

Boucher, O., et al. (2020), Presentation and evaluation of the IPSL-CM6A-LR climate model, *J. Adv. Model. Earth Sys., 12*, e2019MS002010, doi:10.1029/2019MS002010.

Budyko, M. I. (1977). *Climatic changes*: American Geophysical Union.

Collins, W. J., et al. (2011), Development and evaluation of an Earth-system model—HadGEM2, *Geosci. Model. Dev., 4*, 1051–1075, doi:10.5194/ gmd-4-1051-2011.

Crutzen, P. J. (2006), Albedo enhancement by stratospheric sulfur injections: A contribution to resolve a policy dilemma? *Climatic Change*, *77*, 211–220.

Curry, C. L., et al. (2014), A multimodel examination of climate extremes in an idealized geoengineering experiment, *J. Geophys. Res.*, *119*, 3900–3923, doi:10.1002/2013JD020648.

Dufresne, J.-L., et al. (2013), Climate change projections using the IPSL- CM5 Earth System Model: From CMIP3 to CMIP5, *Clim. Dyn., 40*, 2123–2165, doi:10.1007/s00382-012-1636-1.

Eyring, V., S. Bony, G. A. Meehl, C. A. Senior, B. Stevens, R. J. Stouffer, and K. E. Taylor (2016), Overview of the Coupled Model Intercomparison Project Phase 6 (CMIP6) experimental design and organization, *Geosci. Model Dev., 9*, 1937–1958, doi:10.5194/gmd-9-1937-2016.

Flynn, C. M. and T. Mauritsen (2020, On the Climate Sensitivity and Historical Warming Evolution in Recent Coupled Model Ensembles, *Atmos. Chem. Phys. Discuss.,* in review, doi:10.5194/acp-2019-1175.

Gent, P. R., et al. (2011), The Community Climate System Model 4, *J. Clim., 24*, 4973–4991, doi:10.1175/2011JCLI4083.1.

Gertler, C. G., P. A. O'Gorman, B. Kravitz, J. C. Moore, S. J. Phipps, and S. Watanabe (2020), Weakening of the extratropical storm tracks in solar geoengineering scenarios, *Geophys. Res. Lett., 47*, e2020GL087348, doi:10.1029/2020GL087348.

Gettelman, A., et al. (2019), The whole atmosphere community climate model version 6 (WACCM6), *J. Geophys. Res., 124,* 12380–12403, doi:10.1029/2019JD030943.

Giorgetta, M. A., et al. (2013), Climate and carbon cycle changes from 1850 to 2100 in MPI-ESM simulations for the Coupled Model Intercomparison Project phase 5, *J. Adv. Model. Earth Syst.*, 5, 572–597, doi:10.1002/jame.20038.

Glienke, S., P. J. Irvine, and M. G. Lawrence (2015), The impact of geoengineering on vegetation in experiment G1 of the GeoMIP, *Journal of Geophysical Research*, *120*, 10196-10213, doi:10.1002/2015JD024202.

Gordon, C., et al. (2000), The simulation of SST, sea ice extents and ocean heat transports in a version of the Hadley Centre coupled model without flux adjustments, *Clim. Dyn., 16*, 147–168, doi:10.1007/s003820050010.

Govindasamy, B., and K. Caldeira (2000), Geoengineering Earth's radiation balance to mitigate CO_2-induced climate change, *Geophys. Res. Lett., 27*, 2141–2144, doi:10.1029/1999GL006086.

Hansen, J. E., et al. (2005), Efficacy of climate forcings, J. Geophys. Res., *110*, D18104.

Hazeleger, W., et al. (2011), EC-Earth V2.2: Description and validation of a new seamless Earth system prediction model, *Clim. Dyn., 39*, 2611–2629, doi:10.1007/s00382-011-1228-5.

Hourdin, F., et al. (2012), Impact of the LMDZ atmospheric grid configura- tion on the climate and sensitivity of the IPSL-CM5A coupled model, *Clim. Dyn., 40*, 2167–2192, doi:10.1007/s00382-012-1411-3.

Hurrell, J. W., et al. (2013), The Community Earth System Model: A Framework for Collaborative Research. *Bull. Amer. Meteor. Soc.*, *94*, 1339–1360, doi:10.1175/BAMS-D-12-00121.1.

Irvine, P. J., B. Kravitz, H. Muri, and M. G. Lawrence (2016), An overview of the Earth system science of solar geoengineering, *Wiley Interdisciplinary Reviews, 7,* 815-833, doi:10.1002/wcc.423.

Irvine, P., K. Emmanuel, J. He, L. W. Horowitz, G. Vecchi, and D. Keith (2019), Halving warming with idealized solar geoengineering moderates key climate hazards, *Nature Climate Change*, *9*, 295-299.

Ji, D., et al. (2014), Description and basic evaluation of Beijing Normal University Earth System Model (BNU-ESM) version 1, *Geosci. Model Dev.*, *7*, 2039-2064, doi:10.5194/gmd-7-2039-2014.

Jones, A., et al. (2013), The impact of abrupt suspension of solar radiation management (termination effect) in experiment G2 of the Geoengineering Model Intercomparison Project (GeoMIP), *J. Geophys. Res., 118,* 9743-9752, doi:10.1002/jgrd.50762.

Jones A., J.M. Haywood, A.C. Jones, S. Tilmes, A. Robock and B. Kravitz, Why sophisticated aerosol modelling is needed for understanding regional implications of solar radiation management, *Atmos. Chem. Phys.*, in preparation.

Commenté [AR1]: Is this Jones et al. (2020)? I don't know anything about it, even though I am listed as an author.

Kalidindi, S., G. Bala, A. Modak, and K. Caldeira (2015), Modeling of solar radiation management: a comparison of simulations using reduced solar constant and stratospheric sulphate aerosols, *Clim Dyn, 44*, 2909-2925, doi:10.1007/s00382-014-2240-3.

Kelley, M., G.A. Schmidt, L. Nazarenko, R.L. Miller, S.E. Bauer, R. Ruedy, G.L. Russell, I. Aleinov, M. Bauer, R. Bleck, V. Canuto, G. Cesana, Y. Cheng, T.L. Clune, B. Cook, C.A. Cruz, A.D. Del Genio, G.S. Elsaesser, G. Faluvegi, N.Y. Kiang, D. Kim, A.A. Lacis, A. Leboissetier, A.N. LeGrande, K.K. Lo, J.C. Marshall, S. McDermid, E.E. Matthews, K. Mezuman, L.T. Murray, V. Oinas, C. Orbe, C. Pérez García-Pando, J.P. Perlwitz, M.J. Puma, D. Rind, A. Romanou, D.T. Shindell, S. Sun, N. Tausnev, K. Tsigaridis, G. Tselioudis, E. Weng, J. Wu, and M.-S. Yao (2020), GISS-E2.1: Configurations and climatology. *J. Adv. Model. Earth Syst*., accepted, doi:10.1029/2019MS002025.

Kirkevåg, A., et al. (2013), Aerosol-climate interactions in the Norwegian Earth System Model—NorESM1-M, *Geosci. Model. Dev., 6*, 207–244, doi:10.5194/gmd-6-207-2013.

Knutti, R., D. Masson, and A. Gettelman (2013), Climate model genealogy: Generation CMIP5 and how we got there, *Geophys. Res. Lett., 40*, 1194-1199, doi:10.1002/grl.50256.

Kravitz, B. , A. Robock, O. Boucher, H. Schmidt, K. E. Taylor, G. Stenchikov, and M. Schulz (2011), The Geoengineering Model Intercomparison Project (GeoMIP), *Atmosph. Sci. Lett., 12*, 162-167, doi:10.1002/asl.316.

Kravitz, B., et al. (2013a), Climate model response from the Geoengineering Model Intercomparison Project (GeoMIP), *J. Geophys. Res.*, *118*, 1-13, doi:10.1002/jgrd.50646.

Kravitz, B., et al. (2013b), An energetic perspective on hydrological changes in the Geoengineering Model Intercomparison Project (GeoMIP), *J. Geophys. Res.*, *118*, 13087-13102, doi:10.1002/2013JD020502.

Kravitz, B., et al. (2014), A multi-model assessment of regional disparities caused by solar geoengineering, *Environ. Res. Lett.*, *9*, 074013, doi:10.1088/1748-9326/14/074013.

Kravitz, B., A. Robock, S. Tilmes, O. Boucher, J. M. English, P. J. Irvine, A. Jones, M. G. Lawrence, M. MacCracken, H. Muri, J. C. Moore, U. Niemeier, S. J. Phipps, J. Sillmann, T. Storelvmo, H. Wang, and S. Watanabe (2015), The Geoengineering Model Intercomparison Project Phase 6 (GeoMIP6): Simulation design and preliminary results, *Geosci. Model Dev.*, *8*, 3379-3392, doi:10.5194/gmd-8-3379-2015.

Kravitz, B., D. G. MacMartin, H. Wang, and P. J. Rasch (2016), Geoengineering as a design problem, *Earth System Dynamics*, *7*, 469-497, doi:10.5194/esd-7-469-2016.

Kravitz, B., et al. (2017), First simulations of designing stratospheric sulfate aerosol geoengineering to meet multiple simultaneous climate objectives, *J. Geophys. Res., 122*, 12616-12634, doi:10.1002/2017JD026874.

Kravitz, B., D. G. MacMartin, S. Tilmes, J. H. Richter, M. J. Mills, W. Cheng, K. Dagon, A. S. Glanville, J.-F. Lamarque, I. Simpson, J. Tribbia, and F. Vitt (2019), Comparing surface and stratospheric impacts of geoengineering with different SO2 injection strategies, *J. Geophys. Res., 124*, 7900-7918, doi:10.1029/2019JD030329

Lurton, T., et al. (2020), Implementation of the CMIP6 forcing data in the IPSL-CM6A-LR model, *J. Adv. Model. Earth Sys., 12*, e2019MS001940, doi:10.1029/2019MS001940.

MacMartin, D. G., D. W. Keith, B. Kravitz, and K. Caldeira (2013), Management of trade-offs in geoengineering through optimal choice of non-uniform radiative forcing, *Nature Climate Change*, *3*, 365-368, doi:10.1038/nclimate1722.

Mauritsen, T., et al. (2019), Developments in the MPI-M Earth System Model version 1.2 (MPI-ESM1.2) and its response to increasing CO_2, *J. Adv. Model. Earth Sys., 11*, 998– 1038, doi:10.1029/2018MS001400.

Meehl, G. A., C. A. Senior, V. Eyring, G. Flato, J.-F. Lamarque, R. J. Stouffer, K. E. Taylor, and M. Schlund (2020), Context for interpreting equilibrium climate sensitivity and transient climate response from the CMIP6 Earth system models, *Science Advances*, *6*, eaba1981, doi:10.1126/sciadv.aba1981.

Moore, J. C. et al. (2014), Arctic sea ice and atmospheric circulation under the GeoMIP G1 scenario, *J. Geophys. Res.*, *119*, 567-583, doi:10.1002/2013JD021060.

Moreno-Cruz, J. B., K. L. Ricke, and D. W. Keith (2012), A simple model to account for regional inequalities in the effectiveness of solar radiation management, *Climatic Change*, *110*, 649-668.

Neale, R. B., C. Chen, A. Gettelman, P. Lauritzen, S. Park, D. Williamson, A. Conley, R. Garcia, D. Kinnison, and J. Lamarque (2010), Description of the NCAR community atmosphere model (CAM 5.0), NCAR Tech. Note NCAR/TN-486+ STR.

Niemeier, U., H. Schmidt, K. Alterskjær, and J. E. Kristjánsson (2013), Solar irradiance reduction via climate engineering: Impact of different techniques on the energy balance and the hydrological cycle, *J. Geophys. Res. Atmos., 118,* 11,905–11,917, doi:10.1002/2013JD020445.

National Research Council. 2015. Climate Intervention: Reflecting Sunlight to Cool Earth. Washington, DC: The National Academies Press. https://doi.org/10.17226/18988.

Phipps, S. J., L. D. Rotstayn, H. B. Gordon, J. L. Roberts, A. C. Hirst, and W. F. Budd (2011), The CSIRO Mk3L climate system model version 1.0 – Part 1: Description and evaluation, *Geosci. Model Dev., 4*, 483–509, https://doi.org/10.5194/gmd-4-483-2011.

Phipps, S. J., L. D. Rotstayn, H. B. Gordon, J. L. Roberts, A. C. Hirst, and W. F. Budd (2012), The CSIRO Mk3L climate system model version 1.0 – Part 2: Response to external forcings, *Geosci. Model Dev., 5*, 649–682, https://doi.org/10.5194/gmd-5-649-2012.

Pitari, G., V. Aquila, B. Kravitz, A. Robock, S. Watanabe, I. Cionni, N. D. Luca, G. di Genova, E. Mancini, and S. Tilmes (2014), Stratospheric ozone response to sulfate geoengineering: Results from the Geoengineering Model Intercomparison Project (GeoMIP), *J. Geophys. Res.*, *119*, 2629-2653.

Ricke, K. L., M. G. Morgan, and M. R. Allen (2010), Regional climate response to solar-radiation management, *Nat. Geosci., 3*, 537–541, doi:10.1038/ngeo915.

Robock, A. (2000), Volcanic eruptions and climate, *Rev. Geophys.*, 38, 191–219, doi:10.1029/1998RG000054.

Russotto, R. D. and T. P. Ackerman (2018), Changes in clouds and thermodynamics under solar geoengineering and implications for required solar reduction, *Atmos. Chem. Phys., 18*, 11905–11925, doi:10.5194/acp-18-11905-2018.

Schmidt, G. A., et al. (2006), Present-day atmospheric simulations using GISS ModelE: Comparison to in situ, satellite and reanalysis data, *J. Clim., 19*, 153–192, doi:10.1175/JCLI3612.1.

Séférian, R., et al. (2019), Evaluation of CNRM Earth-System model, CNRM-ESM2-1: Role of Earth system processes in present-day and future climate, *J. Adv. Model. Earth Sys., 11*, 4182–4227, doi:10.1029/2019MS001791.

Sellar, A. A., et al. (2019), UKESM1: Description and evaluation of the U.K. Earth System Model, *J. Adv. Model. Earth Sys., 11*, 4513–4558, doi:10.1029/2019MS001739.

Simpson, I., S. Tilmes, J. Richter, B. Kravitz, D. MacMartin, M. Mills, J. Fasullo, and A. Pendergrass (2019), The regional hydroclimate response to stratospheric sulfate geoengineering and the role of stratospheric heating, *J. Geophys. Res., 124*, 12587-12616, doi:10.1029/2019JD031093.

Stevens, B., et al. (2013), The atmospheric component of the MPI-M Earth System Model: ECHAM6, *J. Adv. Model. Earth Syst., 5*, doi:10.1002/jame.20015.

Swart, N. C., et al. (2019), The Canadian Earth System Model version 5 (CanESM5.0.3), *Geosci. Model Dev.*, *12*, 4823-4873, doi:10.5194/gmd-12-4823-2019.

Taylor, K. E., R. J. Stouffer, and G. A. Meehl (2012), An overview of CMIP5 and the experiment design, *Bull. Am. Meteorol. Soc., 93*, 485–498, doi:10.1175/BAMS-D-11-00094.1.

Tilmes, S., et al. (2013), The hydrological impact of geoengineering in the Geoengineering Model Intercomparison Project (GeoMIP), *J. Geophys. Res.*, *118*, 11036-11058, doi:10.1002/jgrd.50868.

Vignesh, P. P., J. H. Jiang, P. Kishore, H. Su, T. Smay, N. Brighton, and I. Velicogna (2020), Assessment of CMIP6 cloud fraction and comparison with satellite observations, *Earth and Space Science*, 7, e2019EA000975, doi:10.1029/2019EA000975.

Visioni, D., D. G. MacMartin, B. Kravitz, S. Tilmes, M. J. Mills, J. H. Richter, and M. P. Boudreau (2019), Seasonal injection strategies for stratospheric aerosol geoengineering, *Geophysical Research Letters, 46,* 7790-7799, doi:10.1029/2019GL083680.

Watanabe, S., et al. (2008), Development of an atmospheric general circulation model for integrated Earth system modeling on the Earth Simulator, *J. Earth Simulator, 9*, 27–35.

Watanabe, S., et al. (2011), MIROC-ESM 2010: Model description and basic results of CMIP5-20c3m experiments, *Geosci. Model Dev., 4*, 845–872, doi:10.5194/gmd-4-845-2011.

Xia, L., et al. (2014), Solar radiation management impacts on agriculture in China: A case study in the Geoengineering Model Intercomparison Project (GeoMIP), *J. Geophys. Res. Atmos., 119*, 8695-8711, doi:10.1002/2013JD020630.

Zelinka, M. D., et al. (2020), Causes of higher climate sensitivity in CMIP6 models, *Geophys. Res. Let.*, 47, e2019GL085782, doi:10.1029/2019GL085782.

#	Model	Gen.	Reference	G1 Solar reduction (%)	Notes
1	BNU-ESM	CMIP5	Ji et al. (2014)	3.80	Cloud forcing not available
2	CanESM2	CMIP5	Arora et al. (2011)	4.00	
3	CCSM4	CMIP5	Gent et al. (2011)	4.25	NPP not available
4	CESM-CAM5.1-FV	CMIP5	Neale et al. (2010) Hurrell et al. (2013)	4.70	
5	CSIRO-Mk3L-1.2	CMIP5	Phipps et al. (2011, 2012)	3.20	Cloud forcing and NPP not available
6	EC-EARTH	CMIP5	Hazeleger et al. (2011)	4.12	Cloud forcing and NPP not available
7	GISS-E2-R	CMIP5	Schmidt et al. (2006)	4.47	
8	HadCM3	CMIP5	Gordon et al. (2000)	4.16	Cloud forcing and NPP not available
9	HadGEM2-ES	CMIP5	Collins et al. (2011)	3.88	
10	IPSL-CM5A-LR	CMIP5	Dufresne et al. (2013) Hourdin et al.(2011)	3.50	NPP not available
11	MIROC-ESM	CMIP5	Watanabe et al. (2008,2011)	5.00	
12	MPI-ESM-LR	CMIP5	Giorgetta et al. (2012) Stevens et al. (2012)	4.68	
13	NorESM1-M	CMIP5	Alterskjær et al. (2012) Kirkevåg et al. (2012)	4.03	
14	CanESM5	CMIP6	Swart et al. (2019)	3.72	
15	CESM2-WACCM	CMIP6	Gettelman et al. (2019)	4.91	
16	CNRM-ESM2.1	CMIP6	Séférian et al. (2019)	3.72	
17	GISS-E2.1-G	CMIP6	Kelley et al. (in revision)	4.13	
18	IPSL-CM6A-LR	CMIP6	Boucher et al. (2020) Lurton et al. (2020)	4.10	
19	MPI-ESM1.2-LR	CMIP6	Mauritsen et al. (2019)	4.57	NPP not available
20	UKESM1.0-LL	CMIP6	Sellar et al. (2019)	3.80	

Table 1. All participating models in both the CMIP5 and CMIP6 eras of GeoMIP, including references. For G1 solar reduction, the percentage is calculated as the percent change in incident solar irradiance at the top-of-atmosphere between G1 and its respective piControl run. Numbers in the first column correspond to the model numbers in Figure 5.

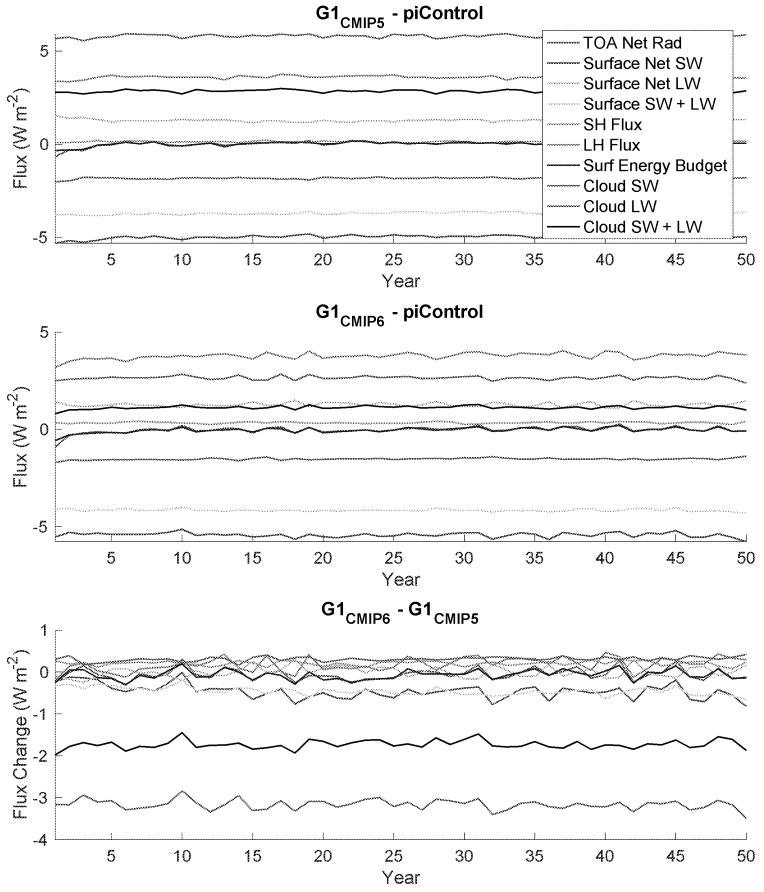

564
565
566 **Figure 1.** Ensemble mean energetics (W m^{-2}) for various flux quantities in $G1_{CMIP5}$ (top), $G1_{CMIP6}$
567 (middle), and the difference (bottom). All fluxes are positive downward, which is
568 counterintuitive for sensible heat (SH) and latent heat (LH). Surf Energy Budget indicates the
569 sum of surface shortwave (SW), surface longwave (LW), SH, and LH. Cloud forcing is calculated
570 as all-sky minus clear-sky.

Commenté [KB2]: Comment from Alan: Do you want to add some indication of the variance between the models with whiskers or shading on each line?

Commenté [KB3R2]: I tried, and it ended up looking more confusing (too much ink).

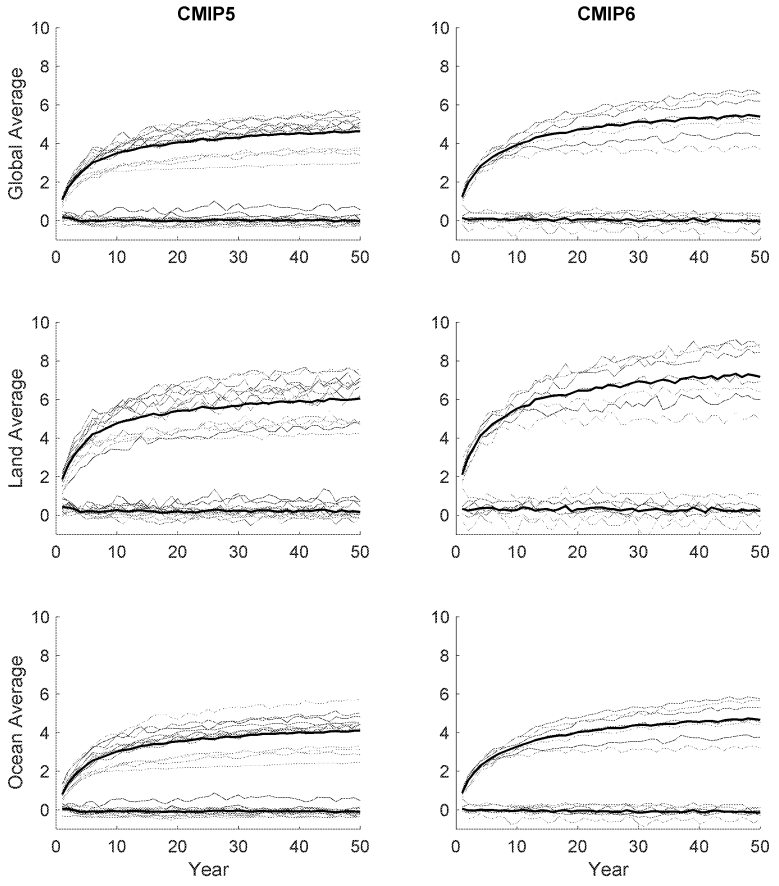

Figure 2. Global mean (top), land mean (middle), and ocean mean (bottom) temperature change (K) for the CMIP5 (left) and CMIP6 (ensembles). Thin colored lines are individual models, and thick black lines are model means. In all panels, the upper cluster of lines is the abrupt4xCO2 simulation, and the lower cluster of lines (approximately zero temperature change for the entire simulation) is experiment G1.

Commenté [KB4]: Still working on how to identify the different models in this figure. I also need to add temperature and units to the y-axes.

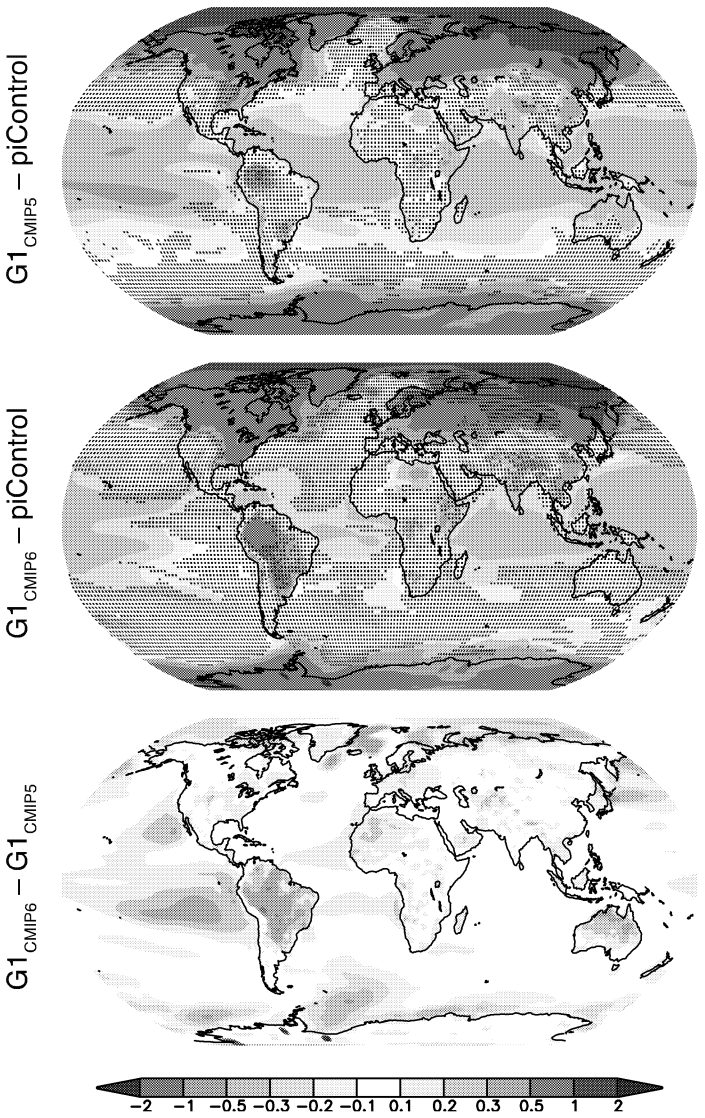

Figure 3. Ensemble average temperature changes (K) for G1 (as compared to the preindustrial control) for CMIP5 (top) and CMIP6 (middle), as well as the difference ($G1_{CMIP6}$ minus $G1_{CMIP5}$, bottom panel). In the top two panels, stippling indicates regions where fewer than 75% of the models in their respective ensembles agree on the sign of the response.

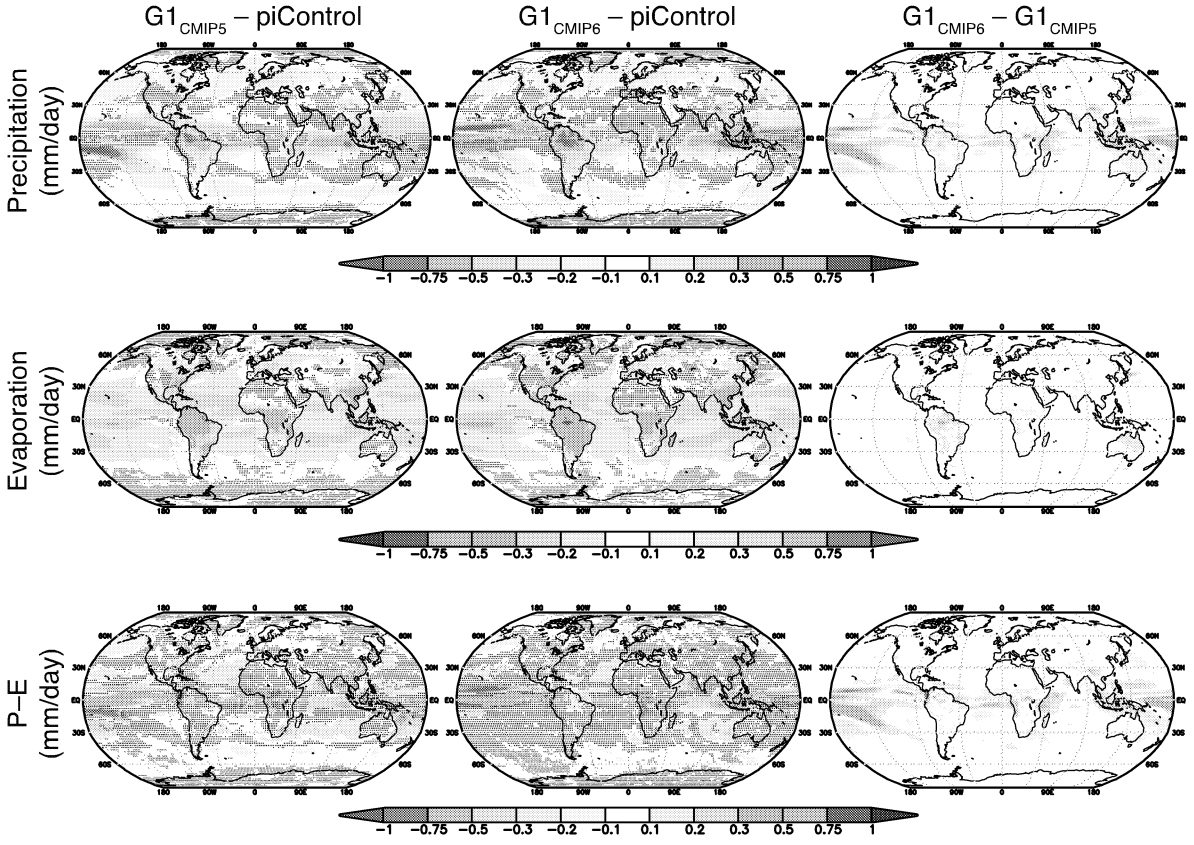

Figure 4. Precipitation (top), evaporation (middle), and precipitation minus evaporation (P-E; bottom) change from preindustrial for the CMIP5 (left) and CMIP6 (middle) ensembles, as well as the ensemble differences (right). All shaded values are ensemble means. Lack of stippling in the left and middle panels indicates agreement on the sign of the values across at least 75% of the models.

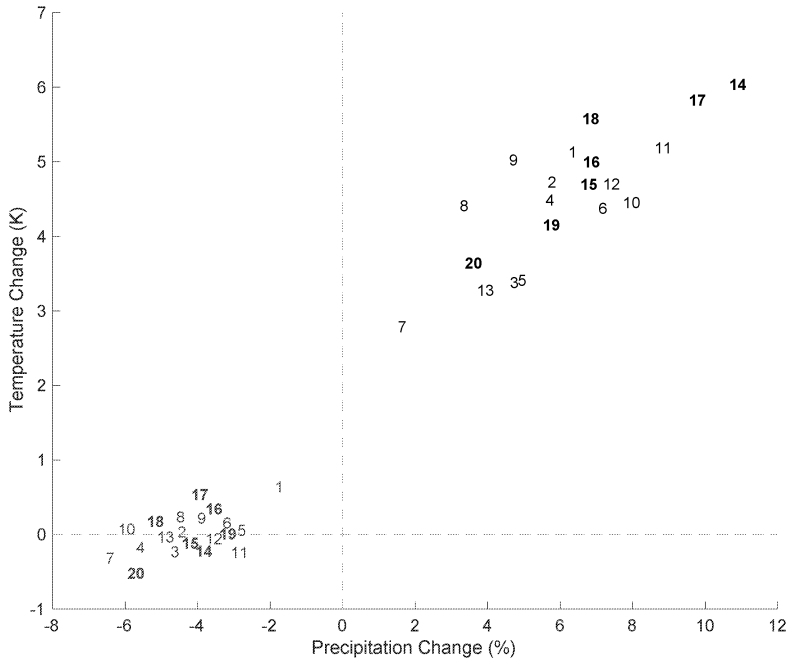

Figure 5. Average (years 11–50) temperature (y-axis; K) and precipitation (x-axis; %) change for each model in this study. Numbers indicate the model number (listed in Table 1, first column). Black numbers are for abrupt4xCO2, and red numbers are for G1. Bolded numbers are for CMIP6.

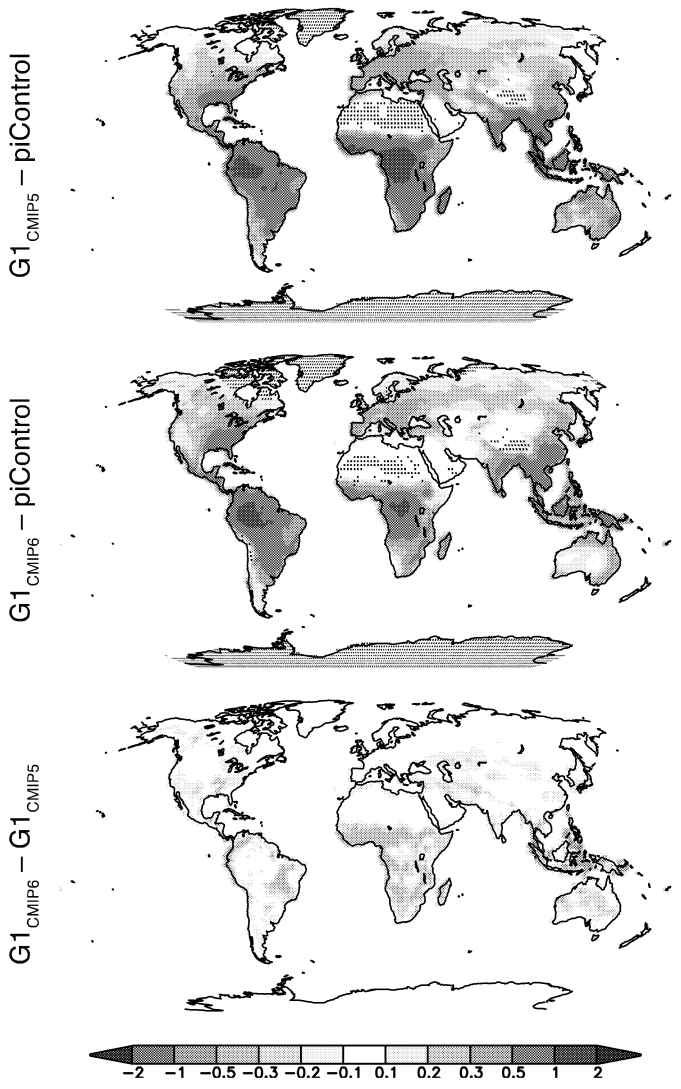

Figure 6. Terrestrial net primary productivity (kg C m^{-2} y^{-1}) for the CMIP5 (top) and CMIP6 (middle) ensembles, as well as the ensemble differences (bottom). All shaded values are ensemble means. Lack of stippling indicates agreement on the sign of the values across at least 75% of the models.

Comparing different generations of idealized solar geoengineering simulations in the Geoengineering Model Intercomparison Project (GeoMIP)

Supplemental Online Material

Ben Kravitz,[1,2,*] Douglas G. MacMartin,[3] Daniele Visioni,[3] Olivier Boucher,[4] Jason N. S. Cole,[5] Jim Haywood,[6,7] Andy Jones,[7] Thibaut Lurton,[4] Michael J. Mills,[8] Pierre Nabat,[9] Ulrike Niemeier,[10] Alan Robock,[11] Roland Séférian,[9] and Simone Tilmes[8]

[1]Department of Earth and Atmospheric Sciences, Indiana University, Bloomington, IN, USA
[2]Atmospheric Sciences and Global Change Division, Pacific Northwest National Laboratory, Richland, WA, USA
[3]Sibley School of Mechanical and Aerospace Engineering, Cornell University, Ithaca, NY, USA
[4]Institut Pierre-Simon Laplace (IPSL), Sorbonne Université/CNRS, Paris, France
[5]Environment and Climate Change Canada, Toronto, Ontario, Canada
[6]College of Engineering, Mathematics and Physical Sciences, University of Exeter, Exeter, United Kingdom
[7]UK Met Office Hadley Centre, Exeter, United Kingdom
[8]Atmospheric Chemistry Observations and Modeling Laboratory, National Center for Atmospheric Research, Boulder, CO, USA
[9]Centre National de Recherches Météorologiques, Université de Toulouse, Météo-France, Toulouse, France
[10]Max Planck Institute for Meteorology, Hamburg, Germany.
[11]Department of Environmental Science, Rutgers University, New Brunswick, NJ, USA

Submission to *Environmental Research Letters*

[*]To whom correspondence should be addressed: 1001 E. 10th Street, Bloomington, IN 47405-1405, USA. bkravitz@iu.edu

S1. Global-scale Temperature Metrics

Supplemental Figure 3 and its associated discussion in Section 3.2 include three temperature metrics (Ban Weiss and Caldeira, 2010; Kravitz et al., 2016): global mean temperature (T_0), the interhemispheric temperature gradient (T_1), and the equator-to-pole temperature gradient (T_2). We define these in terms of the projection of the first three Legendre polynomials onto the temperature field:

$$T_0 = \frac{1}{A} \int_{-\pi/2}^{\pi/2} T(\psi)\, dA$$

$$T_1 = \frac{1}{A} \int_{-\pi/2}^{\pi/2} T(\psi)\, \sin\psi\, dA$$

$$T_2 = \frac{1}{A} \int_{-\pi/2}^{\pi/2} T(\psi)\, (3\sin^2\psi - 1)\, dA$$

where T is temperature, ψ is latitude, and A is area.

S2. Longer-Term Model Behavior

Supplemental Figures 1 and 2 look at G1 behavior over the entire 100-year period of simulation to determine whether there is any drift or trend that would not be revealed by only analyzing 50 years. With the exception of IPSL-CM6A-LR, no model shows any long-term behavior in temperature. Two models (Model X and Model Y) show a slight trend in precipitation and evaporation, with a change of <1% over the first 50 years of simulation. As such, we conclude that our choice to focus on the first 50 years of simulation does not appreciably affect our results.

Supplemental Figure 2 indicates that the temperature trend in IPSL-CM6A-LR is due to temperature changes north of 30°N, possibly related to a slight trend in sea ice coverage (Boucher et al., 2020). This model is also known to have a bicentennial oscillation, which could affect G1–piControl differences, depending on the baseline period used for subtraction. To verify that this oscillation is not impacting our results, we divided the 1200-year piControl run into 50-year chunks and computed the surface air temperature average for each of those chunks. The largest temperature found was 286.0339 K, and the smallest was 285.6384 K. The average over the entire ensemble was 285.8604 K. As such, using the mean of the entire ensemble versus matching the appropriate period in the bicentennial oscillation would have an impact on G1–piControl temperature by at most 0.22 K. Only averaging the first 100 years of the piControl run (which may be the best match to the period covered by G1) yields a

temperature of 285.9084 K, which is 0.048 K different from the mean of the entire piControl run. As such, we conclude that this bicentennial oscillation is unlikely to have substantially influenced our findings.

Supplemental Table 1. Ensemble differences between the CMIP5 and CMIP6 ensembles for each variable evaluated in this study (left column). Column 2 indicates the difference between the ensembles in how much of the Earth's surface is not stippled (more than 75% of models agree on the sign of the response; positive values indicate that CMIP6 has more unstippled area than CMIP5). Column 3 indicates the fraction of the Earth's surface for which the CMIP5 ensemble is statistically different from the CMIP6 ensemble, based on 95th percentile confidence intervals from Welch's *t*-test.

Variable	**Stippling (%)**	**Welch's *t*-test (%)**	**Notes**
Surf. air temperature	-25.77	0.87	
Precipitation	-3.56	11.17	
Evaporation	-2.33	6.47	
Precip minus Evap	-15.23	1.13	
SW Cloud Forcing	-8.02	9.65	
LW Cloud Forcing	11.99	6.57	
Net Primary Prod.	-1.42	1.15	Land surface only

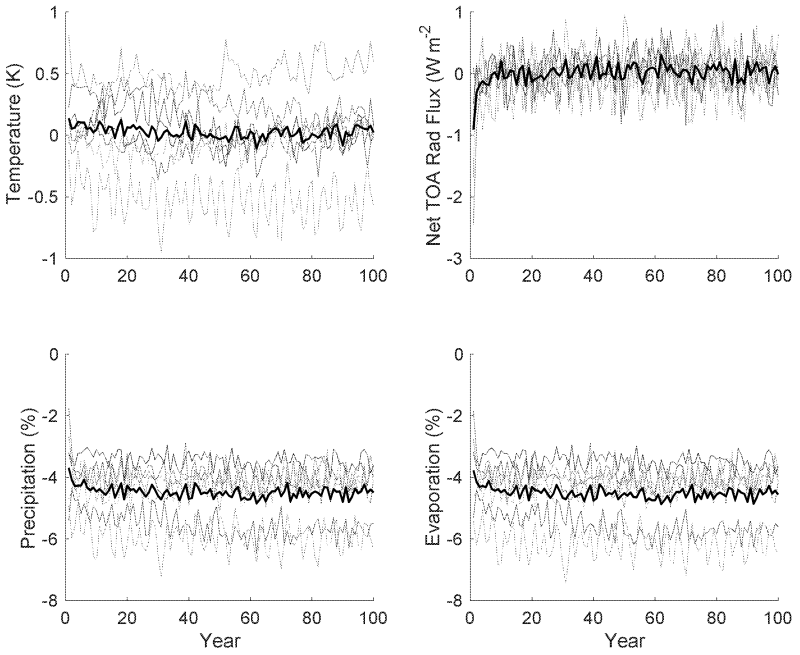

Supplemental Figure 1. Temperature (top left; K), net top-of-atmosphere radiative flux (top right; W m^{-2}), precipitation (bottom left; %), and evaporation (bottom right; %) change in $G1_{CMIP6}$ compared to piControl over 100 years of simulation. Thin colored lines are individual models, and thick black lines are ensemble means.

Commenté [KB5]: Needs a legend

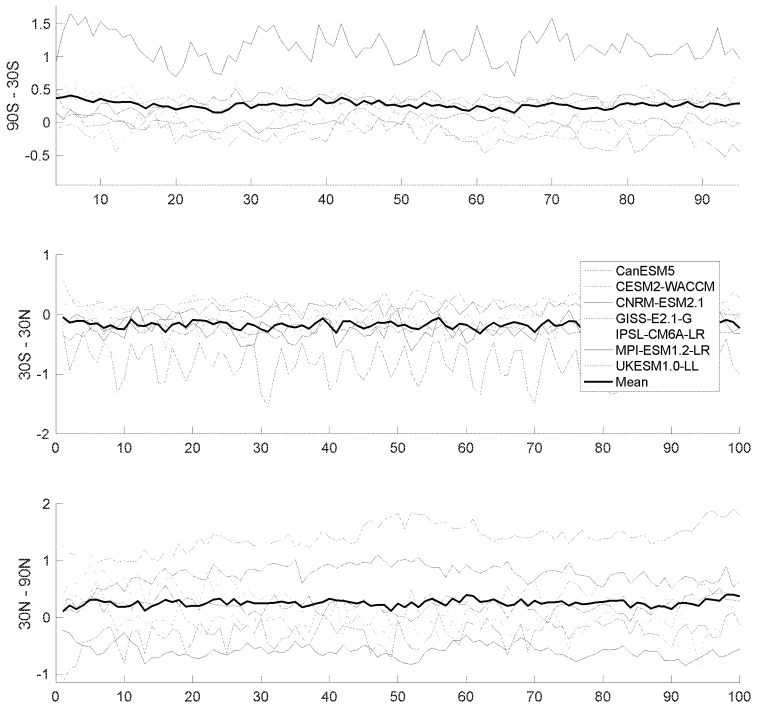

Supplemental Figure 2. Annual mean surface temperature (K) in each model averaged over 90°S-30°S (top), 30°S-30°N (middle), and 30°N-90°N (bottom). The ensemble mean is plotted as thick black lines.

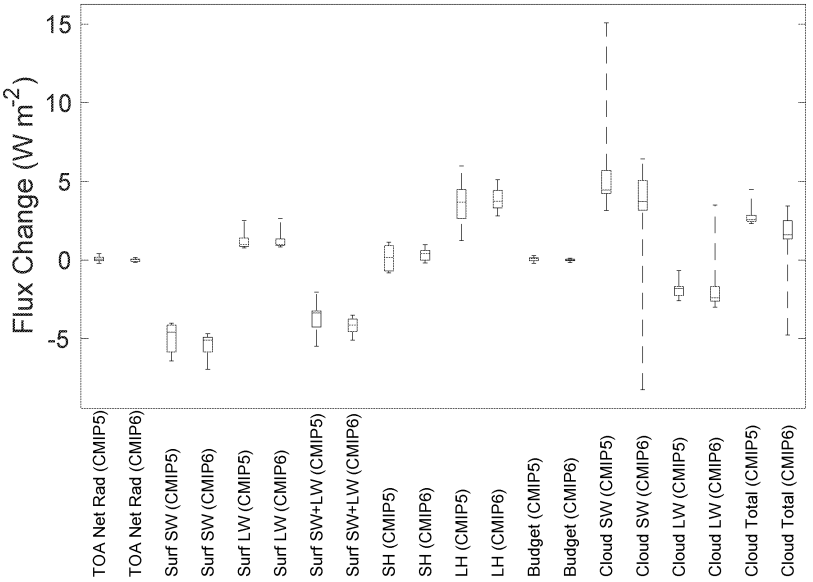

Supplemental Figure 3. Ensemble median (red lines), inter-quartile (blue boxes), and ranges (black whiskers) for the same global mean energetics quantities as in Figure 1 (G1 minus piControl) for both the CMIP5 and CMIP6 ensembles.

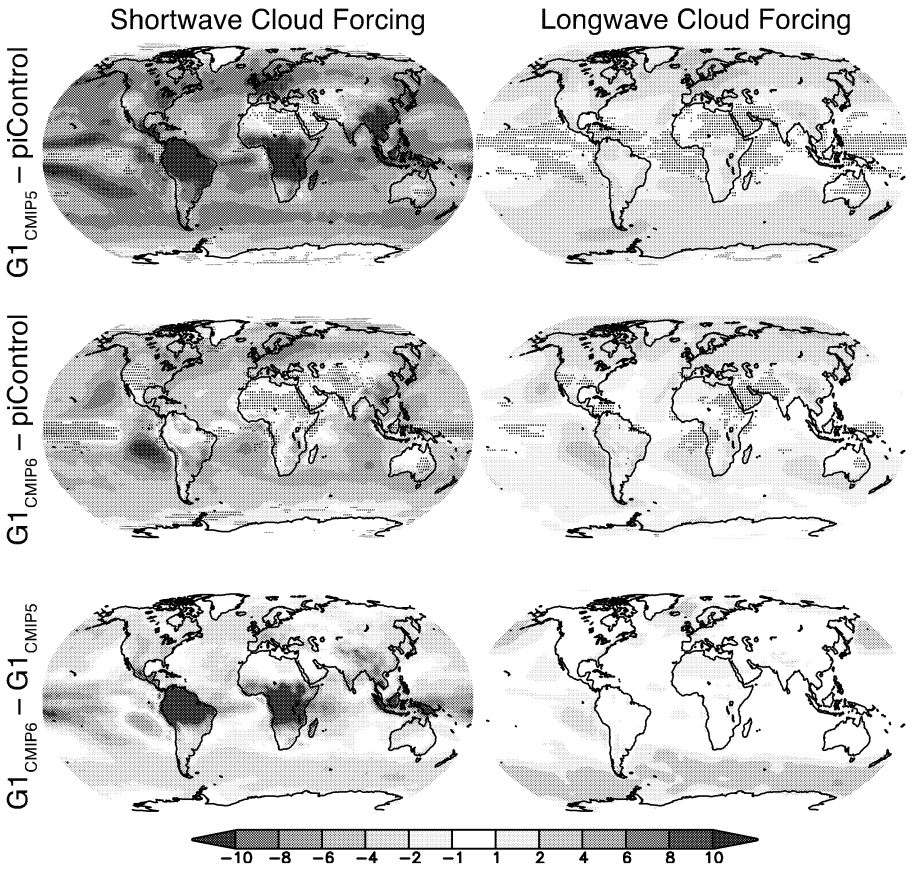

Supplemental Figure 4. Surface shortwave (left) and longwave (right) cloud forcing (W m^{-2}) change from preindustrial for the CMIP5 (top) and CMIP6 (middle) ensembles, as well as the ensemble differences (bottom). Cloud forcing is measured as all-sky minus clear-sky radiative flux. All shaded values are ensemble means. Lack of stippling indicates agreement on the sign of the values across at least 75% of the models.

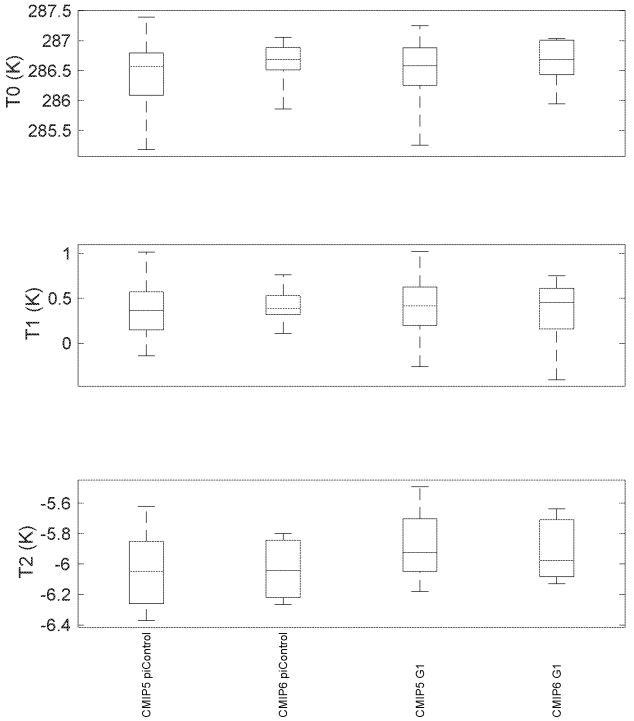

Supplemental Figure 5. Ensemble ranges for global mean temperature (T_0), the interhemispheric temperature gradient (T_1), and the equator-to-pole temperature gradient (T_2), as defined in Supplemental Section 1 (Ban Weiss and Caldeira, 2010; Kravitz et al., 2016). Red lines indicate ensemble medians, blue boxes are the inter-quartile ranges, and black whiskers indicate total ranges.

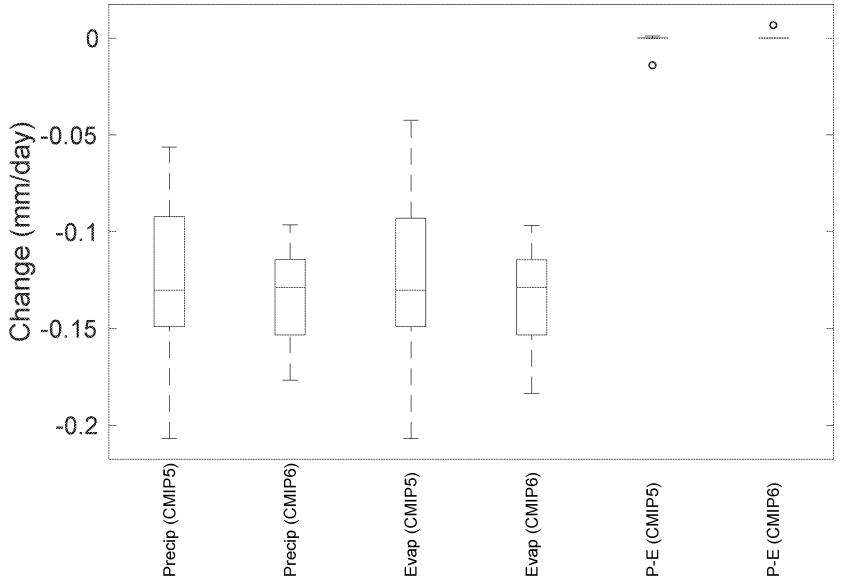

Supplemental Figure 6. Global mean ensemble median (red lines), inter-quartile (blue boxes), and ranges (black whiskers or, for P-E one blue circle indicating an extreme outlier) for the hydrological quantities shown in Figure 4 for both the CMIP5 and CMIP6 ensembles.

Comparing different generations of idealized solar geoengineering simulations in the Geoengineering Model Intercomparison Project (GeoMIP)

Ben Kravitz,[1,2,*] Douglas G. MacMartin,[3] Daniele Visioni,[3] Olivier Boucher,[4] Jason N. S. Cole,[5] Jim Haywood,[6,7] Andy Jones,[7] Thibaut Lurton,[4] Michael J. Mills,[8] Pierre Nabat,[9] Ulrike Niemeier,[10] Alan Robock,[11] Roland Séférian,[9] and Simone Tilmes[8]

[1]Department of Earth and Atmospheric Sciences, Indiana University, Bloomington, IN, USA
[2]Atmospheric Sciences and Global Change Division, Pacific Northwest National Laboratory, Richland, WA, USA
[3]Sibley School of Mechanical and Aerospace Engineering, Cornell University, Ithaca, NY, USA
[4]Institut Pierre-Simon Laplace (IPSL), Sorbonne Université/CNRS, Paris, France
[5]Environment and Climate Change Canada, Toronto, Ontario, Canada
[6]College of Engineering, Mathematics and Physical Sciences, University of Exeter, Exeter, United Kingdom
[7]UK Met Office Hadley Centre, Exeter, United Kingdom
[8]Atmospheric Chemistry Observations and Modeling Laboratory, National Center for Atmospheric Research, Boulder, CO, USA
[9]CNRM, Université de Toulouse, Météo-France, CNRS, Météo-France, Toulouse, France
[10]Max Planck Institute for Meteorology, Hamburg, Germany.
[11]Department of Environmental Sciences, Rutgers University, New Brunswick, NJ, USA

Submission to ~~*Environmental Research Letters*~~ *Atmospheric Chemistry and Physics*

*To whom correspondence should be addressed: 1001 E. 10th Street, Bloomington, IN 47405-1405, USA. bkravitz@iu.edu

Mis en forme : Français (Canada)

Mis en forme : Français (Canada)

Mis en forme : Français (Canada)

Abstract

Solar geoengineering has been receiving increased attention in recent years as a potential temporary solution to offset global warming. One method of approximating global-scale solar geoengineering in climate models is via solar reduction experiments. Two generations of models in the Geoengineering Model Intercomparison Project (GeoMIP) have now simulated offsetting a quadrupling of the CO_2 concentration with solar reduction. Here we show that energetics, temperature, and hydrological cycle changes in this experiment are statistically indistinguishable between the two ensembles. Of the variables analyzed here, the only major differences involve highly parameterized and uncertain processes, such as cloud forcing or terrestrial net primary productivity. ~~W~~Although the climate model experiment analyzed here is artificial and designed to elicit large responses in the models, we conclude that despite numerous structural differences and uncertainties in models over the past 20 years, including an increase in climate sensitivity in the latest generation of models, broad conclusions about the climate response to global solar dimming remain robust.

Keywords: geoengineering, climate engineering, climate intervention, solar radiation management, climate modeling

Three main points

1. The present study investigates the response of the climate system to solar geoengineering across two ensembles of models of different generation
2. Past results about solar dimming remain robust to inter-generational differences in models for most evaluated variables
3. Key ensemble differences are found for highly parameterized and uncertain processes such as clouds and the carbon cycle

Suggested reviewers

- Piers Forster
- Don Wuebbles
- Peter Irvine
- Long Cao
- Ken Caldeira
- Govindasamy Bala
- Jim Hurrell
- Jean-Francois Lamarque

Mis en forme : Police :(Par défaut) Times New Roman

1. Introduction

Solar geoengineering describes a set of technologies designed to (ideally) temporarily, deliberately reduce some of the effects of climate change by changing the radiative balance of the planet, often by reflecting sunlight back to space (NRC, 2015). Numerous methods have been proposed, but ~~arguably~~ the most studied is stratospheric sulfate aerosol injection (Budyko, 1977; Crutzen, 2006). This method involves substantially increasing the stratospheric sulfate aerosol burden, replicating the mechanisms that cause cooling after large volcanic eruptions (Robock, 2000). Climate models remain the most promising tools for understanding the consequences of solar geoengineering. In model simulations of solar geoengineering, insolation reduction is often used as a proxy for actual stratospheric sulfate aerosols, as it captures many of the broad radiative effects of stratospheric aerosol geoengineering as well as some of the important climate effects like surface cooling and hydrological cycle strength reduction (Niemeier et al., 2013; Kalidindi et al., 2015). However, stratospheric sulfate aerosols also absorb longwave radiative flux, which heats the upper troposphere~~/~~ and lower stratosphere. As such, any implementation of stratospheric geoengineering with sulfate aerosols would produce additional effects, such as changing atmospheric circulation in response to stratospheric heating and heating gradients (e.g., Richter et al., 2017; Tilmes et al., 2018; Simpson et al., 2019; Jones et al., 2020) and stratospheric ozone changes (e.g., Pitari et al., 2014), as well as changes in ultraviolet radiative flux and enhanced diffuse radiation at the surface (Madronich et al., 2018). However, here we consider the major, large-scale effect of reflecting sunlight to cool Earth.

Commenté [KB1]: Cut until we get reviews back?

Simulations of solar geoengineering with solar reduction have long shown that solar geoengineering would cool the planet, offsetting global warming (e.g., Govindasamy and Caldeira, 2000; NRC, 2015; Irvine et al., 2016). Idealized simulations of solar reduction have also been simulated in a multi-model context under the Geoengineering Model Intercomparison Project (GeoMIP; Kravitz et al., 2011), to understand the robust model responses to various standardized solar geoengineering simulation designs. Multi-model conclusions from these studies indicate that solar geoengineering would be effective at partially offsetting greenhouse gas-induced temperature changes (Kravitz et al., 2013a), as well as changes in the hydrological cycle (Tilmes et al., 2013), the cryosphere (Moore et al., 2014), extreme events (Curry et al., 2014; Aswathy et al., 2015), vegetation (Glienke et al., 2015), circulation (Guo et al., 2018; Gertler et al., 2020), agriculture (Xia et al., 2014), and numerous other areas. However, the offset is not perfect (Moreno-Cruz et al., 2012), particularly on a regional basis or when considering multiple simultaneous metrics of climate change (Kravitz et al., 2014; Irvine et al., 2019; Jones et al., 2020), leading to concerns about winners and losers from geoengineering (Ricke et al., 2010). To some extent, the effects of solar geoengineering may be tailored or designed (MacMartin et al., 2013; Kravitz et al., 2016, 2017, 2019), but solar geoengineering will still not be able to perfectly offset climate change from greenhouse gases.

Commenté [KB2]: Cut until we get reviews back?

The previous phase of GeoMIP was associated with the Coupled Model Intercomparison Project Phase 5 (CMIP5; Taylor et al., 2012), an international collaboration of climate models to attempt to understand robust model responses to various forcings. GeoMIP has now entered a new phase, concurrent with the Coupled Model Intercomparison Project Phase 6 (CMIP6; Eyring et al., 2016), and with it are new solar geoengineering simulations with new and updated versions of Earth System Models (Kravitz et al., 2015). As such, this is an opportunity to revisit some

central questions in solar geoengineering. Many of the CMIP5 results regarding solar geoengineering showed substantial agreement across the participating GeoMIP models. In this newest iteration of GeoMIP, do the same science conclusions still hold, and do the models still generally agree on the resulting climate effects? Here we address these questions by evaluating and comparing general climate model response to GeoMIP experiment G1 (described in the next section) from both CMIP5 and CMIP6.

2. Simulations and Participating Models

In this study, we evaluate GeoMIP experiment G1, in which, starting from a preindustrial control (piControl) baseline, the atmospheric CO_2 concentration is instantaneously quadrupled (the standard CMIP experiment abrupt4xCO2), and insolation is simultaneously reduced such that net top-of-atmosphere (TOA) radiative flux is approximately unchanged from the baseline in the first decade of simulation (Kravitz et al., 2011, 2015). This experiment was part of the original suite of GeoMIP experiments and was repeated and extended in the newest suite in an effort to understand the role of model structural uncertainty in broad conclusions about solar geoengineering. Participating models are listed in Table 1. We include 13 models from CMIP5 and 7 models from CMIP6.

Because the main focus of this paper is a comparison between the CMIP5 and CMIP6 generations of model results, we have opted for the following to aid comparisons:

- The original G1 experiment was 50 years in length, whereas the CMIP6 version is 100 years in length to allow for better analyses of rare events or to capture very slow responses. Since we are not evaluating any features that require 100 years of statistics, and the results do not show any appreciable time evolution of behavior after the first couple of years (see Supplemental Section 2 and Supplemental Figures 1 and 2), we only evaluate the first 50 years of all simulations. All maps show changes over years 11-50, removing the initial transient period.
- We do not compare previous versions of individual models with current ones, instead only examining ensembles. Even though models may share similar development histories (e.g., atmosphere and ocean dynamical cores, convective parameterizations, radiative transfer modules, terrestrial biosphere and cryosphere~~, etc.~~; Knutti et al., 2013; Zelinka et al., 2020), there have been numerous developments in models in these areas (and others) between CMIP5 and CMIP6 such that in most cases a direct comparison would not be meaningful.
- We focus extensively on the G1 results and, with few exceptions, do not focus on the corresponding abrupt4xCO2 simulations. It has been well documented that the CMIP6 models tend to have higher climate sensitivities than the CMIP5 models (Flynn and Mauritsen, 2020; Meehl et al., 2020; Zelinka et al., 2020), so we do not wish to make conclusions that might be based on a form of selection bias.
- All lack of stippling on map plots, as in previous GeoMIP studies (e.g., Kravitz et al., 2013a), indicates agreement on the sign of the response in at least 75% of models. Because $G1_{CMIP5}$ has more participating models than $G1_{CMIP6}$, this threshold provides some consistency across analyses of the ensembles. When plotting differences between the ensembles ($G1_{CMIP6}$-$G1_{CMIP5}$), there is no stippling, as it is difficult to meaningfully represent such differences between ranges. Aggregate differences between the two

Mis en forme : Police :(Par défaut) Times New Roman

ensembles, as calculated using Welch's *t*-test or differences in stippled area, are discussed in Supplemental Table 1.

3. Results

3.1. Energetics

Ensemble mean radiative and turbulent flux quantities are plotted in Figure 1, and the ensemble ranges are plotted in Supplemental Figure 3. An immediate observation is that, in both ensembles, the models were successful at limiting net TOA radiative flux change to within approximately ±0.1 W m^{-2} of the models' respective preindustrial values. Accomplishing this required an average solar reduction of 4.14% (models range in 3.20–5.00%) in CMIP5 and 4.14% (3.72–4.91%) in CMIP6. As such, despite numerous structural changes between the two generations of models, there is no appreciable change in solar efficacy (Hansen et al., 2005).

None of the radiative flux quantities indicate large transients over 50 years of simulation of G1, other than the initial flux change within the first year or so of simulation. This is consistent with the "perpetual fast response" found by Kravitz et al. (2013b), in which because global mean temperature does not change appreciably over the course of the G1 simulation, climate feedbacks are not excited, and the internal state of the system (as measured by, for example, fluxes and hydrological cycle changes) similarly does not change. Ensemble mean fluxes show few differences (<1 W m^{-2} in magnitude) with the exception of shortwave cloud forcing, defined as all-sky minus clear-sky shortwave flux at the surface. On average, the CMIP6 ensemble has 3–4 W m^{-2} less shortwave cloud forcing than CMIP5. Neglecting some outliers, for each flux except shortwave (and hence total) cloud forcing, the median model in one ensemble is within the inter-quartile range of the other ensemble. This indicates that there are no major differences between the ensembles in how the models handle energy balance and energetics, with the exception of clouds, which is consistent with findings about CMIP6 (Zelinka et al., 2020). Moreover, it appears that most of the major differences in shortwave cloud forcing are due to outliers in each ensemble, positive for CMIP5 and negative for CMIP6.

To further explore these potential differences, Supplemental Figure 4 provides maps of the ensemble means for cloud forcing. In G1, the CMIP5 ensemble showed more positive shortwave cloud forcing and more negative longwave cloud forcing (i.e., more cancellation) than the CMIP6 ensemble. Overall, the CMIP6 ensemble has greatly reduced (in some places by over 10 W m^{-2}) shortwave cloud forcing as compared to CMIP5 under the G1 experiment. This is a widespread result, but the most prominent features are in the tropics, especially over the Amazon, Africa, and the Maritime Continent. These regions encompass tropical forests, indicating a potential for vegetation feedbacks on the temperature reductions. However, the reasons behind these forcing changes are difficult to diagnose, as they could be due to changes in cloud thickness, cloud cover, or cloud level between CMIP5 and CMIP6 models (e.g., Vignesh et al., 2020), differences in how solar geoengineering affects clouds (Russotto and Ackerman, 2018), or artifacts of the analyses (e.g., cloud masking; Andrews et al., 2009; Kravitz et al., 2013b). Moreover, based on the results in Supplemental Figure 3, it is likely that many of these features are exaggerated by outlier models (also see Vignesh et al., 2020). As such, we reserve such detailed investigations for future work.

3.2. Temperature

These small flux changes also lead to few G1 temperature changes between the two ensembles. Figure 2 shows global, land, and ocean-averaged temperatures for the CMIP5 and CMIP6 ensembles. In general, the abrupt4xCO2 simulation in CMIP6 has higher temperatures than in CMIP5, consistent with the noted increase in climate sensitivity (Vial et al., 2013; Flynn and Mauritsen, 2020; Meehl et al., 2020; Zelinka et al., 2020). In both ensembles, G1 is effective at offsetting global mean temperature change, in some cases with a slight positive residual temperature change over land. Supplemental Figure 5 shows three aggregate temperature metrics: global mean temperature, the interhemispheric temperature gradient, and the equator-to-pole temperature gradient (Ban Weiss and Caldeira, 2010; Kravitz et al., 2016). As for the fluxes, the median model in one ensemble is within the inter-quartile range of the other ensemble. This indicates that no ensemble is on average warmer or cooler than another, has a substantially warmer Northern or Southern Hemisphere than the other, or has warmer tropics or poles than the other. We can conclude that spatial patterns of temperature change from G1 are robust across a wide range of structural uncertainty, including an increase in climate sensitivity between the two generations of CMIP.

The spatial structure of temperature change (Figure 3) does have small differences between the two ensembles. G1 in CMIP6 has multiple locations that are warmer than G1 in CMIP5, despite both ensembles achieving net energy balance at TOA and the surface (Figure 1). The majority of the differences are over land and in the tropics, where CMIP6 is slightly warmer than CMIP5 (up to a degree Celsius in some places). Nevertheless, both ensembles show the well noted feature that offsetting a CO_2 increase with globally uniform solar reduction overcools the tropics and undercools the poles (Govindasamy and Caldeira, 2000; Kravitz et al., 2013a). CMIP6 shows slightly less high latitude warming than CMIP5, but temperature differences between the two ensembles are largely negligible. However, the warmer temperatures in CMIP6 near Greenland have important implications for ice sheet melt and consequent sea level rise, as well as bottom water formation. We reserve such analyses for future investigations, particularly since the models used here are not capable of simulating the eustatic component of sea level rise. In any case, these ensemble mean differences between CMIP5 and CMIP6 cannot be deemed statistically significant (Supplemental Table 1 and Supplemental Figure 4).

3.3. Hydrological and Other Integrative Changes

Figure 4 shows ensemble mean changes in precipitation (P), evaporation (E), and P–E for $G1_{CMIP5}$ and $G1_{CMIP6}$. Qualitatively, patterns are similar between both ensembles. Precipitation is slightly (<0.3 mm/day in magnitude) different in the tropics between the two ensembles. The majority of those features can be summarized as a more southward intertropical convergence zone (ITCZ), more precipitation in the South Pacific Convergence Zone, and less precipitation over Southeast Asia and the Maritime Continent in $G1_{CMIP6}$. Evaporation in the two ensembles is nearly identical except for more evaporation in Amazonia and Australia in $G1_{CMIP6}$. As such, the net P–E change between the two ensembles strongly resembles the precipitation changes. Supplemental Figure 6 shows that, like previous evaluations of ensemble ranges, the median model in one ensemble falls well within the interquartile range of the other ensemble for P, E,

and P–E. As such, we cannot conclude any robust hydrological cycle changes between the two ensembles.

Figure 5 shows average (years 11–50) temperature change (with respect to piControl) plotted against average precipitation change for each model, as in Tilmes et al. (2013). Other than a potentially greater climate sensitivity of some CMIP6 models, there is no distinguishable difference in aggregate behavior between the two ensembles. The same conclusion discovered by Tilmes et al. (2013) holds: solar reduction cannot simultaneously offset CO_2-induced changes in both global mean temperature and global mean precipitation.

As an integrator of CO_2, temperature, and precipitation effects over land, Figure 6 shows changes in terrestrial net primary productivity (NPP). Numerous land regions have lower NPP in CMIP6 than in CMIP5. The ensemble average global NPP change (G1–piControl) is 51.2 (4.1–122.1) Pg C y^{-1} in CMIP5 and 38.1 (19.5–77.5) Pg C y^{-1} in CMIP6, representing a 25.6% difference in means. Jones et al. (2013) used NPP to highlight the importance of understanding the influence of structural land model differences on climate results related to geoengineering. While it is beyond the scope of this study to perform a detailed diagnosis of which uncertainties or processes are responsible for this inter-ensemble difference, we show that the ensemble spread of total terrestrial NPP is smaller in CMIP6 than in CMIP5. This result is consistent with the recent assessment of carbon cycle feedbacks conducted by Arora et al. (2020), which demonstrates that the CMIP6 ensemble has reduced overall uncertainty in the land carbon cycle to rising CO_2 compared to their CMIP5 predecessors.

4. Discussion and Conclusions

Based on the results presented here, model response to G1 has not changed substantially between CMIP5 and CMIP6, despite numerous changes to models between the two generations, including an increase in climate sensitivity. The sign of residual climate impacts (for example in temperature) are in better agreement in CMIP5 than CMIP6 (Supplemental Table 1 shows a difference in stippled area between the two ensembles), but this could be a function of the smaller ensemble size in CMIP6. Energetics, temperature, and the hydrological cycle are qualitatively and quantitatively similar in both ensemble means and ensemble ranges, although these variables are somewhat related, so we might expect them to all portray a similar picture. Notable differences do exist in shortwave cloud forcing and NPP, particularly in Amazonia, Africa, and Australia, which are also regions of inter-ensemble difference in precipitation.

From these findings, we can conclude that results obtained over the past 20 years of study have not been overturned by the latest round of simulations. All of the major ensemble differences highlighted above deal with clouds and land surface modeling, both of which are difficult to model and are necessarily highly parameterized. The conclusions that are based on more fundamental knowledge, such as column energetics (in the case of the hydrological cycle), are relatively robust to structural uncertainty, in so far as this study adequately captures representative variations in structural uncertainty. This lends confidence to our conclusions, especially regarding robustness to uncertainty, about the broad climate effects from solar geoengineering methods that can be accurately represented via solar dimming.

We also conclude that the models used in CMIP5 are not obviously biased or inferior as compared to CMIP6. While improvements have been made in the CMIP6 generation of models, and those models are likely better for representing numerous features of the present-day climate that may be important for studies of geoengineering, there are many aspects of climate that are well represented by earlier models. In some cases, more robust analyses may be enabled by augmenting ensemble sizes with archived output from earlier generations of CMIP models.

There are numerous aspects of physical climate that we did not evaluate, nor did we pursue analyses beyond physical climate, including many other aspects of natural science, social science, the humanities, governance, justice, or ethics (to name a few important areas). Moreover, we emphasize that experiment G1 is an idealized experiment aimed at understanding physical climate response to combinations of large forcings and should not be interpreted as a realistic or policy-relevant scenario of geoengineering. A holistic assessment of the consequences of geoengineering, particularly of more policy-relevant scenarios, would certainly need to take these numerous aspects into account. Nevertheless, based on the results presented here, results for geoengineering across several important metrics appear to be robust to some amount of structural uncertainty. This lends confidence to some conclusions drawn from global climate models regarding solar geoengineering.

Many of the broad features of solar geoengineering with sulfate aerosols can be represented by a reduction in solar constant (e.g., Niemeier et al., 2013; Kalidindi et al., 2015). However, the more subtle changes that derive from complex response to stratospheric aerosol heating (for example, the positive wintertime North Atlantic Oscillation; Jones et al., 2020) require detailed assessments with state-of-the-art aerosol microphysical schemes. This is particularly important for understanding regional and seasonal solar geoengineering (Kravitz et al., 2017; Visioni et al., 2019). Such detailed microphysical calculations can only be simulated in a small number of models; in the case of Jones et al. (2020), only two models were available. While simple G1-style experiments enable a robust multi-model ensemble analysis, they cannot capture details that depend on microphysics. We emphasize the importance of a variety of modeling approaches to understand solar geoengineering, particularly the role of model uncertainty in conclusions about solar geoengineering.

Acknowledgments. We acknowledge the World Climate Research Programme, which, through its Working Group on Coupled Modelling, coordinated and promoted CMIP. We thank the climate modeling groups for producing and making available their model output, the Earth System Grid Federation (ESGF) for archiving the data and providing access, and the multiple funding agencies who support CMIP6 and ESGF. We also thank all participants of the Geoengineering Model Intercomparison Project and their model development teams. Support for B.K. was provided in part by the National Science Foundation (NSF) through agreement CBET-1931641, the Indiana University Environmental Resilience Institute, and the *Prepared for Environmental Change* Grand Challenge initiative. The Pacific Northwest National Laboratory is operated for the US Department of Energy by Battelle Memorial Institute under contract DE-AC05-76RL01830. Resources supporting this work were provided by the NASA High-End Computing (HEC) Program through the NASA Center for Climate Simulation (NCCS) at Goddard Space Flight Center. A.R. is supported by NSF grants AGS-1617844 and AGS-2017113. U. N. is supported by the German DFG-funded Research Unit VollImpact FOR2820

Commenté [AR3]: I tried to mention this in the abstract.

Commenté [KB4]: Cut until we get reviews back?

Commenté [KB5]: Cut until we get reviews back?

Mis en forme : Police :(Par défaut) Times New Roman

Mis en forme : Police :(Par défaut) Times New Roman

Mis en forme : Police :(Par défaut) Times New Roman

sub project TI344/2-1 and MPIESM simulation have been performed on the computer of Deutsches Klimarechenzentrum (DKRZ).

Data Availability. All CMIP5 and CMIP6 output, including the respective GeoMIP simulations, is available via the Earth System Grid Federation (https://esgf-node.llnl.gov/projects/esgf-llnl/) or by contacting the respective modeling groups responsible for the output.
For CMIP6 output, see Supplemental Section 3 for data citations.

References

Alterskjær, K., J. E. Kristjansson, and Ø. Seland (2012), Sensitivity to deliberate sea salt seeding of marine clouds – Observations and model simulations, *Atmos. Chem. Phys., 12*, 2,795–2,807, doi:10.5194/acp-12- 2795-2012.

Andrews, T., P. M. Forster, and J. M. Gregory (2009), A surface energy perspective on climate change, *J. Clim., 22*, 2557–2570, doi:10.1175/ 2008JCLI2759.1.

Arora, V. K., and G. J. Boer (2010), Uncertainties in the 20th century carbon budget associated with land use change, *Global Change Biol., 16*, 3327–3348, doi:10.1111/j.1365-2486.2010.02202.x.

Arora, V. K., Katavouta, A., Williams, R. G., Jones, C. D., Brovkin, V., Friedlingstein, P., Schwinger, J., Bopp, L., Boucher, O., Cadule, P., Chamberlain, M. A., Christian, J. R., Delire, C., Fisher, R. A., Hajima, T., Ilyina, T., Joetzjer, E., Kawamiya, M., Koven, C., Krasting, J., Law, R. M., Lawrence, D. M., Lenton, A., Lindsay, K., Pongratz, J., Raddatz, T., Séférian, R., Tachiiri, K., Tjiputra, J. F., Wiltshire, A., Wu, T., and Ziehn, T. (2020), Carbon-concentration and carbon-climate feedbacks in CMIP6 models, and their comparison to CMIP5 models, *Biogeosciences*, in press.

Aswathy, V. N., O. Boucher, M. Quaas, U. Niemeier, H. Muri, J. Mülmenstädt, and J. Quaas (2015), Climate extremes in multi-model simulations of stratospheric aerosol and marine cloud brightening climate engineering, *Atmospheric Chemistry and Physics, 15*, 9593-9610, doi:10.5194/acp-15-9593-2015.

Ban-Weiss, G. A., and K. Caldeira (2010), Geoengineering as an optimization problem, *Environ. Res. Lett., 5*, 034009, doi:10.1088/1748-9326/5/ 3/034009.

Boucher, O., et al. (2020), Presentation and evaluation of the IPSL-CM6A-LR climate model, *J. Adv. Model. Earth Sys., 12*, e2019MS002010, doi:10.1029/2019MS002010.

Budyko, M. I. (1977). *Climatic changes*: American Geophysical Union.

Collins, W. J., et al. (2011), Development and evaluation of an Earth-system model—HadGEM2, *Geosci. Model. Dev., 4*, 1051–1075, doi:10.5194/ gmd-4-1051-2011.

Crutzen, P. J. (2006), Albedo enhancement by stratospheric sulfur injections: A contribution to resolve a policy dilemma? *Climatic Change*, *77*, 211–220.

Curry, C. L., et al. (2014), A multimodel examination of climate extremes in an idealized geoengineering experiment, *J. Geophys. Res.*, *119*, 3900–3923, doi:10.1002/2013JD020648.

Dufresne, J.-L., et al. (2013), Climate change projections using the IPSL- CM5 Earth System Model: From CMIP3 to CMIP5, *Clim. Dyn., 40*, 2123–2165, doi:10.1007/s00382-012-1636-1.

Mis en forme : Police :(Par défaut) Times New Roman

Mis en forme : Police :(Par défaut) Times New Roman

Mis en forme : Police :(Par défaut) Times New Roman

Mis en forme : Police :(Par défaut) Times New Roman, Français (Canada)

Mis en forme : Police :(Par défaut) Times New Roman

Eyring, V., S. Bony, G. A. Meehl, C. A. Senior, B. Stevens, R. J. Stouffer, and K. E. Taylor (2016), Overview of the Coupled Model Intercomparison Project Phase 6 (CMIP6) experimental design and organization, *Geosci. Model Dev., 9*, 1937–1958, doi:10.5194/gmd-9-1937-2016.

Flynn, C. M. and T. Mauritsen (2020, On the Climate Sensitivity and Historical Warming Evolution in Recent Coupled Model Ensembles, *Atmos. Chem. Phys. Discuss.,* in review, doi:10.5194/acp-2019-1175.

Gent, P. R., et al. (2011), The Community Climate System Model 4, *J. Clim., 24*, 4973–4991, doi:10.1175/2011JCLI4083.1.

Gertler, C. G., P. A. O'Gorman, B. Kravitz, J. C. Moore, S. J. Phipps, and S. Watanabe (2020), Weakening of the extratropical storm tracks in solar geoengineering scenarios, *Geophys. Res. Lett., 47*, e2020GL087348, doi:10.1029/2020GL087348.

Gettelman, A., et al. (2019), The whole atmosphere community climate model version 6 (WACCM6), *J. Geophys. Res., 124,* 12380–12403, doi:10.1029/2019JD030943.

Giorgetta, M. A., et al. (2013), Climate and carbon cycle changes from 1850 to 2100 in MPI-ESM simulations for the Coupled Model Intercomparison Project phase 5, *J. Adv. Model. Earth Syst.*, 5, 572–597, doi:10.1002/jame.20038.

Glienke, S., P. J. Irvine, and M. G. Lawrence (2015), The impact of geoengineering on vegetation in experiment G1 of the GeoMIP, *Journal of Geophysical Research*, *120*, 10196-10213, doi:10.1002/2015JD024202.

Gordon, C., et al. (2000), The simulation of SST, sea ice extents and ocean heat transports in a version of the Hadley Centre coupled model without flux adjustments, *Clim. Dyn., 16*, 147–168, doi:10.1007/s003820050010.

Govindasamy, B., and K. Caldeira (2000), Geoengineering Earth's radiation balance to mitigate CO2-induced climate change, *Geophys. Res. Lett., 27*, 2141–2144, doi:10.1029/1999GL006086.

Hansen, J. E., et al. (2005), Efficacy of climate forcings, J. Geophys. Res., *110*, D18104.

Hazeleger, W., et al. (2011), EC-Earth V2.2: Description and validation of a new seamless Earth system prediction model, *Clim. Dyn., 39*, 2611–2629, doi:10.1007/s00382-011-1228-5.

Hourdin, F., et al. (2012), Impact of the LMDZ atmospheric grid configura- tion on the climate and sensitivity of the IPSL-CM5A coupled model, *Clim. Dyn., 40*, 2167–2192, doi:10.1007/s00382-012-1411-3.

Hurrell, J. W., et al. (2013), The Community Earth System Model: A Framework for Collaborative Research. *Bull. Amer. Meteor. Soc.*, *94*, 1339–1360, doi:10.1175/BAMS-D-12-00121.1.

Mis en forme : Police :(Par défaut) Times New Roman, Français (Canada)

Mis en forme : Police :(Par défaut) Times New Roman

Mis en forme : Police :(Par défaut) Times New Roman

Mis en forme : Police :(Par défaut) Times New Roman

Mis en forme : Police :(Par défaut) Times New Roman, Français (Canada)

Mis en forme : Police :(Par défaut) Times New Roman

Irvine, P. J., B. Kravitz, H. Muri, and M. G. Lawrence (2016), An overview of the Earth system science of solar geoengineering, *Wiley Interdisciplinary Reviews, 7,* 815-833, doi:10.1002/wcc.423.

Irvine, P., K. Emmanuel, J. He, L. W. Horowitz, G. Vecchi, and D. Keith (2019), Halving warming with idealized solar geoengineering moderates key climate hazards, *Nature Climate Change*, *9*, 295-299.

Ji, D., et al. (2014), Description and basic evaluation of Beijing Normal University Earth System Model (BNU-ESM) version 1, *Geosci. Model Dev.*, *7*, 2039-2064, doi:10.5194/gmd-7-2039-2014.

Jones, A., et al. (2013), The impact of abrupt suspension of solar radiation management (termination effect) in experiment G2 of the Geoengineering Model Intercomparison Project (GeoMIP), *J. Geophys. Res., 118,* 9743-9752, doi:10.1002/jgrd.50762.

Jones A., J.M. Haywood, A.C. Jones, S. Tilmes, A. Robock and B. Kravitz (2020), Why sophisticated aerosol modelling is needed for understanding regional implications of solar radiation management, *Atmos. Chem. Phys.*, in preparation.

Kalidindi, S., G. Bala, A. Modak, and K. Caldeira (2015), Modeling of solar radiation management: a comparison of simulations using reduced solar constant and stratospheric sulphate aerosols, *Clim Dyn, 44*, 2909-2925, doi:10.1007/s00382-014-2240-3.

Kelley, M., G.A. Schmidt, L. Nazarenko, R.L. Miller, S.E. Bauer, R. Ruedy, G.L. Russell, I. Aleinov, M. Bauer, R. Bleck, V. Canuto, G. Cesana, Y. Cheng, T.L. Clune, B. Cook, C.A. Cruz, A.D. Del Genio, G.S. Elsaesser, G. Faluvegi, N.Y. Kiang, D. Kim, A.A. Lacis, A. Leboissetier, A.N. LeGrande, K.K. Lo, J.C. Marshall, S. McDermid, E.E. Matthews, K. Mezuman, L.T. Murray, V. Oinas, C. Orbe, C. Pérez García-Pando, J.P. Perlwitz, M.J. Puma, D. Rind, A. Romanou, D.T. Shindell, S. Sun, N. Tausnev, K. Tsigaridis, G. Tselioudis, E. Weng, J. Wu, and M.-S. Yao (2020), GISS-E2.1: Configurations and climatology. *J. Adv. Model. Earth Syst*., accepted, doi:10.1029/2019MS002025.

Kirkevåg, A., et al. (2013), Aerosol-climate interactions in the Norwegian Earth System Model—NorESM1-M, *Geosci. Model. Dev., 6*, 207–244, doi:10.5194/gmd-6-207-2013.

Knutti, R., D. Masson, and A. Gettelman (2013), Climate model genealogy: Generation CMIP5 and how we got there, *Geophys. Res. Lett., 40*, 1194-1199, doi:10.1002/grl.50256.

Kravitz, B. , A. Robock, O. Boucher, H. Schmidt, K. E. Taylor, G. Stenchikov, and M. Schulz (2011), The Geoengineering Model Intercomparison Project (GeoMIP), *Atmosph. Sci. Lett., 12*, 162-167, doi:10.1002/asl.316.

Kravitz, B., et al. (2013a), Climate model response from the Geoengineering Model Intercomparison Project (GeoMIP), *J. Geophys. Res.*, *118*, 1-13, doi:10.1002/jgrd.50646.

Mis en forme : Police :(Par défaut) Times New Roman

Commenté [KB6]: Cut until we get reviews back?

Mis en forme : Police :(Par défaut) Times New Roman

Kravitz, B., et al. (2013b), An energetic perspective on hydrological changes in the Geoengineering Model Intercomparison Project (GeoMIP), *J. Geophys. Res.*, *118*, 13087-13102, doi:10.1002/2013JD020502.

Kravitz, B., et al. (2014), A multi-model assessment of regional disparities caused by solar geoengineering, *Environ. Res. Lett.*, *9*, 074013, doi:10.1088/1748-9326/14/074013.

Kravitz, B., A. Robock, S. Tilmes, O. Boucher, J. M. English, P. J. Irvine, A. Jones, M. G. Lawrence, M. MacCracken, H. Muri, J. C. Moore, U. Niemeier, S. J. Phipps, J. Sillmann, T. Storelvmo, H. Wang, and S. Watanabe (2015), The Geoengineering Model Intercomparison Project Phase 6 (GeoMIP6): Simulation design and preliminary results, *Geosci. Model Dev.*, *8*, 3379-3392, doi:10.5194/gmd-8-3379-2015.

Kravitz, B., D. G. MacMartin, H. Wang, and P. J. Rasch (2016), Geoengineering as a design problem, *Earth System Dynamics*, *7*, 469-497, doi:10.5194/esd-7-469-2016.

Kravitz, B., et al. (2017), First simulations of designing stratospheric sulfate aerosol geoengineering to meet multiple simultaneous climate objectives, *J. Geophys. Res., 122*, 12616-12634, doi:10.1002/2017JD026874.

Kravitz, B., D. G. MacMartin, S. Tilmes, J. H. Richter, M. J. Mills, W. Cheng, K. Dagon, A. S. Glanville, J.-F. Lamarque, I. Simpson, J. Tribbia, and F. Vitt (2019), Comparing surface and stratospheric impacts of geoengineering with different SO2 injection strategies, *J. Geophys. Res., 124*, 7900-7918, doi:10.1029/2019JD030329

Lurton, T., et al. (2020), Implementation of the CMIP6 forcing data in the IPSL-CM6A-LR model, *J. Adv. Model. Earth Sys., 12*, e2019MS001940, doi:10.1029/2019MS001940.

MacMartin, D. G., D. W. Keith, B. Kravitz, and K. Caldeira (2013), Management of trade-offs in geoengineering through optimal choice of non-uniform radiative forcing, *Nature Climate Change*, *3*, 365-368, doi:10.1038/nclimate1722.

Madronich, S., S. Tilmes, B. Kravitz, D. G. MacMartin, and J. H. Richter (2018), Response of surface ultraviolet and visible radiation to stratospheric SO_2 injection, *Atmosphere*, *9*, 432, doi:10.3390/atmos9110432.

Mauritsen, T., et al. (2019), Developments in the MPI-M Earth System Model version 1.2 (MPI-ESM1.2) and its response to increasing CO_2, *J. Adv. Model. Earth Sys., 11*, 998– 1038, doi:10.1029/2018MS001400.

Meehl, G. A., C. A. Senior, V. Eyring, G. Flato, J.-F. Lamarque, R. J. Stouffer, K. E. Taylor, and M. Schlund (2020), Context for interpreting equilibrium climate sensitivity and transient climate response from the CMIP6 Earth system models, *Science Advances*, *6*, eaba1981, doi:10.1126/sciadv.aba1981.

Mis en forme : Police :(Par défaut) Times New Roman

Moore, J. C. et al. (2014), Arctic sea ice and atmospheric circulation under the GeoMIP G1 scenario, *J. Geophys. Res.*, *119*, 567-583, doi:10.1002/2013JD021060.

Moreno-Cruz, J. B., K. L. Ricke, and D. W. Keith (2012), A simple model to account for regional inequalities in the effectiveness of solar radiation management, *Climatic Change*, *110*, 649-668.

Neale, R. B., C. Chen, A. Gettelman, P. Lauritzen, S. Park, D. Williamson, A. Conley, R. Garcia, D. Kinnison, and J. Lamarque (2010), Description of the NCAR community atmosphere model (CAM 5.0), NCAR Tech. Note NCAR/TN-486+ STR.

Niemeier, U., H. Schmidt, K. Alterskjær, and J. E. Kristjánsson (2013), Solar irradiance reduction via climate engineering: Impact of different techniques on the energy balance and the hydrological cycle, *J. Geophys. Res. Atmos., 118,* 11,905–11,917, doi:10.1002/2013JD020445.

National Research Council. 2015. Climate Intervention: Reflecting Sunlight to Cool Earth. Washington, DC: The National Academies Press. https://doi.org/10.17226/18988.

Phipps, S. J., L. D. Rotstayn, H. B. Gordon, J. L. Roberts, A. C. Hirst, and W. F. Budd (2011), The CSIRO Mk3L climate system model version 1.0 – Part 1: Description and evaluation, *Geosci. Model Dev., 4*, 483–509, https://doi.org/10.5194/gmd-4-483-2011.

Phipps, S. J., L. D. Rotstayn, H. B. Gordon, J. L. Roberts, A. C. Hirst, and W. F. Budd (2012), The CSIRO Mk3L climate system model version 1.0 – Part 2: Response to external forcings, *Geosci. Model Dev., 5*, 649–682, https://doi.org/10.5194/gmd-5-649-2012.

Pitari, G., V. Aquila, B. Kravitz, A. Robock, S. Watanabe, I. Cionni, N. D. Luca, G. di Genova, E. Mancini, and S. Tilmes (2014), Stratospheric ozone response to sulfate geoengineering: Results from the Geoengineering Model Intercomparison Project (GeoMIP), *J. Geophys. Res.*, *119*, 2629-2653.

Richter, J. H., S. Tilmes, A. Glanville, B. Kravitz, D. G. MacMartin, M. J. Mills, I. R. Simpson, F. Vitt, J. J. Tribbia, and J.-F. Lamarque (2018), Stratospheric response in the first geoengineering simulation meeting multiple surface climate objectives, *J. Geophys. Res., 123*, 5762-5782, doi:10.1029/2018JD028285.

Ricke, K. L., M. G. Morgan, and M. R. Allen (2010), Regional climate response to solar-radiation management, *Nat. Geosci., 3*, 537–541, doi:10.1038/ngeo915.

Robock, A. (2000), Volcanic eruptions and climate, *Rev. Geophys.*, 38, 191–219, doi:10.1029/1998RG000054.

Russotto, R. D. and T. P. Ackerman (2018), Changes in clouds and thermodynamics under solar geoengineering and implications for required solar reduction, *Atmos. Chem. Phys., 18*, 11905–11925, doi:10.5194/acp-18-11905-2018.

Mis en forme : Police :(Par défaut) Times New Roman, Français (Canada)

Mis en forme : Police :(Par défaut) Times New Roman

Mis en forme : Police :(Par défaut) Times New Roman

Mis en forme : Police :(Par défaut) Times New Roman

Mis en forme : Police :(Par défaut) Times New Roman

Mis en forme : Police :(Par défaut) Times New Roman

Mis en forme : Police :(Par défaut) Times New Roman

Mis en forme : Police :(Par défaut) Times New Roman

Mis en forme : Police :(Par défaut) Times New Roman

Schmidt, G. A., et al. (2006), Present-day atmospheric simulations using GISS ModelE: Comparison to in situ, satellite and reanalysis data, *J. Clim., 19*, 153–192, doi:10.1175/JCLI3612.1.

Séférian, R., et al. (2019), Evaluation of CNRM Earth-System model, CNRM-ESM2-1: Role of Earth system processes in present-day and future climate, *J. Adv. Model. Earth Sys., 11*, 4182–4227, doi:10.1029/2019MS001791.

Sellar, A. A., et al. (2019), UKESM1: Description and evaluation of the U.K. Earth System Model, *J. Adv. Model. Earth Sys., 11*, 4513–4558, doi:10.1029/2019MS001739.

Simpson, I., S. Tilmes, J. Richter, B. Kravitz, D. MacMartin, M. Mills, J. Fasullo, and A. Pendergrass (2019), The regional hydroclimate response to stratospheric sulfate geoengineering and the role of stratospheric heating, *J. Geophys. Res., 124*, 12587-12616, doi:10.1029/2019JD031093.

Stevens, B., et al. (2013), The atmospheric component of the MPI-M Earth System Model: ECHAM6, *J. Adv. Model. Earth Syst., 5*, doi:10.1002/jame.20015.

Swart, N. C., et al. (2019), The Canadian Earth System Model version 5 (CanESM5.0.3), *Geosci. Model Dev.*, *12*, 4823-4873, doi:10.5194/gmd-12-4823-2019.

Taylor, K. E., R. J. Stouffer, and G. A. Meehl (2012), An overview of CMIP5 and the experiment design, *Bull. Am. Meteorol. Soc., 93*, 485–498, doi:10.1175/BAMS-D-11-00094.1.

Tilmes, S., et al. (2013), The hydrological impact of geoengineering in the Geoengineering Model Intercomparison Project (GeoMIP), *J. Geophys. Res.*, *118*, 11036-11058, doi:10.1002/jgrd.50868.

Tilmes, S., J. Richter, M. Mills, B. Kravitz, D. G. MacMartin, R. Garcia, D. Kinnison, J.-F. Lamarque, J. Tribbia, and F. Vitt (2018), Effects of different stratospheric SO_2 injection altitudes on stratospheric chemistry and dynamics*, J. Geophys. Res., 123*, 4654-4673, doi:10.1002/2017JD028146.

Vial, J., J.-L. Dufresne, and S. Bony (2013), On the interpretation of inter-model spread in CMIP5 climate sensitivity estimates, *Climate Dynamics*, *41*, 3339-3362, doi:10.1007/s00382-013-1725-9.

Vignesh, P. P., J. H. Jiang, P. Kishore, H. Su, T. Smay, N. Brighton, and I. Velicogna (2020), Assessment of CMIP6 cloud fraction and comparison with satellite observations, *Earth and Space Science*, 7, e2019EA000975, doi:10.1029/2019EA000975.

Visioni, D., D. G. MacMartin, B. Kravitz, S. Tilmes, M. J. Mills, J. H. Richter, and M. P. Boudreau (2019), Seasonal injection strategies for stratospheric aerosol geoengineering, *Geophysical Research Letters, 46,* 7790-7799, doi:10.1029/2019GL083680.

Mis en forme : Police :(Par défaut) Times New Roman, Français (Canada)

Mis en forme : Police :(Par défaut) Times New Roman

Mis en forme : Police :(Par défaut) Times New Roman, Non souligné

Mis en forme : Police :(Par défaut) Times New Roman

Watanabe, S., et al. (2008), Development of an atmospheric general circulation model for integrated Earth system modeling on the Earth Simulator, *J. Earth Simulator, 9*, 27–35.

Watanabe, S., et al. (2011), MIROC-ESM 2010: Model description and basic results of CMIP5-20c3m experiments, *Geosci. Model Dev., 4*, 845–872, doi:10.5194/gmd-4-845-2011.

Xia, L., et al. (2014), Solar radiation management impacts on agriculture in China: A case study in the Geoengineering Model Intercomparison Project (GeoMIP), *J. Geophys. Res. Atmos., 119*, 8695-8711, doi:10.1002/2013JD020630.

Zelinka, M. D., et al. (2020), Causes of higher climate sensitivity in CMIP6 models, *Geophys. Res. Let.*, 47, e2019GL085782, doi:10.1029/2019GL085782.

#	Model	Gen.	Reference	G1 Solar reduction (%)	Notes
1	BNU-ESM	CMIP5	Ji et al. (2014)	3.80	Cloud forcing not available
2	CanESM2	CMIP5	Arora et al. (2011)	4.00	
3	CCSM4	CMIP5	Gent et al. (2011)	4.25	NPP not available
4	CESM-CAM5.1-FV	CMIP5	Neale et al. (2010) Hurrell et al. (2013)	4.70	
5	CSIRO-Mk3L-1.2	CMIP5	Phipps et al. (2011, 2012)	3.20	Cloud forcing and NPP not available
6	EC-EARTH	CMIP5	Hazeleger et al. (2011)	4.12	Cloud forcing and NPP not available
7	GISS-E2-R	CMIP5	Schmidt et al. (2006)	4.47	
8	HadCM3	CMIP5	Gordon et al. (2000)	4.16	Cloud forcing and NPP not available
9	HadGEM2-ES	CMIP5	Collins et al. (2011)	3.88	
10	IPSL-CM5A-LR	CMIP5	Dufresne et al. (2013) Hourdin et al.(2011)	3.50	NPP not available
11	MIROC-ESM	CMIP5	Watanabe et al. (2008,2011)	5.00	
12	MPI-ESM-LR	CMIP5	Giorgetta et al. (2012) Stevens et al. (2012)	4.68	
13	NorESM1-M	CMIP5	Alterskjær et al. (2012) Kirkevåg et al. (2012)	4.03	
14	CanESM5	CMIP6	Swart et al. (2019)	3.72	
15	CESM2-WACCM	CMIP6	Gettelman et al. (2019)	4.91	
16	CNRM-ESM2.1	CMIP6	Séférian et al. (2019)	3.72	
17	GISS-E2.1-G	CMIP6	Kelley et al. (in revision)	4.13	
18	IPSL-CM6A-LR	CMIP6	Boucher et al. (2020) Lurton et al. (2020)	4.10	
19	MPI-ESM1.2-LR	CMIP6	Mauritsen et al. (2019)	4.57	
20	UKESM1.0-LL	CMIP6	Sellar et al. (2019)	3.80	

Mis en forme : Police :(Par défaut) Times New Roman
Tableau mis en forme
Mis en forme : Police :(Par défaut) Times New Roman
Mis en forme : Police :(Par défaut) Times New Roman
Mis en forme : Police :(Par défaut) Times New Roman
Mis en forme : Police :(Par défaut) Times New Roman
Mis en forme : Police :(Par défaut) Times New Roman
Mis en forme : Police :(Par défaut) Times New Roman
Mis en forme : Police :(Par défaut) Times New Roman
Mis en forme : Police :(Par défaut) Times New Roman
Mis en forme : Police :(Par défaut) Times New Roman
Mis en forme : Police :(Par défaut) Times New Roman
Mis en forme : Police :(Par défaut) Times New Roman
Mis en forme : Police :(Par défaut) Times New Roman
Mis en forme : Police :(Par défaut) Times New Roman
Mis en forme : Police :(Par défaut) Times New Roman
Mis en forme : Police :(Par défaut) Times New Roman
Mis en forme : Police :(Par défaut) Times New Roman
Mis en forme : Police :(Par défaut) Times New Roman
Mis en forme : Police :(Par défaut) Times New Roman
Mis en forme : Police :(Par défaut) Times New Roman

Table 1. All participating models in both the CMIP5 and CMIP6 eras of GeoMIP, including references. For G1 solar reduction, the percentage is calculated as the percent change in incident solar irradiance at the top-of-atmosphere between G1 and its respective piControl run. Numbers in the first column correspond to the model numbers in Figure 5.

#	Model	Gen.	Reference	G1 Solar reduction (%)	Notes
1	BNU-ESM	CMIP5	Ji et al. (2014)	3.80	Cloud forcing not available
2	CanESM2	CMIP5	Arora et al. (2011)	4.00	
3	CCSM4	CMIP5	Gent et al. (2011)	4.25	NPP not available
4	CESM-CAM5.1-FV	CMIP5	Neale et al. (2010) Hurrell et al. (2013)	4.70	
5	CSIRO-Mk3L-1.2	CMIP5	Phipps et al. (2011, 2012)	3.20	Cloud forcing and NPP not available
6	EC-EARTH	CMIP5	Hazeleger et al. (2011)	4.12	Cloud forcing and NPP not available
7	GISS-E2-R	CMIP5	Schmidt et al. (2006)	4.47	

8	HadCM3	CMIP5	Gordon et al. (2000)	4.16	Cloud forcing and NPP not available
9	HadGEM2-ES	CMIP5	Collins et al. (2011)	3.88	
10	IPSL-CM5A-LR	CMIP5	Dufresne et al. (2013) Hourdin et al.(2011)	3.50	NPP not available
11	MIROC-ESM	CMIP5	Watanabe et al. (2008,2011)	5.00	
12	MPI-ESM-LR	CMIP5	Giorgetta et al. (2012) Stevens et al. (2012)	4.68	
13	NorESM1-M	CMIP5	Alterskjær et al. (2012) Kirkevåg et al. (2012)	4.03	
14	CanESM5	CMIP6	Swart et al. (2019)	3.72	
15	CESM2-WACCM	CMIP6	Gettelman et al. (2019)	4.91	
16	CNRM-ESM2.1	CMIP6	Séférian et al. (2019)	3.72	
17	GISS-E2.1-G	CMIP6	Kelley et al. (in revision)	4.13	
18	IPSL-CM6A-LR	CMIP6	Boucher et al. (2020) Lurton et al. (2020)	4.10	
19	MPI-ESM1.2-LR	CMIP6	Mauritsen et al. (2019)	4.57	
20	UKESM1.0-LL	CMIP6	Sellar et al. (2019)	3.80	

617

618

Comparing different generations of idealized solar geoengineering simulations in the Geoengineering Model Intercomparison Project (GeoMIP)

Ben Kravitz,[1,2,*] Douglas G. MacMartin,[3] Daniele Visioni,[3] Olivier Boucher,[4] Jason N. S. Cole,[5] Jim Haywood,[6,7] Andy Jones,[7] Thibaut Lurton,[4] Michael J. Mills,[8] Pierre Nabat,[9] Ulrike Niemeier,[10] Alan Robock,[11] Roland Séférian,[9] and Simone Tilmes[8]

[1]Department of Earth and Atmospheric Sciences, Indiana University, Bloomington, IN, USA
[2]Atmospheric Sciences and Global Change Division, Pacific Northwest National Laboratory, Richland, WA, USA
[3]Sibley School of Mechanical and Aerospace Engineering, Cornell University, Ithaca, NY, USA
[4]Institut Pierre-Simon Laplace (IPSL), Sorbonne Université/CNRS, Paris, France
[5]Environment and Climate Change Canada, Toronto, Ontario, Canada
[6]College of Engineering, Mathematics and Physical Sciences, University of Exeter, Exeter, United Kingdom
[7]UK Met Office Hadley Centre, Exeter, United Kingdom
[8]Atmospheric Chemistry Observations and Modeling Laboratory, National Center for Atmospheric Research, Boulder, CO, USA
[9]CNRM, Université de Toulouse, Météo-France, CNRS, Météo-France, Toulouse, France
[10]Max Planck Institute for Meteorology, Hamburg, Germany
[11]Department of Environmental Sciences, Rutgers University, New Brunswick, NJ, USA

Submission to ~~*Environmental Research Letters*~~ *Atmospheric Chemistry and Physics*

[*]To whom correspondence should be addressed: 1001 E. 10th Street, Bloomington, IN 47405-1405, USA. bkravitz@iu.edu

Abstract

Solar geoengineering has been receiving increased attention in recent years as a potential temporary solution to offset global warming. One method of approximating global-scale solar geoengineering in climate models is via solar reduction experiments. Two generations of models in the Geoengineering Model Intercomparison Project (GeoMIP) have now simulated offsetting a quadrupling of the CO_2 concentration with solar reduction. Here we show that energetics, temperature, and hydrological cycle changes in this experiment are statistically indistinguishable between the two ensembles. Of the variables analyzed here, the only major differences involve highly parameterized and uncertain processes, such as cloud forcing or terrestrial net primary productivity. ~~W~~Although the climate model experiment analyzed here is artificial and designed to elicit large responses in the models, we conclude that despite numerous structural differences and uncertainties in models over the past 20 years, including an increase in climate sensitivity in the latest generation of models, broad conclusions about the climate response to global solar dimming remain robust.

Keywords: geoengineering, climate engineering, climate intervention, solar radiation management, climate modeling

Three main points

1. The present study investigates the response of the climate system to solar geoengineering across two ensembles of models of different generation
2. Past results about solar dimming remain robust to inter-generational differences in models for most evaluated variables
3. Key ensemble differences are found for highly parameterized and uncertain processes such as clouds and the carbon cycle

Suggested reviewers

- Piers Forster
- Don Wuebbles
- Peter Irvine
- Long Cao
- Ken Caldeira
- Govindasamy Bala
- Jim Hurrell
- Jean-Francois Lamarque

1. Introduction

Solar geoengineering describes a set of technologies designed to (ideally) temporarily, deliberately reduce some of the effects of climate change by changing the radiative balance of the planet, often by reflecting sunlight back to space (NRC, 2015). Numerous methods have been proposed, but ~~arguably~~ the most studied is stratospheric sulfate aerosol injection (Budyko, 1977; Crutzen, 2006). This method involves substantially increasing the stratospheric sulfate aerosol burden, replicating the mechanisms that cause cooling after large volcanic eruptions (Robock, 2000). Climate models remain the most promising tools for understanding the consequences of solar geoengineering. In model simulations of solar geoengineering, insolation reduction is often used as a proxy for actual stratospheric sulfate aerosols, as it captures many of the broad radiative effects of stratospheric aerosol geoengineering as well as some of the important climate effects like surface cooling and hydrological cycle strength reduction (Niemeier et al., 2013; Kalidindi et al., 2015). However, stratospheric sulfate aerosols also absorb longwave radiative flux, which heats the upper troposphere~~/~~ and lower stratosphere. As such, any implementation of stratospheric geoengineering with sulfate aerosols would produce additional effects, such as changing atmospheric circulation in response to stratospheric heating and heating gradients (e.g., Richter et al., 2017; Tilmes et al., 2018; Simpson et al., 2019; Jones et al., 2020) and stratospheric ozone changes (e.g., Pitari et al., 2014), as well as changes in ultraviolet radiative flux and enhanced diffuse radiation at the surface (Madronich et al., 2018). However, here we consider the major, large-scale effect of reflecting sunlight to cool Earth.

Commenté [KB1]: Cut until we get reviews back?

Simulations of solar geoengineering with solar reduction have long shown that solar geoengineering would cool the planet, offsetting global warming (e.g., Govindasamy and Caldeira, 2000; NRC, 2015; Irvine et al., 2016). Idealized simulations of solar reduction have also been simulated in a multi-model context under the Geoengineering Model Intercomparison Project (GeoMIP; Kravitz et al., 2011), to understand the robust model responses to various standardized solar geoengineering simulation designs. Multi-model conclusions from these studies indicate that solar geoengineering would be effective at partially offsetting greenhouse gas-induced temperature changes (Kravitz et al., 2013a), as well as changes in the hydrological cycle (Tilmes et al., 2013), the cryosphere (Moore et al., 2014), extreme events (Curry et al., 2014; Aswathy et al., 2015), vegetation (Glienke et al., 2015), circulation (Guo et al., 2018; Gertler et al., 2020), agriculture (Xia et al., 2014), and numerous other areas. However, the offset is not perfect (Moreno-Cruz et al., 2012), particularly on a regional basis or when considering multiple simultaneous metrics of climate change (Kravitz et al., 2014; Irvine et al., 2019; Jones et al., 2020), leading to concerns about winners and losers from geoengineering (Ricke et al., 2010). To some extent, the effects of solar geoengineering may be tailored or designed (MacMartin et al., 2013; Kravitz et al., 2016, 2017, 2019), but solar geoengineering will still not be able to perfectly offset climate change from greenhouse gases.

Commenté [KB2]: Cut until we get reviews back?

The previous phase of GeoMIP was associated with the Coupled Model Intercomparison Project Phase 5 (CMIP5; Taylor et al., 2012), an international collaboration of climate models to attempt to understand robust model responses to various forcings. GeoMIP has now entered a new phase, concurrent with the Coupled Model Intercomparison Project Phase 6 (CMIP6; Eyring et al., 2016), and with it are new solar geoengineering simulations with new and updated versions of Earth System Models (Kravitz et al., 2015). As such, this is an opportunity to revisit some

central questions in solar geoengineering. Many of the CMIP5 results regarding solar geoengineering showed substantial agreement across the participating GeoMIP models. In this newest iteration of GeoMIP, do the same science conclusions still hold, and do the models still generally agree on the resulting climate effects? Here we address these questions by evaluating and comparing general climate model response to GeoMIP experiment G1 (described in the next section) from both CMIP5 and CMIP6.

2. Simulations and Participating Models

In this study, we evaluate GeoMIP experiment G1, in which, starting from a preindustrial control (piControl) baseline, the atmospheric CO_2 concentration is instantaneously quadrupled (the standard CMIP experiment abrupt4xCO2), and insolation is simultaneously reduced such that net top-of-atmosphere (TOA) radiative flux is approximately unchanged from the baseline in the first decade of simulation (Kravitz et al., 2011, 2015). This experiment was part of the original suite of GeoMIP experiments and was repeated and extended in the newest suite in an effort to understand the role of model structural uncertainty in broad conclusions about solar geoengineering. Participating models are listed in Table 1. We include 13 models from CMIP5 and 7 models from CMIP6.

Because the main focus of this paper is a comparison between the CMIP5 and CMIP6 generations of model results, we have opted for the following to aid comparisons:

- The original G1 experiment was 50 years in length, whereas the CMIP6 version is 100 years in length to allow for better analyses of rare events or to capture very slow responses. Since we are not evaluating any features that require 100 years of statistics, and the results do not show any appreciable time evolution of behavior after the first couple of years (see Supplemental Section 2 and Supplemental Figures 1 and 2), we only evaluate the first 50 years of all simulations. All maps show changes over years 11-50, removing the initial transient period.
- We do not compare previous versions of individual models with current ones, instead only examining ensembles. Even though models may share similar development histories (e.g., atmosphere and ocean dynamical cores, convective parameterizations, radiative transfer modules, terrestrial biosphere and cryosphere~~, etc.~~; Knutti et al., 2013; Zelinka et al., 2020), there have been numerous developments in models in these areas (and others) between CMIP5 and CMIP6 such that in most cases a direct comparison would not be meaningful.
- We focus extensively on the G1 results and, with few exceptions, do not focus on the corresponding abrupt4xCO2 simulations. It has been well documented that the CMIP6 models tend to have higher climate sensitivities than the CMIP5 models (Flynn and Mauritsen, 2020; Meehl et al., 2020; Zelinka et al., 2020), so we do not wish to make conclusions that might be based on a form of selection bias.
- All lack of stippling on map plots, as in previous GeoMIP studies (e.g., Kravitz et al., 2013a), indicates agreement on the sign of the response in at least 75% of models. Because $G1_{CMIP5}$ has more participating models than $G1_{CMIP6}$, this threshold provides some consistency across analyses of the ensembles. When plotting differences between the ensembles ($G1_{CMIP6}$-$G1_{CMIP5}$), there is no stippling, as it is difficult to meaningfully represent such differences between ranges. Aggregate differences between the two

ensembles, as calculated using Welch's *t*-test or differences in stippled area, are discussed in Supplemental Table 1.

3. Results

3.1. Energetics

Ensemble mean radiative and turbulent flux quantities are plotted in Figure 1, and the ensemble ranges are plotted in Supplemental Figure 3. An immediate observation is that, in both ensembles, the models were successful at limiting net TOA radiative flux change to within approximately ±0.1 W m^{-2} of the models' respective preindustrial values. Accomplishing this required an average solar reduction of 4.14% (models range in 3.20–5.00%) in CMIP5 and 4.14% (3.72–4.91%) in CMIP6. As such, despite numerous structural changes between the two generations of models, there is no appreciable change in solar efficacy (Hansen et al., 2005).

None of the radiative flux quantities indicate large transients over 50 years of simulation of G1, other than the initial flux change within the first year or so of simulation. This is consistent with the "perpetual fast response" found by Kravitz et al. (2013b), in which because global mean temperature does not change appreciably over the course of the G1 simulation, climate feedbacks are not excited, and the internal state of the system (as measured by, for example, fluxes and hydrological cycle changes) similarly does not change. Ensemble mean fluxes show few differences (<1 W m^{-2} in magnitude) with the exception of shortwave cloud forcing, defined as all-sky minus clear-sky shortwave flux at the surface. On average, the CMIP6 ensemble has 3–4 W m^{-2} less shortwave cloud forcing than CMIP5. Neglecting some outliers, for each flux except shortwave (and hence total) cloud forcing, the median model in one ensemble is within the inter-quartile range of the other ensemble. This indicates that there are no major differences between the ensembles in how the models handle energy balance and energetics, with the exception of clouds, which is consistent with findings about CMIP6 (Zelinka et al., 2020). Moreover, it appears that most of the major differences in shortwave cloud forcing are due to outliers in each ensemble, positive for CMIP5 and negative for CMIP6.

To further explore these potential differences, Supplemental Figure 4 provides maps of the ensemble means for cloud forcing. In G1, the CMIP5 ensemble showed more positive shortwave cloud forcing and more negative longwave cloud forcing (i.e., more cancellation) than the CMIP6 ensemble. Overall, the CMIP6 ensemble has greatly reduced (in some places by over 10 W m^{-2}) shortwave cloud forcing as compared to CMIP5 under the G1 experiment. This is a widespread result, but the most prominent features are in the tropics, especially over the Amazon, Africa, and the Maritime Continent. These regions encompass tropical forests, indicating a potential for vegetation feedbacks on the temperature reductions. However, the reasons behind these forcing changes are difficult to diagnose, as they could be due to changes in cloud thickness, cloud cover, or cloud level between CMIP5 and CMIP6 models (e.g., Vignesh et al., 2020), differences in how solar geoengineering affects clouds (Russotto and Ackerman, 2018), or artifacts of the analyses (e.g., cloud masking; Andrews et al., 2009; Kravitz et al., 2013b). Moreover, based on the results in Supplemental Figure 3, it is likely that many of these features are exaggerated by outlier models (also see Vignesh et al., 2020). As such, we reserve such detailed investigations for future work.

3.2. Temperature

These small flux changes also lead to few G1 temperature changes between the two ensembles. Figure 2 shows global, land, and ocean-averaged temperatures for the CMIP5 and CMIP6 ensembles. In general, the abrupt4xCO2 simulation in CMIP6 has higher temperatures than in CMIP5, consistent with the noted increase in climate sensitivity (Vial et al., 2013; Flynn and Mauritsen, 2020; Meehl et al., 2020; Zelinka et al., 2020). In both ensembles, G1 is effective at offsetting global mean temperature change, in some cases with a slight positive residual temperature change over land. Supplemental Figure 5 shows three aggregate temperature metrics: global mean temperature, the interhemispheric temperature gradient, and the equator-to-pole temperature gradient (Ban Weiss and Caldeira, 2010; Kravitz et al., 2016). As for the fluxes, the median model in one ensemble is within the inter-quartile range of the other ensemble. This indicates that no ensemble is on average warmer or cooler than another, has a substantially warmer Northern or Southern Hemisphere than the other, or has warmer tropics or poles than the other. We can conclude that spatial patterns of temperature change from G1 are robust across a wide range of structural uncertainty, including an increase in climate sensitivity between the two generations of CMIP.

The spatial structure of temperature change (Figure 3) does have small differences between the two ensembles. G1 in CMIP6 has multiple locations that are warmer than G1 in CMIP5, despite both ensembles achieving net energy balance at TOA and the surface (Figure 1). The majority of the differences are over land and in the tropics, where CMIP6 is slightly warmer than CMIP5 (up to a degree Celsius in some places). Nevertheless, both ensembles show the well noted feature that offsetting a CO_2 increase with globally uniform solar reduction overcools the tropics and undercools the poles (Govindasamy and Caldeira, 2000; Kravitz et al., 2013a). CMIP6 shows slightly less high latitude warming than CMIP5, but temperature differences between the two ensembles are largely negligible. However, the warmer temperatures in CMIP6 near Greenland have important implications for ice sheet melt and consequent sea level rise, as well as bottom water formation. We reserve such analyses for future investigations, particularly since the models used here are not capable of simulating the eustatic component of sea level rise. In any case, these ensemble mean differences between CMIP5 and CMIP6 cannot be deemed statistically significant (Supplemental Table 1 and Supplemental Figure 4).

3.3. Hydrological and Other Integrative Changes

Figure 4 shows ensemble mean changes in precipitation (P), evaporation (E), and P–E for $G1_{CMIP5}$ and $G1_{CMIP6}$. Qualitatively, patterns are similar between both ensembles. Precipitation is slightly (<0.3 mm/day in magnitude) different in the tropics between the two ensembles. The majority of those features can be summarized as a more southward intertropical convergence zone (ITCZ), more precipitation in the South Pacific Convergence Zone, and less precipitation over Southeast Asia and the Maritime Continent in $G1_{CMIP6}$. Evaporation in the two ensembles is nearly identical except for more evaporation in Amazonia and Australia in $G1_{CMIP6}$. As such, the net P–E change between the two ensembles strongly resembles the precipitation changes. Supplemental Figure 6 shows that, like previous evaluations of ensemble ranges, the median model in one ensemble falls well within the interquartile range of the other ensemble for P, E,

and P–E. As such, we cannot conclude any robust hydrological cycle changes between the two ensembles.

Figure 5 shows average (years 11–50) temperature change (with respect to piControl) plotted against average precipitation change for each model, as in Tilmes et al. (2013). Other than a potentially greater climate sensitivity of some CMIP6 models, there is no distinguishable difference in aggregate behavior between the two ensembles. The same conclusion discovered by Tilmes et al. (2013) holds: solar reduction cannot simultaneously offset CO_2-induced changes in both global mean temperature and global mean precipitation.

As an integrator of CO_2, temperature, and precipitation effects over land, Figure 6 shows changes in terrestrial net primary productivity (NPP). Numerous land regions have lower NPP in CMIP6 than in CMIP5. The ensemble average global NPP change (G1–piControl) is 51.2 (4.1–122.1) Pg C y^{-1} in CMIP5 and 38.1 (19.5–77.5) Pg C y^{-1} in CMIP6, representing a 25.6% difference in means. Jones et al. (2013) used NPP to highlight the importance of understanding the influence of structural land model differences on climate results related to geoengineering. While it is beyond the scope of this study to perform a detailed diagnosis of which uncertainties or processes are responsible for this inter-ensemble difference, we show that the ensemble spread of total terrestrial NPP is smaller in CMIP6 than in CMIP5. This result is consistent with the recent assessment of carbon cycle feedbacks conducted by Arora et al. (2020), which demonstrates that the CMIP6 ensemble has reduced overall uncertainty in the land carbon cycle to rising CO_2 compared to their CMIP5 predecessors.

4. Discussion and Conclusions

Based on the results presented here, model response to G1 has not changed substantially between CMIP5 and CMIP6, despite numerous changes to models between the two generations, including an increase in climate sensitivity. The sign of residual climate impacts (for example in temperature) are in better agreement in CMIP5 than CMIP6 (Supplemental Table 1 shows a difference in stippled area between the two ensembles), but this could be a function of the smaller ensemble size in CMIP6. Energetics, temperature, and the hydrological cycle are qualitatively and quantitatively similar in both ensemble means and ensemble ranges, although these variables are somewhat related, so we might expect them to all portray a similar picture. Notable differences do exist in shortwave cloud forcing and NPP, particularly in Amazonia, Africa, and Australia, which are also regions of inter-ensemble difference in precipitation.

From these findings, we can conclude that results obtained over the past 20 years of study have not been overturned by the latest round of simulations. All of the major ensemble differences highlighted above deal with clouds and land surface modeling, both of which are difficult to model and are necessarily highly parameterized. The conclusions that are based on more fundamental knowledge, such as column energetics (in the case of the hydrological cycle), are relatively robust to structural uncertainty, in so far as this study adequately captures representative variations in structural uncertainty. This lends confidence to our conclusions, especially regarding robustness to uncertainty, about the broad climate effects from solar geoengineering methods that can be accurately represented via solar dimming.

We also conclude that the models used in CMIP5 are not obviously biased or inferior as compared to CMIP6. While improvements have been made in the CMIP6 generation of models, and those models are likely better for representing numerous features of the present-day climate that may be important for studies of geoengineering, there are many aspects of climate that are well represented by earlier models. In some cases, more robust analyses may be enabled by augmenting ensemble sizes with archived output from earlier generations of CMIP models.

There are numerous aspects of physical climate that we did not evaluate, nor did we pursue analyses beyond physical climate, including many other aspects of natural science, social science, the humanities, governance, justice, or ethics (to name a few important areas). Moreover, we emphasize that experiment G1 is an idealized experiment aimed at understanding physical climate response to combinations of large forcings and should not be interpreted as a realistic or policy-relevant scenario of geoengineering. A holistic assessment of the consequences of geoengineering, particularly of more policy-relevant scenarios, would certainly need to take these numerous aspects into account. Nevertheless, based on the results presented here, results for geoengineering across several important metrics appear to be robust to some amount of structural uncertainty. This lends confidence to some conclusions drawn from global climate models regarding solar geoengineering.

Many of the broad features of solar geoengineering with sulfate aerosols can be represented by a reduction in solar constant (e.g., Niemeier et al., 2013; Kalidindi et al., 2015). However, the more subtle changes that derive from complex response to stratospheric aerosol heating (for example, the positive wintertime North Atlantic Oscillation; Jones et al., 2020) require detailed assessments with state-of-the-art aerosol microphysical schemes. This is particularly important for understanding regional and seasonal solar geoengineering (Kravitz et al., 2017; Visioni et al., 2019). Such detailed microphysical calculations can only be simulated in a small number of models; in the case of Jones et al. (2020), only two models were available. While simple G1-style experiments enable a robust multi-model ensemble analysis, they cannot capture details that depend on microphysics. We emphasize the importance of a variety of modeling approaches to understand solar geoengineering, particularly the role of model uncertainty in conclusions about solar geoengineering.

Acknowledgments. We acknowledge the World Climate Research Programme, which, through its Working Group on Coupled Modelling, coordinated and promoted CMIP. We thank the climate modeling groups for producing and making available their model output, the Earth System Grid Federation (ESGF) for archiving the data and providing access, and the multiple funding agencies who support CMIP6 and ESGF. We also thank all participants of the Geoengineering Model Intercomparison Project and their model development teams. Support for B.K. was provided in part by the National Science Foundation (NSF) through agreement CBET-1931641, the Indiana University Environmental Resilience Institute, and the *Prepared for Environmental Change* Grand Challenge initiative. The Pacific Northwest National Laboratory is operated for the US Department of Energy by Battelle Memorial Institute under contract DE-AC05-76RL01830. Resources supporting this work were provided by the NASA High-End Computing (HEC) Program through the NASA Center for Climate Simulation (NCCS) at Goddard Space Flight Center. A.R. is supported by NSF grants AGS-1617844 and AGS-2017113. U_4N_4 is supported by the German DFG-funded Research Unit VollImpact FOR2820

Commenté [AR3]: I tried to mention this in the abstract.

Commenté [KB4]: Cut until we get reviews back?

Commenté [KB5]: Cut until we get reviews back?

Mis en forme : Police :(Par défaut) Times New Roman

Mis en forme : Police :(Par défaut) Times New Roman

sub project TI344/2-1 and MPIESM simulation have been performed on the computer of Deutsches Klimarechenzentrum (DKRZ). O.B. and T.L. were supported by the IPSL Climate Graduate School EUR (ANR grant ANR-11-IDEX-0004 - 17-EURE-0006). The CMIP6 project at IPSL used the HPC resources of TGCC under the allocations 2016-A0030107732, 2017-R0040110492 and 2018-R0040110492 (project gencmip6) provided by GENCI (Grand \'Equipement National de Calcul Intensif).

Data Availability. All CMIP5 and CMIP6 output, including the respective GeoMIP simulations, is available via the Earth System Grid Federation (https://esgf-node.llnl.gov/projects/esgf-llnl/) or by contacting the respective modeling groups responsible for the output.
For CMIP6 output, see Supplemental Section 3 for data citations.

Mis en forme : Police :(Par défaut) Times New Roman

References

Alterskjær, K., J. E. Kristjansson, and Ø. Seland (2012), Sensitivity to deliberate sea salt seeding of marine clouds – Observations and model simulations, *Atmos. Chem. Phys., 12*, 2,795–2,807, doi:10.5194/acp-12- 2795-2012.

Andrews, T., P. M. Forster, and J. M. Gregory (2009), A surface energy perspective on climate change, *J. Clim., 22*, 2557–2570, doi:10.1175/ 2008JCLI2759.1.

Arora, V. K., and G. J. Boer (2010), Uncertainties in the 20th century carbon budget associated with land use change, *Global Change Biol., 16*, 3327–3348, doi:10.1111/j.1365-2486.2010.02202.x.

Arora, V. K., Katavouta, A., Williams, R. G., Jones, C. D., Brovkin, V., Friedlingstein, P., Schwinger, J., Bopp, L., Boucher, O., Cadule, P., Chamberlain, M. A., Christian, J. R., Delire, C., Fisher, R. A., Hajima, T., Ilyina, T., Joetzjer, E., Kawamiya, M., Koven, C., Krasting, J., Law, R. M., Lawrence, D. M., Lenton, A., Lindsay, K., Pongratz, J., Raddatz, T., Séférian, R., Tachiiri, K., Tjiputra, J. F., Wiltshire, A., Wu, T., and Ziehn, T. (2020), Carbon-concentration and carbon-climate feedbacks in CMIP6 models, and their comparison to CMIP5 models, *Biogeosciences*, in press.

Aswathy, V. N., O. Boucher, M. Quaas, U. Niemeier, H. Muri, J. Mülmenstädt, and J. Quaas (2015), Climate extremes in multi-model simulations of stratospheric aerosol and marine cloud brightening climate engineering, *Atmospheric Chemistry and Physics, 15*, 9593-9610, doi:10.5194/acp-15-9593-2015.

Ban-Weiss, G. A., and K. Caldeira (2010), Geoengineering as an optimization problem, *Environ. Res. Lett., 5*, 034009, doi:10.1088/1748-9326/5/ 3/034009.

Boucher, O., et al. (2020), Presentation and evaluation of the IPSL-CM6A-LR climate model, *J. Adv. Model. Earth Sys., 12*, e2019MS002010, doi:10.1029/2019MS002010.

Budyko, M. I. (1977). *Climatic changes*: American Geophysical Union.

Collins, W. J., et al. (2011), Development and evaluation of an Earth-system model—HadGEM2, *Geosci. Model. Dev., 4*, 1051–1075, doi:10.5194/ gmd-4-1051-2011.

Crutzen, P. J. (2006), Albedo enhancement by stratospheric sulfur injections: A contribution to resolve a policy dilemma? *Climatic Change*, *77*, 211–220.

Curry, C. L., et al. (2014), A multimodel examination of climate extremes in an idealized geoengineering experiment, *J. Geophys. Res.*, *119*, 3900–3923, doi:10.1002/2013JD020648.

Dufresne, J.-L., et al. (2013), Climate change projections using the IPSL- CM5 Earth System Model: From CMIP3 to CMIP5, *Clim. Dyn., 40*, 2123–2165, doi:10.1007/s00382-012-1636-1.

Mis en forme : Police :(Par défaut) Times New Roman

Mis en forme : Police :(Par défaut) Times New Roman

Mis en forme : Police :(Par défaut) Times New Roman

Mis en forme : Police :(Par défaut) Times New Roman, Français (France)

Mis en forme : Police :(Par défaut) Times New Roman

Eyring, V., S. Bony, G. A. Meehl, C. A. Senior, B. Stevens, R. J. Stouffer, and K. E. Taylor (2016), Overview of the Coupled Model Intercomparison Project Phase 6 (CMIP6) experimental design and organization, *Geosci. Model Dev., 9*, 1937–1958, doi:10.5194/gmd-9-1937-2016.

Flynn, C. M. and T. Mauritsen (2020, On the Climate Sensitivity and Historical Warming Evolution in Recent Coupled Model Ensembles, *Atmos. Chem. Phys. Discuss.,* in review, doi:10.5194/acp-2019-1175.

Gent, P. R., et al. (2011), The Community Climate System Model 4, *J. Clim., 24*, 4973–4991, doi:10.1175/2011JCLI4083.1.

Gertler, C. G., P. A. O'Gorman, B. Kravitz, J. C. Moore, S. J. Phipps, and S. Watanabe (2020), Weakening of the extratropical storm tracks in solar geoengineering scenarios, *Geophys. Res. Lett., 47*, e2020GL087348, doi:10.1029/2020GL087348.

Gettelman, A., et al. (2019), The whole atmosphere community climate model version 6 (WACCM6), *J. Geophys. Res., 124,* 12380–12403, doi:10.1029/2019JD030943.

Giorgetta, M. A., et al. (2013), Climate and carbon cycle changes from 1850 to 2100 in MPI-ESM simulations for the Coupled Model Intercomparison Project phase 5, *J. Adv. Model. Earth Syst.*, 5, 572–597, doi:10.1002/jame.20038.

Glienke, S., P. J. Irvine, and M. G. Lawrence (2015), The impact of geoengineering on vegetation in experiment G1 of the GeoMIP, *Journal of Geophysical Research*, *120*, 10196-10213, doi:10.1002/2015JD024202.

Gordon, C., et al. (2000), The simulation of SST, sea ice extents and ocean heat transports in a version of the Hadley Centre coupled model without flux adjustments, *Clim. Dyn., 16*, 147–168, doi:10.1007/s003820050010.

Govindasamy, B., and K. Caldeira (2000), Geoengineering Earth's radiation balance to mitigate CO2-induced climate change, *Geophys. Res. Lett., 27*, 2141–2144, doi:10.1029/1999GL006086.

Hansen, J. E., et al. (2005), Efficacy of climate forcings, J. Geophys. Res., *110*, D18104.

Hazeleger, W., et al. (2011), EC-Earth V2.2: Description and validation of a new seamless Earth system prediction model, *Clim. Dyn., 39*, 2611–2629, doi:10.1007/s00382-011-1228-5.

Hourdin, F., et al. (2012), Impact of the LMDZ atmospheric grid configura- tion on the climate and sensitivity of the IPSL-CM5A coupled model, *Clim. Dyn., 40*, 2167–2192, doi:10.1007/s00382-012-1411-3.

Hurrell, J. W., et al. (2013), The Community Earth System Model: A Framework for Collaborative Research. *Bull. Amer. Meteor. Soc.*, *94*, 1339–1360, doi:10.1175/BAMS-D-12-00121.1.

Mis en forme : Police :(Par défaut) Times New Roman, Français (Canada)

Mis en forme : Police :(Par défaut) Times New Roman

Mis en forme : Police :(Par défaut) Times New Roman

Mis en forme : Police :(Par défaut) Times New Roman

Mis en forme : Police :(Par défaut) Times New Roman, Français (France)

Mis en forme : Police :(Par défaut) Times New Roman

Irvine, P. J., B. Kravitz, H. Muri, and M. G. Lawrence (2016), An overview of the Earth system science of solar geoengineering, *Wiley Interdisciplinary Reviews, 7,* 815-833, doi:10.1002/wcc.423.

Irvine, P., K. Emmanuel, J. He, L. W. Horowitz, G. Vecchi, and D. Keith (2019), Halving warming with idealized solar geoengineering moderates key climate hazards, *Nature Climate Change*, *9*, 295-299.

Ji, D., et al. (2014), Description and basic evaluation of Beijing Normal University Earth System Model (BNU-ESM) version 1, *Geosci. Model Dev.*, *7*, 2039-2064, doi:10.5194/gmd-7-2039-2014.

Jones, A., et al. (2013), The impact of abrupt suspension of solar radiation management (termination effect) in experiment G2 of the Geoengineering Model Intercomparison Project (GeoMIP), *J. Geophys. Res., 118,* 9743-9752, doi:10.1002/jgrd.50762.

Jones A., J.M. Haywood, A.C. Jones, S. Tilmes, A. Robock and B. Kravitz (2020), Why sophisticated aerosol modelling is needed for understanding regional implications of solar radiation management, *Atmos. Chem. Phys.*, in preparation.

Kalidindi, S., G. Bala, A. Modak, and K. Caldeira (2015), Modeling of solar radiation management: a comparison of simulations using reduced solar constant and stratospheric sulphate aerosols, *Clim Dyn, 44*, 2909-2925, doi:10.1007/s00382-014-2240-3.

Kelley, M., G.A. Schmidt, L. Nazarenko, R.L. Miller, S.E. Bauer, R. Ruedy, G.L. Russell, I. Aleinov, M. Bauer, R. Bleck, V. Canuto, G. Cesana, Y. Cheng, T.L. Clune, B. Cook, C.A. Cruz, A.D. Del Genio, G.S. Elsaesser, G. Faluvegi, N.Y. Kiang, D. Kim, A.A. Lacis, A. Leboissetier, A.N. LeGrande, K.K. Lo, J.C. Marshall, S. McDermid, E.E. Matthews, K. Mezuman, L.T. Murray, V. Oinas, C. Orbe, C. Pérez García-Pando, J.P. Perlwitz, M.J. Puma, D. Rind, A. Romanou, D.T. Shindell, S. Sun, N. Tausnev, K. Tsigaridis, G. Tselioudis, E. Weng, J. Wu, and M.-S. Yao (2020), GISS-E2.1: Configurations and climatology. *J. Adv. Model. Earth Syst*., accepted, doi:10.1029/2019MS002025.

Kirkevåg, A., et al. (2013), Aerosol-climate interactions in the Norwegian Earth System Model—NorESM1-M, *Geosci. Model. Dev., 6*, 207–244, doi:10.5194/gmd-6-207-2013.

Knutti, R., D. Masson, and A. Gettelman (2013), Climate model genealogy: Generation CMIP5 and how we got there, *Geophys. Res. Lett., 40*, 1194-1199, doi:10.1002/grl.50256.

Kravitz, B. , A. Robock, O. Boucher, H. Schmidt, K. E. Taylor, G. Stenchikov, and M. Schulz (2011), The Geoengineering Model Intercomparison Project (GeoMIP), *Atmosph. Sci. Lett., 12*, 162-167, doi:10.1002/asl.316.

Kravitz, B., et al. (2013a), Climate model response from the Geoengineering Model Intercomparison Project (GeoMIP), *J. Geophys. Res.*, *118*, 1-13, doi:10.1002/jgrd.50646.

Mis en forme : Police :(Par défaut) Times New Roman

Commenté [KB6]: Cut until we get reviews back?

Mis en forme : Police :(Par défaut) Times New Roman

Kravitz, B., et al. (2013b), An energetic perspective on hydrological changes in the Geoengineering Model Intercomparison Project (GeoMIP), *J. Geophys. Res.*, *118*, 13087-13102, doi:10.1002/2013JD020502.

Kravitz, B., et al. (2014), A multi-model assessment of regional disparities caused by solar geoengineering, *Environ. Res. Lett.*, *9*, 074013, doi:10.1088/1748-9326/14/074013.

Kravitz, B., A. Robock, S. Tilmes, O. Boucher, J. M. English, P. J. Irvine, A. Jones, M. G. Lawrence, M. MacCracken, H. Muri, J. C. Moore, U. Niemeier, S. J. Phipps, J. Sillmann, T. Storelvmo, H. Wang, and S. Watanabe (2015), The Geoengineering Model Intercomparison Project Phase 6 (GeoMIP6): Simulation design and preliminary results, *Geosci. Model Dev.*, *8*, 3379-3392, doi:10.5194/gmd-8-3379-2015.

Kravitz, B., D. G. MacMartin, H. Wang, and P. J. Rasch (2016), Geoengineering as a design problem, *Earth System Dynamics*, *7*, 469-497, doi:10.5194/esd-7-469-2016.

Kravitz, B., et al. (2017), First simulations of designing stratospheric sulfate aerosol geoengineering to meet multiple simultaneous climate objectives, *J. Geophys. Res., 122*, 12616-12634, doi:10.1002/2017JD026874.

Kravitz, B., D. G. MacMartin, S. Tilmes, J. H. Richter, M. J. Mills, W. Cheng, K. Dagon, A. S. Glanville, J.-F. Lamarque, I. Simpson, J. Tribbia, and F. Vitt (2019), Comparing surface and stratospheric impacts of geoengineering with different SO2 injection strategies, *J. Geophys. Res., 124*, 7900-7918, doi:10.1029/2019JD030329

Lurton, T., et al. (2020), Implementation of the CMIP6 forcing data in the IPSL-CM6A-LR model, *J. Adv. Model. Earth Sys., 12*, e2019MS001940, doi:10.1029/2019MS001940.

MacMartin, D. G., D. W. Keith, B. Kravitz, and K. Caldeira (2013), Management of trade-offs in geoengineering through optimal choice of non-uniform radiative forcing, *Nature Climate Change*, *3*, 365-368, doi:10.1038/nclimate1722.

Madronich, S., S. Tilmes, B. Kravitz, D. G. MacMartin, and J. H. Richter (2018), Response of surface ultraviolet and visible radiation to stratospheric SO_2 injection, *Atmosphere*, *9*, 432, doi:10.3390/atmos9110432.

Mauritsen, T., et al. (2019), Developments in the MPI-M Earth System Model version 1.2 (MPI-ESM1.2) and its response to increasing CO_2, *J. Adv. Model. Earth Sys., 11*, 998– 1038, doi:10.1029/2018MS001400.

Meehl, G. A., C. A. Senior, V. Eyring, G. Flato, J.-F. Lamarque, R. J. Stouffer, K. E. Taylor, and M. Schlund (2020), Context for interpreting equilibrium climate sensitivity and transient climate response from the CMIP6 Earth system models, *Science Advances*, *6*, eaba1981, doi:10.1126/sciadv.aba1981.

Mis en forme : Police :(Par défaut) Times New Roman

Moore, J. C. et al. (2014), Arctic sea ice and atmospheric circulation under the GeoMIP G1 scenario, *J. Geophys. Res.*, *119*, 567-583, doi:10.1002/2013JD021060.

Moreno-Cruz, J. B., K. L. Ricke, and D. W. Keith (2012), A simple model to account for regional inequalities in the effectiveness of solar radiation management, *Climatic Change*, *110*, 649-668.

Neale, R. B., C. Chen, A. Gettelman, P. Lauritzen, S. Park, D. Williamson, A. Conley, R. Garcia, D. Kinnison, and J. Lamarque (2010), Description of the NCAR community atmosphere model (CAM 5.0), NCAR Tech. Note NCAR/TN-486+ STR.

Niemeier, U., H. Schmidt, K. Alterskjær, and J. E. Kristjánsson (2013), Solar irradiance reduction via climate engineering: Impact of different techniques on the energy balance and the hydrological cycle, *J. Geophys. Res. Atmos., 118,* 11,905–11,917, doi:10.1002/2013JD020445.

National Research Council. 2015. Climate Intervention: Reflecting Sunlight to Cool Earth. Washington, DC: The National Academies Press. https://doi.org/10.17226/18988.

Phipps, S. J., L. D. Rotstayn, H. B. Gordon, J. L. Roberts, A. C. Hirst, and W. F. Budd (2011), The CSIRO Mk3L climate system model version 1.0 – Part 1: Description and evaluation, *Geosci. Model Dev., 4*, 483–509, https://doi.org/10.5194/gmd-4-483-2011.

Phipps, S. J., L. D. Rotstayn, H. B. Gordon, J. L. Roberts, A. C. Hirst, and W. F. Budd (2012), The CSIRO Mk3L climate system model version 1.0 – Part 2: Response to external forcings, *Geosci. Model Dev., 5*, 649–682, https://doi.org/10.5194/gmd-5-649-2012.

Pitari, G., V. Aquila, B. Kravitz, A. Robock, S. Watanabe, I. Cionni, N. D. Luca, G. di Genova, E. Mancini, and S. Tilmes (2014), Stratospheric ozone response to sulfate geoengineering: Results from the Geoengineering Model Intercomparison Project (GeoMIP), *J. Geophys. Res.*, *119*, 2629-2653.

Richter, J. H., S. Tilmes, A. Glanville, B. Kravitz, D. G. MacMartin, M. J. Mills, I. R. Simpson, F. Vitt, J. J. Tribbia, and J.-F. Lamarque (2018), Stratospheric response in the first geoengineering simulation meeting multiple surface climate objectives, *J. Geophys. Res., 123*, 5762-5782, doi:10.1029/2018JD028285.

Ricke, K. L., M. G. Morgan, and M. R. Allen (2010), Regional climate response to solar-radiation management, *Nat. Geosci., 3*, 537–541, doi:10.1038/ngeo915.

Robock, A. (2000), Volcanic eruptions and climate, *Rev. Geophys.*, 38, 191–219, doi:10.1029/1998RG000054.

Russotto, R. D. and T. P. Ackerman (2018), Changes in clouds and thermodynamics under solar geoengineering and implications for required solar reduction, *Atmos. Chem. Phys., 18*, 11905–11925, doi:10.5194/acp-18-11905-2018.

Mis en forme : Police :(Par défaut) Times New Roman, Français (France)

Mis en forme : Police :(Par défaut) Times New Roman

Mis en forme : Police :(Par défaut) Times New Roman

Mis en forme : Police :(Par défaut) Times New Roman

Mis en forme : Police :(Par défaut) Times New Roman

Mis en forme : Police :(Par défaut) Times New Roman

Mis en forme : Police :(Par défaut) Times New Roman

Mis en forme : Police :(Par défaut) Times New Roman

Mis en forme : Police :(Par défaut) Times New Roman

Schmidt, G. A., et al. (2006), Present-day atmospheric simulations using GISS ModelE: Comparison to in situ, satellite and reanalysis data, *J. Clim., 19*, 153–192, doi:10.1175/JCLI3612.1.

Séférian, R., et al. (2019), Evaluation of CNRM Earth-System model, CNRM-ESM2-1: Role of Earth system processes in present-day and future climate, *J. Adv. Model. Earth Sys., 11*, 4182–4227, doi:10.1029/2019MS001791.

Sellar, A. A., et al. (2019), UKESM1: Description and evaluation of the U.K. Earth System Model, *J. Adv. Model. Earth Sys., 11*, 4513–4558, doi:10.1029/2019MS001739.

Simpson, I., S. Tilmes, J. Richter, B. Kravitz, D. MacMartin, M. Mills, J. Fasullo, and A. Pendergrass (2019), The regional hydroclimate response to stratospheric sulfate geoengineering and the role of stratospheric heating, *J. Geophys. Res., 124*, 12587-12616, doi:10.1029/2019JD031093.

Stevens, B., et al. (2013), The atmospheric component of the MPI-M Earth System Model: ECHAM6, *J. Adv. Model. Earth Syst., 5*, doi:10.1002/jame.20015.

Swart, N. C., et al. (2019), The Canadian Earth System Model version 5 (CanESM5.0.3), *Geosci. Model Dev.*, *12*, 4823-4873, doi:10.5194/gmd-12-4823-2019.

Taylor, K. E., R. J. Stouffer, and G. A. Meehl (2012), An overview of CMIP5 and the experiment design, *Bull. Am. Meteorol. Soc., 93*, 485–498, doi:10.1175/BAMS-D-11-00094.1.

Tilmes, S., et al. (2013), The hydrological impact of geoengineering in the Geoengineering Model Intercomparison Project (GeoMIP), *J. Geophys. Res.*, *118*, 11036-11058, doi:10.1002/jgrd.50868.

Tilmes, S., J. Richter, M. Mills, B. Kravitz, D. G. MacMartin, R. Garcia, D. Kinnison, J.-F. Lamarque, J. Tribbia, and F. Vitt (2018), Effects of different stratospheric SO_2 injection altitudes on stratospheric chemistry and dynamics*, J. Geophys. Res., 123*, 4654-4673, doi:10.1002/2017JD028146.

Vial, J., J.-L. Dufresne, and S. Bony (2013), On the interpretation of inter-model spread in CMIP5 climate sensitivity estimates, *Climate Dynamics*, *41*, 3339-3362, doi:10.1007/s00382-013-1725-9.

Vignesh, P. P., J. H. Jiang, P. Kishore, H. Su, T. Smay, N. Brighton, and I. Velicogna (2020), Assessment of CMIP6 cloud fraction and comparison with satellite observations, *Earth and Space Science*, 7, e2019EA000975, doi:10.1029/2019EA000975.

Visioni, D., D. G. MacMartin, B. Kravitz, S. Tilmes, M. J. Mills, J. H. Richter, and M. P. Boudreau (2019), Seasonal injection strategies for stratospheric aerosol geoengineering, *Geophysical Research Letters, 46,* 7790-7799, doi:10.1029/2019GL083680.

Mis en forme : Police :(Par défaut) Times New Roman, Français (Canada)

Mis en forme : Police :(Par défaut) Times New Roman

Mis en forme : Police :(Par défaut) Times New Roman, Non souligné

Mis en forme : Police :(Par défaut) Times New Roman

Watanabe, S., et al. (2008), Development of an atmospheric general circulation model for integrated Earth system modeling on the Earth Simulator, *J. Earth Simulator, 9*, 27–35.

Watanabe, S., et al. (2011), MIROC-ESM 2010: Model description and basic results of CMIP5-20c3m experiments, *Geosci. Model Dev., 4*, 845–872, doi:10.5194/gmd-4-845-2011.

Xia, L., et al. (2014), Solar radiation management impacts on agriculture in China: A case study in the Geoengineering Model Intercomparison Project (GeoMIP), *J. Geophys. Res. Atmos., 119*, 8695-8711, doi:10.1002/2013JD020630.

Zelinka, M. D., et al. (2020), Causes of higher climate sensitivity in CMIP6 models, *Geophys. Res. Let.*, 47, e2019GL085782, doi:10.1029/2019GL085782.

#	Model	Gen.	Reference	G1 Solar reduction (%)	Notes
1	BNU-ESM	CMIP5	Ji et al. (2014)	3.80	Cloud forcing not available
2	CanESM2	CMIP5	Arora et al. (2011)	4.00	
3	CCSM4	CMIP5	Gent et al. (2011)	4.25	NPP not available
4	CESM-CAM5.1-FV	CMIP5	Neale et al. (2010) Hurrell et al. (2013)	4.70	
5	CSIRO-Mk3L-1.2	CMIP5	Phipps et al. (2011, 2012)	3.20	Cloud forcing and NPP not available
6	EC-EARTH	CMIP5	Hazeleger et al. (2011)	4.12	Cloud forcing and NPP not available
7	GISS-E2-R	CMIP5	Schmidt et al. (2006)	4.47	
8	HadCM3	CMIP5	Gordon et al. (2000)	4.16	Cloud forcing and NPP not available
9	HadGEM2-ES	CMIP5	Collins et al. (2011)	3.88	
10	IPSL-CM5A-LR	CMIP5	Dufresne et al. (2013) Hourdin et al.(2011)	3.50	NPP not available
11	MIROC-ESM	CMIP5	Watanabe et al. (2008,2011)	5.00	
12	MPI-ESM-LR	CMIP5	Giorgetta et al. (2012) Stevens et al. (2012)	4.68	
13	NorESM1-M	CMIP5	Alterskjær et al. (2012) Kirkevåg et al. (2012)	4.03	
14	CanESM5	CMIP6	Swart et al. (2019)	3.72	
15	CESM2-WACCM	CMIP6	Gettelman et al. (2019)	4.91	
16	CNRM-ESM2-1	CMIP6	Séférian et al. (2019)	3.72	
17	GISS-E2-1-G	CMIP6	Kelley et al. (in revision)	4.13	
18	IPSL-CM6A-LR	CMIP6	Boucher et al. (2020) Lurton et al. (2020)	4.10	
19	MPI-ESM1-2-LR	CMIP6	Mauritsen et al. (2019)	4.57	
20	UKESM1-0-LL	CMIP6	Sellar et al. (2019)	3.80	

Table 1. All participating models in both the CMIP5 and CMIP6 eras of GeoMIP, including references. For G1 solar reduction, the percentage is calculated as the percent change in incident solar irradiance at the top-of-atmosphere between G1 and its respective piControl run. Numbers in the first column correspond to the model numbers in Figure 5.

#	Model	Gen.	Reference	G1 Solar reduction (%)	Notes
1	BNU-ESM	CMIP5	Ji et al. (2014)	3.80	Cloud forcing not available
2	CanESM2	CMIP5	Arora et al. (2011)	4.00	
3	CCSM4	CMIP5	Gent et al. (2011)	4.25	NPP not available
4	CESM-CAM5.1-FV	CMIP5	Neale et al. (2010) Hurrell et al. (2013)	4.70	
5	CSIRO-Mk3L-1.2	CMIP5	Phipps et al. (2011, 2012)	3.20	Cloud forcing and NPP not available
6	EC-EARTH	CMIP5	Hazeleger et al. (2011)	4.12	Cloud forcing and NPP not available
7	GISS-E2-R	CMIP5	Schmidt et al. (2006)	4.47	
8	HadCM3	CMIP5	Gordon et al. (2000)	4.16	Cloud forcing and NPP not

Mis en forme : Police :(Par défaut) Times New Roman
Tableau mis en forme
Mis en forme : Police :(Par défaut) Times New Roman
Mis en forme : Police :(Par défaut) Times New Roman
Mis en forme : Police :(Par défaut) Times New Roman
Mis en forme : Police :(Par défaut) Times New Roman
Mis en forme : Police :(Par défaut) Times New Roman
Mis en forme : Police :(Par défaut) Times New Roman
Mis en forme : Police :(Par défaut) Times New Roman
Mis en forme : Police :(Par défaut) Times New Roman
Mis en forme : Police :(Par défaut) Times New Roman
Mis en forme : Police :(Par défaut) Times New Roman
Mis en forme : Police :(Par défaut) Times New Roman
Mis en forme : Police :(Par défaut) Times New Roman
Mis en forme : Police :(Par défaut) Times New Roman
Mis en forme : Police :(Par défaut) Times New Roman
Mis en forme : Police :(Par défaut) Times New Roman
Mis en forme : Police :(Par défaut) Times New Roman
Mis en forme : Police :(Par défaut) Times New Roman
Mis en forme : Police :(Par défaut) Times New Roman
Mis en forme : Français (France)

					available
9	HadGEM2-ES	CMIP5	Collins et al. (2011)	3.88	
10	IPSL-CM5A-LR	CMIP5	Dufresne et al. (2013) Hourdin et al.(2011)	3.50	NPP not available
11	MIROC-ESM	CMIP5	Watanabe et al. (2008,2011)	5.00	
12	MPI-ESM-LR	CMIP5	Giorgetta et al. (2012) Stevens et al. (2012)	4.68	
13	NorESM1-M	CMIP5	Alterskjær et al. (2012) Kirkevåg et al. (2012)	4.03	
14	CanESM5	CMIP6	Swart et al. (2019)	3.72	
15	CESM2-WACCM	CMIP6	Gettelman et al. (2019)	4.91	
16	CNRM-ESM2.1	CMIP6	Séférian et al. (2019)	3.72	
17	GISS-E2.1-G	CMIP6	Kelley et al. (in revision)	4.13	
18	IPSL-CM6A-LR	CMIP6	Boucher et al. (2020) Lurton et al. (2020)	4.10	
19	MPI-ESM1.2-LR	CMIP6	Mauritsen et al. (2019)	4.57	
20	UKESM1.0-LL	CMIP6	Sellar et al. (2019)	3.80	

Mis en forme : Français (France)

Mis en forme : Français (France)

Mis en forme : Français (France)

Mis en forme : Français (France)

621

Comparing different generations of idealized solar geoengineering simulations in the Geoengineering Model Intercomparison Project (GeoMIP)

Ben Kravitz[1,2], Douglas G. MacMartin[3], Daniele Visioni[3], Olivier Boucher[4], Jason N. S. Cole[5], Jim Haywood[6,7], Andy Jones[7], Thibaut Lurton[4], Pierre Nabat[8], Ulrike Niemeier[9], Alan Robock[10], Roland Séférian[8], and Simone Tilmes[11]

[1]Department of Earth and Atmospheric Sciences, Indiana University, Bloomington, IN, USA
[2]Atmospheric Sciences and Global Change Division, Pacific Northwest National Laboratory, Richland, WA, USA
[3]Sibley School of Mechanical and Aerospace Engineering, Cornell University, Ithaca, NY, USA
[4]Institut Pierre-Simon Laplace (IPSL), Sorbonne Université/CNRS, Paris, France
[5]Environment and Climate Change Canada, Toronto, Ontario, Canada
[6]College of Engineering, Mathematics and Physical Sciences, University of Exeter, Exeter, United Kingdom
[7]UK Met Office Hadley Centre, Exeter, United Kingdom
[8]CNRM, Université de Toulouse, Météo-France, CNRS, Météo-France, Toulouse, France
[9]Max Planck Institute for Meteorology, Hamburg, Germany
[10]Department of Environmental Sciences, Rutgers University, New Brunswick, NJ, USA
[11]Atmospheric Chemistry Observations and Modeling Laboratory, National Center for Atmospheric Research, Boulder, CO, USA

Correspondence: Ben Kravitz, 1001 E. 10th Street, Bloomington, IN 47405-1405, USA. (bkravitz@iu.edu)

Abstract. Solar geoengineering has been receiving increased attention in recent years as a potential temporary solution to offset global warming. One method of approximating global-scale solar geoengineering in climate models is via solar reduction experiments. Two generations of models in the Geoengineering Model Intercomparison Project (GeoMIP) have now simulated offsetting a quadrupling of the CO_2 concentration with solar reduction. This simulation is idealized and designed to elicit large responses in the models. Here we show that energetics, temperature, and hydrological cycle changes in this experiment are statistically indistinguishable between the two ensembles. Of the variables analyzed here, the only major differences involve highly parameterized and uncertain processes, such as cloud forcing or terrestrial net primary productivity. We conclude that despite numerous structural differences and uncertainties in models over the past 20 years, including an increase in climate sensitivity in the latest generation of models, broad conclusions about the climate response to global solar dimming remain robust.

1 Introduction

Solar geoengineering describes a set of technologies designed to (ideally) temporarily, deliberately reduce some of the effects of climate change by changing the radiative balance of the planet, often by reflecting sunlight back to space (NRC, 2015). Numerous methods have been proposed, but the most studied is stratospheric sulfate aerosol injection (Budyko, 1977; Crutzen, 2006). This method involves substantially increasing the stratospheric sulfate aerosol burden, replicating the mechanisms that cause cooling after large volcanic eruptions (Robock, 2000). Climate models are currently the only tools for understanding the climatic consequences of solar geoengineering. In model simulations of solar geoengineering, insolation reduction is often used as a proxy for actual stratospheric sulfate aerosols, as it captures many of the broad radiative effects of stratospheric aerosol geoengineering as well as some of the important climate effects like surface cooling and hydrological cycle strength reduction (Niemeier et al., 2013; Kalidindi et al., 2015). However, stratospheric sulfate aerosols also absorb longwave radiative flux, which heats the upper troposphere and lower stratosphere. As such, any implementation of stratospheric geoengineering with sulfate aerosols would produce additional effects, such as changing atmospheric circulation in response to stratospheric heating and heating gradients (e.g., Richter et al., 2017; Tilmes et al., 2018; Simpson et al., 2019) and stratospheric ozone changes (e.g., Pitari et al., 2014), as well as changes in ultraviolet radiative flux and enhanced diffuse radiation at the surface (Madronich et al., 2018). However, here we consider the major, large-scale effect of reflecting sunlight to cool Earth.

Simulations of solar geoengineering with solar reduction have long shown that solar geoengineering would cool the planet, offsetting global warming (e.g., Govindasamy and Caldeira, 2000; NRC, 2015; Irvine et al., 2016). Idealized simulations of solar reduction have also been simulated in a multi-model context under the Geoengineering Model Intercomparison Project (GeoMIP; Kravitz et al., 2011), to understand the robust model responses to various standardized solar geoengineering simulation designs. Multi-model conclusions from these studies indicate that solar geoengineering would be effective at partially offsetting greenhouse gas-induced temperature changes (Kravitz et al., 2013), as well as changes in the hydrological cycle (Tilmes et al., 2013), the cryosphere (Moore et al., 2014), extreme events (Curry et al., 2014; Aswathy et al., 2015), vegetation (Glienke et al., 2015), circulation (Guo et al., 2018; Gertler et al., 2020), agricultural yield potential (Xia et al., 2014), and numerous other areas. However, the offset is not exact (Moreno-Cruz et al., 2012), particularly on a regional basis or when considering multiple simultaneous metrics of climate change (Kravitz et al., 2014; Irvine et al., 2019), leading to concerns about winners and losers from geoengineering (Ricke et al., 2010). To some extent, the effects of solar geoengineering may be tailored or designed (MacMartin et al., 2013; Kravitz et al., 2016, 2017, 2019), but solar geoengineering will still not be able to completely offset climate change from greenhouse gases.

The previous phase of GeoMIP was associated with the Coupled Model Intercomparison Project Phase 5 (CMIP5; Taylor et al., 2012), an international collaboration of climate models to attempt to understand robust model responses to various forcings. GeoMIP has now entered a new phase, concurrent with the Coupled Model Intercomparison Project Phase 6 (CMIP6; Eyring et al., 2016), and with it are new solar geoengineering simulations with new and updated versions of the participating Earth System Models (Kravitz et al., 2015). As such, this is an opportunity to revisit some central questions in solar geoengineering. Many of the CMIP5 results regarding solar geoengineering showed substantial agreement across the participating

GeoMIP models. In this newest iteration of GeoMIP, do the same science conclusions still hold, and do the models still generally agree on the resulting climate effects? Here we address these questions by evaluating and comparing general climate model response to GeoMIP experiment G1 (described in the next section) from both CMIP5 and CMIP6.

2 Simulations and Participating Models

In this study, we evaluate GeoMIP experiment G1, in which, starting from a preindustrial control (piControl) baseline, the atmospheric CO_2 concentration is instantaneously quadrupled (the standard CMIP experiment abrupt4xCO2), and insolation is simultaneously reduced such that net top-of-atmosphere (TOA) radiative flux is within ± 0.1 W m^{-2} of the baseline value in the first decade of simulation (Kravitz et al., 2011, 2015). This experiment was part of the original suite of GeoMIP experiments and was repeated and extended in the newest suite in an effort to understand the role of model structural uncertainty in broad conclusions about solar geoengineering. Participating models are listed in Table 1. We include 13 models from CMIP5 and 7 models from CMIP6. Experiment G1 is an idealized experiment aimed at understanding physical climate response, with limited policy relevance.

The original G1 experiment was 50 years in length, whereas the CMIP6 version is 100 years in length to allow for better analyses of rare events and to capture very slow responses. Comparison between the two ensembles necessitates only using the first 50 years, but we need to verify that this can be done without losing important longer-term evolution in features. Figures 1 and 2 look at G1 behavior over the entire 100-year period of the CMIP6 simulations to determine whether there is any drift or trend that would not be revealed by only analyzing the first 50 years. (Also see Table 2 for quantitative information.) CNRM-ESM2.1 and IPSL-CM6A-LR show appreciable (greater than 0.1 K/decade in magnitude) negative trends in temperature, and CESM2(WACCM) and UKESM1.0-LL show appreciable positive trends. This is despite no model showing a trend in net TOA radiative flux greater in magnitude than 0.02 W m^{-2}/decade. Beyond an initial transient period, CESM2(WACCM), CNRM-ESM2.1, and IPSL-CM6A-LR show appreciable (approximately 0.06%/decade) trends in precipitation and evaporation of the same sign as the temperature trends. Nevertheless, these trends are orders of magnitude lower than the changes in these variables in experiment G1 as compared to piControl (Figure 1). As such, we conclude that our choice to focus on the first 50 years of simulation does not appreciably affect our results.

Figure 2 shows relatively flat lines for the 90°S-30°S and 30°S-30°N regions, whereas this is not the case for the region north of 30°N. In this region, CESM2(WACCM), CNRM-ESM2.1, IPSL-CM6A-LR, and UKESM1.0-LL have some time-varying behavior, indicating that the temperature changes are possibly related to a slight trend in sea ice coverage (Boucher et al., 2020).

IPSL-CM6A-LR is also known to have a bicentennial oscillation, which could affect G1–piControl differences, depending on the baseline period used for subtraction. To verify that this oscillation is not impacting our results, we divided that model's 1200-year piControl run into 50-year chunks and computed the surface air temperature average for each of those chunks. The largest temperature found was 286.0339 K, and the smallest was 285.6384 K. The average over the entire ensemble was 285.8604 K. As such, using the mean of the entire ensemble versus matching the appropriate period in the bicentennial

oscillation would have an impact on G1–piControl temperature by at most 0.22 K. Only averaging the first 100 years of the piControl run (which may be the best match to the period covered by G1) yields a temperature of 285.9084 K, which is 0.048 K different from the mean of the entire piControl run. As such, we conclude that this bicentennial oscillation is unlikely to have substantially influenced our findings.

Per the results in Figure 1, IPSL-CM6A-LR and GISS-E2.1-G appear to have a different responsiveness of the hydrological cycle to the combined CO_2-solar forcing than the other models. We are reluctant to attribute this feature to any potential shortcomings or lack of fidelity to observations because there are no observations of this type of experiment. Although these models are outliers, there is no evidential basis on which to assume they are more or less valid than the other models for this study.

Because the main focus of this paper is a comparison between the CMIP5 and CMIP6 generations of model results, we have opted for the following to aid comparisons:

- Since we are not evaluating any features that require 100 years of statistics, and the results do not show any appreciable time evolution of behavior after the first couple of years (see discussion above), we only evaluate the first 50 years of all simulations. All maps show changes over years 11-50, removing the initial transient period.

- We do not compare previous versions of individual models with current ones, instead only examining ensembles. Even though models may share similar development histories (e.g., atmosphere and ocean dynamical cores, convective parameterizations, radiative transfer modules, terrestrial biosphere and cryosphere; Knutti et al., 2013; Zelinka et al., 2020), there have been numerous developments in models in these areas (and others) between CMIP5 and CMIP6 such that in most cases a direct comparison would not be meaningful.

- We focus extensively on the G1 results and, with few exceptions, do not focus on the corresponding abrupt4xCO2 simulations. It has been well documented that the CMIP6 models tend to have higher climate sensitivities than the CMIP5 models (Flynn and Mauritsen, 2020; Meehl et al., 2020; Zelinka et al., 2020), so we do not wish to make conclusions that might be based on a form of selection bias.

- All lack of stippling on map plots, as in previous GeoMIP studies (e.g., Kravitz et al., 2013), indicates agreement on the sign of the response in at least 75% of models. Because $\mathrm{G1}_{\mathrm{CMIP5}}$ has more participating models than $\mathrm{G1}_{\mathrm{CMIP6}}$, this threshold provides some consistency across analyses of the ensembles. When plotting differences between the ensembles ($\mathrm{G1}_{\mathrm{CMIP6}}$–$\mathrm{G1}_{\mathrm{CMIP5}}$), there is no stippling, as it is difficult to meaningfully represent such differences between ranges. Aggregate differences between the two ensembles, as calculated using Welch's t-test or differences in stippled area, are discussed in Table 3.

3 Results

3.1 Energetics

Ensemble mean radiative and turbulent flux quantities are plotted in Figure 3, and the ensemble ranges are plotted in Figure 4. An immediate observation is that, in both ensembles, the models were successful at limiting net TOA radiative flux change to within approximately ± 0.1 W m^{-2} of the models' respective preindustrial values. Accomplishing this required an average solar reduction of 4.14% (models range in 3.20–5.00%) in CMIP5 and 4.14% (3.72–4.91%) in CMIP6. As such, despite numerous structural changes between the two generations of models, there is no appreciable change in solar efficacy (Hansen et al., 2005).

None of the radiative flux quantities indicate large transients over 50 years of simulation of G1, other than the initial flux change within the first year or so of simulation. This is consistent with the "perpetual fast response" found by Kravitz et al. (2013b), in which because global mean temperature does not change appreciably over the course of the G1 simulation, climate feedbacks are not excited, and the internal state of the system (as measured by, for example, fluxes and hydrological cycle changes) similarly does not change. Ensemble mean fluxes show few differences (<1 W m^{-2} in magnitude) with the exception of shortwave cloud forcing, defined as all-sky minus clear-sky shortwave flux at the surface. On average, the CMIP6 ensemble has 3–4 W m^{-2} less shortwave cloud forcing than CMIP5. Neglecting some outliers, for each flux except shortwave (and hence total) cloud forcing, the median model in one ensemble is within the inter-quartile range of the other ensemble. This indicates that there are no major differences between the ensembles in how the models handle energy balance and energetics, with the exception of clouds, which is consistent with findings about CMIP6 (Zelinka et al., 2020). Moreover, it appears that most of the major differences in shortwave cloud forcing are due to outliers in each ensemble, positive for CMIP5 and negative for CMIP6. To further explore these potential differences, Figure 5 provides maps of the ensemble means for cloud forcing. In G1, the CMIP5 ensemble showed more positive shortwave cloud forcing and more negative longwave cloud forcing (i.e., more cancellation) than the CMIP6 ensemble. Overall, the CMIP6 ensemble has greatly reduced (in some places by over 10 W m^{-2}) shortwave cloud forcing as compared to CMIP5 under the G1 experiment. This is a widespread result, but the most prominent features are in the tropics, especially over the Amazon, Africa, and the Maritime Continent. These regions encompass tropical forests, indicating a potential for vegetation feedbacks on the temperature reductions. However, the reasons behind these forcing changes are difficult to diagnose, as they could be due to changes in cloud thickness, cloud cover, or cloud level between CMIP5 and CMIP6 models (e.g., Vignesh et al., 2020), differences in how solar geoengineering affects clouds (Russotto and Ackerman, 2018), or artifacts of the analyses (e.g., cloud masking; Andrews et al., 2009; Kravitz et al., 2013b). Moreover, based on the results in Figure 4, it is likely that many of these features are exaggerated by outlier models (also see Vignesh et al., 2020). As such, we reserve such detailed investigations for future work.

3.2 Temperature

These small flux changes also lead to few G1 temperature changes between the two ensembles. Figure 6 shows global, land, and ocean-averaged temperatures for the CMIP5 and CMIP6 ensembles. In general, the abrupt4xCO2 simulation in CMIP6 has higher temperatures than in CMIP5, consistent with the noted increase in climate sensitivity (Vial et al., 2013; Flynn

and Mauritsen, 2020; Meehl et al., 2020; Zelinka et al., 2020). In both ensembles, G1 is effective at offsetting global mean temperature change, in some cases with a slight positive residual temperature change over land. Figure 7 shows three aggregate temperature metrics: global mean temperature (T_0), the interhemispheric temperature gradient (T_1), and the equator-to-pole temperature gradient (T_2) (Ban-Weiss and Caldeira, 2010; Kravitz et al., 2016):

$$T_0 = \frac{1}{A}\int_{-\pi/2}^{\pi/2} T(\psi)\,\mathrm{d}A$$

$$T_1 = \frac{1}{A}\int_{-\pi/2}^{\pi/2} T(\psi)\sin\psi\,\mathrm{d}A \quad (1)$$

$$T_2 = \frac{1}{A}\int_{-\pi/2}^{\pi/2} T(\psi)\frac{1}{2}(3\sin^2\psi - 1)\,\mathrm{d}A$$

where A is area. As for the fluxes, the median model in one ensemble is within the inter-quartile range of the other ensemble. This indicates that no ensemble is on average warmer or cooler than another, has a substantially warmer Northern or Southern Hemisphere than the other, nor has warmer tropics or poles than the other. We can conclude that spatial patterns of temperature change from G1 are robust across a wide range of structural uncertainty, including an increase in climate sensitivity between the two generations of CMIP.

The spatial structure of temperature change (Figure 8) does have small differences between the two ensembles. G1 in CMIP6 has multiple locations that are warmer than G1 in CMIP5, despite both ensembles achieving net energy balance at TOA and the surface (Figure 3). The majority of the differences are over land and in the tropics, where CMIP6 is slightly warmer than CMIP5 (up to 1°C in some places). Nevertheless, both ensembles show the well noted feature that offsetting a CO_2 increase with globally uniform solar reduction overcools the tropics and undercools the poles (Govindasamy and Caldeira, 2000; Kravitz et al., 2013). CMIP6 shows slightly less high latitude warming than CMIP5, but temperature differences between the two ensembles are largely negligible. However, the warmer temperatures in CMIP6 near Greenland have important implications for ice sheet melt and consequent sea level rise, as well as bottom water formation. We reserve such analyses for future investigations, particularly since the models used here are not capable of simulating the eustatic component of sea level rise. In any case, these ensemble mean differences between CMIP5 and CMIP6 cannot be deemed statistically significant (Table 3 and Figure 7).

3.3 Hydrological and Other Integrative Changes

Figure 9 shows ensemble mean changes in precipitation (P), evaporation (E), and P–E for $\mathrm{G1}_{\mathrm{CMIP5}}$ and $\mathrm{G1}_{\mathrm{CMIP6}}$. Qualitatively, patterns are similar between both ensembles. Precipitation is slightly (<0.3 mm/day in magnitude) different in the tropics between the two ensembles. The majority of those features can be summarized as a more southward Intertropical Convergence Zone (ITCZ), more precipitation in the South Pacific Convergence Zone, and less precipitation over Southeast Asia and the

Maritime Continent in $G1_{CMIP6}$. Evaporation in the two ensembles is nearly identical except for more evaporation in Amazonia and Australia in $G1_{CMIP6}$. As such, the net P–E change between the two ensembles strongly resembles the precipitation changes. Figure 10 shows that, like previous evaluations of ensemble ranges, the median model in one ensemble falls well within the interquartile range of the other ensemble for P, E, and P–E. As such, we cannot conclude any robust hydrological cycle changes between the two ensembles.

Figure 11 shows average (years 11–50) temperature change (with respect to piControl) plotted against average precipitation change for each model, as in Tilmes et al. (2013). Other than a potentially greater climate sensitivity of some CMIP6 models, there is no distinguishable difference in aggregate behavior between the two ensembles. The same conclusion discovered by Tilmes et al. (2013) holds: solar reduction cannot simultaneously offset CO_2-induced changes in both global mean temperature and global mean precipitation.

As an integrator of CO_2, temperature, and precipitation effects over land, Figure 12 shows changes in terrestrial net primary productivity (NPP). Numerous land regions have lower NPP in CMIP6 than in CMIP5. The ensemble average global NPP change (G1–piControl) is 51.2 (4.1–122.1) Pg C y^{-1} in CMIP5 and 38.1 (19.5–77.5) Pg C y^{-1} in CMIP6, representing a 25.6% difference in means. Jones et al. (2013) used NPP to highlight the importance of understanding the influence of structural land model differences on climate results related to geoengineering. While it is beyond the scope of this study to perform a detailed diagnosis of which uncertainties or processes are responsible for this inter-ensemble difference (and indeed the present setup does not allow for a controlled experiment to rigorously test structural uncertainty), we show that the ensemble spread of total terrestrial NPP is smaller in CMIP6 than in CMIP5. This result is consistent with the recent assessment of carbon cycle feedbacks conducted by Arora et al. (2020), who showed that the CMIP6 ensemble has reduced overall uncertainty in the land carbon cycle to rising CO_2 compared to their CMIP5 predecessors.

4 Discussion and Conclusions

Based on the results presented here, model response to G1 has not changed substantially between CMIP5 and CMIP6, despite numerous changes to models between the two generations, including an increase in climate sensitivity. The sign of residual climate impacts (for example in temperature) are in better agreement in CMIP5 than CMIP6 (Table 3 shows a difference in stippled area between the two ensembles), but this could be a function of the smaller ensemble size in CMIP6. Energetics, temperature, and the hydrological cycle are qualitatively and quantitatively similar in both ensemble means and ensemble ranges, although these variables are somewhat related, so we might expect them to all portray a similar picture. Notable differences do exist in shortwave cloud forcing and NPP, particularly in Amazonia, Africa, and Australia, which are also regions of inter-ensemble difference in precipitation.

From these findings, we can conclude that results obtained over the past 20 years of study have not been overturned by the latest round of simulations. All of the major ensemble differences highlighted above deal with clouds and land surface modeling, both of which are difficult to model and are necessarily highly parameterized. The conclusions that are based on more fundamental knowledge, such as column energetics (in the case of the hydrological cycle), are relatively robust to structural

uncertainty, in so far as this study adequately captures representative variations in structural uncertainty. This lends confidence to our conclusions, especially regarding robustness to uncertainty, about the broad climate effects from solar geoengineering methods that can be accurately represented via solar dimming.

We also conclude that the models used in CMIP5 are not obviously biased or inferior as compared to CMIP6. While improvements have been made in the CMIP6 generation of models, and those models are likely better for representing numerous features of the present-day climate that may be important for studies of geoengineering, there are many aspects of climate that are well represented by earlier models. In some cases, more robust analyses may be enabled by augmenting ensemble sizes with archived output from earlier generations of CMIP models.

Many of the broad features of solar geoengineering with sulfate aerosols can be represented by a reduction in solar constant (e.g., Niemeier et al., 2013; Kalidindi et al., 2015). However, the more subtle changes that derive from complex response to stratospheric aerosol heating (for example, consequences of stratospheric heating like the positive wintertime North Atlantic Oscillation; Simpson et al., 2019) require detailed assessments with state-of-the-art aerosol microphysical schemes. This is particularly important for understanding regional and seasonal solar geoengineering (Kravitz et al., 2017; Visioni et al., 2019). Such detailed microphysical calculations can only be simulated in a small number of models. While simple G1-style experiments enable a robust multi-model ensemble analysis, they cannot capture details that depend on microphysics. We emphasize the importance of a variety of modeling approaches to understand solar geoengineering, particularly the role of model uncertainty in conclusions about solar geoengineering.

There are numerous aspects of physical climate that we did not evaluate, nor did we pursue analyses beyond physical climate, including many other aspects of natural science, social science, the humanities, governance, justice, or ethics (to name a few important areas). Moreover, we emphasize that experiment G1 is an idealized experiment aimed at understanding physical climate response to combinations of large forcings and should not be interpreted as a realistic or policy-relevant scenario of geoengineering. A holistic assessment of the consequences of geoengineering, particularly of more policy-relevant scenarios, would certainly need to take these numerous aspects into account. Nevertheless, based on the results presented here, results for geoengineering across several important metrics appear to be robust to some amount of structural uncertainty. This lends confidence to some conclusions drawn from global climate models regarding solar geoengineering.

Data availability. All CMIP5 and CMIP6 output, including the respective GeoMIP simulations, is available via the Earth System Grid Federation (https://esgf-node.llnl.gov/projects/esgf-llnl/) or by contacting the respective modeling groups responsible for the output. For CMIP6 output, seeTable 1 data citations.

Author contributions. BK, OB, JNSC, JH, AJ, TL, PN, UN, RS, and ST contributed model output. BK performed the analysis. BK, DGM, and DV wrote the manuscript with all coauthors.

Competing interests. None.

Acknowledgements. We acknowledge the World Climate Research Programme, which, through its Working Group on Coupled Modelling, coordinated and promoted CMIP. We thank the climate modeling groups for producing and making available their model output, the Earth System Grid Federation (ESGF) for archiving the data and providing access, and the multiple funding agencies who support CMIP6 and ESGF. We also thank all participants of the Geoengineering Model Intercomparison Project and their model development teams. Support for B.K. was provided in part by the National Science Foundation (NSF) through agreement CBET-1931641, the Indiana University Environmental Resilience Institute, and the Prepared for Environmental Change Grand Challenge initiative. The Pacific Northwest National Laboratory is operated for the US Department of Energy by Battelle Memorial Institute under contract DE-AC05-76RL01830. Resources supporting this work were provided by the NASA High-End Computing (HEC) Program through the NASA Center for Climate Simulation (NCCS) at Goddard Space Flight Center. A.R. is supported by NSF grants AGS-1617844 and AGS-2017113. J.H. and A.J. were supported by the Met Office Hadley Centre Climate Programme funded by BEIS and Defra. U.N. is supported by the German DFG-funded Research Unit VolImpact FOR2820 sub project TI344/2-1 and MPIESM simulation have been performed on the computer of Deutsches Klimarechenzentrum (DKRZ). O.B. and T.L. were supported by the IPSL Climate Graduate School EUR (ANR grant ANR-11-IDEX-0004 - 17-EURE-0006). The CMIP6 project at IPSL used the HPC resources of TGCC under the allocations 2016-A0030107732, 2017-R0040110492 and 2018-R0040110492 (project gencmip6) provided by GENCI (Grand Équipement National de Calcul Intensif). R.S. and P.N. were supported by the H2020 CONSTRAIN under the grant agreement No 820829 and the Météo-France/DSI supercomputing center.

References

Alterskjær, K., Kristjánsson, J. E., and Seland, Ø.: Sensitivity to deliberate sea salt seeding of marine clouds – Observations and model simulations, Atmos. Chem. Phys., 12, 2795–2807, https://doi.org/10.5194/acp-12- 2795-2012, 2012.

Andrews, T., Forster, P. M., and Gregory, J. M.: A surface energy perspective on climate change, J. Clim., 22, 2557–2570, https://doi.org/10.1175/2008JCLI2759.1, 2009.

Arora, V. K., Scinocca, J. F., Boer, G. J., Christian, J. R., Denman, K. L., Flato, G. M., Kharin, V. V., Lee, W. G., and Merryfield, W. J.: Carbon emission limits required to satisfy future representative concentration pathways of greenhouse gases, Geophys. Res. Lett., 38, L05 805, https://doi.org/10.1029/2010GL046270, 2011.

Arora, V. K., Katavouta, A., Williams, R. G., Jones, C. D., Brovkin, V., Friedlingstein, P., Schwinger, J., Bopp, L., Boucher, O., Cadule, P., Chamberlain, M. A., Christian, J. R., Delire, C., Fisher, R. A., Hajima, T., Ilyina, T., Joetzjer, E., Kawamiya, M., Koven, C., Krasting, J., Law, R. M., Lawrence, D. M., Lenton, A., Lindsay, K., Pongratz, J., Raddatz, T., Séférian, R., Tachiiri, K., Tjiputra, J. F., Wiltshire, A., Wu, T., and Ziehn, T.: Carbon-concentration and carbon-climate feedbacks in CMIP6 models, and their comparison to CMIP5 models, Biogeosciences, p. in press, 2020.

Aswathy, V. N., Boucher, O., Quaas, M., Niemeier, U., Muri, H., Mülmenstädt, J., and Quaas, J.: Climate extremes in multi-model simulations of stratospheric aerosol and marine cloud brightening climate engineering, Atmospheric Chemistry and Physics, 15, 9593–9610, https://doi.org/10.5194/acp-15-9593-2015, 2015.

Ban-Weiss, G. A. and Caldeira, K.: Geoengineering as an optimization problem, Environ. Res. Lett., 5, 031 001, https://doi.org/10.1088/1748-9326/5/3/034009, 2010.

Boucher, O., Denvil, S., Caubel, A., and Foujols, M. A.: IPSL IPSL-CM6A-LR model output prepared for CMIP6 GeoMIP G1, Earth System Grid Federation, https://doi.org/10.22033/ESGF/CMIP6.5054, 2018a.

Boucher, O., Denvil, S., Caubel, A., and Foujols, M. A.: IPSL IPSL-CM6A-LR model output prepared for CMIP6 CMIP abrupt-4xCO2, Earth System Grid Federation, https://doi.org/10.22033/ESGF/CMIP6.5109, 2018b.

Boucher, O., Denvil, S., Caubel, A., and Foujols, M. A.: IPSL IPSL-CM6A-LR model output prepared for CMIP6 CMIP piControl, Earth System Grid Federation, https://doi.org/10.22033/ESGF/CMIP6.5251, 2018c.

Boucher, O., Servonnat, J., Albright, A. L., Aumont, O., Balkanski, Y., Bastrikov, V., Bekki, S., Bonnet, R., Bony, S., Bopp, L., Braconnot, P., Brockmann, P., Cadule, P., Caubel, A., Cheruy, F., Codron, F., Cozic, A., Cugnet, D., D'Andrea, F., Davini, P., de Lavergne, C., Denvil, S., Deshayes, J., Devilliers, M., Ducharne, A., Dufresne, J.-L., Dupont, E., Éthé, C., Fairhead, L., Falletti, L., Flavoni, S., Foujols, M.-A., Gardoll, S., Gastineau, G., Ghattas, J., Grandpeix, J.-Y., Guenet, B., Guez, L., Guilyardi, E., Guimberteau, M., Hauglustaine, D., Hourdin, F., Idelkadi, A., Joussaume, S., Kageyama, M., Khodri, M., Krinner, G., Lebas, N., Levavasseur, G., Lévy, C., Li, L., Lott, F., Lurton, T., Luyssaert, S., Madec, G., Madeleine, J.-B., Maignan, F., Marchand, M., Marti, O., Mellul, L., Meurdesoif, Y., Mignot, J., Musat, I., Ottlé, C., Peylin, P., Planton, Y., Polcher, J., Rio, C., Rochetin, N., Rousset, C., Sepulchre, P., Sima, A., Swingedouw, D., Thiéblemont, R., Traore, A. K., Vancoppenolle, M., Vial, J., Vialard, J., Viovy, N., and Vuichard, N.: Presentation and evaluation of the IPSL-CM6A-LR climate model, Journal of Advances in Modeling Earth Systems, in press, e2019MS002 010, https://doi.org/10.1029/2019MS002010, 2020.

Budyko, M. I.: Climatic Changes, American Geophysical Union, 1977.

Cole, J. N., Swart, N. C., Kharin, V. V., Lazare, M., Scinocca, J. F., Gillett, N. P., Anstey, J., Arora, V., Christian, J. R., Jiao, Y., Lee, W. G., Majaess, F., Saenko, O. A., Seiler, C., Seinen, C., Shao, A., Solheim, L., von Salzen, K., Yang, D., Winter, B., and Sigmond, M.: CCCma

CanESM5 model output prepared for CMIP6 GeoMIP G1, Earth System Grid Federation, https://doi.org/10.22033/ESGF/CMIP6.3158, 2019.

Collins, W. J., Bellouin, N., Doutriaux-Boucher, M., Gedney, N., Halloran, P., Hinton, T., Hughes, J., Jones, C. D., Joshi, M., Liddicoat, S., Martin, G., O'Connor, F., Rae, J., Senior, C., Sitch, S., Totterdell, I., Wiltshire, A., and Woodward, S.: Development and evaluation of an Earth-System model—HadGEM2, Geosci. Model Dev., 4, 1051–1075, https://doi.org/10.5194/gmd-4-1051-2011, 2011.

Crutzen, P. J.: Albedo enhancement by stratospheric sulfur injections: A contribution to resolve a policy dilemma?, Climatic Change, 77, 211–220, https://doi.org/10.1007/s10584-006-9101-y, 2006.

Curry, C. L., Sillmann, J., Bronaugh, D., Alterskjær, K., Cole, J. N. S., Kravitz., B., Kristjánsson, J. E., Muri, H., Niemeier, U., Robock, A., and Tilmes, S.: A multi-model examination of climate extremes in an idealized geoengineering experiment, J. Geophys. Res., 119, 3900–3923, https://doi.org/10.1002/2013JD020648, 2014.

Danabasoglu, G.: NCAR CESM2-WACCM model output prepared for CMIP6 GeoMIP G1, Earth System Grid Federation, https://doi.org/10.22033/ESGF/CMIP6.10029, 2019a.

Danabasoglu, G.: NCAR CESM2-WACCM model output prepared for CMIP6 CMIP abrupt-4xCO2, Earth System Grid Federation, https://doi.org/10.22033/ESGF/CMIP6.10039, 2019b.

Danabasoglu, G.: NCAR CESM2-WACCM-FV2 model output prepared for CMIP6 CMIP piControl, Earth System Grid Federation, https://doi.org/10.22033/ESGF/CMIP6.11302, 2019c.

Dufresne, J.-L., Foujols, M.-A., Denvil, S., Caubel, A., Marti, O., Aumont, O., Balkanski, Y., Bekki, S., Bellenger, H., Benshila, R., Bony, S., Bopp, L., Braconnot, P., Brockmann, P., Cadule, P., Cheruy, F., Codron, F., Cozic, A., Cugnet, D., de Noblet, N., Duvel, J.-P., Ethé, C., Fairhead, L., Fichefet, T., Flavoni, S., Friedlingstein, P., Grandpeix, J.-Y., Guez, L., Guilyardi, E., Hauglustaine, D., Hourdin, F., Idelkadi, A., Ghattas, J., Joussaume, S., Kageyama, M., Krinner, G., Labetoulle, S., Lahellec, A., Lefebvre, M.-P., Lefevre, F., Levy, C., Li, Z. X., Lloyd, J., Lott, F., Madec, G., Mancip, M., Marchand, M., Masson, S., Meurdesoif, Y., Mignot, J., Musat, I., Parouty, S., Polcher, J., Rio, C., Schulz, M., Swingedouw, D., Szopa, S., Talandier, C., Terray, P., Viovy, N., and Vuichard, N.: Climate change projections using the IPSL-CM5 Earth System Model: From CMIP3 to CMIP5, Clim. Dynam., 40, 2123–2165, https://doi.org/10.1007/s00382-012-1636-1, 2013.

Eyring, V., Bony, S., Meehl, G. A., Senior, C. A., Stevens, B., Stouffer, R. J., and Taylor, K. E.: Overview of the Coupled Model Intercomparison Project Phase 6 (CMIP6) experimental design and organization, Geosci. Model Dev., 9, 1937–1958, https://doi.org/10.5194/gmd-9-1937-2016, 2016.

Flynn, C. M. and Mauritsen, T.: On the climate sensitivity and historical warming evolution in recent coupled model ensembles, Atmospheric Chemistry and Physics, 20, 7829–7842, https://doi.org/10.5194/acp-20-7829-2020, https://www.atmos-chem-phys.net/20/7829/2020/, 2020.

Gent, P. R., Danabasoglu, G., Donner, L. J., Holland, M. M., Hunke, E. C., Jayne, S. R., Lawrence, D. M., Neale, R. B., Rasch, P. J., Vertenstein, M., Worley, P. H., Yang, Z.-L., and Zhang, M.: The Community Climate System Model Version 4, Journal of Climate, 24, 4973–4991, https://doi.org/10.1175/2011JCLI4083.1, 2011.

Gertler, C. G., O'Gorman, P. A., Kravitz, B., Moore, J. C., Phipps, S. J., and Watanabe, S.: Weakening of the extratropical storm tracks in solar geoengineering scenarios, Geophys. Res. Lett., 47, e2020GL087348, https://doi.org/10.1029/2020GL087348, 2020.

Gettelman, A., Mills, M. J., Kinnison, D. E., Garcia, R. R., Smith, A. K., Marsh, D. R., Tilmes, S., Vitt, F., Bardeen, C. G., McInerny, J., Liu, H.-L., Solomon, S. C., Polvani, L. M., Emmons, L. K., Lamarque, J.-F., Richter, J. H., Glanville, A. S., Bacmeister, J. T., Phillips, A. S.,

Neale, R. B., Simpson, I. R., DuVivier, A. K., Hodzic, A., and Randel, W. J.: The Whole Atmosphere Community Climate Model Version 6 (WACCM6), Journal of Geophysical Research: Atmospheres, 124, 12 380–12 403, https://doi.org/10.1029/2019JD030943, 2019.

Giorgetta, M. A., Jungclaus, J., Reick, C. H., Legutke, S., Bader, J., Böttinger, M., Brovkin, V., Crueger, T., Esch, M., Fieg, K., Glushak, K., Gayler, V., Haak, H., Hollweg, H.-D., Ilyina, T., Kinne, S., Kornblueh, L., Matei, D., Mauritsen, T., Mikolajewicz, U., Mueller, W., Notz, D., Pithan, F., Raddatz, T., Rast, S., Redler, R., Roeckner, E., Schmidt, H., Schnur, R., Segschneider, J., Six, K. D., Stockhause, M., Timmreck, C., Wegner, J., Widmann, H., Wieners, K.-H., Claussen, M., Marotzke, J., and Stevens, B.: Climate and carbon cycle changes from 1850 to 2100 in MPI-ESM simulations for the Coupled Model Intercomparison Project Phase 5, J. Adv. Model. Earth Syst., 5, 572–597, https://doi.org/10.1002/jame.20038, 2013.

Glienke, S., Irvine, P. J., and Lawrence, M. G.: The impact of geoengineering on vegetation in experiment G1 of the GeoMIP, J. Geophys. Res., 120, 10 196–10 213, https://doi.org/10.1002/2015JD024202, 2015.

Gordon, C., Cooper, C., Senior, C. A., Banks, H., Gregory, J. M., Johns, T. C., Mitchell, J. F. B., and Wood, R. A.: The simulation of SST, sea ice extents and ocean heat transports in a version of the Hadley Centre coupled model without flux adjustments, Clim. Dyn., 16, 147–168, https://doi.org/10.1007/s003820050010, 2000.

Govindasamy, B. and Caldeira, K.: Geoengineering Earth's radiation balance to mitigate CO_2-induced climate change, Geophys. Res. Lett., 27, 2141–2144, https://doi.org/10.1029/1999GL006086, 2000.

Guo, A., Moore, J. C., and Ji, D.: Tropical atmospheric circulation response to the G1 sunshade geoengineering radiative forcing experiment, Atmospheric Chemistry and Physics, 18, 8689–8706, https://doi.org/10.5194/acp-2018-8689, 2018.

Hansen, J., Sato, M., Ruedy, R., Nazarenko, L., Lacis, A., Schmidt, G. A., Russell, G., Aleinov, I., Bauer, M., Bauer, S., Bell, N., Cairns, B., Canuto, V., Chandler, M., Cheng, Y., Del Genio, A., Faluvegi, G., Fleming, E., Friend, A., Hall, T., Jackman, C., Kelley, M., Kiang, N., Koch, D., Lean, J., Lerner, J., Lo, K., Menon, S., Miller, R., Minnis, P., Novakov, T., Oinas, V., Perlwitz, J., Perlwitz, J., Rind, D., Romanou, A., Shindell, D., Stone, P., Sun, S., Tausnev, N., Thresher, D., Wielicki, B., Wong, T., Yaho, M., and Zhang, S.: Efficacy of Climate Forcings, J. Geophys. Res., 110, D18 104, https://doi.org/10.1029/2005JD005776, 2005.

Hazeleger, W., Wang, X., Severijns, C., Ştefănescu, S., Bintanja, R., Sterl, A., Wyser, K., Semmler, T., Yang, S., van den Hurk, B., van Noije, T., van der Linden, E., and van der Wiel, K.: EC-Earth V2.2: Description and validation of a new seamless Earth system prediction model, Clim. Dynam., 39, 2611–2629, https://doi.org/10.1007/s00382-011-1228-5, 2011.

Hourdin, F., Foujols, M.-A., Codron, F., Guemas, V., Dufresne, J.-L., Bony, S., Denvil, S., Guez, L., Lott, F., Ghattas, J., Braconnot, P., Marti, O., Meurdesoif, Y., and Bopp, L.: Impact of the LMDZ atmospheric grid configuration on the climate and sensitivity of the IPSL-CM5A coupled model, Clim. Dyn., 40, 2167–2192, https://doi.org/10.1007/s00382-012-1411-3, 2012.

Hurrell, J. W., Holland, M. M., Gent, P. R., Ghan, S., Kay, J. E., Kushner, P. J., Lamarque, J.-F., Large, W. G., Lawrence, D., Lindsay, K., Lipscomb, W. H., Long, M. C., Mahowald, N., Marsh, D. R., Neale, R. B., Rasch, P., Vavrus, S., Vertenstein, M., Bader, D., Collins, W. D., Hack, J. J., Kiehl, J., , and Marshall, S.: The Community Earth System Model: A Framework for Collaborative Research, Bull. Amer. Meteor. Soc., 94, 1339–1360, https://doi.org/10.1175/BAMS-D-12-00121.1, 2013.

Irvine, P., Emmanuel, K., He, J., Horowitz, L. W., Vecchi, G., and Keith, D.: Halving warming with idealized solar geoengineering moderates key climate hazards, Nature Climate Change, 9, 295–299, 2019.

Irvine, P. J., Kravitz, B., Lawrence, M. G., and Muri, H.: An overview of the Earth system science of solar geoengineering, WIREs Climate Change, 7, 815–833, https://doi.org/10.1002/wcc.423, 2016.

Ji, D., Wang, L., Feng, J., Wu, Q., Cheng, H., Zhang, Q., Yang, J., Dong, W., Dai, Y., Gong, D., Zhang, R.-H., Wang, X., Liu, J., Moore, J. C., Chen, D., and Zhou, M.: Description and basic evaluation of Beijing Normal University Earth System Model (BNU-ESM) version 1, Geosci. Model. Dev., 7, 2039–2064, https://doi.org/10.5194/gmd-7-2039-2014, 2014.

Jones, A.: MOHC UKESM1.0-LL model output prepared for CMIP6 GeoMIP G1, Earth System Grid Federation, https://doi.org/10.22033/ESGF/CMIP6.5812, 2019.

Jones, A., Haywood, J. M., Alterskjær, K., Boucher, O., Cole, J. N. S., J., C. L. C. P., Irvine, Ji, D., Kravitz, B., Moore, J. E. K. J. C., Niemeier, U., Robock, A., Schmidt, H., Singh, B., Tilmes, S., Watanabe, S., and Yoon, J.-H.: The impact of abrupt suspension of solar radiation management (termination effect) in experiment G2 of the Geoengineering Model Intercomparison Project (GeoMIP), Journal of Geophysical Research: Atmospheres, 118, 9743–9752, https://doi.org/10.1002/jgrd.50762, 2013.

Kalidindi, S., Bala, G., Modak, A., and Caldeira, K.: Modeling of solar radiation management: A comparison of simulations using reduced solar constant and stratospheric sulfate aerosols, Clim. Dynam., 44, 2909–2925, https://doi.org/10.1007/s00382-014-2240-3, 2015.

Kelley, M., Schmidt, G. A., Nazarenko, L. S., Bauer, S. E., Ruedy, R., Russell, G. L., Ackerman, A. S., Aleinov, I., Bauer, M., Bleck, R., Canuto, V., Cesana, G., Cheng, Y., Clune, T. L., Cook, B. I., Cruz, C. A., Del Genio, A. D., Elsaesser, G. S., Faluvegi, G., Kiang, N. Y., Kim, D., Lacis, A. A., Leboissetier, A., LeGrande, A. N., Lo, K. K., Marshall, J., Matthews, E. E., McDermid, S., Mezuman, K., Miller, R. L., Murray, L. T., Oinas, V., Orbe, C., Pérez García-Pando, C., Perlwitz, J. P., Puma, M. J., Rind, D., Romanou, A., Shindell, D. T., Sun, S., Tausnev, N., Tsigaridis, K., Tselioudis, G., Weng, E., Wu, J., and Yao, M.-S.: GISS-E2.1: Configurations and Climatology, Journal of Advances in Modeling Earth Systems, in press, e2019MS002 025, https://doi.org/10.1029/2019MS002025, 2020.

Kirkevåg, A., Iversen, T., Seland, Ø., Hoose, C., Kristjánsson, J. E., Struthers, H., Ekman, A. M. L., Ghan, S., Griesfeller, J., Nilsson, E. D., and Schulz, M.: Aerosol–climate interactions in the Norwegian Earth System Model – NorESM1-M, Geoscientific Model Development, 6, 207–244, https://doi.org/10.5194/gmd-6-207-2013, https://gmd.copernicus.org/articles/6/207/2013/, 2013.

Knutti, R., Masson, D., and Gettelman, A.: Climate model genealogy: Generation CMIP5 and how we got there, Geophys. Res. Lett., 40, 1194–1199, https://doi.org/10.1002/grl.50256, 2013.

Kravitz, B., Robock, A., Boucher, O., Schmidt, H., Taylor, K. E., Stenchikov, G., and Schulz, M.: The Geoengineering Model Intercomparison Project (GeoMIP), Atmos. Sci. Lett., 12, 162–167, https://doi.org/10.1002/asl.316, 2011.

Kravitz, B., Caldeira, K., Boucher, O., Robock, A., Rasch, P. J., Alterskjær, K., Karam, D. B., Cole, J. N. S., Curry, C. L., Haywood, J. M., Irvine, P. J., Ji, D., Jones, A., Kristjánsson, J. E., Lunt, D. J., Moore, J., Niemeier, U., Schmidt, H., Schulz, M., Singh, B., Tilmes, S., Watanabe, S., Yang, S., , and Yoon, J.-H.: Climate model response from the Geoengineering Model Intercomparison Project (GeoMIP), J. Geophys. Res., 118, 8320–8332, https://doi.org/10.1002/jgrd.50646, 2013.

Kravitz, B., Rasch, P. J., Forster, P. M., Andrews, T., Cole, J. N. S., Irvine, P. J., Ji, D., Kristjánsson, J. E., Moore, J. C., Muri, H., Niemeier, U., Robock, A., Singh, B., Tilmes, S., Watanabe, S., , and Yoon, J.-H.: An energetic perspective on hydrological cycle changes in the Geoengineering Model Intercomparison Project (GeoMIP), J. Geophys. Res., 118, 13 087–13 102, https://doi.org/10.1002/2013JD020502, 2013b.

Kravitz, B., MacMartin, D. G., Robock, A., Rasch, P. J., Ricke, K. L., Cole, J. N. S., Curry, C. L., Irvine, P. J., Ji, D., Keith, D. W., Kristjánsson, J. E., Moore, J. C., Muri, H., Singh, B., Tilmes, S., Watanabe, S., Yang, S., and Yoon, J.-H.: A multi-model assessment of regional climate disparities caused by solar geoengineering, Environ. Res. Lett., 9, 074 013, https://doi.org/10.1088/1748-9326/9/7/074013, 2014.

Kravitz, B., Robock, A., Tilmes, S., Boucher, O., English, J. M., Irvine, P. J., Jones, A., Lawrence, M. G., MacCracken, M., Muri, H., Moore, J. C., Niemeier, U., Phipps, S. J., Sillmann, J., Storelvmo, T., Wang, H., and Watanabe, S.: The Geoengineering Model Intercomparison

Project Phase 6 (GeoMIP6): Simulation design and preliminary results, Geosci. Model Dev., 8, 3379–3392, https://doi.org/10.5194/gmd-8-3379-2015, 2015.

Kravitz, B., MacMartin, D. G., Wang, H., and Rasch, P. J.: Geoengineering as a design problem, Earth System Dynamics, 7, 469–497, https://doi.org/10.5194/esd-469-2016, 2016.

Kravitz, B., MacMartin, D. G., Mills, M. J., Richter, J. H., Tilmes, S., Lamarque, J., Tribbia, J. J., and Vitt, F.: First Simulations of Designing Stratospheric Sulfate Aerosol Geoengineering to Meet Multiple Simultaneous Climate Objectives, J. Geophys. Res., 122, 12 616–12 634, https://doi.org/10.1002/2017JD026874, 2017.

Kravitz, B., MacMartin, D. G., Tilmes, S., Richter, J. H., Mills, M. J., Cheng, W., Dagon, K., Glanville, A. S., Lamarque, J.-F., Simpson, I., Tribbia, J., and Vitt, F.: Comparing surface and stratospheric impacts of geoengineering with different SO_2 injection strategies, J. Geophys. Res., 124, 7900–7918, https://doi.org/10.1029/2019JD030329, 2019.

Lurton, T., Balkanski, Y., Bastrikov, V., Bekki, S., Bopp, L., Braconnot, P., Brockmann, P., Cadule, P., Contoux, C., Cozic, A., Cugnet, D., Dufresne, J.-L., Éthé, C., Foujols, M.-A., Ghattas, J., Hauglustaine, D., Hu, R.-M., Kageyama, M., Khodri, M., Lebas, N., Levavasseur, G., Marchand, M., Ottlé, C., Peylin, P., Sima, A., Szopa, S., Thiéblemont, R., Vuichard, N., and Boucher, O.: Implementation of the CMIP6 Forcing Data in the IPSL-CM6A-LR Model, Journal of Advances in Modeling Earth Systems, 12, e2019MS001 940, https://doi.org/10.1029/2019MS001940, 2020.

MacMartin, D. G., Keith, D. W., Kravitz, B., and Caldeira, K.: Management of trade-offs in geoengineering through optimal choice of non-uniform radiative forcing, Nature Climate Change, 3, 365–368, https://doi.org/10.1038/nclimate1722, 2013.

Madronich, S., Tilmes, S., Kravitz, B., MacMartin, D. G., and Richter, J. H.: Response of surface ultraviolet and visible radiation to stratospheric SO_2 injection, Atmosphere, 9, 432, https://doi.org/10.3390/atmos9110432, 2018.

Mauritsen, T., Bader, J., Becker, T., Behrens, J., Bittner, M., Brokopf, R., Brovkin, V., Claussen, M., Crueger, T., Esch, M., Fast, I., Fiedler, S., Fläschner, D., Gayler, V., Giorgetta, M., Goll, D. S., Haak, H., Hagemann, S., Hedemann, C., Hohenegger, C., Ilyina, T., Jahns, T., Jimenéz-de-la Cuesta, D., Jungclaus, J., Kleinen, T., Kloster, S., Kracher, D., Kinne, S., Kleberg, D., Lasslop, G., Kornblueh, L., Marotzke, J., Matei, D., Meraner, K., Mikolajewicz, U., Modali, K., Möbis, B., Müller, W. A., Nabel, J. E. M. S., Nam, C. C. W., Notz, D., Nyawira, S.-S., Paulsen, H., Peters, K., Pincus, R., Pohlmann, H., Pongratz, J., Popp, M., Raddatz, T. J., Rast, S., Redler, R., Reick, C. H., Rohrschneider, T., Schemann, V., Schmidt, H., Schnur, R., Schulzweida, U., Six, K. D., Stein, L., Stemmler, I., Stevens, B., von Storch, J.-S., Tian, F., Voigt, A., Vrese, P., Wieners, K.-H., Wilkenskjeld, S., Winkler, A., and Roeckner, E.: Developments in the MPI-M Earth System Model version 1.2 (MPI-ESM1.2) and Its Response to Increasing CO_2, Journal of Advances in Modeling Earth Systems, 11, 998–1038, https://doi.org/10.1029/2018MS001400, 2019.

Meehl, G. A., Senior, C. A., Eyring, V., Flato, G., Lamarque, J.-F., Stouffer, R. J., Taylor, K. E., and Schlund, M.: Context for interpreting equilibrium climate sensitivity and transient climate response from the CMIP6 Earth system models, Science Advances, 6, eaba1981, https://doi.org/10.1126/sciadv.aba1981, 2020.

Moore, J. C., Rinke, A., Yu, X., Ji, D., Cui, X., Li, Y., Alterskjær, K., Kristjánsson, J. E., Boucher, O., Huneeus, N., Kravitz, B., Robock, A., Niemeier, U., Schmidt, H., Schulz, M., Tilmes, S., and Watanabe, S.: Arctic sea ice and atmospheric circulation under the GeoMIP G1 scenario, J. Geophys. Res., 119, 567–583, https://doi.org/10.1002/2013JD021060, 2014.

Moreno-Cruz, J. B., Ricke, K. L., and Keith, D. W.: A simple model to account for regional inequalities in the effectiveness of solar radiation management, Climatic Change, 110, 649–668, 2012.

NASA Goddard Institute for Space Studies (NASA/GISS): NASA-GISS GISS-E2.1G model output prepared for CMIP6 CMIP abrupt-4xCO2, Earth System Grid Federation, https://doi.org/10.22033/ESGF/CMIP6.6976, 2018.

NASA Goddard Institute for Space Studies (NASA/GISS): NASA-GISS GISS-E2-1-G-CC model output prepared for CMIP6 CMIP piControl, Earth System Grid Federation, https://doi.org/10.22033/ESGF/CMIP6.11856, 2019.

Neale, R. B., Chen, C., Gettelman, A., Lauritzen, P., Park, S., Williamson, D., Conley, A., Garcia, R., Kinnison, D., and Lamarque, J.: Description of the NCAR community atmosphere model (CAM 5.0), Tech. rep., National Center for Atmospheric Research, 2010.

Niemeier, U., Schmidt, H., Alterskjær, K., and Kristjánsson, J. E.: Solar irradiance reduction via climate engineering: Impact of different techniques on the energy balance and the hydrological cycle, J. Geophys. Res., 118, 11 905–11 917, https://doi.org/10.1002/2013JD020445, 2013.

NRC: Climate Intervention: Reflecting Sunlight to Cool Earth, Tech. rep., National Research Council, http://www.nap.edu/catalog/18988/climate-intervention-reflecting-sunlight-to-cool-earth, (last access: 7 May 2015), 2015.

Phipps, S. J., Rotstayn, L. D., Gordon, H. B., Roberts, J. L., Hirst, A. C., , and Budd, W. F.: The CSIRO Mk3L climate system model version 1.0 – Part 1: Description and evaluation, Geosci. Model Dev., 4, 483–509, https://doi.org/10.5194/gmd-4-483-2011, 2011.

Phipps, S. J., Rotstayn, L. D., Gordon, H. B., Roberts, J. L., Hirst, A. C., and Budd, W. F.: The CSIRO Mk3L climate system model version 1.0 – Part 2: Response to external forcings, Geosci. Model Dev., 5, 649–682, https://doi.org/10.5194/gmd-5-649-2012, 2012.

Pitari, G., Aquila, V., Kravitz, B., Robock, A., Watanabe, S., Cionni, I., Luca, N. D., di Genova, G., Mancini, E., and Tilmes, S.: Stratospheric ozone response to sulfate geoengineering: Results from the Geoengineering Model Intercomparison Project (GeoMIP), J. Geophys. Res., 119, 2629–2653, 2014.

Richter, J. H., Tilmes, S., Mills, M. J., Tribbia, J. J., Kravitz, B., MacMartin, D. G., Vitt, F., and Lamarque, J.: Stratospheric Dynamical Response and Ozone Feedbacks in the Presence of SO_2 Injections, J. Geophys. Res., 122, 12 557–12 573, https://doi.org/10.1002/2017JD026912, 2017.

Ricke, K. L., Morgan, M. G., and Allen, M. R.: Regional climate response to solar-radiation management, Nat. Geosci., 3, 537–541, https://doi.org/10.1038/ngeo915, 2010.

Robock, A.: Volcanic eruptions and climate, Rev. Geophys., 38, 191–219, https://doi.org/10.1029/1998RG000054, 2000.

Russotto, R. D. and Ackerman, T. P.: Changes in clouds and thermodynamics under solar geoengineering and implications for required solar reduction, Atmos. Chem. Phys., 18, 11 905–11 925, https://doi.org/10.5194/acp-18-11905-2018, 2018.

Schmidt, G. A., Kelley, M., Nazarenko, L., Ruedy, R., Russell, G. L., Aleinov, I., Bauer, M., Bauer, S. E., Bhat, M. K., Bleck, R., Canuto, V., Chen, Y.-H., Cheng, Y., Clune, T. L., Genio, A. D., de Fainchtein, R., Faluvegi, G., Hansen, J. E., Healy, R. J., Kiang, N. Y., Koch, D., Lacis, A. A., LeGrande, A. N., Lerner, J., Lo, K. K., Matthews, E. E., Menon, S., Miller, R. L., Oinas, V., Oloso, A. O., Perlwitz, J. P., Puma, M. J., Putman, W. M., Rind, D., Romanou, A., Sato, M., Shindell, D. T., Sun, S., Syed, R. A., Tausnev, N., Tsigaridis, K., Under, N., Volugarakis, A., Yao, M.-S., and Zhang, J.: Configuration and assessment of the GISS ModelE2 contributions to the CMIP5 archive, J. Adv. Modell. Earth Syst., 6, 141–184, https://doi.org/10.1002/2013MS000265, 2014.

Séférian, R.: CNRM-CERFACS CNRM-ESM2-1 model output prepared for CMIP6 CMIP abrupt-4xCO2, Earth System Grid Federation, https://doi.org/10.22033/ESGF/CMIP6.3918, 2018a.

Séférian, R.: CNRM-CERFACS CNRM-ESM2-1 model output prepared for CMIP6 CMIP piControl, Earth System Grid Federation, https://doi.org/10.22033/ESGF/CMIP6.4165, 2018b.

Séférian, R.: CNRM-CERFACS CNRM-ESM2-1 model output prepared for CMIP6 CMIP G1, Earth System Grid Federation, https://doi.org/10.22033/ESGF/CMIP6.3902, 2018c.

Séférian, R., Nabat, P., Michou, M., Saint-Martin, D., Voldoire, A., Colin, J., Decharme, B., Delire, C., Berthet, S., Chevallier, M., Sénési, S., Franchisteguy, L., Vial, J., Mallet, M., Joetzjer, E., Geoffroy, O., Guérémy, J.-F., Moine, M.-P., Msadek, R., Ribes, A., Rocher, M.,

Roehrig, R., Salas-y Mélia, D., Sanchez, E., Terray, L., Valcke, S., Waldman, R., Aumont, O., Bopp, L., Deshayes, J., Éthé, C., and Madec, G.: Evaluation of CNRM Earth System Model, CNRM-ESM2-1: Role of Earth System Processes in Present-Day and Future Climate, Journal of Advances in Modeling Earth Systems, 11, 4182–4227, https://doi.org/10.1029/2019MS001791, 2019.

Sellar, A. A., Jones, C. G., Mulcahy, J. P., Tang, Y., Yool, A., Wiltshire, A., O'Connor, F. M., Stringer, M., Hill, R., Palmieri, J., Woodward, S., de Mora, L., Kuhlbrodt, T., Rumbold, S. T., Kelley, D. I., Ellis, R., Johnson, C. E., Walton, J., Abraham, N. L., Andrews, M. B., Andrews, T., Archibald, A. T., Berthou, S., Burke, E., Blockley, E., Carslaw, K., Dalvi, M., Edwards, J., Folberth, G. A., Gedney, N., Griffiths, P. T., Harper, A. B., Hendry, M. A., Hewitt, A. J., Johnson, B., Jones, A., Jones, C. D., Keeble, J., Liddicoat, S., Morgenstern, O., Parker, R. J., Predoi, V., Robertson, E., Siahaan, A., Smith, R. S., Swaminathan, R., Woodhouse, M. T., Zeng, G., and Zerroukat, M.: UKESM1: Description and Evaluation of the U.K. Earth System Model, Journal of Advances in Modeling Earth Systems, 11, 4513–4558, https://doi.org/10.1029/2019MS001739, 2019.

Simpson, I., Tilmes, S., Richter, J., Kravitz, B., MacMartin, D., Mills, M., Fasullo, J., and Pendergrass, A.: The regional hydroclimate response to stratospheric sulfate geoengineering and the role of stratospheric heating, J. Geophys. Res., 124, 12 587–12 616, https://doi.org/10.1029/2019JD031093, 2019.

Stevens, B., Giorgetta, M., Esch, M., Mauritsen, T., Crueger, T., Rast, S., Salzmann, M., Schmidt, H., Bader, J., Block, K., Brokopf, R., Fast, I., Kinne, S., Kornblueh, L., Lohmann, U., Pincus, R., Reichler, T., and Roeckner, E.: Atmospheric component of the MPI-M Earth System Model: ECHAM6, Journal of Advances in Modeling Earth Systems, 5, 146–172, https://doi.org/10.1002/jame.20015, 2013.

Swart, N. C., Cole, J. N., Kharin, V. V., Lazare, M., Scinocca, J. F., Gillett, N. P., Anstey, J., Arora, V., Christian, J. R., Jiao, Y., Lee, W. G., Majaess, F., Saenko, O. A., Seiler, C., Seinen, C., Shao, A., Solheim, L., von Salzen, K., Yang, D., Winter, B., and Sigmond, M.: CCCma CanESM5 model output prepared for CMIP6 CMIP abrupt-4xCO2, Earth System Grid Federation, https://doi.org/10.22033/ESGF/CMIP6.3532, 2019a.

Swart, N. C., Cole, J. N., Kharin, V. V., Lazare, M., Scinocca, J. F., Gillett, N. P., Anstey, J., Arora, V., Christian, J. R., Jiao, Y., Lee, W. G., Majaess, F., Saenko, O. A., Seiler, C., Seinen, C., Shao, A., Solheim, L., von Salzen, K., Yang, D., Winter, B., and Sigmond, M.: CCCma CanESM5 model output prepared for CMIP6 CMIP piControl, Earth System Grid Federation, https://doi.org/10.22033/ESGF/CMIP6.3673, 2019b.

Swart, N. C., Cole, J. N. S., Kharin, V. V., Lazare, M., Scinocca, J. F., Gillett, N. P., Anstey, J., Arora, V., Christian, J. R., Hanna, S., Jiao, Y., Lee, W. G., Majaess, F., Saenko, O. A., Seiler, C., Seinen, C., Shao, A., Sigmond, M., Solheim, L., von Salzen, K., Yang, D., and Winter, B.: The Canadian Earth System Model version 5 (CanESM5.0.3), Geoscientific Model Development, 12, 4823–4873, https://doi.org/10.5194/gmd-12-4823-2019, https://gmd.copernicus.org/articles/12/4823/2019/, 2019c.

Tang, Y., Rumbold, S., Ellis, R., Kelley, D., Mulcahy, J., Sellar, A., Walton, J., and Jones, C.: MOHC UKESM1.0-LL model output prepared for CMIP6 CMIP abrupt-4xCO2, Earth System Grid Federation, https://doi.org/10.22033/ESGF/CMIP6.5843, 2019a.

Tang, Y., Rumbold, S., Ellis, R., Kelley, D., Mulcahy, J., Sellar, A., Walton, J., and Jones, C.: MOHC UKESM1.0-LL model output prepared for CMIP6 CMIP piControl, Earth System Grid Federation, https://doi.org/10.22033/ESGF/CMIP6.6298, 2019b.

Taylor, K. E., Stouffer, R. J., and Meehl, G. A.: An overview of CMIP5 and the experiment design, Bull. Amer. Meteor. Soc., 93, 485–498, https://doi.org/10.1175/BAMS-D-11-00094.1, 2012.

Tilmes, S., Fasullo, J., Lamarque, J.-F., Marsh, D. R., Mills, M., Alterskjær, K., Muri, H., Kristjánsson, J. E., Boucher, O., Schulz, M., Cole, J. N. S., Curry, C. L., Jones, A., Haywood, J., Irvine, P. J., Ji, D., Moore, J. C., Karam, D. B., Kravitz, B., Rasch, P. J., Singh, B., Yoon, J.-H., Niemeier, U., Schmidt, H., Robock, A., Yang, S., and Watanabe, S.: The hydrological impact of geoengineering in the Geoengineering Model Intercomparison Project (GeoMIP), J. Geophys. Res., 118, 11 036–11 058, https://doi.org/10.1002/jgrd.50868, 2013.

Tilmes, S., Richter, J. H., Mills, M. J., Kravitz, B., MacMartin, D. G., Garcia, R. R., Kinnison, D. E., Lamarque, J.-F., Tribbia, J., and Vitt, F.: Effects of Different Stratospheric SO_2 Injection Altitudes on Stratospheric Chemistry and Dynamics, J. Geophys. Res., 123, 4654–4673, https://doi.org/10.1002/2017JD028146, 2018.

Vial, J., Dufresne, J.-L., and Bony, S.: On the interpretation of inter-model spread in CMIP5 climate sensitivity estimates, Climate Dynamics, 41, 3339–3362, https://doi.org/10.1007/s00382-013-1725-9, 2013.

Vignesh, P. P., Jiang, J. H., Kishore, P., Su, H., Smay, T., Brighton, N., and Velicogna, I.: Assessment of CMIP6 cloud fraction and comparison with satellite observations, Earth and Space Science, 7, e2019EA000975, https://doi.org/10.1029/2019EA000975, 2020.

Visioni, D., MacMartin, D. G., Kravitz, B., Tilmes, S., Mills, M. J., Richter, J. H., and Boudreau, M. P.: Seasonal injection strategies for stratospheric aerosol geoengineering, Geophysical Research Letters, 46, 7790–7799, https://doi.org/10.1029/2019GL083680, 2019.

Watanabe, S., Miura, H., Sekiguchi, M., Nagashima, T., Sudo, K., Emori, S., and Kawamiya, M.: Development of an atmospheric general circulation model for integrated Earth system modeling on the Earth Simulator, J. Earth Simulator, 9, 27–35, 2008.

Watanabe, S., Hajima, T., Sudo, K., Nagashima, T., Takemura, T., Okajima, H., Nozawa, T., Kawase, H., Abe, M., Yokohata, T., Ise, T., Sato, H., Kato, E., Takata, K., Emori, S., and Kawamiya, M.: MIROC-ESM 2010: Model description and basic results of CMIP5-20c3m experiments, Geosci. Mod. Dev., 4, 845–872, https://doi.org/10.5194/gmd-4-845-2011, 2011.

Wieners, K.-H., Giorgetta, M., Jungclaus, J., Reick, C., Esch, M., Bittner, M., Legutke, S., Schupfner, M., Wachsmann, F., Gayler, V., Haak, H., de Vrese, P., Raddatz, T., Mauritsen, T., von Storch, J.-S., Behrens, J., Brovkin, V., Claussen, M., Crueger, T., Fast, I., Fiedler, S., Hagemann, S., Hohenegger, C., Jahns, T., Kloster, S., Kinne, S., Lasslop, G., Kornblueh, L., Marotzke, J., Matei, D., Meraner, K., Mikolajewicz, U., Modali, K., Müller, W., Nabel, J., Notz, D., Peters, K., Pincus, R., Pohlmann, H., Pongratz, J., Rast, S., Schmidt, H., Schnur, R., Schulzweida, U., Six, K., Stevens, B., Voigt, A., and Roeckner, E.: MPI-M MPI-ESM1.2-LR model output prepared for CMIP6 CMIP piControl, Earth System Grid Federation, https://doi.org/10.22033/ESGF/CMIP6.6675, 2019a.

Wieners, K.-H., Giorgetta, M., Jungclaus, J., Reick, C., Esch, M., Bittner, M., Legutke, S., Schupfner, M., Wachsmann, F., Gayler, V., Haak, H., de Vrese, P., Raddatz, T., Mauritsen, T., von Storch, J.-S., Behrens, J., Brovkin, V., Claussen, M., Crueger, T., Fast, I., Fiedler, S., Hagemann, S., Hohenegger, C., Jahns, T., Kloster, S., Kinne, S., Lasslop, G., Kornblueh, L., Marotzke, J., Matei, D., Meraner, K., Mikolajewicz, U., Modali, K., Müller, W., Nabel, J., Notz, D., Peters, K., Pincus, R., Pohlmann, H., Pongratz, J., Rast, S., Schmidt, H., Schnur, R., Schulzweida, U., Six, K., Stevens, B., Voigt, A., and Roeckner, E.: MPI-M MPI-ESM1.2-LR model output prepared for CMIP6 CMIP abrupt-4xCO2, Earth System Grid Federation, https://doi.org/10.22033/ESGF/CMIP6.6459, 2019b.

Xia, L., Robock, A., Cole, J. N. S., Curry, C. L., Ji, D., Jones, A., Kravitz, B., Moore, J. C., Muri, H., Niemeier, U., Singh, B., Tilmes, S., Watanabe, S., and Yoon, J.-H.: Solar Radiation Management impacts on agriculture in China: A case study in the Geoengineering Model Intercomparison Project (GeoMIP), J. Geophys. Res., 119, 8695–8711, https://doi.org/10.1002/2013JD020630, 2014.

Zelinka, M. D., Myers, T. A., McCoy, D. T., Po-Chedley, S., Caldwell, P. M., Ceppi, P., Klein, S. A., and Taylor, K. E.: Causes of higher climate sensitivity in CMIP6 models, Geophys. Res. Let., 47, e2019GL085782, https://doi.org/10.1029/2019GL085782, 2020.

Table 1. All participating models in both the CMIP5 and CMIP6 eras of GeoMIP, including references. For G1 solar reduction, the percentage is calculated as the percent change in incident solar irradiance at the top-of-atmosphere between G1 and its respective piControl run. Numbers in the first column correspond to the model numbers in Figure 11.

#	Model	Generation	Reference	G1 Solar Reduction (%)	Data not available	Data Citations (CMIP6 only)
1	BNU-ESM	CMIP5	Ji et al. (2014)	3.80	Cloud forcing	
2	CanESM2	CMIP5	Arora et al. (2011)	4.00		
3	CCSM4	CMIP5	Gent et al. (2011)	4.25	NPP	
4	CESM-CAM5.1-FV	CMIP5	Neale et al. (2010); Hurrell et al. (2013)	4.70		
5	CSIRO-Mk3L-1.2	CMIP5	Phipps et al. (2011, 2012)	3.20	Cloud forcing, NPP	
6	EC-EARTH	CMIP5	Hazeleger et al. (2011)	4.12	Cloud forcing, NPP	
7	GISS-E2-R	CMIP5	Schmidt et al. (2014)	4.47		
8	HadCM3	CMIP5	Gordon et al. (2000)	4.16	Cloud forcing, NPP	
9	HadGEM2-ES	CMIP5	Collins et al. (2011)	3.88		
10	IPSL-CM5A-LR	CMIP5	Dufresne et al. (2013); Hourdin et al. (2012)	3.50	NPP	
11	MIROC-ESM	CMIP5	Watanabe et al. (2008, 2011)	5.00		
12	MPI-ESM-LR	CMIP5	Giorgetta et al. (2013); Stevens et al. (2013)	4.68		
13	NorESM1-M	CMIP5	Alterskjær et al. (2012); Kirkevåg et al. (2013)	4.03		
14	CanESM5	CMIP6	Swart et al. (2019c)	3.72		Swart et al. (2019b, a); Cole et al. (
15	CESM2-WACCM	CMIP6	Gettelman et al. (2019)	4.91		Danabasoglu (2019c, b, a)
16	CNRM-ESM2.1	CMIP6	Séférian et al. (2019)	3.72		Séférian (2018b, a, c)
17	GISS-E2.1-G	CMIP6	Kelley et al. (2020)	4.13		NASA Goddard Institute for Space
18	IPSL-CM6A-LR	CMIP6	Boucher et al. (2020); Lurton et al. (2020)	4.10		Boucher et al. (2018c, b, a)
19	MPI-ESM1.2-LR	CMIP6	Mauritsen et al. (2019)	4.57		Wieners et al. (2019a, b)
20	UKESM1.0-LL	CMIP6	Sellar et al. (2019)	3.80		Tang et al. (2019b, a); Jones (2019)

Table 2. Decadal trends in the global mean temperature, Net TOA radiative flux, precipitation, and evaporation values shown in Figure 1 for each model. Trends are calculated across the years 11-100 to eliminate any effects due to initial transient adjustment to the abrupt forcing.

Model	Temperature (K/decade)	Rad Flux (W m^{-2}/decade)	Precipitation (%/decade)	Evaporation (%/decade)
CanESM5	0.010	-0.005	0.011	0.011
CESM2(WACCM)	0.023	-0.009	0.067	0.067
CNRM-ESM2.1	-0.033	0.016	-0.058	-0.058
GISS-E2.1-G	-0.005	0.018	-0.006	-0.006
IPSL-CM6A-LR	-0.027	0.015	-0.062	-0.063
MPI-ESM1.2-LR	-0.003	-0.000	-0.015	-0.016
UKESM1.0-LL	0.018	0.008	0.018	0.018
Ensemble Mean	-0.002	0.006	-0.006	-0.007

Table 3. Ensemble differences between the CMIP5 and CMIP6 ensembles for each variable evaluated in this study (left column). Column 2 indicates the difference between the ensembles in how much of the Earth's surface is not stippled (more than 75% of models agree on the sign of the response; positive values indicate that CMIP6 has more unstippled area than CMIP5). Column 3 indicates the percent of the Earth's surface for which the CMIP5 ensemble is statistically different from the CMIP6 ensemble, based on 95th percentile confidence intervals from Welch's *t*-test.

Variable	Stippling (%)	Welch's *t*-test (%)	Notes
Surface air temperature	-25.77	0.87	
Precipitation	-3.56	11.17	
Evaporation	-2.33	6.47	
P–E	-15.23	1.13	
SW Cloud Forcing	-8.02	9.65	
LW Cloud Forcing	11.99	6.57	
Net Primary Productivity	-1.42	1.15	Land surface only

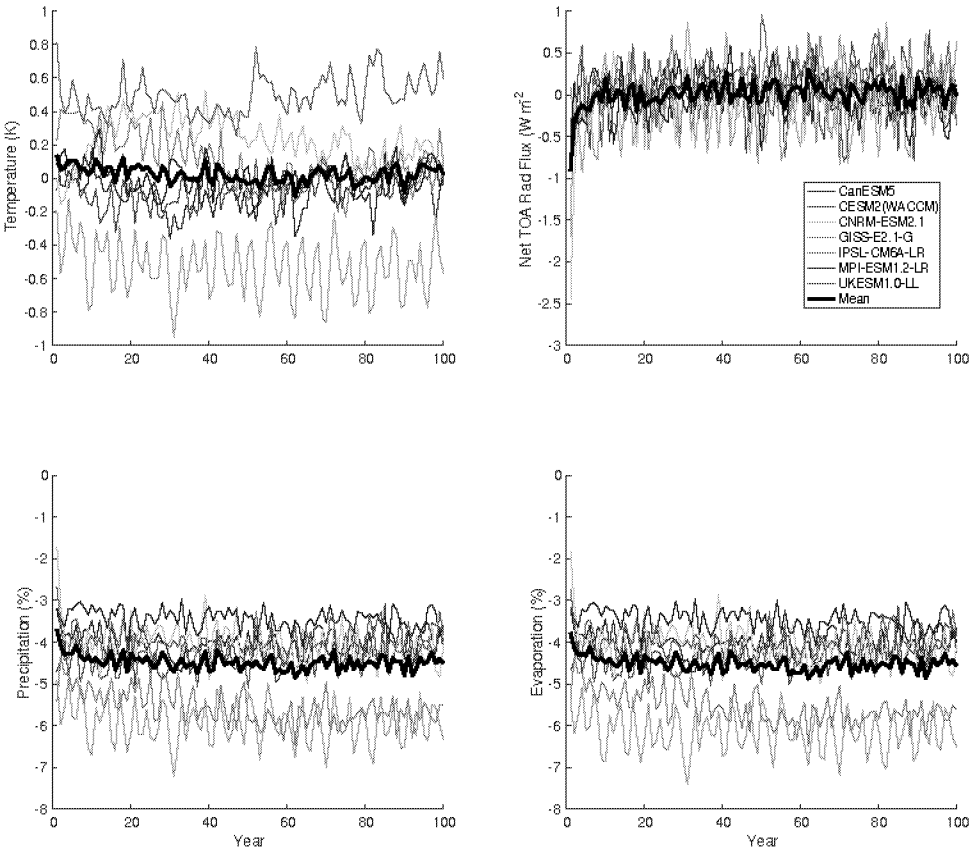

Figure 1. Temperature (top left; K), net top-of-atmosphere radiative flux (top right; W m^{-2}), precipitation (bottom left; %), and evaporation (bottom right; %) change in $G1_{CMIP6}$ compared to piControl over 100 years of simulation. Thin colored lines are individual models, and thick black lines are ensemble means.

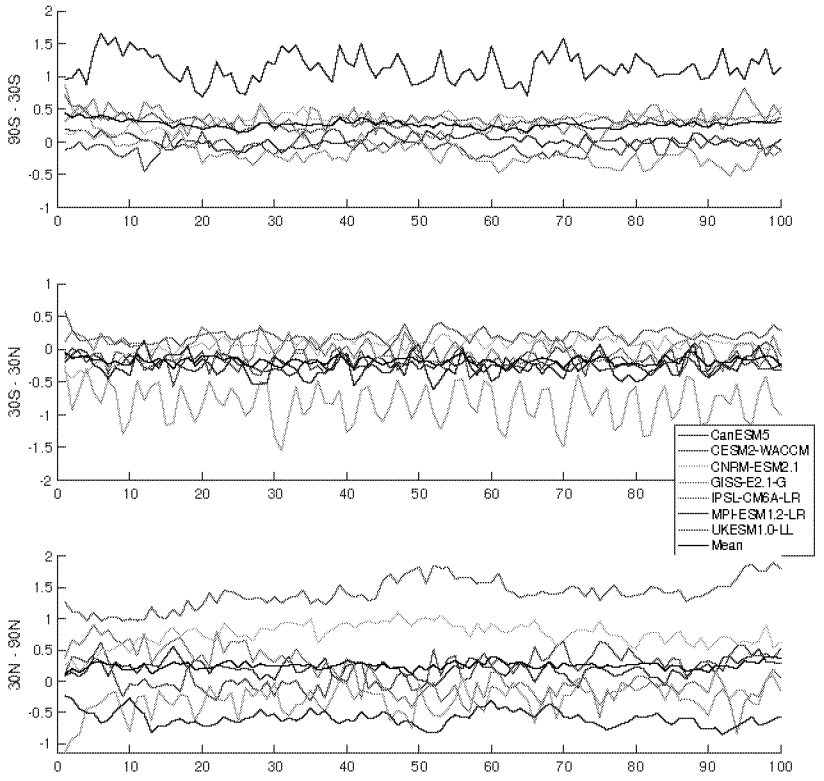

Figure 2. Annual mean surface temperature (K) in each model averaged over 90°S-30°S (top), 30°S-30°N (middle), and 30°N-90°N (bottom). The ensemble mean is plotted as thick black lines.

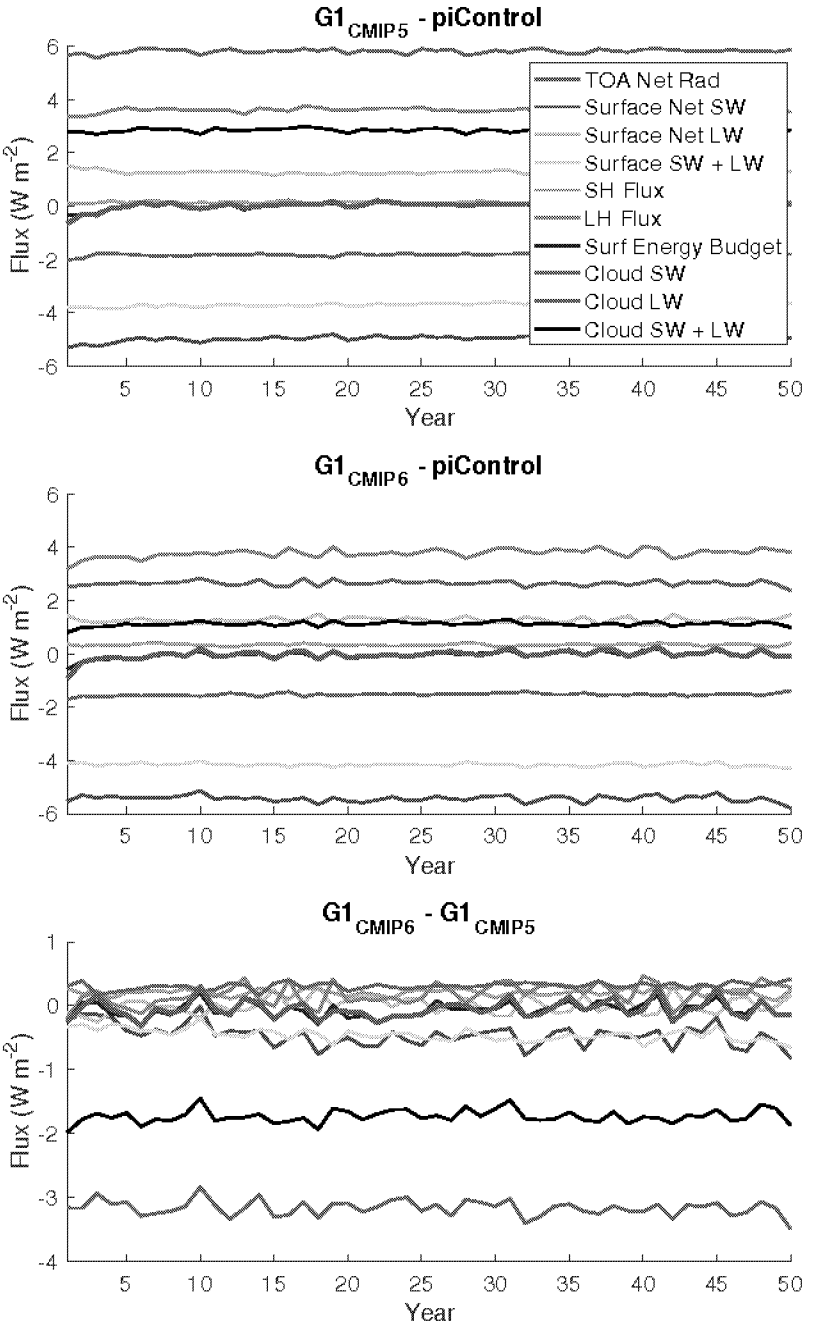

Figure 3. Ensemble mean energetics (W m^{-2}) for various flux quantities in $G1_{CMIP5}$ (top), $G1_{CMIP6}$ (middle), and their difference (bottom). All fluxes are positive downward, which is counterintuitive for sensible heat (SH) and latent heat (LH). Surf Energy Budget indicates the sum of surface shortwave (SW), surface longwave (LW), SH, and LH. Cloud forcing is calculated as all-sky minus clear-sky.

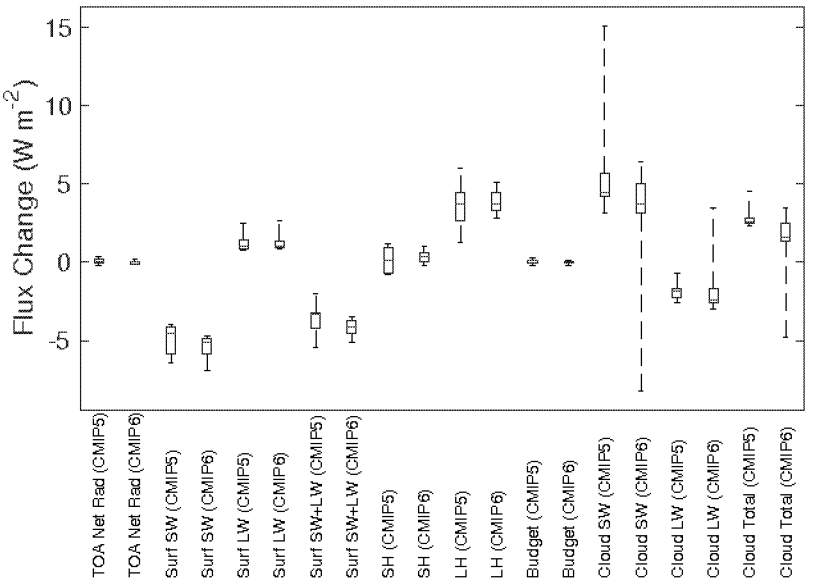

Figure 4. Ensemble median (red lines), inter-quartile (blue boxes), and ranges (black whiskers) for the same global mean energetics quantities as in Figure 3 (G1 minus piControl) for both the CMIP5 and CMIP6 ensembles.

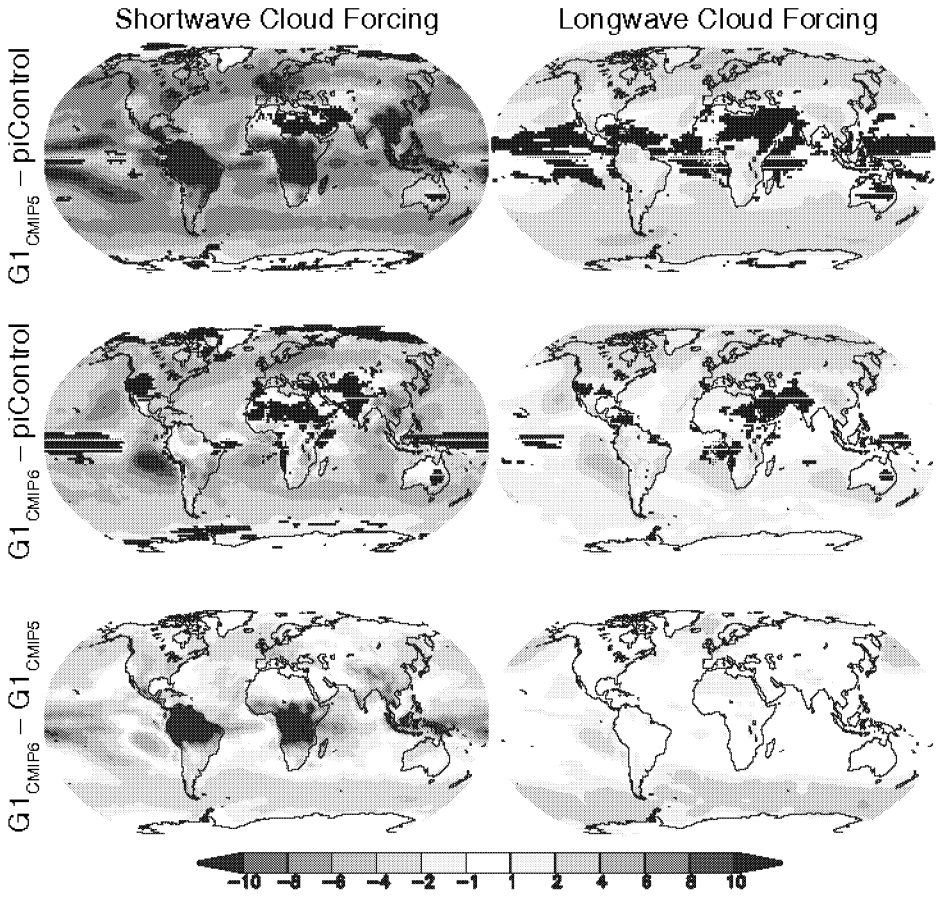

Figure 5. Surface shortwave (left) and longwave (right) cloud forcing (W m^{-2}) change from preindustrial for the CMIP5 (top) and CMIP6 (middle) ensembles, as well as the ensemble differences (bottom). Cloud forcing is measured as all-sky minus clear-sky radiative flux. All shaded values are ensemble means. Lack of stippling indicates agreement on the sign of the values across at least 75% of the models.

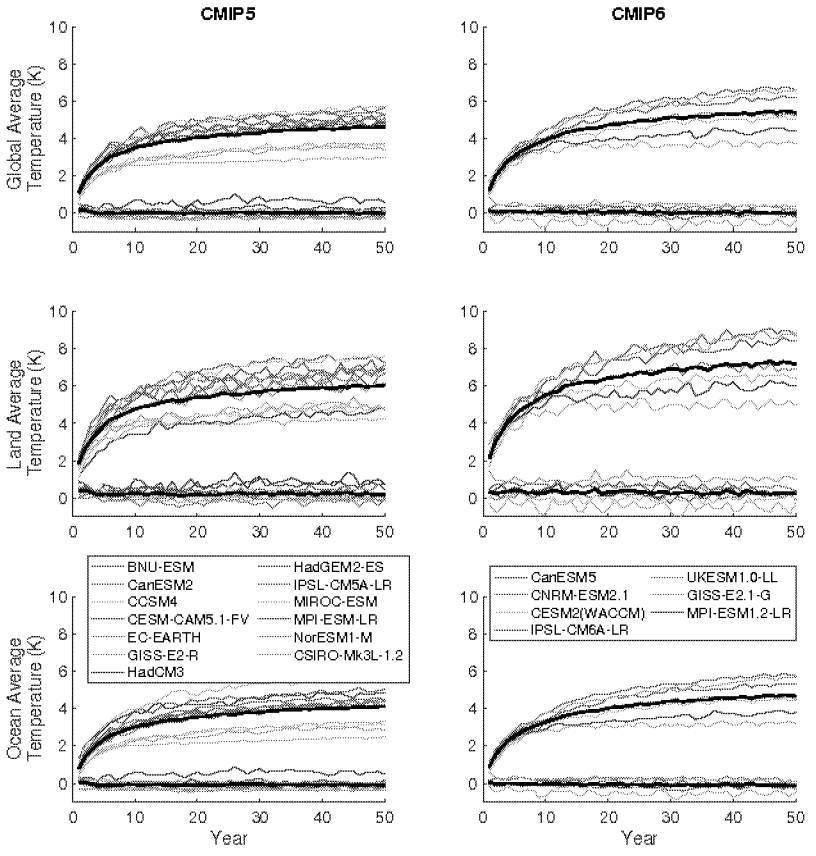

Figure 6. Global mean (top), land mean (middle), and ocean mean (bottom) temperature change (K) for the CMIP5 (left) and CMIP6 (ensembles). Thin colored lines are individual models, and thick black lines are model means. In all panels, the upper cluster of lines is the abrupt4xCO2 simulation, and the lower cluster of lines (approximately zero temperature change for the entire simulation) is experiment G1.

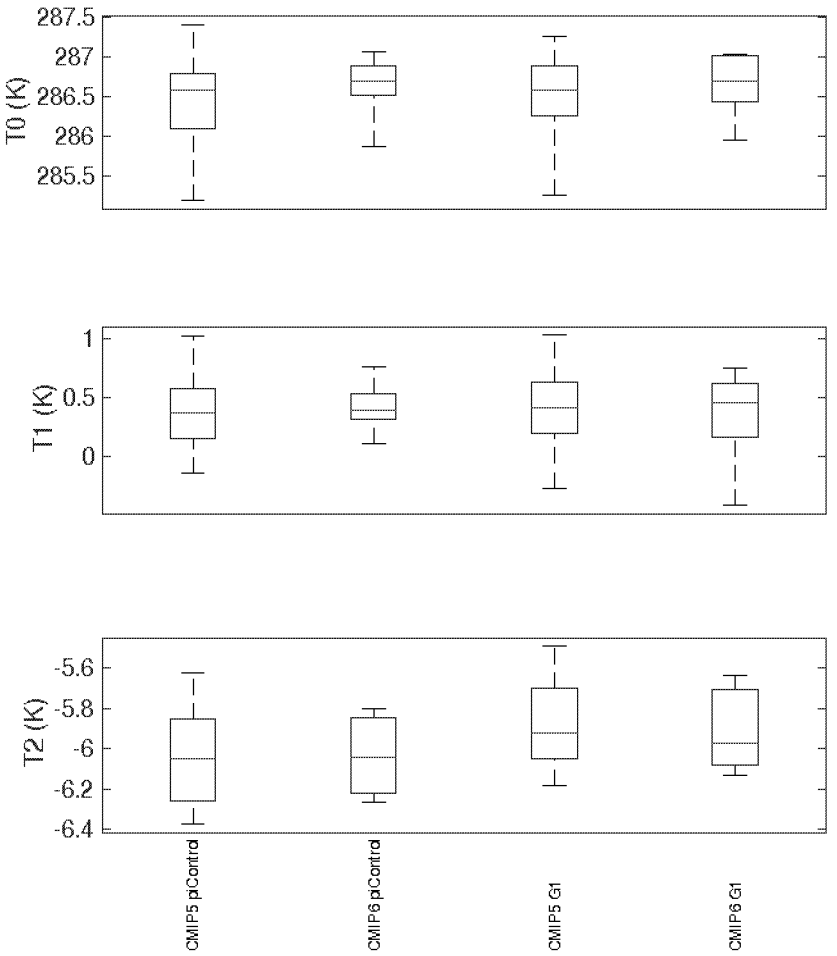

Figure 7. Ensemble ranges for global mean temperature (T_0), the interhemispheric temperature gradient (T_1), and the equator-to-pole temperature gradient (T_2), as defined in Equation 1 (Ban-Weiss and Caldeira, 2010; Kravitz et al., 2016). Red lines indicate ensemble medians, blue boxes are the inter-quartile ranges, and black whiskers indicate total ranges.

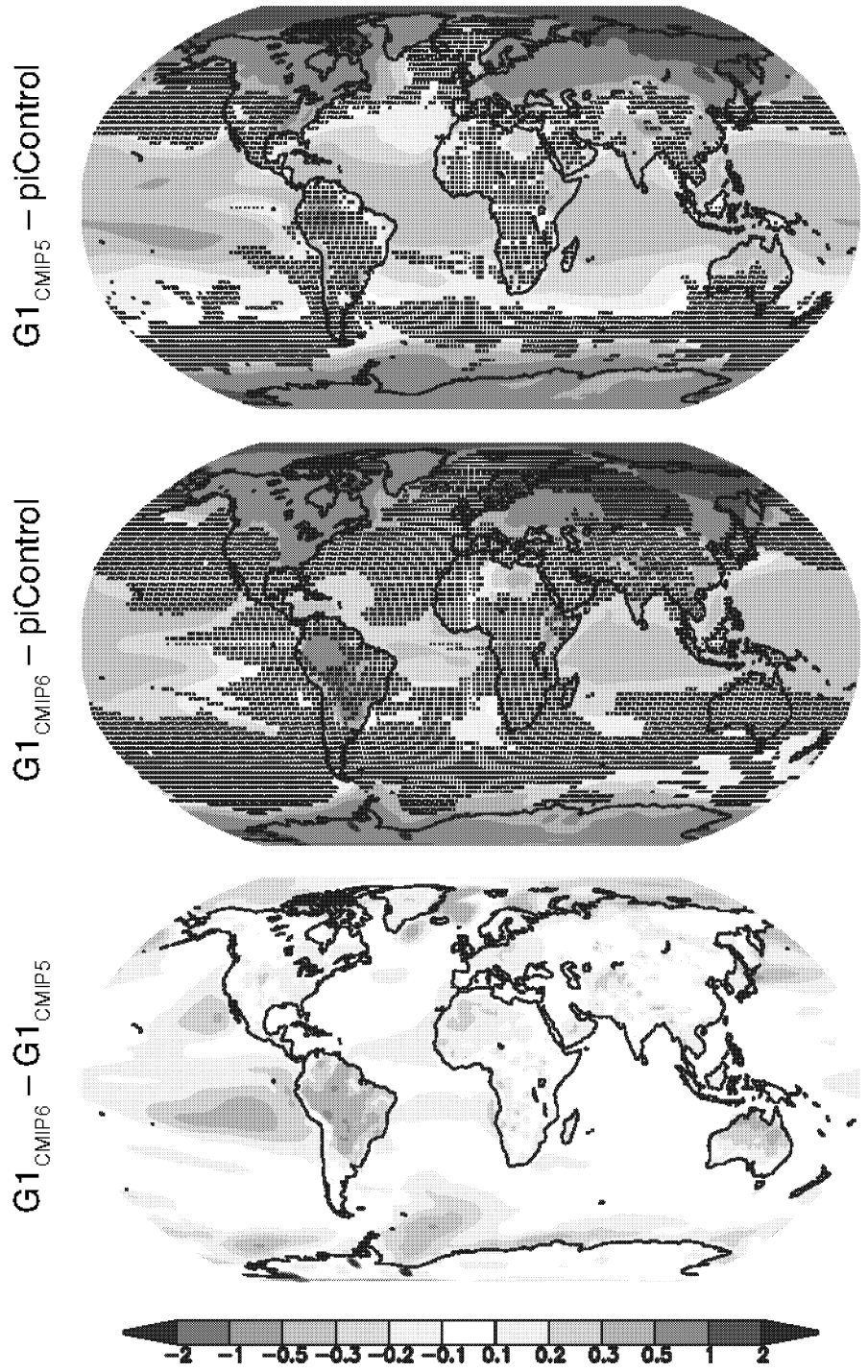

Figure 8. Ensemble average temperature changes (K) for G1 (as compared to the preindustrial control) for CMIP5 (top) and CMIP6 (middle), as well as their difference ($G1_{CMIP6}$ minus $G1_{CMIP5}$, bottom panel). In the top two panels, stippling indicates regions where fewer than 75% of the models in their respective ensembles agree on the sign of the response.

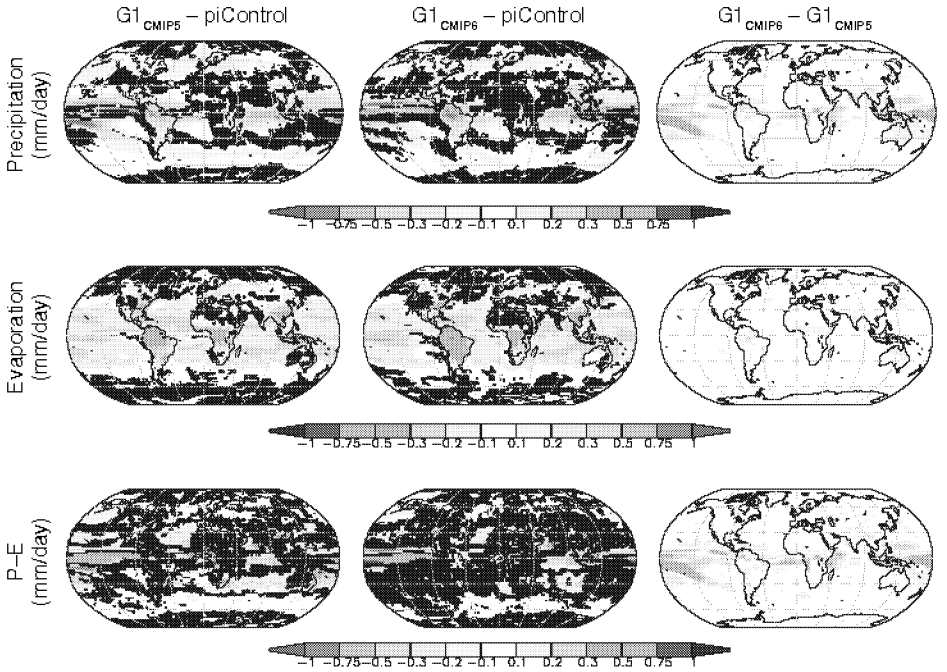

Figure 9. Precipitation (top), evaporation (middle), and precipitation minus evaporation (P–E; bottom) change from preindustrial for the CMIP5 (left) and CMIP6 (middle) ensembles, as well as the ensemble differences (right). All shaded values are ensemble means. Lack of stippling in the left and middle panels indicates agreement on the sign of the values across at least 75% of the models.

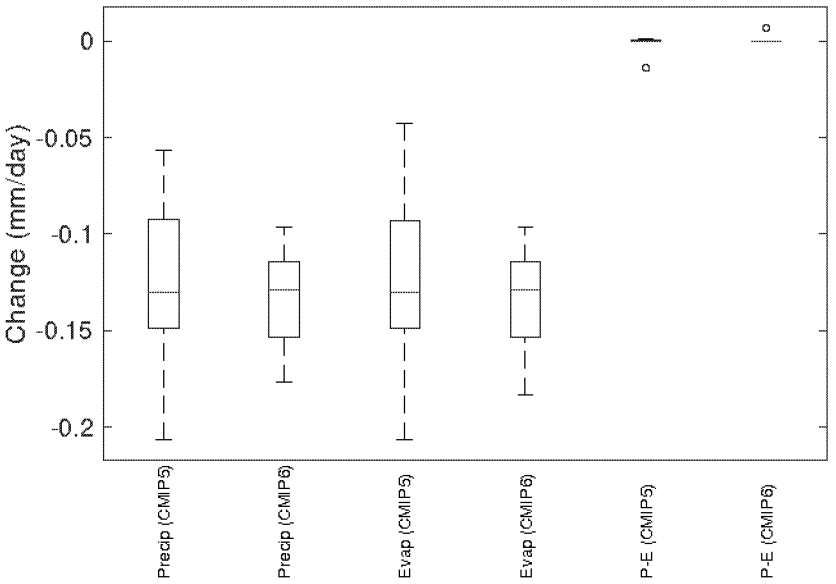

Figure 10. Global mean ensemble median (red lines), inter-quartile (blue boxes), and ranges (black whiskers or, for P–E one blue circle indicating an extreme outlier) for the hydrological quantities shown in Figure 9 for both the CMIP5 and CMIP6 ensembles.

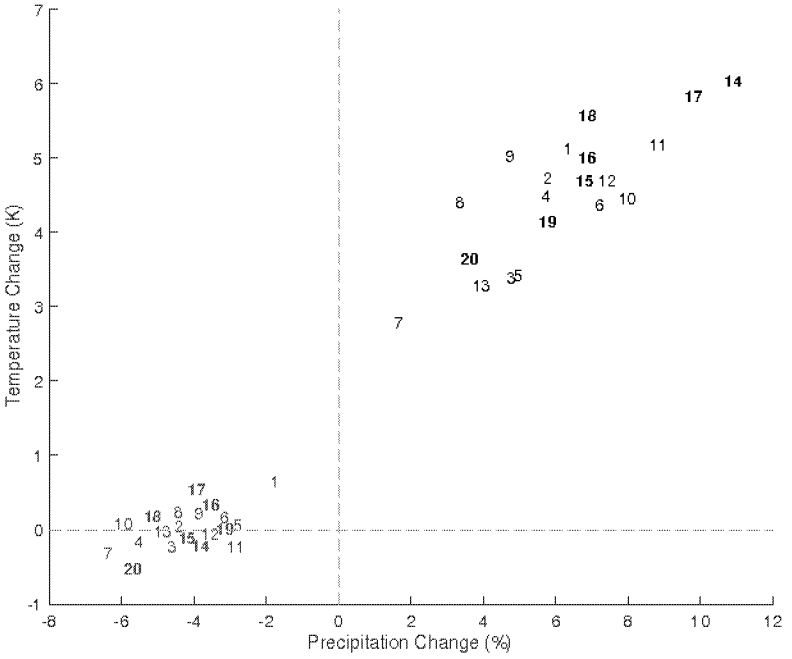

Figure 11. Average (years 11-50) temperature (y-axis; K) and precipitation (x-axis; %) change for each model in this study. Numbers indicate the model number (listed in Table 1, first column). Black numbers are for abrupt4xCO2, and red numbers are for G1. Bolded numbers are for CMIP6

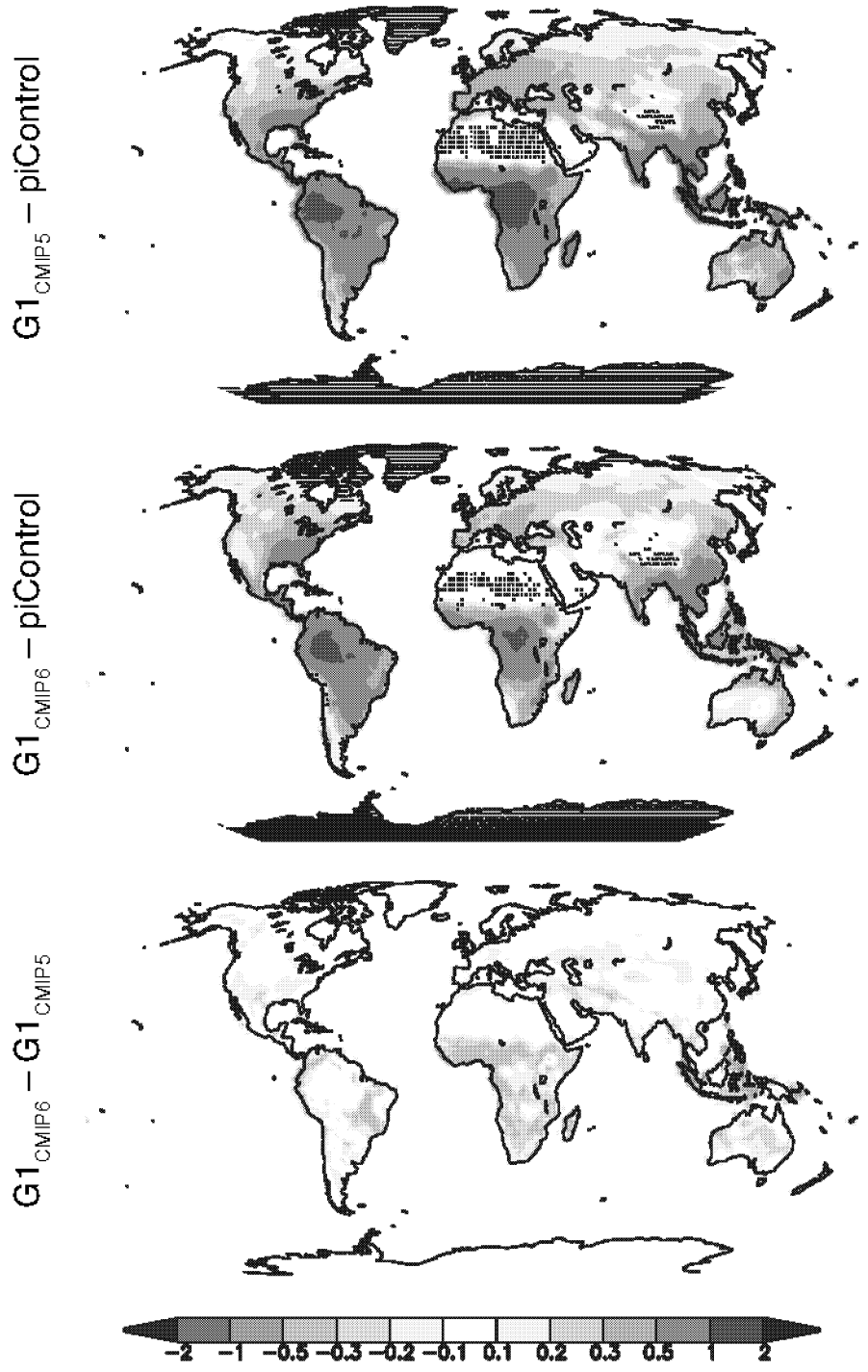

Figure 12. Terrestrial net primary productivity (kg C m^{-2} y^{-1}) for the CMIP5 (top) and CMIP6 (middle) ensembles, as well as the ensemble differences (bottom). All shaded values are ensemble means. Lack of stippling indicates agreement on the sign of the values across at least 75% of the models.

https://doi.org/10.5194/acp-2020-732
Preprint. Discussion started: 28 August 2020

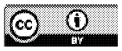

Atmospheric Chemistry and Physics Discussions

Comparing different generations of idealized solar geoengineering simulations in the Geoengineering Model Intercomparison Project (GeoMIP)

Ben Kravitz[1,2], Douglas G. MacMartin[3], Daniele Visioni[3], Olivier Boucher[4], Jason N. S. Cole[5], Jim Haywood[6,7], Andy Jones[7], Thibaut Lurton[4], Pierre Nabat[8], Ulrike Niemeier[9], Alan Robock[10], Roland Séférian[8], and Simone Tilmes[11]

[1]Department of Earth and Atmospheric Sciences, Indiana University, Bloomington, IN, USA
[2]Atmospheric Sciences and Global Change Division, Pacific Northwest National Laboratory, Richland, WA, USA
[3]Sibley School of Mechanical and Aerospace Engineering, Cornell University, Ithaca, NY, USA
[4]Institut Pierre-Simon Laplace (IPSL), Sorbonne Université/CNRS, Paris, France
[5]Environment and Climate Change Canada, Toronto, Ontario, Canada
[6]College of Engineering, Mathematics and Physical Sciences, University of Exeter, Exeter, United Kingdom
[7]UK Met Office Hadley Centre, Exeter, United Kingdom
[8]CNRM, Université de Toulouse, Météo-France, CNRS, Météo-France, Toulouse, France
[9]Max Planck Institute for Meteorology, Hamburg, Germany
[10]Department of Environmental Sciences, Rutgers University, New Brunswick, NJ, USA
[11]Atmospheric Chemistry Observations and Modeling Laboratory, National Center for Atmospheric Research, Boulder, CO, USA

Correspondence: Ben Kravitz, 1001 E. 10th Street, Bloomington, IN 47405-1405, USA. (bkravitz@iu.edu)

Abstract. Solar geoengineering has been receiving increased attention in recent years as a potential temporary solution to offset global warming. One method of approximating global-scale solar geoengineering in climate models is via solar reduction experiments. Two generations of models in the Geoengineering Model Intercomparison Project (GeoMIP) have now simulated offsetting a quadrupling of the CO_2 concentration with solar reduction. This simulation is artificial and designed to elicit large responses in the models. Here we show that energetics, temperature, and hydrological cycle changes in this experiment are statistically indistinguishable between the two ensembles. Of the variables analyzed here, the only major differences involve highly parameterized and uncertain processes, such as cloud forcing or terrestrial net primary productivity. We conclude that despite numerous structural differences and uncertainties in models over the past 20 years, including an increase in climate sensitivity in the latest generation of models, broad conclusions about the climate response to global solar dimming remain robust.

https://doi.org/10.5194/acp-2020-732
Preprint. Discussion started: 28 August 2020

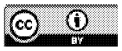

Atmospheric Chemistry and Physics Discussions

1 Introduction

Solar geoengineering describes a set of technologies designed to (ideally) temporarily, deliberately reduce some of the effects of climate change by changing the radiative balance of the planet, often by reflecting sunlight back to space (NRC, 2015). Numerous methods have been proposed, but the most studied is stratospheric sulfate aerosol injection (Budyko, 1977; Crutzen, 2006). This method involves substantially increasing the stratospheric sulfate aerosol burden, replicating the mechanisms that cause cooling after large volcanic eruptions (Robock, 2000). Climate models remain the most promising tools for understanding the consequences of solar geoengineering. In model simulations of solar geoengineering, insolation reduction is often used as a proxy for actual stratospheric sulfate aerosols, as it captures many of the broad radiative effects of stratospheric aerosol geoengineering as well as some of the important climate effects like surface cooling and hydrological cycle strength reduction (Niemeier et al., 2013; Kalidindi et al., 2015). However, stratospheric sulfate aerosols also absorb longwave radiative flux, which heats the upper troposphere and lower stratosphere. As such, any implementation of stratospheric geoengineering with sulfate aerosols would produce additional effects, such as changing atmospheric circulation in response to stratospheric heating and heating gradients (e.g., Richter et al., 2017; Tilmes et al., 2018; Simpson et al., 2019) and stratospheric ozone changes (e.g., Pitari et al., 2014), as well as changes in ultraviolet radiative flux and enhanced diffuse radiation at the surface (Madronich et al., 2018). However, here we consider the major, large-scale effect of reflecting sunlight to cool Earth.

Simulations of solar geoengineering with solar reduction have long shown that solar geoengineering would cool the planet, offsetting global warming (e.g., Govindasamy and Caldeira, 2000; NRC, 2015; Irvine et al., 2016). Idealized simulations of solar reduction have also been simulated in a multi-model context under the Geoengineering Model Intercomparison Project (GeoMIP; Kravitz et al., 2011), to understand the robust model responses to various standardized solar geoengineering simulation designs. Multi-model conclusions from these studies indicate that solar geoengineering would be effective at partially offsetting greenhouse gas-induced temperature changes (Kravitz et al., 2013), as well as changes in the hydrological cycle (Tilmes et al., 2013), the cryosphere (Moore et al., 2014), extreme events (Curry et al., 2014; Aswathy et al., 2015), vegetation (Glienke et al., 2015), circulation (Guo et al., 2018; Gertler et al., 2020), agriculture (Xia et al., 2014), and numerous other areas. However, the offset is not perfect (Moreno-Cruz et al., 2012), particularly on a regional basis or when considering multiple simultaneous metrics of climate change (Kravitz et al., 2014; Irvine et al., 2019), leading to concerns about winners and losers from geoengineering (Ricke et al., 2010). To some extent, the effects of solar geoengineering may be tailored or designed (MacMartin et al., 2013; Kravitz et al., 2016, 2017, 2019), but solar geoengineering will still not be able to perfectly offset climate change from greenhouse gases.

The previous phase of GeoMIP was associated with the Coupled Model Intercomparison Project Phase 5 (CMIP5; Taylor et al., 2012), an international collaboration of climate models to attempt to understand robust model responses to various forcings. GeoMIP has now entered a new phase, concurrent with the Coupled Model Intercomparison Project Phase 6 (CMIP6; Eyring et al., 2016), and with it are new solar geoengineering simulations with new and updated versions of Earth System Models (Kravitz et al., 2015). As such, this is an opportunity to revisit some central questions in solar geoengineering. Many of the CMIP5 results regarding solar geoengineering showed substantial agreement across the participating GeoMIP models.

https://doi.org/10.5194/acp-2020-732
Preprint. Discussion started: 28 August 2020

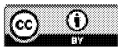

Atmospheric Chemistry and Physics Discussions

In this newest iteration of GeoMIP, do the same science conclusions still hold, and do the models still generally agree on the resulting climate effects? Here we address these questions by evaluating and comparing general climate model response to GeoMIP experiment G1 (described in the next section) from both CMIP5 and CMIP6.

2 Simulations and Participating Models

In this study, we evaluate GeoMIP experiment G1, in which, starting from a preindustrial control (piControl) baseline, the atmospheric CO_2 concentration is instantaneously quadrupled (the standard CMIP experiment abrupt4xCO2), and insolation is simultaneously reduced such that net top-of-atmosphere (TOA) radiative flux is approximately unchanged from the baseline in the first decade of simulation (Kravitz et al., 2011, 2015). This experiment was part of the original suite of GeoMIP experiments and was repeated and extended in the newest suite in an effort to understand the role of model structural uncertainty in broad conclusions about solar geoengineering. Participating models are listed in Table 1. We include 13 models from CMIP5 and 7 models from CMIP6.

The original G1 experiment was 50 years in length, whereas the CMIP6 version is 100 years in length to allow for better analyses of rare events or to capture very slow responses. Comparison between the two ensembles necessitates only using the first 50 years, but we need to verify that this can be done without losing important longer-term evolution in features. Figures 1 and 2 look at G1 behavior over the entire 100-year period of the CMIP6 simulations to determine whether there is any drift or trend that would not be revealed by only analyzing 50 years. With the exception of IPSL-CM6A-LR, no model shows any long-term behavior in temperature. Two models (IPSL-CM6A-LR and GISS-E2.1-G) show a slight trend in precipitation and evaporation, with a change of <1% over the first 50 years of simulation. As such, we conclude that our choice to focus on the first 50 years of simulation does not appreciably affect our results.

Figure 2 indicates that the temperature trend in IPSL-CM6A-LR is due to temperature changes north of 30°N, possibly related to a slight trend in sea ice coverage (Boucher et al., 2020). This model is also known to have a bicentennial oscillation, which could affect G1–piControl differences, depending on the baseline period used for subtraction. To verify that this oscillation is not impacting our results, we divided that model's 1200-year piControl run into 50-year chunks and computed the surface air temperature average for each of those chunks. The largest temperature found was 286.0339 K, and the smallest was 285.6384 K. The average over the entire ensemble was 285.8604 K. As such, using the mean of the entire ensemble versus matching the appropriate period in the bicentennial oscillation would have an impact on G1–piControl temperature by at most 0.22 K. Only averaging the first 100 years of the piControl run (which may be the best match to the period covered by G1) yields a temperature of 285.9084 K, which is 0.048 K different from the mean of the entire piControl run. As such, we conclude that this bicentennial oscillation is unlikely to have substantially influenced our findings.

Because the main focus of this paper is a comparison between the CMIP5 and CMIP6 generations of model results, we have opted for the following to aid comparisons:

https://doi.org/10.5194/acp-2020-732
Preprint. Discussion started: 28 August 2020

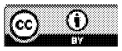

Atmospheric Chemistry and Physics Discussions

- Since we are not evaluating any features that require 100 years of statistics, and the results do not show any appreciable time evolution of behavior after the first couple of years (see discussion above), we only evaluate the first 50 years of all simulations. All maps show changes over years 11-50, removing the initial transient period.

- We do not compare previous versions of individual models with current ones, instead only examining ensembles. Even though models may share similar development histories (e.g., atmosphere and ocean dynamical cores, convective parameterizations, radiative transfer modules, terrestrial biosphere and cryosphere; Knutti et al., 2013; Zelinka et al., 2020), there have been numerous developments in models in these areas (and others) between CMIP5 and CMIP6 such that in most cases a direct comparison would not be meaningful.

- We focus extensively on the G1 results and, with few exceptions, do not focus on the corresponding abrupt4xCO2 simulations. It has been well documented that the CMIP6 models tend to have higher climate sensitivities than the CMIP5 models (Flynn and Mauritsen, 2020; Meehl et al., 2020; Zelinka et al., 2020), so we do not wish to make conclusions that might be based on a form of selection bias.

- All lack of stippling on map plots, as in previous GeoMIP studies (e.g., Kravitz et al., 2013), indicates agreement on the sign of the response in at least 75% of models. Because $\mathrm{G1}_{\mathrm{CMIP5}}$ has more participating models than $\mathrm{G1}_{\mathrm{CMIP6}}$, this threshold provides some consistency across analyses of the ensembles. When plotting differences between the ensembles ($\mathrm{G1}_{\mathrm{CMIP6}}$–$\mathrm{G1}_{\mathrm{CMIP5}}$), there is no stippling, as it is difficult to meaningfully represent such differences between ranges. Aggregate differences between the two ensembles, as calculated using Welch's t-test or differences in stippled area, are discussed in Table 2.

3 Results

3.1 Energetics

Ensemble mean radiative and turbulent flux quantities are plotted in Figure 3, and the ensemble ranges are plotted in Figure 4. An immediate observation is that, in both ensembles, the models were successful at limiting net TOA radiative flux change to within approximately ± 0.1 W m^{-2} of the models' respective preindustrial values. Accomplishing this required an average solar reduction of 4.14% (models range in 3.20–5.00%) in CMIP5 and 4.14% (3.72–4.91%) in CMIP6. As such, despite numerous structural changes between the two generations of models, there is no appreciable change in solar efficacy (Hansen et al., 2005).

None of the radiative flux quantities indicate large transients over 50 years of simulation of G1, other than the initial flux change within the first year or so of simulation. This is consistent with the "perpetual fast response" found by Kravitz et al. (2013b), in which because global mean temperature does not change appreciably over the course of the G1 simulation, climate feedbacks are not excited, and the internal state of the system (as measured by, for example, fluxes and hydrological cycle changes) similarly does not change. Ensemble mean fluxes show few differences (<1 W m^{-2} in magnitude) with the exception of shortwave cloud forcing, defined as all-sky minus clear-sky shortwave flux at the surface. On average, the CMIP6 ensemble

https://doi.org/10.5194/acp-2020-732
Preprint. Discussion started: 28 August 2020

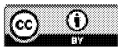

Atmospheric Chemistry and Physics Discussions

has 3–4 W m^{-2} less shortwave cloud forcing than CMIP5. Neglecting some outliers, for each flux except shortwave (and hence total) cloud forcing, the median model in one ensemble is within the inter-quartile range of the other ensemble. This indicates that there are no major differences between the ensembles in how the models handle energy balance and energetics, with the exception of clouds, which is consistent with findings about CMIP6 (Zelinka et al., 2020). Moreover, it appears that most of the major differences in shortwave cloud forcing are due to outliers in each ensemble, positive for CMIP5 and negative for CMIP6. To further explore these potential differences, Figure 5 provides maps of the ensemble means for cloud forcing. In G1, the CMIP5 ensemble showed more positive shortwave cloud forcing and more negative longwave cloud forcing (i.e., more cancellation) than the CMIP6 ensemble. Overall, the CMIP6 ensemble has greatly reduced (in some places by over 10 W m^{-2}) shortwave cloud forcing as compared to CMIP5 under the G1 experiment. This is a widespread result, but the most prominent features are in the tropics, especially over the Amazon, Africa, and the Maritime Continent. These regions encompass tropical forests, indicating a potential for vegetation feedbacks on the temperature reductions. However, the reasons behind these forcing changes are difficult to diagnose, as they could be due to changes in cloud thickness, cloud cover, or cloud level between CMIP5 and CMIP6 models (e.g., Vignesh et al., 2020), differences in how solar geoengineering affects clouds (Russotto and Ackerman, 2018), or artifacts of the analyses (e.g., cloud masking; Andrews et al., 2009; Kravitz et al., 2013b). Moreover, based on the results in Figure 4, it is likely that many of these features are exaggerated by outlier models (also see Vignesh et al., 2020). As such, we reserve such detailed investigations for future work.

3.2 Temperature

These small flux changes also lead to few G1 temperature changes between the two ensembles. Figure 6 shows global, land, and ocean-averaged temperatures for the CMIP5 and CMIP6 ensembles. In general, the abrupt4xCO2 simulation in CMIP6 has higher temperatures than in CMIP5, consistent with the noted increase in climate sensitivity (Vial et al., 2013; Flynn and Mauritsen, 2020; Meehl et al., 2020; Zelinka et al., 2020). In both ensembles, G1 is effective at offsetting global mean temperature change, in some cases with a slight positive residual temperature change over land. Figure 7 shows three aggregate temperature metrics: global mean temperature (T_0), the interhemispheric temperature gradient (T_1), and the equator-to-pole temperature gradient (T_2) (Ban-Weiss and Caldeira, 2010; Kravitz et al., 2016):

$$
\begin{aligned}
T_0 &= \frac{1}{A}\int_{-\pi/2}^{\pi/2} T(\psi)\,\mathrm{d}A \\
T_1 &= \frac{1}{A}\int_{-\pi/2}^{\pi/2} T(\psi)\sin\psi\,\mathrm{d}A \\
T_2 &= \frac{1}{A}\int_{-\pi/2}^{\pi/2} T(\psi)\frac{1}{2}(3\sin^2\psi - 1)\,\mathrm{d}A
\end{aligned}
\tag{1}
$$

https://doi.org/10.5194/acp-2020-732
Preprint. Discussion started: 28 August 2020

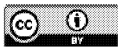

Atmospheric Chemistry and Physics Discussions

where A is area. As for the fluxes, the median model in one ensemble is within the inter-quartile range of the other ensemble. This indicates that no ensemble is on average warmer or cooler than another, has a substantially warmer Northern or Southern Hemisphere than the other, or has warmer tropics or poles than the other. We can conclude that spatial patterns of temperature change from G1 are robust across a wide range of structural uncertainty, including an increase in climate sensitivity between the two generations of CMIP.

The spatial structure of temperature change (Figure 8) does have small differences between the two ensembles. G1 in CMIP6 has multiple locations that are warmer than G1 in CMIP5, despite both ensembles achieving net energy balance at TOA and the surface (Figure 3). The majority of the differences are over land and in the tropics, where CMIP6 is slightly warmer than CMIP5 (up to 1°C in some places). Nevertheless, both ensembles show the well noted feature that offsetting a CO_2 increase with globally uniform solar reduction overcools the tropics and undercools the poles (Govindasamy and Caldeira, 2000; Kravitz et al., 2013). CMIP6 shows slightly less high latitude warming than CMIP5, but temperature differences between the two ensembles are largely negligible. However, the warmer temperatures in CMIP6 near Greenland have important implications for ice sheet melt and consequent sea level rise, as well as bottom water formation. We reserve such analyses for future investigations, particularly since the models used here are not capable of simulating the eustatic component of sea level rise. In any case, these ensemble mean differences between CMIP5 and CMIP6 cannot be deemed statistically significant (Table 2 and Figure 7).

3.3 Hydrological and Other Integrative Changes

Figure 9 shows ensemble mean changes in precipitation (P), evaporation (E), and P–E for $G1_{CMIP5}$ and $G1_{CMIP6}$. Qualitatively, patterns are similar between both ensembles. Precipitation is slightly (<0.3 mm/day in magnitude) different in the tropics between the two ensembles. The majority of those features can be summarized as a more southward Intertropical Convergence Zone (ITCZ), more precipitation in the South Pacific Convergence Zone, and less precipitation over Southeast Asia and the Maritime Continent in $G1_{CMIP6}$. Evaporation in the two ensembles is nearly identical except for more evaporation in Amazonia and Australia in $G1_{CMIP6}$. As such, the net P–E change between the two ensembles strongly resembles the precipitation changes. Figure 10 shows that, like previous evaluations of ensemble ranges, the median model in one ensemble falls well within the interquartile range of the other ensemble for P, E, and P–E. As such, we cannot conclude any robust hydrological cycle changes between the two ensembles.

Figure 11 shows average (years 11–50) temperature change (with respect to piControl) plotted against average precipitation change for each model, as in Tilmes et al. (2013). Other than a potentially greater climate sensitivity of some CMIP6 models, there is no distinguishable difference in aggregate behavior between the two ensembles. The same conclusion discovered by Tilmes et al. (2013) holds: solar reduction cannot simultaneously offset CO_2-induced changes in both global mean temperature and global mean precipitation.

As an integrator of CO_2, temperature, and precipitation effects over land, Figure 12 shows changes in terrestrial net primary productivity (NPP). Numerous land regions have lower NPP in CMIP6 than in CMIP5. The ensemble average global NPP change (G1–piControl) is 51.2 (4.1–122.1) Pg C y^{-1} in CMIP5 and 38.1 (19.5–77.5) Pg C y^{-1} in CMIP6, representing a 25.6%

https://doi.org/10.5194/acp-2020-732
Preprint. Discussion started: 28 August 2020

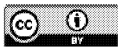

Atmospheric Chemistry and Physics Discussions

difference in means. Jones et al. (2013) used NPP to highlight the importance of understanding the influence of structural land model differences on climate results related to geoengineering. While it is beyond the scope of this study to perform a detailed diagnosis of which uncertainties or processes are responsible for this inter-ensemble difference, we show that the ensemble spread of total terrestrial NPP is smaller in CMIP6 than in CMIP5. This result is consistent with the recent assessment of carbon cycle feedbacks conducted by Arora et al. (2020), which demonstrates that the CMIP6 ensemble has reduced overall uncertainty in the land carbon cycle to rising CO_2 compared to their CMIP5 predecessors.

4 Discussion and Conclusions

Based on the results presented here, model response to G1 has not changed substantially between CMIP5 and CMIP6, despite numerous changes to models between the two generations, including an increase in climate sensitivity. The sign of residual climate impacts (for example in temperature) are in better agreement in CMIP5 than CMIP6 (Table 2 shows a difference in stippled area between the two ensembles), but this could be a function of the smaller ensemble size in CMIP6. Energetics, temperature, and the hydrological cycle are qualitatively and quantitatively similar in both ensemble means and ensemble ranges, although these variables are somewhat related, so we might expect them to all portray a similar picture. Notable differences do exist in shortwave cloud forcing and NPP, particularly in Amazonia, Africa, and Australia, which are also regions of inter-ensemble difference in precipitation.

From these findings, we can conclude that results obtained over the past 20 years of study have not been overturned by the latest round of simulations. All of the major ensemble differences highlighted above deal with clouds and land surface modeling, both of which are difficult to model and are necessarily highly parameterized. The conclusions that are based on more fundamental knowledge, such as column energetics (in the case of the hydrological cycle), are relatively robust to structural uncertainty, in so far as this study adequately captures representative variations in structural uncertainty. This lends confidence to our conclusions, especially regarding robustness to uncertainty, about the broad climate effects from solar geoengineering methods that can be accurately represented via solar dimming.

We also conclude that the models used in CMIP5 are not obviously biased or inferior as compared to CMIP6. While improvements have been made in the CMIP6 generation of models, and those models are likely better for representing numerous features of the present-day climate that may be important for studies of geoengineering, there are many aspects of climate that are well represented by earlier models. In some cases, more robust analyses may be enabled by augmenting ensemble sizes with archived output from earlier generations of CMIP models.

Many of the broad features of solar geoengineering with sulfate aerosols can be represented by a reduction in solar constant (e.g., Niemeier et al., 2013; Kalidindi et al., 2015). However, the more subtle changes that derive from complex response to stratospheric aerosol heating (for example, consequences of stratospheric heating like the positive wintertime North Atlantic Oscillation; Simpson et al., 2019) require detailed assessments with state-of-the-art aerosol microphysical schemes. This is particularly important for understanding regional and seasonal solar geoengineering (Kravitz et al., 2017; Visioni et al., 2019). Such detailed microphysical calculations can only be simulated in a small number of models While simple G1-style experiments

https://doi.org/10.5194/acp-2020-732
Preprint. Discussion started: 28 August 2020

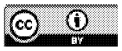

Atmospheric Chemistry and Physics Discussions

enable a robust multi-model ensemble analysis, they cannot capture details that depend on microphysics. We emphasize the importance of a variety of modeling approaches to understand solar geoengineering, particularly the role of model uncertainty in conclusions about solar geoengineering.

There are numerous aspects of physical climate that we did not evaluate, nor did we pursue analyses beyond physical climate, including many other aspects of natural science, social science, the humanities, governance, justice, or ethics (to name a few important areas). Moreover, we emphasize that experiment G1 is an idealized experiment aimed at understanding physical climate response to combinations of large forcings and should not be interpreted as a realistic or policy-relevant scenario of geoengineering. A holistic assessment of the consequences of geoengineering, particularly of more policy-relevant scenarios, would certainly need to take these numerous aspects into account. Nevertheless, based on the results presented here, results for geoengineering across several important metrics appear to be robust to some amount of structural uncertainty. This lends confidence to some conclusions drawn from global climate models regarding solar geoengineering.

Data availability. All CMIP5 and CMIP6 output, including the respective GeoMIP simulations, is available via the Earth System Grid Federation (https://esgf-node.llnl.gov/projects/esgf-llnl/) or by contacting the respective modeling groups responsible for the output. For CMIP6 output, seeTable 1 data citations.

Author contributions. BK, OB, JNSC, JH, AJ, TL, PN, UN, RS, and ST contributed model output. BK performed the analysis. BK, DGM, and DV wrote the manuscript with all coauthors.

Competing interests. None.

Acknowledgements. We acknowledge the World Climate Research Programme, which, through its Working Group on Coupled Modelling, coordinated and promoted CMIP. We thank the climate modeling groups for producing and making available their model output, the Earth System Grid Federation (ESGF) for archiving the data and providing access, and the multiple funding agencies who support CMIP6 and ESGF. We also thank all participants of the Geoengineering Model Intercomparison Project and their model development teams. Support for B.K. was provided in part by the National Science Foundation (NSF) through agreement CBET-1931641, the Indiana University Environmental Resilience Institute, and the Prepared for Environmental Change Grand Challenge initiative. The Pacific Northwest National Laboratory is operated for the US Department of Energy by Battelle Memorial Institute under contract DE-AC05-76RL01830. Resources supporting this work were provided by the NASA High-End Computing (HEC) Program through the NASA Center for Climate Simulation (NCCS) at Goddard Space Flight Center. A.R. is supported by NSF grants AGS-1617844 and AGS-2017113. U.N. is supported by the German DFG-funded Research Unit VolImpact FOR2820 sub project TI344/2-1 and MPIESM simulation have been performed on the computer of Deutsches Klimarechenzentrum (DKRZ). O.B. and T.L. were supported by the IPSL Climate Graduate School EUR (ANR grant ANR-

https://doi.org/10.5194/acp-2020-732
Preprint. Discussion started: 28 August 2020

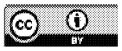

Atmospheric Chemistry and Physics Discussions

11-IDEX-0004 - 17-EURE-0006). The CMIP6 project at IPSL used the HPC resources of TGCC under the allocations 2016-A0030107732, 2017-R0040110492 and 2018-R0040110492 (project gencmip6) provided by GENCI (Grand Équipement National de Calcul Intensif). R.S. and P.N. were supported by the H2020 CONSTRAIN under the grant agreement No 820829 and the Météo-France/DSI supercomputing center.

https://doi.org/10.5194/acp-2020-732
Preprint. Discussion started: 28 August 2020

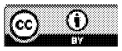

Atmospheric Chemistry and Physics Discussions

References

Alterskjær, K., Kristjánsson, J. E., and Seland, Ø.: Sensitivity to deliberate sea salt seeding of marine clouds – Observations and model simulations, Atmos. Chem. Phys., 12, 2795–2807, https://doi.org/10.5194/acp-12- 2795-2012, 2012.

Andrews, T., Forster, P. M., and Gregory, J. M.: A surface energy perspective on climate change, J. Clim., 22, 2557–2570, https://doi.org/10.1175/2008JCLI2759.1, 2009.

Arora, V. K., Scinocca, J. F., Boer, G. J., Christian, J. R., Denman, K. L., Flato, G. M., Kharin, V. V., Lee, W. G., and Merryfield, W. J.: Carbon emission limits required to satisfy future representative concentration pathways of greenhouse gases, Geophys. Res. Lett., 38, L05805, https://doi.org/10.1029/2010GL046270, 2011.

Arora, V. K., Katavouta, A., Williams, R. G., Jones, C. D., Brovkin, V., Friedlingstein, P., Schwinger, J., Bopp, L., Boucher, O., Cadule, P., Chamberlain, M. A., Christian, J. R., Delire, C., Fisher, R. A., Hajima, T., Ilyina, T., Joetzjer, E., Kawamiya, M., Koven, C., Krasting, J., Law, R. M., Lawrence, D. M., Lenton, A., Lindsay, K., Pongratz, J., Raddatz, T., Séférian, R., Tachiiri, K., Tjiputra, J. F., Wiltshire, A., Wu, T., and Ziehn, T.: Carbon-concentration and carbon-climate feedbacks in CMIP6 models, and their comparison to CMIP5 models, Biogeosciences, p. in press, 2020.

Aswathy, V. N., Boucher, O., Quaas, M., Niemeier, U., Muri, H., Mülmenstädt, J., and Quaas, J.: Climate extremes in multi-model simulations of stratospheric aerosol and marine cloud brightening climate engineering, Atmospheric Chemistry and Physics, 15, 9593–9610, https://doi.org/10.5194/acp-15-9593-2015, 2015.

Ban-Weiss, G. A. and Caldeira, K.: Geoengineering as an optimization problem, Environ. Res. Lett., 5, 031 001, https://doi.org/10.1088/1748-9326/5/3/034009, 2010.

Boucher, O., Denvil, S., Caubel, A., and Foujols, M. A.: IPSL IPSL-CM6A-LR model output prepared for CMIP6 GeoMIP G1, Earth System Grid Federation, https://doi.org/10.22033/ESGF/CMIP6.5054, 2018a.

Boucher, O., Denvil, S., Caubel, A., and Foujols, M. A.: IPSL IPSL-CM6A-LR model output prepared for CMIP6 CMIP abrupt-4xCO2, Earth System Grid Federation, https://doi.org/10.22033/ESGF/CMIP6.5109, 2018b.

Boucher, O., Denvil, S., Caubel, A., and Foujols, M. A.: IPSL IPSL-CM6A-LR model output prepared for CMIP6 CMIP piControl, Earth System Grid Federation, https://doi.org/10.22033/ESGF/CMIP6.5251, 2018c.

Boucher, O., Servonnat, J., Albright, A. L., Aumont, O., Balkanski, Y., Bastrikov, V., Bekki, S., Bonnet, R., Bony, S., Bopp, L., Braconnot, P., Brockmann, P., Cadule, P., Caubel, A., Cheruy, F., Codron, F., Cozic, A., Cugnet, D., D'Andrea, F., Davini, P., de Lavergne, C., Denvil, S., Deshayes, J., Devilliers, M., Ducharne, A., Dufresne, J.-L., Dupont, E., Éthé, C., Fairhead, L., Falletti, L., Flavoni, S., Foujols, M.-A., Gardoll, S., Gastineau, G., Ghattas, J., Grandpeix, J.-Y., Guenet, B., Guez, L., Guilyardi, E., Guimberteau, M., Hauglustaine, D., Hourdin, F., Idelkadi, A., Joussaume, S., Kageyama, M., Khodri, M., Krinner, G., Lebas, N., Levavasseur, G., Lévy, C., Li, L., Lott, F., Lurton, T., Luyssaert, S., Madec, G., Madeleine, J.-B., Maignan, F., Marchand, M., Marti, O., Mellul, L., Meurdesoif, Y., Mignot, J., Musat, I., Ottlé, C., Peylin, P., Planton, Y., Polcher, J., Rio, C., Rochetin, N., Rousset, C., Sepulchre, P., Sima, A., Swingedouw, D., Thiéblemont, R., Traore, A. K., Vancoppenolle, M., Vial, J., Vialard, J., Viovy, N., and Vuichard, N.: Presentation and evaluation of the IPSL-CM6A-LR climate model, Journal of Advances in Modeling Earth Systems, in press, e2019MS002 010, https://doi.org/10.1029/2019MS002010, 2020.

Budyko, M. I.: Climatic Changes, American Geophysical Union, 1977.

Cole, J. N., Swart, N. C., Kharin, V. V., Lazare, M., Scinocca, J. F., Gillett, N. P., Anstey, J., Arora, V., Christian, J. R., Jiao, Y., Lee, W. G., Majaess, F., Saenko, O. A., Seiler, C., Seinen, C., Shao, A., Solheim, L., von Salzen, K., Yang, D., Winter, B., and Sigmond, M.: CCCma

https://doi.org/10.5194/acp-2020-732
Preprint. Discussion started: 28 August 2020

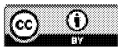

Atmospheric Chemistry and Physics Discussions

CanESM5 model output prepared for CMIP6 GeoMIP G1, Earth System Grid Federation, https://doi.org/10.22033/ESGF/CMIP6.3158, 2019.

Collins, W. J., Bellouin, N., Doutriaux-Boucher, M., Gedney, N., Halloran, P., Hinton, T., Hughes, J., Jones, C. D., Joshi, M., Liddicoat, S., Martin, G., O'Connor, F., Rae, J., Senior, C., Sitch, S., Totterdell, I., Wiltshire, A., and Woodward, S.: Development and evaluation of an Earth-System model—HadGEM2, Geosci. Model Dev., 4, 1051–1075, https://doi.org/10.5194/gmd-4-1051-2011, 2011.

Crutzen, P. J.: Albedo enhancement by stratospheric sulfur injections: A contribution to resolve a policy dilemma?, Climatic Change, 77, 211–220, https://doi.org/10.1007/s10584-006-9101-y, 2006.

Curry, C. L., Sillmann, J., Bronaugh, D., Alterskjær, K., Cole, J. N. S., Kravitz., B., Kristjánsson, J. E., Muri, H., Niemeier, U., Robock, A., and Tilmes, S.: A multi-model examination of climate extremes in an idealized geoengineering experiment, J. Geophys. Res., 119, 3900–3923, https://doi.org/10.1002/2013JD020648, 2014.

Danabasoglu, G.: NCAR CESM2-WACCM model output prepared for CMIP6 GeoMIP G1, Earth System Grid Federation, https://doi.org/10.22033/ESGF/CMIP6.10029, 2019a.

Danabasoglu, G.: NCAR CESM2-WACCM model output prepared for CMIP6 CMIP abrupt-4xCO2, Earth System Grid Federation, https://doi.org/10.22033/ESGF/CMIP6.10039, 2019b.

Danabasoglu, G.: NCAR CESM2-WACCM-FV2 model output prepared for CMIP6 CMIP piControl, Earth System Grid Federation, https://doi.org/10.22033/ESGF/CMIP6.11302, 2019c.

Dufresne, J.-L., Foujols, M.-A., Denvil, S., Caubel, A., Marti, O., Aumont, O., Balkanski, Y., Bekki, S., Bellenger, H., Benshila, R., Bony, S., Bopp, L., Braconnot, P., Brockmann, P., Cadule, P., Cheruy, F., Codron, F., Cozic, A., Cugnet, D., de Noblet, N., Duvel, J.-P., Ethé, C., Fairhead, L., Fichefet, T., Flavoni, S., Friedlingstein, P., Grandpeix, J.-Y., Guez, L., Guilyardi, E., Hauglustaine, D., Hourdin, F., Idelkadi, A., Ghattas, J., Joussaume, S., Kageyama, M., Krinner, G., Labetoulle, S., Lahellec, A., Lefebvre, M.-P., Lefevre, F., Levy, C., Li, Z. X., Lloyd, J., Lott, F., Madec, G., Mancip, M., Marchand, M., Masson, S., Meurdesoif, Y., Mignot, J., Musat, I., Parouty, S., Polcher, J., Rio, C., Schulz, M., Swingedouw, D., Szopa, S., Talandier, C., Terray, P., Viovy, N., and Vuichard, N.: Climate change projections using the IPSL-CM5 Earth System Model: From CMIP3 to CMIP5, Clim. Dynam., 40, 2123–2165, https://doi.org/10.1007/s00382-012-1636-1, 2013.

Eyring, V., Bony, S., Meehl, G. A., Senior, C. A., Stevens, B., Stouffer, R. J., and Taylor, K. E.: Overview of the Coupled Model Intercomparison Project Phase 6 (CMIP6) experimental design and organization, Geosci. Model Dev., 9, 1937–1958, https://doi.org/10.5194/gmd-9-1937-2016, 2016.

Flynn, C. M. and Mauritsen, T.: On the climate sensitivity and historical warming evolution in recent coupled model ensembles, Atmospheric Chemistry and Physics, 20, 7829–7842, https://doi.org/10.5194/acp-20-7829-2020, https://www.atmos-chem-phys.net/20/7829/2020/, 2020.

Gent, P. R., Danabasoglu, G., Donner, L. J., Holland, M. M., Hunke, E. C., Jayne, S. R., Lawrence, D. M., Neale, R. B., Rasch, P. J., Vertenstein, M., Worley, P. H., Yang, Z.-L., and Zhang, M.: The Community Climate System Model Version 4, Journal of Climate, 24, 4973–4991, https://doi.org/10.1175/2011JCLI4083.1, 2011.

Gertler, C. G., O'Gorman, P. A., Kravitz, B., Moore, J. C., Phipps, S. J., and Watanabe, S.: Weakening of the extratropical storm tracks in solar geoengineering scenarios, Geophys. Res. Lett., 47, e2020GL087348, https://doi.org/10.1029/2020GL087348, 2020.

Gettelman, A., Mills, M. J., Kinnison, D. E., Garcia, R. R., Smith, A. K., Marsh, D. R., Tilmes, S., Vitt, F., Bardeen, C. G., McInerny, J., Liu, H.-L., Solomon, S. C., Polvani, L. M., Emmons, L. K., Lamarque, J.-F., Richter, J. H., Glanville, A. S., Bacmeister, J. T., Phillips, A. S.,

https://doi.org/10.5194/acp-2020-732
Preprint. Discussion started: 28 August 2020

Neale, R. B., Simpson, I. R., DuVivier, A. K., Hodzic, A., and Randel, W. J.: The Whole Atmosphere Community Climate Model Version 6 (WACCM6), Journal of Geophysical Research: Atmospheres, 124, 12 380–12 403, https://doi.org/10.1029/2019JD030943, 2019.

Giorgetta, M. A., Jungclaus, J., Reick, C. H., Legutke, S., Bader, J., Böttinger, M., Brovkin, V., Crueger, T., Esch, M., Fieg, K., Glushak, K., Gayler, V., Haak, H., Hollweg, H.-D., Ilyina, T., Kinne, S., Kornblueh, L., Matei, D., Mauritsen, T., Mikolajewicz, U., Mueller, W., Notz, D., Pithan, F., Raddatz, T., Rast, S., Redler, R., Roeckner, E., Schmidt, H., Schnur, R., Segschneider, J., Six, K. D., Stockhause, M., Timmreck, C., Wegner, J., Widmann, H., Wieners, K.-H., Claussen, M., Marotzke, J., and Stevens, B.: Climate and carbon cycle changes from 1850 to 2100 in MPI-ESM simulations for the Coupled Model Intercomparison Project Phase 5, J. Adv. Model. Earth Syst., 5, 572–597, https://doi.org/10.1002/jame.20038, 2013.

Glienke, S., Irvine, P. J., and Lawrence, M. G.: The impact of geoengineering on vegetation in experiment G1 of the GeoMIP, J. Geophys. Res., 120, 10 196–10 213, https://doi.org/10.1002/2015JD024202, 2015.

Gordon, C., Cooper, C., Senior, C. A., Banks, H., Gregory, J. M., Johns, T. C., Mitchell, J. F. B., and Wood, R. A.: The simulation of SST, sea ice extents and ocean heat transports in a version of the Hadley Centre coupled model without flux adjustments, Clim. Dyn., 16, 147–168, https://doi.org/10.1007/s003820050010, 2000.

Govindasamy, B. and Caldeira, K.: Geoengineering Earth's radiation balance to mitigate CO_2-induced climate change, Geophys. Res. Lett., 27, 2141–2144, https://doi.org/10.1029/1999GL006086, 2000.

Guo, A., Moore, J. C., and Ji, D.: Tropical atmospheric circulation response to the G1 sunshade geoengineering radiative forcing experiment, Atmospheric Chemistry and Physics, 18, 8689–8706, https://doi.org/10.5194/acp-2018-8689, 2018.

Hansen, J., Sato, M., Ruedy, R., Nazarenko, L., Lacis, A., Schmidt, G. A., Russell, G., Aleinov, I., Bauer, M., Bauer, S., Bell, N., Cairns, B., Canuto, V., Chandler, M., Cheng, Y., Del Genio, A., Faluvegi, G., Fleming, E., Friend, A., Hall, T., Jackman, C., Kelley, M., Kiang, N., Koch, D., Lean, J., Lerner, J., Lo, K., Menon, S., Miller, R., Minnis, P., Novakov, T., Oinas, V., Perlwitz, J., Perlwitz, J., Rind, D., Romanou, A., Shindell, D., Stone, P., Sun, S., Tausnev, N., Thresher, D., Wielicki, B., Wong, T., Yaho, M., and Zhang, S.: Efficacy of Climate Forcings, J. Geophys. Res., 110, D18 104, https://doi.org/10.1029/2005JD005776, 2005.

Hazeleger, W., Wang, X., Severijns, C., Ştefănescu, S., Bintanja, R., Sterl, A., Wyser, K., Semmler, T., Yang, S., van den Hurk, B., van Noije, T., van der Linden, E., and van der Wiel, K.: EC-Earth V2.2: Description and validation of a new seamless Earth system prediction model, Clim. Dynam., 39, 2611–2629, https://doi.org/10.1007/s00382-011-1228-5, 2011.

Hourdin, F., Foujols, M.-A., Codron, F., Guemas, V., Dufresne, J.-L., Bony, S., Denvil, S., Guez, L., Lott, F., Ghattas, J., Braconnot, P., Marti, O., Meurdesoif, Y., and Bopp, L.: Impact of the LMDZ atmospheric grid configuration on the climate and sensitivity of the IPSL-CM5A coupled model, Clim. Dyn., 40, 2167–2192, https://doi.org/10.1007/s00382-012-1411-3, 2012.

Hurrell, J. W., Holland, M. M., Gent, P. R., Ghan, S., Kay, J. E., Kushner, P. J., Lamarque, J.-F., Large, W. G., Lawrence, D., Lindsay, K., Lipscomb, W. H., Long, M. C., Mahowald, N., Marsh, D. R., Neale, R. B., Rasch, P., Vavrus, S., Vertenstein, M., Bader, D., Collins, W. D., Hack, J. J., Kiehl, J., , and Marshall, S.: The Community Earth System Model: A Framework for Collaborative Research, Bull. Amer. Meteor. Soc., 94, 1339–1360, https://doi.org/10.1175/BAMS-D-12-00121.1, 2013.

Irvine, P., Emmanuel, K., He, J., Horowitz, L. W., Vecchi, G., and Keith, D.: Halving warming with idealized solar geoengineering moderates key climate hazards, Nature Climate Change, 9, 295–299, 2019.

Irvine, P. J., Kravitz, B., Lawrence, M. G., and Muri, H.: An overview of the Earth system science of solar geoengineering, WIREs Climate Change, 7, 815–833, https://doi.org/10.1002/wcc.423, 2016.

https://doi.org/10.5194/acp-2020-732
Preprint. Discussion started: 28 August 2020

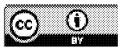

Atmospheric Chemistry and Physics Discussions

Ji, D., Wang, L., Feng, J., Wu, Q., Cheng, H., Zhang, Q., Yang, J., Dong, W., Dai, Y., Gong, D., Zhang, R.-H., Wang, X., Liu, J., Moore, J. C., Chen, D., and Zhou, M.: Description and basic evaluation of Beijing Normal University Earth System Model (BNU-ESM) version 1, Geosci. Model. Dev., 7, 2039–2064, https://doi.org/10.5194/gmd-7-2039-2014, 2014.

Jones, A.: MOHC UKESM1.0-LL model output prepared for CMIP6 GeoMIP G1, Earth System Grid Federation, https://doi.org/10.22033/ESGF/CMIP6.5812, 2019.

Jones, A., Haywood, J. M., Alterskjær, K., Boucher, O., Cole, J. N. S., J., C. L. C. P., Irvine, Ji, D., Kravitz, B., Moore, J. E. K. J. C., Niemeier, U., Robock, A., Schmidt, H., Singh, B., Tilmes, S., Watanabe, S., and Yoon, J.-H.: The impact of abrupt suspension of solar radiation management (termination effect) in experiment G2 of the Geoengineering Model Intercomparison Project (GeoMIP), Journal of Geophysical Research: Atmospheres, 118, 9743–9752, https://doi.org/10.1002/jgrd.50762, 2013.

Kalidindi, S., Bala, G., Modak, A., and Caldeira, K.: Modeling of solar radiation management: A comparison of simulations using reduced solar constant and stratospheric sulfate aerosols, Clim. Dynam., 44, 2909–2925, https://doi.org/10.1007/s00382-014-2240-3, 2015.

Kelley, M., Schmidt, G. A., Nazarenko, L. S., Bauer, S. E., Ruedy, R., Russell, G. L., Ackerman, A. S., Aleinov, I., Bauer, M., Bleck, R., Canuto, V., Cesana, G., Cheng, Y., Clune, T. L., Cook, B. I., Cruz, C. A., Del Genio, A. D., Elsaesser, G. S., Faluvegi, G., Kiang, N. Y., Kim, D., Lacis, A. A., Leboissetier, A., LeGrande, A. N., Lo, K. K., Marshall, J., Matthews, E. E., McDermid, S., Mezuman, K., Miller, R. L., Murray, L. T., Oinas, V., Orbe, C., Pérez García-Pando, C., Perlwitz, J. P., Puma, M. J., Rind, D., Romanou, A., Shindell, D. T., Sun, S., Tausnev, N., Tsigaridis, K., Tselioudis, G., Weng, E., Wu, J., and Yao, M.-S.: GISS-E2.1: Configurations and Climatology, Journal of Advances in Modeling Earth Systems, in press, e2019MS002025, https://doi.org/10.1029/2019MS002025, 2020.

Kirkevåg, A., Iversen, T., Seland, Ø., Hoose, C., Kristjánsson, J. E., Struthers, H., Ekman, A. M. L., Ghan, S., Griesfeller, J., Nilsson, E. D., and Schulz, M.: Aerosol–climate interactions in the Norwegian Earth System Model – NorESM1-M, Geoscientific Model Development, 6, 207–244, https://doi.org/10.5194/gmd-6-207-2013, https://gmd.copernicus.org/articles/6/207/2013/, 2013.

Knutti, R., Masson, D., and Gettelman, A.: Climate model genealogy: Generation CMIP5 and how we got there, Geophys. Res. Lett., 40, 1194–1199, https://doi.org/10.1002/grl.50256, 2013.

Kravitz, B., Robock, A., Boucher, O., Schmidt, H., Taylor, K. E., Stenchikov, G., and Schulz, M.: The Geoengineering Model Intercomparison Project (GeoMIP), Atmos. Sci. Lett., 12, 162–167, https://doi.org/10.1002/asl.316, 2011.

Kravitz, B., Caldeira, K., Boucher, O., Robock, A., Rasch, P. J., Alterskjær, K., Karam, D. B., Cole, J. N. S., Curry, C. L., Haywood, J. M., Irvine, P. J., Ji, D., Jones, A., Kristjánsson, J. E., Lunt, D. J., Moore, J., Niemeier, U., Schmidt, H., Schulz, M., Singh, B., Tilmes, S., Watanabe, S., Yang, S., , and Yoon, J.-H.: Climate model response from the Geoengineering Model Intercomparison Project (GeoMIP), J. Geophys. Res., 118, 8320–8332, https://doi.org/10.1002/jgrd.50646, 2013.

Kravitz, B., Rasch, P. J., Forster, P. M., Andrews, T., Cole, J. N. S., Irvine, P. J., Ji, D., Kristjánsson, J. E., Moore, J. C., Muri, H., Niemeier, U., Robock, A., Singh, B., Tilmes, S., Watanabe, S., , and Yoon, J.-H.: An energetic perspective on hydrological cycle changes in the Geoengineering Model Intercomparison Project (GeoMIP), J. Geophys. Res., 118, 13 087–13 102, https://doi.org/10.1002/2013JD020502, 2013b.

Kravitz, B., MacMartin, D. G., Robock, A., Rasch, P. J., Ricke, K. L., Cole, J. N. S., Curry, C. L., Irvine, P. J., Ji, D., Keith, D. W., Kristjánsson, J. E., Moore, J. C., Muri, H., Singh, B., Tilmes, S., Watanabe, S., Yang, S., and Yoon, J.-H.: A multi-model assessment of regional climate disparities caused by solar geoengineering, Environ. Res. Lett., 9, 074013, https://doi.org/10.1088/1748-9326/9/7/074013, 2014.

Kravitz, B., Robock, A., Tilmes, S., Boucher, O., English, J. M., Irvine, P. J., Jones, A., Lawrence, M. G., MacCracken, M., Muri, H., Moore, J. C., Niemeier, U., Phipps, S. J., Sillmann, J., Storelvmo, T., Wang, H., and Watanabe, S.: The Geoengineering Model Intercomparison

https://doi.org/10.5194/acp-2020-732
Preprint. Discussion started: 28 August 2020

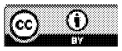

Atmospheric Chemistry and Physics Discussions

Project Phase 6 (GeoMIP6): Simulation design and preliminary results, Geosci. Model Dev., 8, 3379–3392, https://doi.org/10.5194/gmd-8-3379-2015, 2015.

Kravitz, B., MacMartin, D. G., Wang, H., and Rasch, P. J.: Geoengineering as a design problem, Earth System Dynamics, 7, 469–497, https://doi.org/10.5194/esd-469-2016, 2016.

Kravitz, B., MacMartin, D. G., Mills, M. J., Richter, J. H., Tilmes, S., Lamarque, J., Tribbia, J. J., and Vitt, F.: First Simulations of Designing Stratospheric Sulfate Aerosol Geoengineering to Meet Multiple Simultaneous Climate Objectives, J. Geophys. Res., 122, 12616–12634, https://doi.org/10.1002/2017JD026874, 2017.

Kravitz, B., MacMartin, D. G., Tilmes, S., Richter, J. H., Mills, M. J., Cheng, W., Dagon, K., Glanville, A. S., Lamarque, J.-F., Simpson, I., Tribbia, J., and Vitt, F.: Comparing surface and stratospheric impacts of geoengineering with different SO_2 injection strategies, J. Geophys. Res., 124, 7900–7918, https://doi.org/10.1029/2019JD030329, 2019.

Lurton, T., Balkanski, Y., Bastrikov, V., Bekki, S., Bopp, L., Braconnot, P., Brockmann, P., Cadule, P., Contoux, C., Cozic, A., Cugnet, D., Dufresne, J.-L., Éthé, C., Foujols, M.-A., Ghattas, J., Hauglustaine, D., Hu, R.-M., Kageyama, M., Khodri, M., Lebas, N., Levavasseur, G., Marchand, M., Ottlé, C., Peylin, P., Sima, A., Szopa, S., Thiéblemont, R., Vuichard, N., and Boucher, O.: Implementation of the CMIP6 Forcing Data in the IPSL-CM6A-LR Model, Journal of Advances in Modeling Earth Systems, 12, e2019MS001940, https://doi.org/10.1029/2019MS001940, 2020.

MacMartin, D. G., Keith, D. W., Kravitz, B., and Caldeira, K.: Management of trade-offs in geoengineering through optimal choice of non-uniform radiative forcing, Nature Climate Change, 3, 365–368, https://doi.org/10.1038/nclimate1722, 2013.

Madronich, S., Tilmes, S., Kravitz, B., MacMartin, D. G., and Richter, J. H.: Response of surface ultraviolet and visible radiation to stratospheric SO_2 injection, Atmosphere, 9, 432, https://doi.org/10.3390/atmos9110432, 2018.

Mauritsen, T., Bader, J., Becker, T., Behrens, J., Bittner, M., Brokopf, R., Brovkin, V., Claussen, M., Crueger, T., Esch, M., Fast, I., Fiedler, S., Fläschner, D., Gayler, V., Giorgetta, M., Goll, D. S., Haak, H., Hagemann, S., Hedemann, C., Hohenegger, C., Ilyina, T., Jahns, T., Jimenéz-de-la Cuesta, D., Jungclaus, J., Kleinen, T., Kloster, S., Kracher, D., Kinne, S., Kleberg, D., Lasslop, G., Kornblueh, L., Marotzke, J., Matei, D., Meraner, K., Mikolajewicz, U., Modali, K., Möbis, B., Müller, W. A., Nabel, J. E. M. S., Nam, C. C. W., Notz, D., Nyawira, S.-S., Paulsen, H., Peters, K., Pincus, R., Pohlmann, H., Pongratz, J., Popp, M., Raddatz, T. J., Rast, S., Redler, R., Reick, C. H., Rohrschneider, T., Schemann, V., Schmidt, H., Schnur, R., Schulzweida, U., Six, K. D., Stein, L., Stemmler, I., Stevens, B., von Storch, J.-S., Tian, F., Voigt, A., Vrese, P., Wieners, K.-H., Wilkenskjeld, S., Winkler, A., and Roeckner, E.: Developments in the MPI-M Earth System Model version 1.2 (MPI-ESM1.2) and Its Response to Increasing CO_2, Journal of Advances in Modeling Earth Systems, 11, 998–1038, https://doi.org/10.1029/2018MS001400, 2019.

Meehl, G. A., Senior, C. A., Eyring, V., Flato, G., Lamarque, J.-F., Stouffer, R. J., Taylor, K. E., and Schlund, M.: Context for interpreting equilibrium climate sensitivity and transient climate response from the CMIP6 Earth system models, Science Advances, 6, eaba1981, https://doi.org/10.1126/sciadv.aba1981, 2020.

Moore, J. C., Rinke, A., Yu, X., Ji, D., Cui, X., Li, Y., Alterskjær, K., Kristjánsson, J. E., Boucher, O., Huneeus, N., Kravitz, B., Robock, A., Niemeier, U., Schmidt, H., Schulz, M., Tilmes, S., and Watanabe, S.: Arctic sea ice and atmospheric circulation under the GeoMIP G1 scenario, J. Geophys. Res., 119, 567–583, https://doi.org/10.1002/2013JD021060, 2014.

Moreno-Cruz, J. B., Ricke, K. L., and Keith, D. W.: A simple model to account for regional inequalities in the effectiveness of solar radiation management, Climatic Change, 110, 649–668, 2012.

NASA Goddard Institute for Space Studies (NASA/GISS): NASA-GISS GISS-E2.1G model output prepared for CMIP6 CMIP abrupt-4xCO2, Earth System Grid Federation, https://doi.org/10.22033/ESGF/CMIP6.6976, 2018.

https://doi.org/10.5194/acp-2020-732
Preprint. Discussion started: 28 August 2020

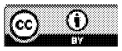

Atmospheric Chemistry and Physics Discussions

NASA Goddard Institute for Space Studies (NASA/GISS): NASA-GISS GISS-E2-1-G-CC model output prepared for CMIP6 CMIP piControl, Earth System Grid Federation, https://doi.org/10.22033/ESGF/CMIP6.11856, 2019.

Neale, R. B., Chen, C., Gettelman, A., Lauritzen, P., Park, S., Williamson, D., Conley, A., Garcia, R., Kinnison, D., and Lamarque, J.: Description of the NCAR community atmosphere model (CAM 5.0), Tech. rep., National Center for Atmospheric Research, 2010.

Niemeier, U., Schmidt, H., Alterskjær, K., and Kristjánsson, J. E.: Solar irradiance reduction via climate engineering: Impact of different techniques on the energy balance and the hydrological cycle, J. Geophys. Res., 118, 11 905–11 917, https://doi.org/10.1002/2013JD020445, 2013.

NRC: Climate Intervention: Reflecting Sunlight to Cool Earth, Tech. rep., National Research Council, http://www.nap.edu/catalog/18988/climate-intervention-reflecting-sunlight-to-cool-earth, (last access: 7 May 2015), 2015.

Phipps, S. J., Rotstayn, L. D., Gordon, H. B., Roberts, J. L., Hirst, A. C., , and Budd, W. F.: The CSIRO Mk3L climate system model version 1.0 – Part 1: Description and evaluation, Geosci. Model Dev., 4, 483–509, https://doi.org/10.5194/gmd-4-483-2011, 2011.

Phipps, S. J., Rotstayn, L. D., Gordon, H. B., Roberts, J. L., Hirst, A. C., and Budd, W. F.: The CSIRO Mk3L climate system model version 1.0 – Part 2: Response to external forcings, Geosci. Model Dev., 5, 649–682, https://doi.org/10.5194/gmd-5-649-2012, 2012.

Pitari, G., Aquila, V., Kravitz, B., Robock, A., Watanabe, S., Cionni, I., Luca, N. D., di Genova, G., Mancini, E., and Tilmes, S.: Stratospheric ozone response to sulfate geoengineering: Results from the Geoengineering Model Intercomparison Project (GeoMIP), J. Geophys. Res., 119, 2629–2653, 2014.

Richter, J. H., Tilmes, S., Mills, M. J., Tribbia, J. J., Kravitz, B., MacMartin, D. G., Vitt, F., and Lamarque, J.: Stratospheric Dynamical Response and Ozone Feedbacks in the Presence of SO_2 Injections, J. Geophys. Res., 122, 12 557–12 573, https://doi.org/10.1002/2017JD026912, 2017.

Ricke, K. L., Morgan, M. G., and Allen, M. R.: Regional climate response to solar-radiation management, Nat. Geosci., 3, 537–541, https://doi.org/10.1038/ngeo915, 2010.

Robock, A.: Volcanic eruptions and climate, Rev. Geophys., 38, 191–219, https://doi.org/10.1029/1998RG000054, 2000.

Russotto, R. D. and Ackerman, T. P.: Changes in clouds and thermodynamics under solar geoengineering and implications for required solar reduction, Atmos. Chem. Phys., 18, 11 905–11 925, https://doi.org/10.5194/acp-18-11905-2018, 2018.

Schmidt, G. A., Kelley, M., Nazarenko, L., Ruedy, R., Russell, G. L., Aleinov, I., Bauer, M., Bauer, S. E., Bhat, M. K., Bleck, R., Canuto, V., Chen, Y.-H., Cheng, Y., Clune, T. L., Genio, A. D., de Fainchtein, R., Faluvegi, G., Hansen, J. E., Healy, R. J., Kiang, N. Y., Koch, D., Lacis, A. A., LeGrande, A. N., Lerner, J., Lo, K. K., Matthews, E. E., Menon, S., Miller, R. L., Oinas, V., Oloso, A. O., Perlwitz, J. P., Puma, M. J., Putman, W. M., Rind, D., Romanou, A., Sato, M., Shindell, D. T., Sun, S., Syed, R. A., Tausnev, N., Tsigaridis, K., Under, N., Volugarakis, A., Yao, M.-S., and Zhang, J.: Configuration and assessment of the GISS ModelE2 contributions to the CMIP5 archive, J. Adv. Modell. Earth Syst., 6, 141–184, https://doi.org/10.1002/2013MS000265, 2014.

Séférian, R.: CNRM-CERFACS CNRM-ESM2-1 model output prepared for CMIP6 CMIP abrupt-4xCO2, Earth System Grid Federation, https://doi.org/10.22033/ESGF/CMIP6.3918, 2018a.

Séférian, R.: CNRM-CERFACS CNRM-ESM2-1 model output prepared for CMIP6 CMIP piControl, Earth System Grid Federation, https://doi.org/10.22033/ESGF/CMIP6.4165, 2018b.

Séférian, R.: CNRM-CERFACS CNRM-ESM2-1 model output prepared for CMIP6 CMIP G1, Earth System Grid Federation, https://doi.org/10.22033/ESGF/CMIP6.3902, 2018c.

Séférian, R., Nabat, P., Michou, M., Saint-Martin, D., Voldoire, A., Colin, J., Decharme, B., Delire, C., Berthet, S., Chevallier, M., Sénési, S., Franchisteguy, L., Vial, J., Mallet, M., Joetzjer, E., Geoffroy, O., Guérémy, J.-F., Moine, M.-P., Msadek, R., Ribes, A., Rocher, M.,

https://doi.org/10.5194/acp-2020-732
Preprint. Discussion started: 28 August 2020

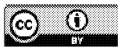

Roehrig, R., Salas-y Mélia, D., Sanchez, E., Terray, L., Valcke, S., Waldman, R., Aumont, O., Bopp, L., Deshayes, J., Éthé, C., and Madec, G.: Evaluation of CNRM Earth System Model, CNRM-ESM2-1: Role of Earth System Processes in Present-Day and Future Climate, Journal of Advances in Modeling Earth Systems, 11, 4182–4227, https://doi.org/10.1029/2019MS001791, 2019.

Sellar, A. A., Jones, C. G., Mulcahy, J. P., Tang, Y., Yool, A., Wiltshire, A., O'Connor, F. M., Stringer, M., Hill, R., Palmieri, J., Woodward, S., de Mora, L., Kuhlbrodt, T., Rumbold, S. T., Kelley, D. I., Ellis, R., Johnson, C. E., Walton, J., Abraham, N. L., Andrews, M. B., Andrews, T., Archibald, A. T., Berthou, S., Burke, E., Blockley, E., Carslaw, K., Dalvi, M., Edwards, J., Folberth, G. A., Gedney, N., Griffiths, P. T., Harper, A. B., Hendry, M. A., Hewitt, A. J., Johnson, B., Jones, A., Jones, C. D., Keeble, J., Liddicoat, S., Morgenstern, O., Parker, R. J., Predoi, V., Robertson, E., Siahaan, A., Smith, R. S., Swaminathan, R., Woodhouse, M. T., Zeng, G., and Zerroukat, M.: UKESM1: Description and Evaluation of the U.K. Earth System Model, Journal of Advances in Modeling Earth Systems, 11, 4513–4558, https://doi.org/10.1029/2019MS001739, 2019.

Simpson, I., Tilmes, S., Richter, J., Kravitz, B., MacMartin, D., Mills, M., Fasullo, J., and Pendergrass, A.: The regional hydroclimate response to stratospheric sulfate geoengineering and the role of stratospheric heating, J. Geophys. Res., 124, 12587–12616, https://doi.org/10.1029/2019JD031093, 2019.

Stevens, B., Giorgetta, M., Esch, M., Mauritsen, T., Crueger, T., Rast, S., Salzmann, M., Schmidt, H., Bader, J., Block, K., Brokopf, R., Fast, I., Kinne, S., Kornblueh, L., Lohmann, U., Pincus, R., Reichler, T., and Roeckner, E.: Atmospheric component of the MPI-M Earth System Model: ECHAM6, Journal of Advances in Modeling Earth Systems, 5, 146–172, https://doi.org/10.1002/jame.20015, 2013.

Swart, N. C., Cole, J. N., Kharin, V. V., Lazare, M., Scinocca, J. F., Gillett, N. P., Anstey, J., Arora, V., Christian, J. R., Jiao, Y., Lee, W. G., Majaess, F., Saenko, O. A., Seiler, C., Seinen, C., Shao, A., Solheim, L., von Salzen, K., Yang, D., Winter, B., and Sigmond, M.: CCCma CanESM5 model output prepared for CMIP6 CMIP piControl, Earth System Grid Federation, https://doi.org/10.22033/ESGF/CMIP6.3673, 2019a.

Swart, N. C., Cole, J. N., Kharin, V. V., Lazare, M., Scinocca, J. F., Gillett, N. P., Anstey, J., Arora, V., Christian, J. R., Jiao, Y., Lee, W. G., Majaess, F., Saenko, O. A., Seiler, C., Seinen, C., Shao, A., Solheim, L., von Salzen, K., Yang, D., Winter, B., and Sigmond, M.: CCCma CanESM5 model output prepared for CMIP6 CMIP abrupt-4xCO2, Earth System Grid Federation, https://doi.org/10.22033/ESGF/CMIP6.3532, 2019b.

Swart, N. C., Cole, J. N. S., Kharin, V. V., Lazare, M., Scinocca, J. F., Gillett, N. P., Anstey, J., Arora, V., Christian, J. R., Hanna, S., Jiao, Y., Lee, W. G., Majaess, F., Saenko, O. A., Seiler, C., Seinen, C., Shao, A., Sigmond, M., Solheim, L., von Salzen, K., Yang, D., and Winter, B.: The Canadian Earth System Model version 5 (CanESM5.0.3), Geoscientific Model Development, 12, 4823–4873, https://doi.org/10.5194/gmd-12-4823-2019, https://gmd.copernicus.org/articles/12/4823/2019/, 2019c.

Tang, Y., Rumbold, S., Ellis, R., Kelley, D., Mulcahy, J., Sellar, A., Walton, J., and Jones, C.: MOHC UKESM1.0-LL model output prepared for CMIP6 CMIP abrupt-4xCO2, Earth System Grid Federation, https://doi.org/10.22033/ESGF/CMIP6.5843, 2019a.

Tang, Y., Rumbold, S., Ellis, R., Kelley, D., Mulcahy, J., Sellar, A., Walton, J., and Jones, C.: MOHC UKESM1.0-LL model output prepared for CMIP6 CMIP piControl, Earth System Grid Federation, https://doi.org/10.22033/ESGF/CMIP6.6298, 2019b.

Taylor, K. E., Stouffer, R. J., and Meehl, G. A.: An overview of CMIP5 and the experiment design, Bull. Amer. Meteor. Soc., 93, 485–498, https://doi.org/10.1175/BAMS-D-11-00094.1, 2012.

Tilmes, S., Fasullo, J., Lamarque, J.-F., Marsh, D. R., Mills, M., Alterskjær, K., Muri, H., Kristjánsson, J. E., Boucher, O., Schulz, M., Cole, J. N. S., Curry, C. L., Jones, A., Haywood, J., Irvine, P. J., Ji, D., Moore, J. C., Karam, D. B., Kravitz, B., Rasch, P. J., Singh, B., Yoon, J.-H., Niemeier, U., Schmidt, H., Robock, A., Yang, S., and Watanabe, S.: The hydrological impact of geoengineering in the Geoengineering Model Intercomparison Project (GeoMIP), J. Geophys. Res., 118, 11 036–11 058, https://doi.org/10.1002/jgrd.50868, 2013.

https://doi.org/10.5194/acp-2020-732
Preprint. Discussion started: 28 August 2020

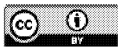

Atmospheric Chemistry and Physics Discussions

Tilmes, S., Richter, J. H., Mills, M. J., Kravitz, B., MacMartin, D. G., Garcia, R. R., Kinnison, D. E., Lamarque, J.-F., Tribbia, J., and Vitt, F.: Effects of Different Stratospheric SO_2 Injection Altitudes on Stratospheric Chemistry and Dynamics, J. Geophys. Res., 123, 4654–4673, https://doi.org/10.1002/2017JD028146, 2018.

Vial, J., Dufresne, J.-L., and Bony, S.: On the interpretation of inter-model spread in CMIP5 climate sensitivity estimates, Climate Dynamics, 41, 3339–3362, https://doi.org/10.1007/s00382-013-1725-9, 2013.

Vignesh, P. P., Jiang, J. H., Kishore, P., Su, H., Smay, T., Brighton, N., and Velicogna, I.: Assessment of CMIP6 cloud fraction and comparison with satellite observations, Earth and Space Science, 7, e2019EA000975, https://doi.org/10.1029/2019EA000975, 2020.

Visioni, D., MacMartin, D. G., Kravitz, B., Tilmes, S., Mills, M. J., Richter, J. H., and Boudreau, M. P.: Seasonal injection strategies for stratospheric aerosol geoengineering, Geophysical Research Letters, 46, 7790–7799, https://doi.org/10.1029/2019GL083680, 2019.

Watanabe, S., Miura, H., Sekiguchi, M., Nagashima, T., Sudo, K., Emori, S., and Kawamiya, M.: Development of an atmospheric general circulation model for integrated Earth system modeling on the Earth Simulator, J. Earth Simulator, 9, 27–35, 2008.

Watanabe, S., Hajima, T., Sudo, K., Nagashima, T., Takemura, T., Okajima, H., Nozawa, T., Kawase, H., Abe, M., Yokohata, T., Ise, T., Sato, H., Kato, E., Takata, K., Emori, S., and Kawamiya, M.: MIROC-ESM 2010: Model description and basic results of CMIP5-20c3m experiments, Geosci. Mod. Dev., 4, 845–872, https://doi.org/10.5194/gmd-4-845-2011, 2011.

Wieners, K.-H., Giorgetta, M., Jungclaus, J., Reick, C., Esch, M., Bittner, M., Legutke, S., Schupfner, M., Wachsmann, F., Gayler, V., Haak, H., de Vrese, P., Raddatz, T., Mauritsen, T., von Storch, J.-S., Behrens, J., Brovkin, V., Claussen, M., Crueger, T., Fast, I., Fiedler, S., Hagemann, S., Hohenegger, C., Jahns, T., Kloster, S., Kinne, S., Lasslop, G., Kornblueh, L., Marotzke, J., Matei, D., Meraner, K., Mikolajewicz, U., Modali, K., Müller, W., Nabel, J., Notz, D., Peters, K., Pincus, R., Pohlmann, H., Pongratz, J., Rast, S., Schmidt, H., Schnur, R., Schulzweida, U., Six, K., Stevens, B., Voigt, A., and Roeckner, E.: MPI-M MPI-ESM1.2-LR model output prepared for CMIP6 CMIP piControl, Earth System Grid Federation, https://doi.org/10.22033/ESGF/CMIP6.6675, 2019a.

Wieners, K.-H., Giorgetta, M., Jungclaus, J., Reick, C., Esch, M., Bittner, M., Legutke, S., Schupfner, M., Wachsmann, F., Gayler, V., Haak, H., de Vrese, P., Raddatz, T., Mauritsen, T., von Storch, J.-S., Behrens, J., Brovkin, V., Claussen, M., Crueger, T., Fast, I., Fiedler, S., Hagemann, S., Hohenegger, C., Jahns, T., Kloster, S., Kinne, S., Lasslop, G., Kornblueh, L., Marotzke, J., Matei, D., Meraner, K., Mikolajewicz, U., Modali, K., Müller, W., Nabel, J., Notz, D., Peters, K., Pincus, R., Pohlmann, H., Pongratz, J., Rast, S., Schmidt, H., Schnur, R., Schulzweida, U., Six, K., Stevens, B., Voigt, A., and Roeckner, E.: MPI-M MPI-ESM1.2-LR model output prepared for CMIP6 CMIP abrupt-4xCO2, Earth System Grid Federation, https://doi.org/10.22033/ESGF/CMIP6.6459, 2019b.

Xia, L., Robock, A., Cole, J. N. S., Curry, C. L., Ji, D., Jones, A., Kravitz, B., Moore, J. C., Muri, H., Niemeier, U., Singh, B., Tilmes, S., Watanabe, S., and Yoon, J.-H.: Solar Radiation Management impacts on agriculture in China: A case study in the Geoengineering Model Intercomparison Project (GeoMIP), J. Geophys. Res., 119, 8695–8711, https://doi.org/10.1002/2013JD020630, 2014.

Zelinka, M. D., Myers, T. A., McCoy, D. T., Po-Chedley, S., Caldwell, P. M., Ceppi, P., Klein, S. A., and Taylor, K. E.: Causes of higher climate sensitivity in CMIP6 models, Geophys. Res. Let., 47, e2019GL085782, https://doi.org/10.1029/2019GL085782, 2020.

https://doi.org/10.5194/acp-2020-732
Preprint. Discussion started: 28 August 2020

Table 1. All participating models in both the CMIP5 and CMIP6 eras of GeoMIP, including references. For G1 solar reduction, the percentage is calculated as the percent change in incident solar irradiance at the top-of-atmosphere between G1 and its respective piControl run. Numbers in the first column correspond to the model numbers in Figure 11.

#	Model	Generation	Reference	G1 Solar Reduction (%)	Data not available	Data Citations (CMIP6 only)
1	BNU-ESM	CMIP5	Ji et al. (2014)	3.80	Cloud forcing	
2	CanESM2	CMIP5	Arora et al. (2011)	4.00		
3	CCSM4	CMIP5	Gent et al. (2011)	4.25	NPP	
4	CESM-CAM5.1-FV	CMIP5	Neale et al. (2010); Hurrell et al. (2013)	4.70		
5	CSIRO-Mk3L-1.2	CMIP5	Phipps et al. (2011, 2012)	3.20	Cloud forcing, NPP	
6	EC-EARTH	CMIP5	Hazeleger et al. (2011)	4.12	Cloud forcing, NPP	
7	GISS-E2-R	CMIP5	Schmidt et al. (2014)	4.47		
8	HadCM3	CMIP5	Gordon et al. (2000)	4.16	Cloud forcing, NPP	
9	HadGEM2-ES	CMIP5	Collins et al. (2011)	3.88		
10	IPSL-CM5A-LR	CMIP5	Dufresne et al. (2013); Hourdin et al. (2012)	3.50	NPP	
11	MIROC-ESM	CMIP5	Watanabe et al. (2008, 2011)	5.00		
12	MPI-ESM-LR	CMIP5	Giorgetta et al. (2013); Stevens et al. (2013)	4.68		
13	NorESM1-M	CMIP5	Alterskjær et al. (2012); Kirkevåg et al. (2013)	4.03		
14	CanESM5	CMIP6	Swart et al. (2019c)	3.72		Swart et al. (2019a, b); Cole et al. (
15	CESM2-WACCM	CMIP6	Gettelman et al. (2019)	4.91		Danabasoglu (2019c, b, a)
16	CNRM-ESM2.1	CMIP6	Séférian et al. (2019)	3.72		Séférian (2018b, a, c)
17	GISS-E2.1-G	CMIP6	Kelley et al. (2020)	4.13		NASA Goddard Institute for Space
18	IPSL-CM6A-LR	CMIP6	Boucher et al. (2020); Lurton et al. (2020)	4.10		Boucher et al. (2018c, b, a)
19	MPI-ESM1.2-LR	CMIP6	Mauritsen et al. (2019)	4.57		Wieners et al. (2019a, b)
20	UKESM1.0-LL	CMIP6	Sellar et al. (2019)	3.80		Tang et al. (2019b, a); Jones (2019

https://doi.org/10.5194/acp-2020-732
Preprint. Discussion started: 28 August 2020

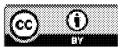

Atmospheric Chemistry and Physics Discussions

Table 2. Ensemble differences between the CMIP5 and CMIP6 ensembles for each variable evaluated in this study (left column). Column 2 indicates the difference between the ensembles in how much of the Earth's surface is not stippled (more than 75% of models agree on the sign of the response; positive values indicate that CMIP6 has more unstippled area than CMIP5). Column 3 indicates the fraction of the Earth's surface for which the CMIP5 ensemble is statistically different from the CMIP6 ensemble, based on 95th percentile confidence intervals from Welch's *t*-test.

Variable	Stippling (%)	Welch's *t*-test (%)	Notes
Surface air temperature	-25.77	0.87	
Precipitation	-3.56	11.17	
Evaporation	-2.33	6.47	
P–E	-15.23	1.13	
SW Cloud Forcing	-8.02	9.65	
LW Cloud Forcing	11.99	6.57	
Net Primary Productivity	-1.42	1.15	Land surface only

https://doi.org/10.5194/acp-2020-732
Preprint. Discussion started: 28 August 2020

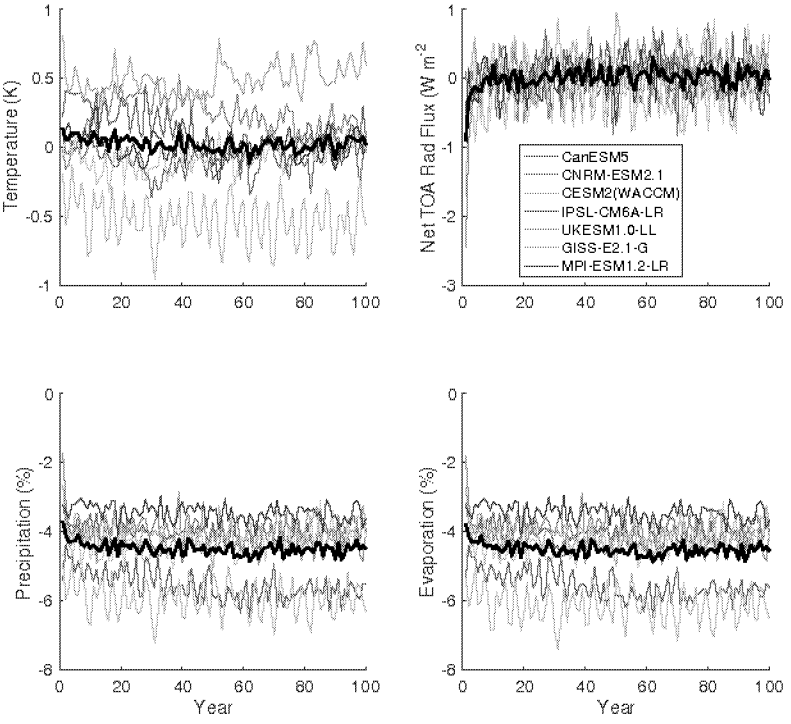

Figure 1. Temperature (top left; K), net top-of-atmosphere radiative flux (top right; W m^{-2}), precipitation (bottom left; %), and evaporation (bottom right; %) change in $G1_{CMIP6}$ compared to piControl over 100 years of simulation. Thin colored lines are individual models, and thick black lines are ensemble means.

https://doi.org/10.5194/acp-2020-732
Preprint. Discussion started: 28 August 2020

Atmospheric Chemistry and Physics Discussions

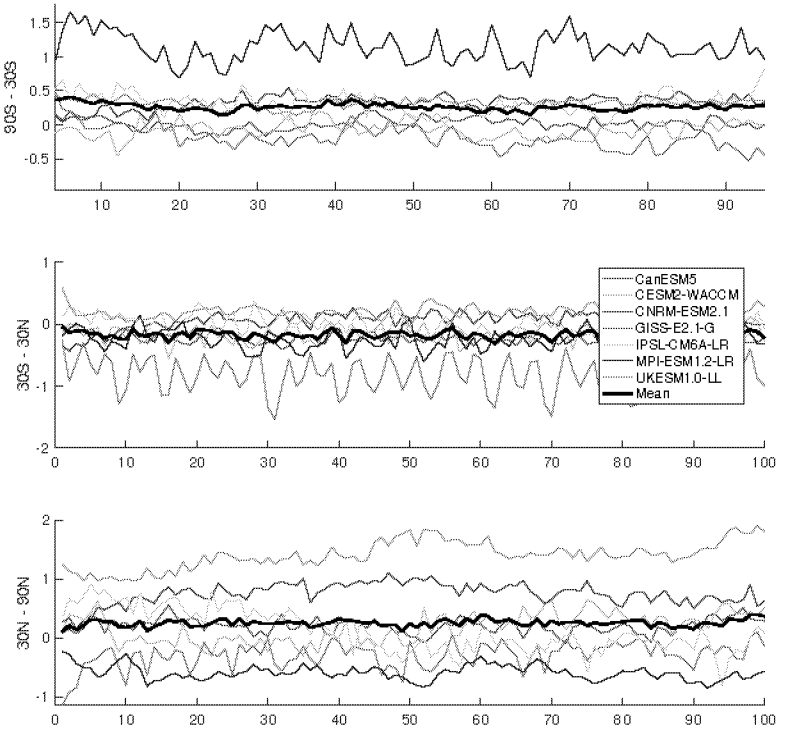

Figure 2. Annual mean surface temperature (K) in each model averaged over 90°S-30°S (top), 30°S-30°N (middle), and 30°N-90°N (bottom). The ensemble mean is plotted as thick black lines.

https://doi.org/10.5194/acp-2020-732
Preprint. Discussion started: 28 August 2020

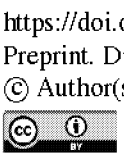

Atmospheric Chemistry and Physics Discussions

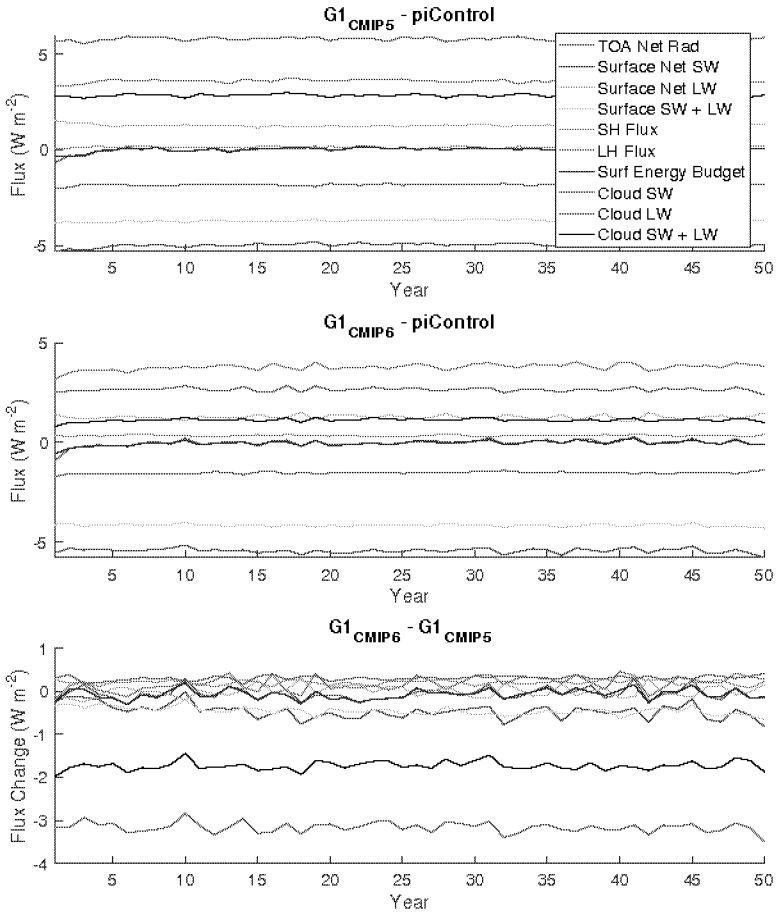

Figure 3. Ensemble mean energetics (W m^{-2}) for various flux quantities in $G1_{CMIP5}$ (top), $G1_{CMIP6}$ (middle), and the difference (bottom). All fluxes are positive downward, which is counterintuitive for sensible heat (SH) and latent heat (LH). Surf Energy Budget indicates the sum of surface shortwave (SW), surface longwave (LW), SH, and LH. Cloud forcing is calculated as all-sky minus clear-sky.

https://doi.org/10.5194/acp-2020-732
Preprint. Discussion started: 28 August 2020

Atmospheric Chemistry and Physics Discussions

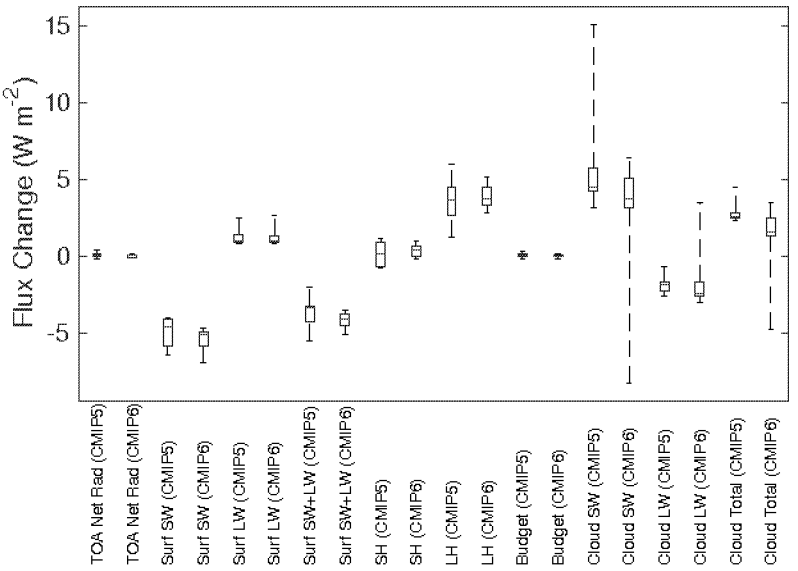

Figure 4. Ensemble median (red lines), inter-quartile (blue boxes), and ranges (black whiskers) for the same global mean energetics quantities as in Figure 3 (G1 minus piControl) for both the CMIP5 and CMIP6 ensembles.

https://doi.org/10.5194/acp-2020-732
Preprint. Discussion started: 28 August 2020

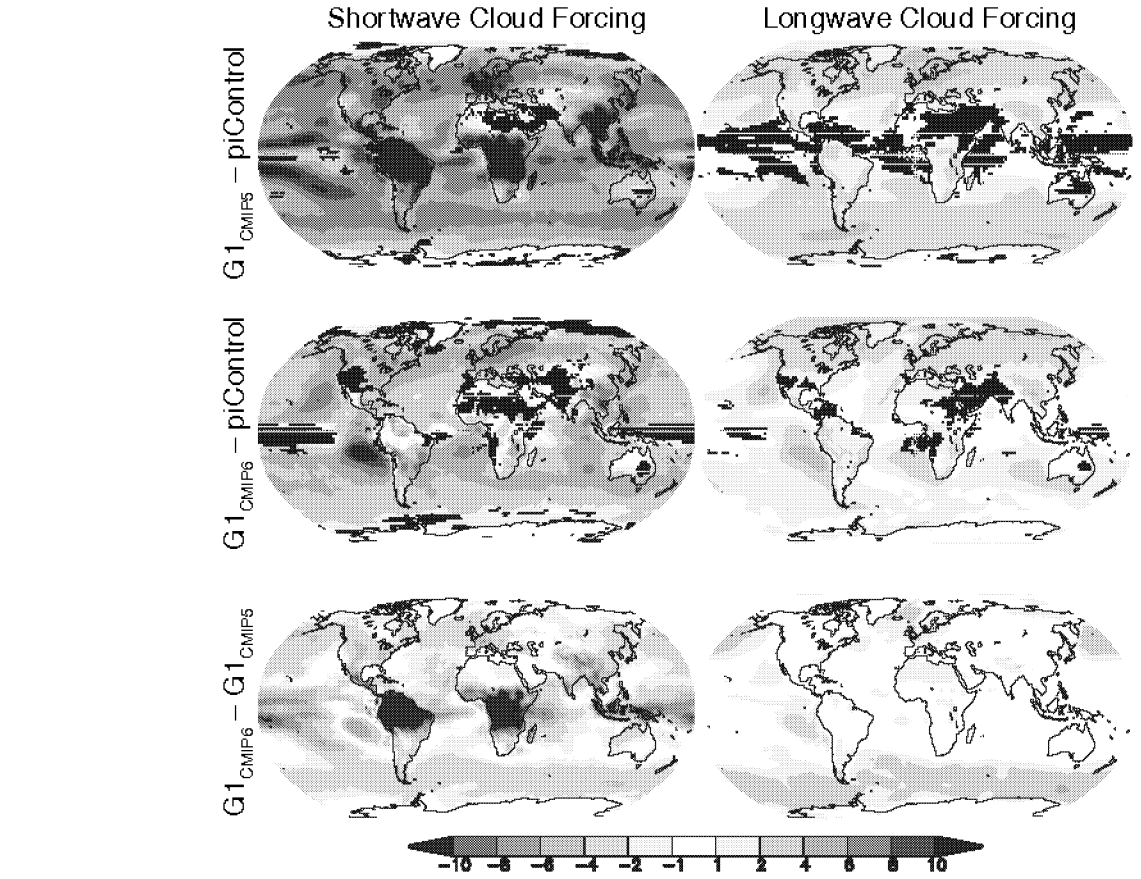

Figure 5. Surface shortwave (left) and longwave (right) cloud forcing (W m^{-2}) change from preindustrial for the CMIP5 (top) and CMIP6 (middle) ensembles, as well as the ensemble differences (bottom). Cloud forcing is measured as all-sky minus clear-sky radiative flux. All shaded values are ensemble means. Lack of stippling indicates agreement on the sign of the values across at least 75% of the models.

https://doi.org/10.5194/acp-2020-732
Preprint. Discussion started: 28 August 2020

Atmospheric Chemistry and Physics Discussions

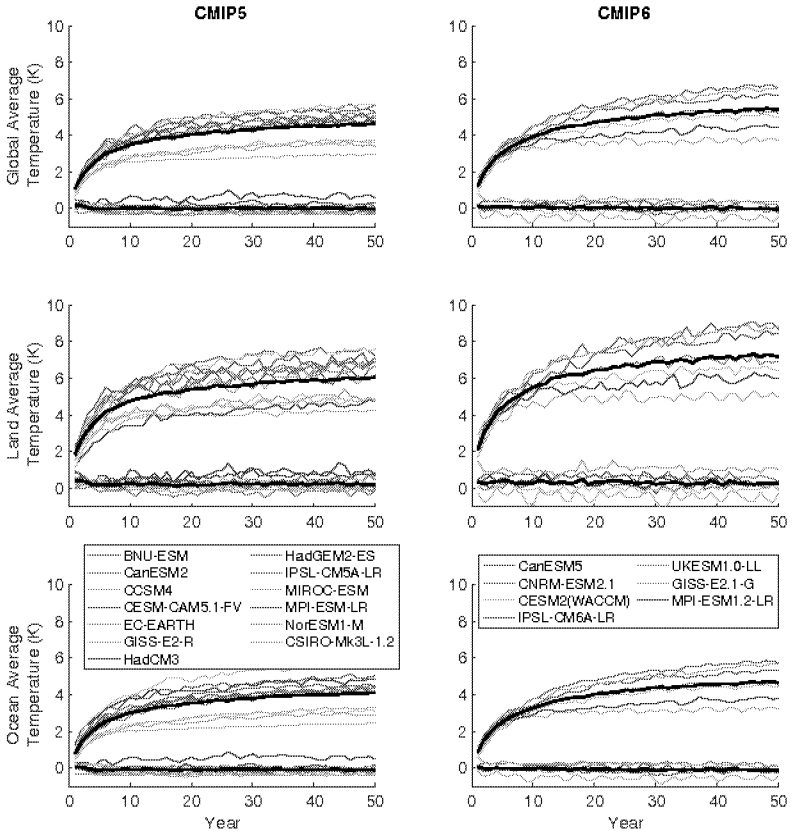

Figure 6. Global mean (top), land mean (middle), and ocean mean (bottom) temperature change (K) for the CMIP5 (left) and CMIP6 (ensembles). Thin colored lines are individual models, and thick black lines are model means. In all panels, the upper cluster of lines is the abrupt4xCO2 simulation, and the lower cluster of lines (approximately zero temperature change for the entire simulation) is experiment G1.

https://doi.org/10.5194/acp-2020-732
Preprint. Discussion started: 28 August 2020

Atmospheric Chemistry and Physics Discussions

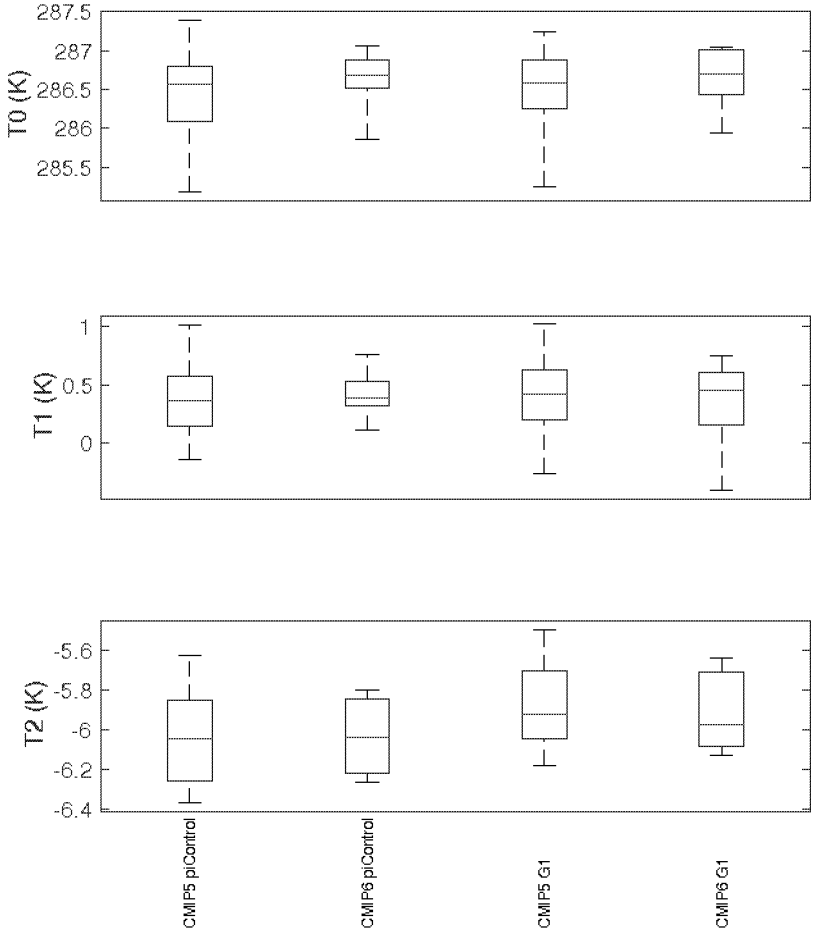

Figure 7. Ensemble ranges for global mean temperature (T_0), the interhemispheric temperature gradient (T_1), and the equator-to-pole temperature gradient (T_2), as defined in Equation 1 (Ban-Weiss and Caldeira, 2010; Kravitz et al., 2016). Red lines indicate ensemble medians, blue boxes are the inter-quartile ranges, and black whiskers indicate total ranges.

https://doi.org/10.5194/acp-2020-732
Preprint. Discussion started: 28 August 2020

Atmospheric Chemistry and Physics Discussions

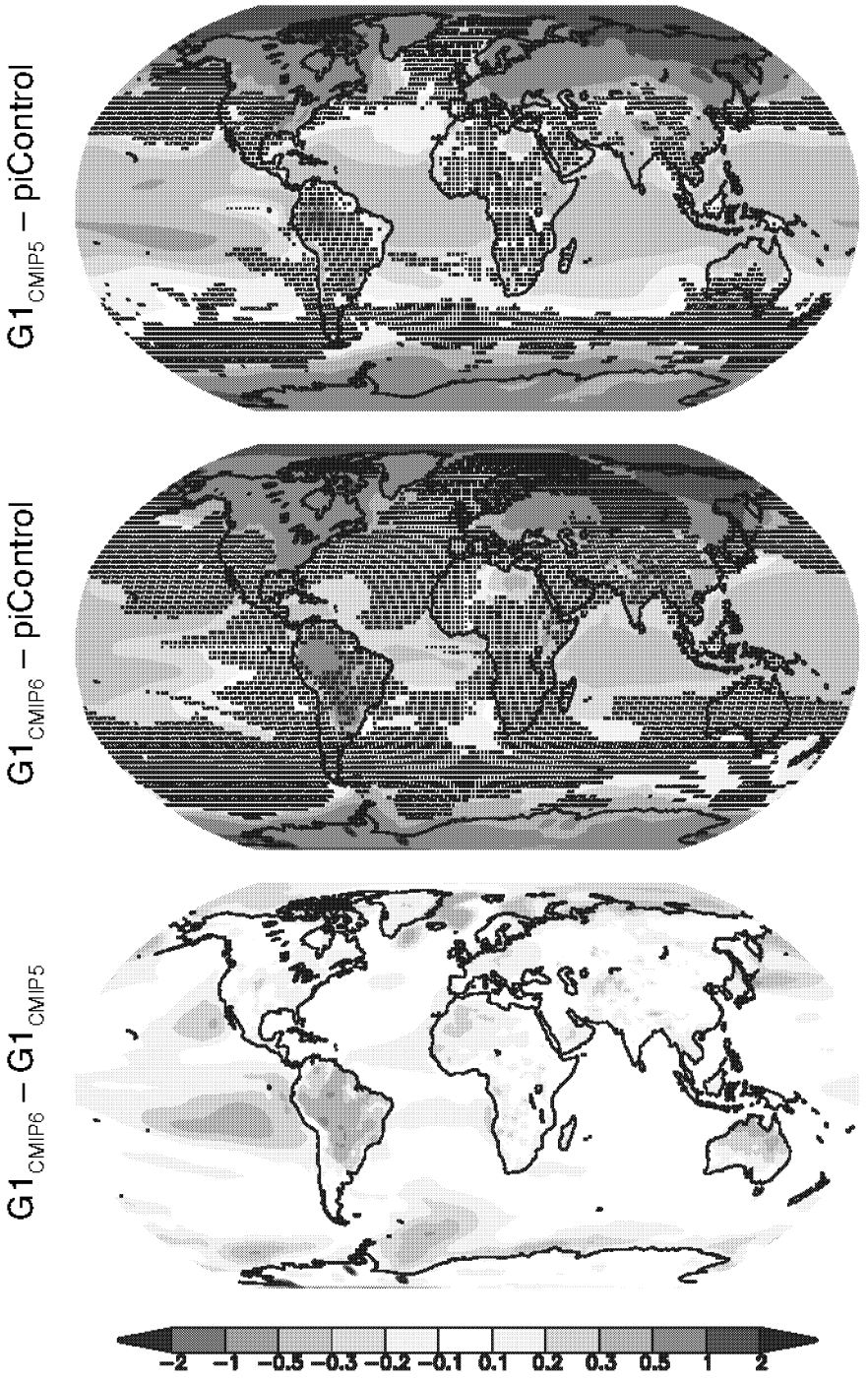

Figure 8. Ensemble average temperature changes (K) for G1 (as compared to the preindustrial control) for CMIP5 (top) and CMIP6 (middle), as well as the difference ($G1_{CMIP6}$ minus $G1_{CMIP5}$, bottom panel). In the top two panels, stippling indicates regions where fewer than 75% of the models in their respective ensembles agree on the sign of the response.

https://doi.org/10.5194/acp-2020-732
Preprint. Discussion started: 28 August 2020

Atmospheric Chemistry and Physics Discussions

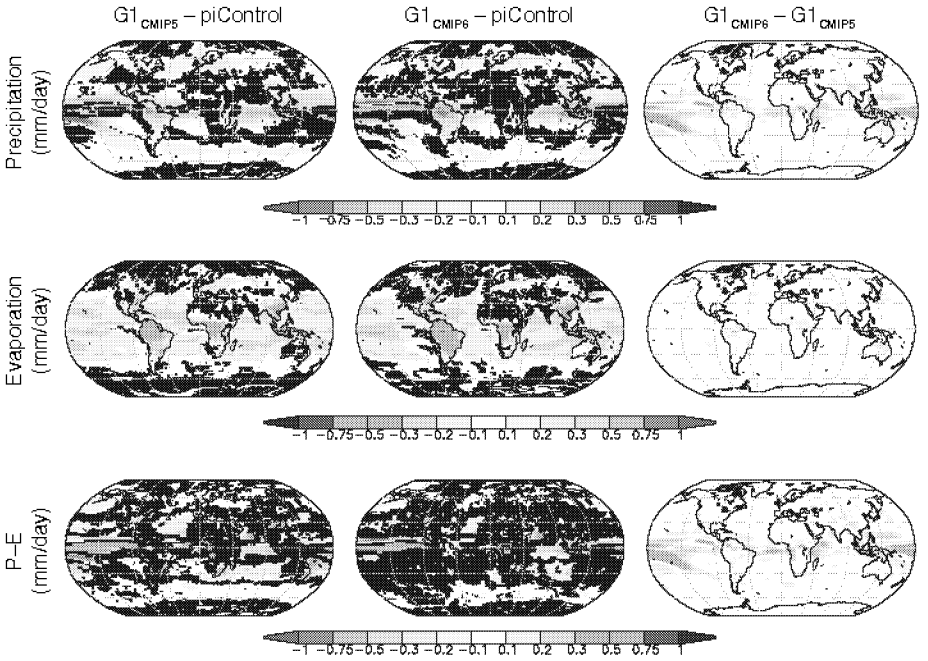

Figure 9. Precipitation (top), evaporation (middle), and precipitation minus evaporation (P–E; bottom) change from preindustrial for the CMIP5 (left) and CMIP6 (middle) ensembles, as well as the ensemble differences (right). All shaded values are ensemble means. Lack of stippling in the left and middle panels indicates agreement on the sign of the values across at least 75% of the models.

https://doi.org/10.5194/acp-2020-732
Preprint. Discussion started: 28 August 2020

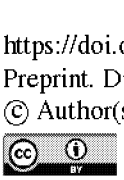

Atmospheric Chemistry and Physics Discussions

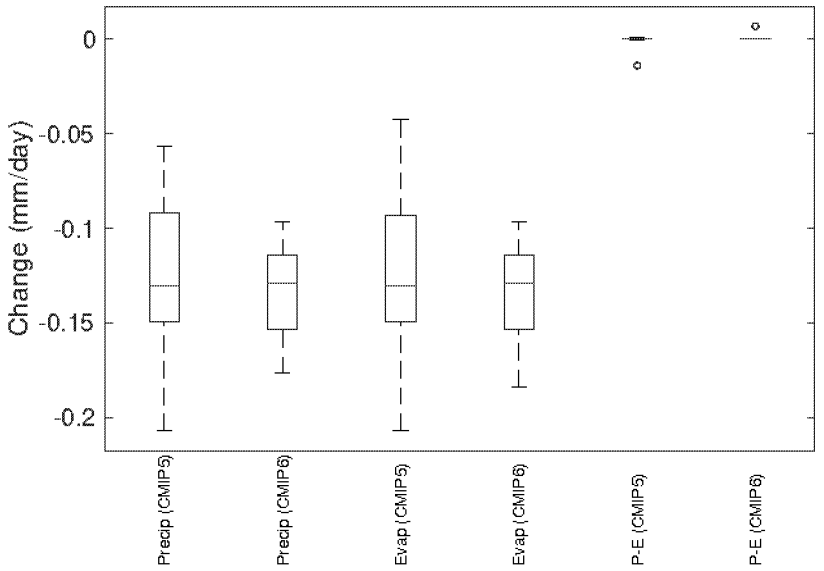

Figure 10. Global mean ensemble median (red lines), inter-quartile (blue boxes), and ranges (black whiskers or, for P–E one blue circle indicating an extreme outlier) for the hydrological quantities shown in Figure 9 for both the CMIP5 and CMIP6 ensembles.

https://doi.org/10.5194/acp-2020-732
Preprint. Discussion started: 28 August 2020

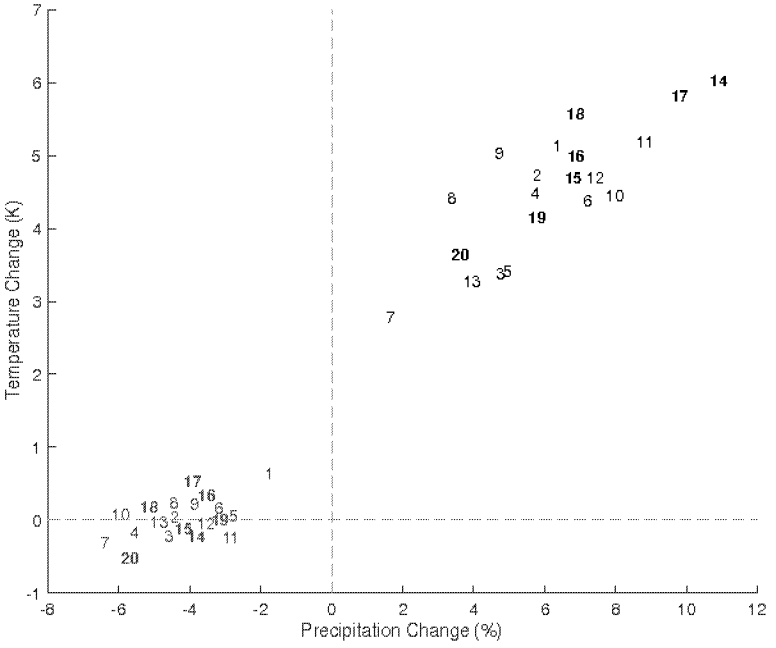

Figure 11. Average (years 11-50) temperature (y-axis; K) and precipitation (x-axis; %) change for each model in this study. Numbers indicate the model number (listed in Table 1, first column). Black numbers are for abrupt4xCO2, and red numbers are for G1. Bolded numbers are for CMIP6

https://doi.org/10.5194/acp-2020-732
Preprint. Discussion started: 28 August 2020

Atmospheric Chemistry and Physics Discussions

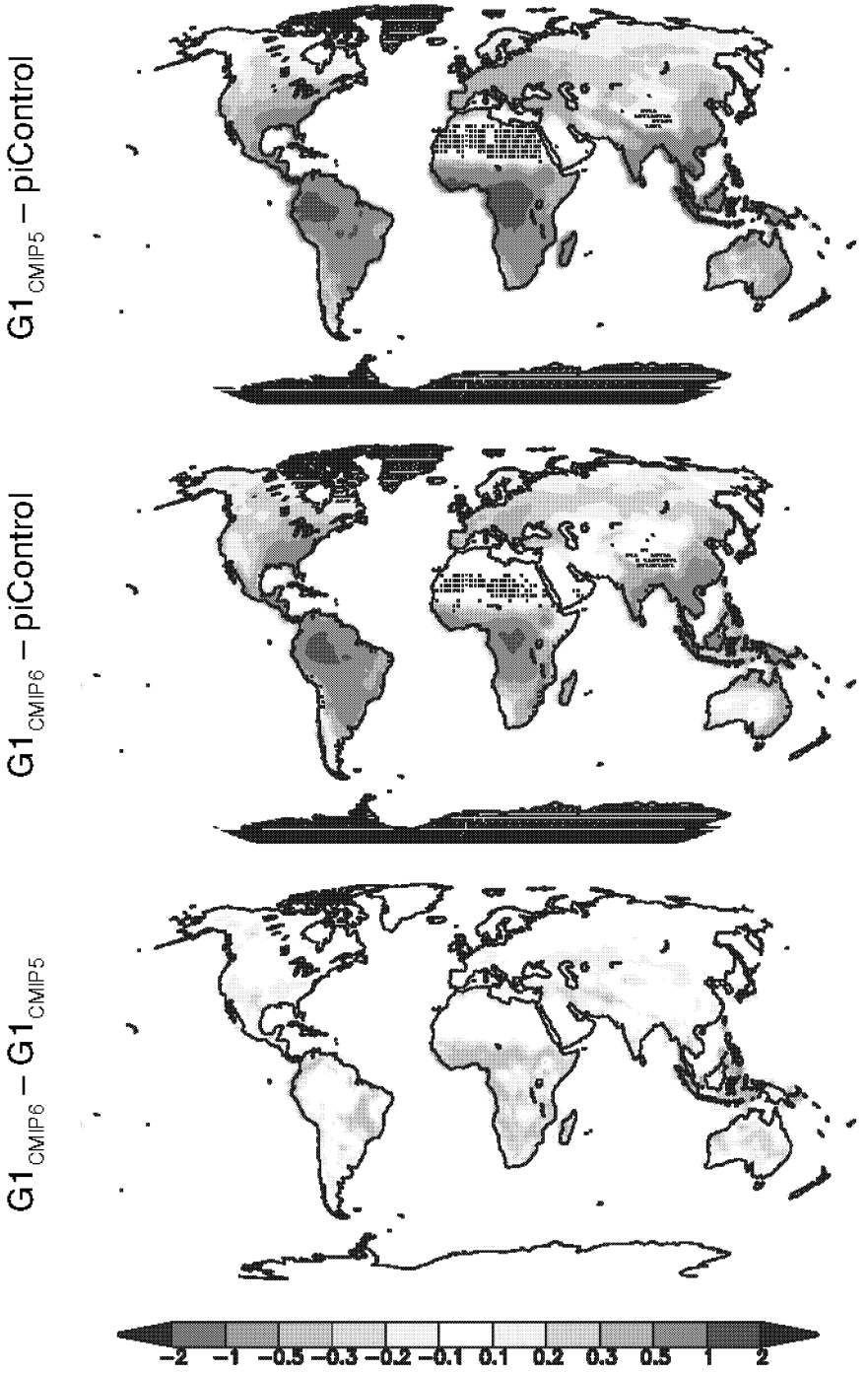

Figure 12. Terrestrial net primary productivity (kg C m^{-2} y^{-1}) for the CMIP5 (top) and CMIP6 (middle) ensembles, as well as the ensemble differences (bottom). All shaded values are ensemble means. Lack of stippling indicates agreement on the sign of the values across at least 75% of the models.

Response to reviewer comments
Kravitz et al. (acp-2020-732)
Original review comments in normal text. **Responses in bold.**

Anonymous Referee #3

This paper compares how two generations of Geoengineering models perform in a 50 year G1 experiment, where CO2 is instantaneously quadrupled and at the same time, insolation is reduced so the net TOA radiative flux is essentially unchanged. Key aspects of the CMIP5 vs. CMIP6 model ensemble results remain unchanged.
This is a worthwhile exercise for identifying where to focus more detailed analysis in future studies. However, it should also be stated clearly that consistency among ensembles of two generations of models demonstrates only that the differences do not significantly affect the results, at least when aggregated into ensemble averages; it by no means shows the results to be robust in any deeper sense. (E.g., lines 186-188) This is especially important, as there are policymakers who cite the model results as support for proposed action in response to a possible severe climate crisis. The statement in lines 205-207 does not seem to be enough; this point also needs to be made much earlier in the paper in my opinion.

We thank the reviewer for their comments on our manuscript. We agree with these points and have adjusted our language so as not to overstate our conclusions. We have also made the point in lines 205-207 earlier in the manuscript.

Without exploring more specifically the similarities and differences among the models, one cannot assess how significant the model diversity really is for generating the parameter values analyzed here. As such, this paper could go further in at least identifying which processes are most important for future focus (in addition to cloud parameterizations, which is already well known).

We appreciate the reviewer's point. We would like to acknowledge the difficulty of what the reviewer suggests. In some cases, large parts of the model have been completely overhauled between versions, which does not provide a controlled enough experiment to identify which processes are most important for future focus. Cloud parameterizations and land surface parameterizations were obvious ones (as the reviewer states), but beyond that we don't have enough information to even conduct informed speculation. We found it interesting that despite these large differences, the two generations of models largely resulted in similar climate outcomes. We agree that these points were not necessarily communicated as clearly as they could have been. We have gone through the manuscript to address this.

Notes

Figure 1. I can see that IPSL-CM6A-LR shows a long-term trend in temperature, as stated, but it seems CNRM has one too. UKESM1.0-LL has a jump at about 50 years that produces an overall

pattern with the opposite sign. And if GISS shows trends in precipitation and evaporation, MPI seems to have these features as well.

We have added a more thorough discussion of trends to the manuscript, including a new Table that provides quantitative estimates of trends.

Figure 1. For precipitation (and evaporation), two models are systematically below all the others, bringing the ensemble average to below the larger model cluster. This might require some explanation. For example, is there a fundamental unresolved issue in modeling precipitation, where a poorly constrained choice produces dramatically different results?

This is a fair point. There are no observations of geoengineering, so it's difficult to say why these two models are different. We are reluctant to focus on these two because being an outlier doesn't necessarily mean being wrong. We have added some discussion of this to the manuscript.

Lines 170-173. The fact that the CMIP6 models show less diversity does not mean that the uncertainty is lower. As more model inter-comparisons take place, it is not surprising that model behavior tends to converge. But to make a statement about model uncertainty requires critical tests, based on measurements at least of the processes involved.

Our original language was unclear – this statement was about the findings of Arora et al. (2020). We have clarified this in the manuscript.

Minor Notes

Table 2. The caption says Column 3 reports a fraction, whereas the column itself is labeled "%," which seems correct.

That's a typo in the caption. Thanks for catching that.

Figures 1 and 2. The colors assigned to the different models are not the same in these two figures, which seems unnecessarily confusing.

Corrected. Thanks for catching that oversight.

Anonymous Referee #4

This paper presents an interesting comparison between two generations of models performing a geoengineering experiment where quadrupling of CO2 is offset by solar reduction. The goal of the study is to assess the consistency of model results between the two generations and the validity of the overall scientific conclusions.

This is attained applying standard statistical methods, in order to derive quantitative figures to support the conclusions. Although this study does not go into the details of specific models, but rather looks at the ensemble perspective, I think the topic is scientifically relevant and makes this study worthy of publication in ACP.
The paper is well written, concise and understandable. I have, however, a few minor remarks and suggestions for improvement that should be taken into account.

Thank you!

Remarks
L4: "This simulation is artificial", I think every model simulation is somewhat artificial, so maybe you could write "idealized".

Agreed. Changed.

L17: "Climate models remain the most promising tools...". Aren't they actually the only tool for that?

Not entirely – one could gain information from natural analogues like volcanic eruptions. Nevertheless, the reviewer makes a valid point, and we have updated the manuscript accordingly.

L34: What do you mean exactly with "agriculture"? Could you please be more specific?

This has been clarified.

L52: "unchanged from the baseline": does this mean that it has the same insolation as the 1850-1860 period of the piControl experiment? Please clarify.

We have clarified this in the manuscript.

L57-64: the trend in TOA net flux is not mentioned in this paragraph, although Fig. 1 shows it. Moreover, it would be interesting to have some numbers about the trends of the ensemble mean for each variable shown in Fig. 1.

Agreed. We have added a discussion of this to the manuscript, including a new table.

Fig. 2: The legend hides some important parts of the plot, please consider shifting it to a different position.

Done.

Fig. 3: The brown line for the TOA net radiative flux change is probably the most interesting results in this figure but it's hardly visible. You may consider drawing it in the foreground above the other lines.

Done.

Text corrections

L35: I would replace "perfect" with "exact".
L38: I would replace "perfeclty" with "completely".
L43: I would replace "version of Earth System Models" with "version of the participating Earth System Models".
L58: I would replace "rare events or" with "rare events and".
L61: "by only analysing 50 years", do you mean "the first 50 years"?
L135: I think "or has warmer tropics" should be "nor has warmer tropics".
L199: It looks like punctuation is missing.
Fig. 1: Please add the mean to the legend (as in Fig. 2).
Fig. 3: I would replace "the difference" with "their difference".

All of these text corrections have been made.

Response to reviewer comments
Kravitz et al. (acp-2020-732)
Original review comments in normal text. **Responses in bold.**

Anonymous Referee #3

This paper compares how two generations of Geoengineering models perform in a 50 year G1 experiment, where CO2 is instantaneously quadrupled and at the same time, insolation is reduced so the net TOA radiative flux is essentially unchanged. Key aspects of the CMIP5 vs. CMIP6 model ensemble results remain unchanged.
This is a worthwhile exercise for identifying where to focus more detailed analysis in future studies. However, it should also be stated clearly that consistency among ensembles of two generations of models demonstrates only that the differences do not significantly affect the results, at least when aggregated into ensemble averages; it by no means shows the results to be robust in any deeper sense. (E.g., lines 186-188) This is especially important, as there are policymakers who cite the model results as support for proposed action in response to a possible severe climate crisis. The statement in lines 205-207 does not seem to be enough; this point also needs to be made much earlier in the paper in my opinion.

We thank the reviewer for their comments on our manuscript. We agree with these points and have adjusted our language so as not to overstate our conclusions. We have also made the point in lines 205-207 earlier in the manuscript.

Without exploring more specifically the similarities and differences among the models, one cannot assess how significant the model diversity really is for generating the parameter values analyzed here. As such, this paper could go further in at least identifying which processes are most important for future focus (in addition to cloud parameterizations, which is already well known).

We appreciate the reviewer's point. We would like to acknowledge the difficulty of what the reviewer suggests. In some cases, large parts of the model have been completely overhauled between versions, which does not provide a controlled enough experiment to identify which processes are most important for future focus. Cloud parameterizations and land surface parameterizations were obvious ones (as the reviewer states), but beyond that we don't have enough information to even conduct informed speculation. We found it interesting that despite these large differences, the two generations of models largely resulted in similar climate outcomes. We agree that these points were not necessarily communicated as clearly as they could have been. We have gone through the manuscript to address this.

Commenté [o1]: You could cite the genealogy paper: https://agupubs.onlinelibrary.wiley.com/doi/full/10.1002/grl.50256

Notes

Figure 1. I can see that IPSL-CM6A-LR shows a long-term trend in temperature, as stated, but it seems CNRM has one too. UKESM1.0-LL has a jump at about 50 years that produces an overall

pattern with the opposite sign. And if GISS shows trends in precipitation and evaporation, MPI seems to have these features as well.

We have added a more thorough discussion of trends to the manuscript, including a new Table that provides quantitative estimates of trends.

Figure 1. For precipitation (and evaporation), two models are systematically below all the others, bringing the ensemble average to below the larger model cluster. This might require some explanation. For example, is there a fundamental unresolved issue in modeling precipitation, where a poorly constrained choice produces dramatically different results?

This is a fair point. There are no observations of geoengineering, so it's difficult to say why these two models are different. We are reluctant to focus on these two because being an outlier doesn't necessarily mean being wrong. We have added some discussion of this to the manuscript.

Commenté [o2]: You could speculate a bit though. GISS cools more than others, and a colder model is also one with less E or P (by 2-3% per K). I don't know for sure for IPSL-CM6A-LR but we know that precipitation change is largely correlated with atmospheric heating rate (at the global scale). You may want to compare change in SW atmospheric absorption across the models (difference between toa and surface net radiation). I would no tbe surprised if IPSL is an outlier

Lines 170-173. The fact that the CMIP6 models show less diversity does not mean that the uncertainty is lower. As more model inter-comparisons take place, it is not surprising that model behavior tends to converge. But to make a statement about model uncertainty requires critical tests, based on measurements at least of the processes involved.

Our original language was unclear – this statement was about the findings of Arora et al. (2020). We have clarified this in the manuscript.

Minor Notes

Table 2. The caption says Column 3 reports a fraction, whereas the column itself is labeled "%," which seems correct.

That's a typo in the caption. Thanks for catching that.

Figures 1 and 2. The colors assigned to the different models are not the same in these two figures, which seems unnecessarily confusing.

Corrected. Thanks for catching that oversight.

Anonymous Referee #4

This paper presents an interesting comparison between two generations of models performing a geoengineering experiment where quadrupling of CO_2 is offset by solar reduction. The goal of the study is to assess the consistency of model results between the two generations and the validity of the overall scientific conclusions.

This is attained applying standard statistical methods, in order to derive quantitative figures to support the conclusions. Although this study does not go into the details of specific models, but rather looks at the ensemble perspective, I think the topic is scientifically relevant and makes this study worthy of publication in ACP.
The paper is well written, concise and understandable. I have, however, a few minor remarks and suggestions for improvement that should be taken into account.

Thank you!

Remarks
L4: "This simulation is artificial", I think every model simulation is somewhat artificial, so maybe you could write "idealized".

Agreed. Changed.

L17: "Climate models remain the most promising tools...". Aren't they actually the only tool for that?

Not entirely – one could gain information from natural analogues like volcanic eruptions. Nevertheless, the reviewer makes a valid point, and we have updated the manuscript accordingly.

Commenté [o3]: You could say that physical understanding is also required, and the model helps at that.

L34: What do you mean exactly with "agriculture"? Could you please be more specific?

This has been clarified.

L52: "unchanged from the baseline": does this mean that it has the same insolation as the 1850-1860 period of the piControl experiment? Please clarify.

We have clarified this in the manuscript.

L57-64: the trend in TOA net flux is not mentioned in this paragraph, although Fig. 1 shows it. Moreover, it would be interesting to have some numbers about the trends of the ensemble mean for each variable shown in Fig. 1.

Agreed. We have added a discussion of this to the manuscript, including a new table.

Fig. 2: The legend hides some important parts of the plot, please consider shifting it to a different position.

Done.

Fig. 3: The brown line for the TOA net radiative flux change is probably the most interesting results in this figure but it's hardly visible. You may consider drawing it in the foreground above the other lines.

Done.

Text corrections

L35: I would replace "perfect" with "exact".
L38: I would replace "perfeclty" with "completely".
L43: I would replace "version of Earth System Models" with "version of the participating Earth System Models".
L58: I would replace "rare events or" with "rare events and".
L61: "by only analysing 50 years", do you mean "the first 50 years"?
L135: I think "or has warmer tropics" should be "nor has warmer tropics".
L199: It looks like punctuation is missing.
Fig. 1: Please add the mean to the legend (as in Fig. 2).
Fig. 3: I would replace "the difference" with "their difference".

All of these text corrections have been made.

Interactive comment on "The climate effects of increasing ocean albedo: An idealized representation of solar geoengineering" by Ben Kravitz et al.

Received and published: 2 May 2018

I am surprised that in discussing an experiment that finds:

> Eleven Earth System Models are relatively consistent in their temperature, radiative flux, and hydrological cycle responses...

GeoMIP should elide:

> an abrupt quadrupling of ocean albedo to maintain approximate net top-of-atmosphere radiative flux balance "

with the doubling of CO2 in one of the references it discusses. Seitz 2011 reported the initial CAM3.1 modeling of the combined effect of higher ocean albedo and CO2 doubling to 780ppm, approximating the forcing in IPCC Representative Concentration Pathway 6.0

In contrast, Kravitz et al 2018 instantaneously quadruple CO2 to 1600 ppm, considerably outside the IPCC envelope, which only extends to ~1230 ppm CO2 eq. in RCP 8.5, as seen in the accompanying graph.

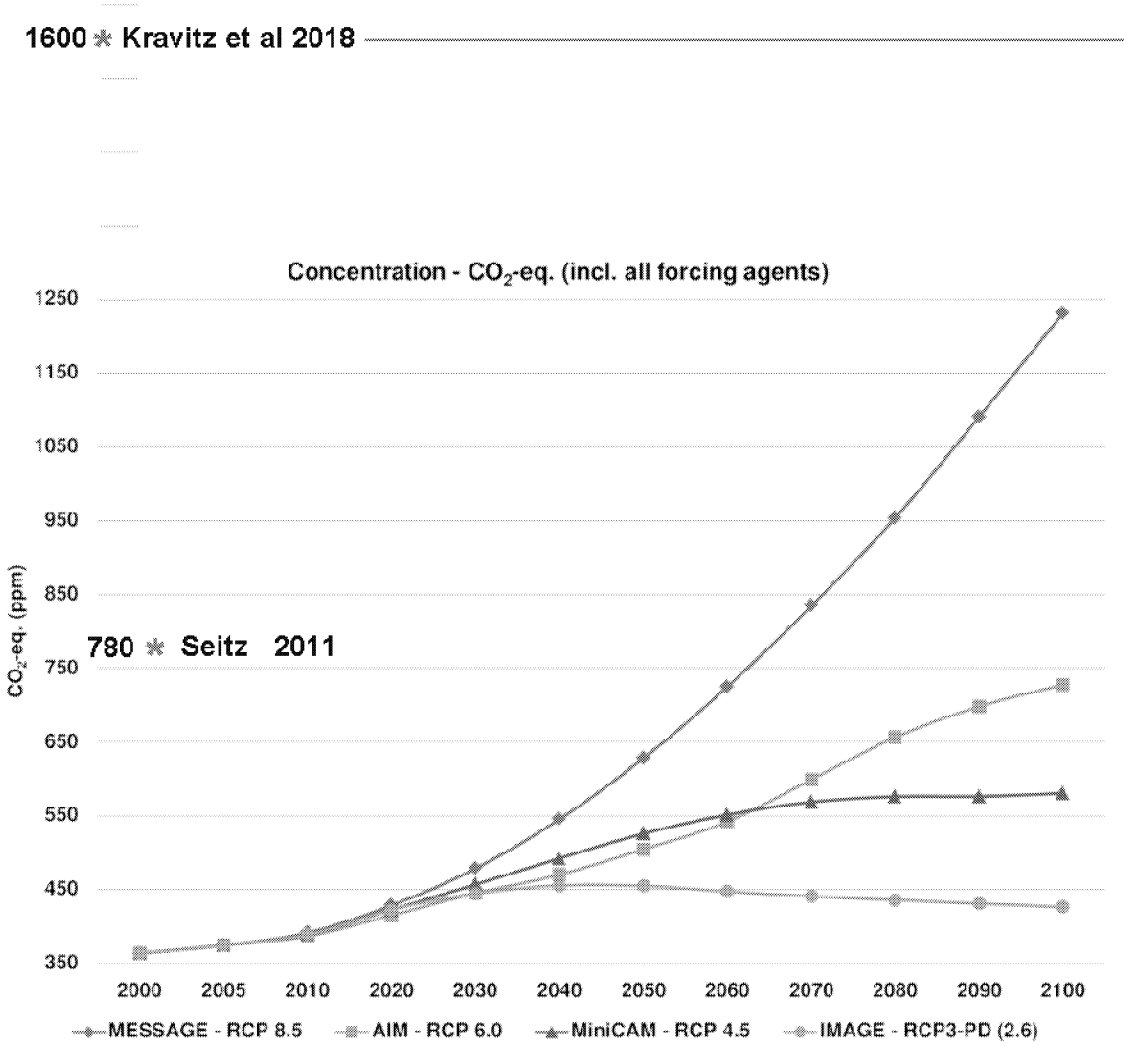

While Seitz 2011 is primarily concerned with fresh water conservation, it used the CAM3.1 model to quantify the coupled climate impact of increased sea surface albedo and doubled CO2 forcing ,and found substantial continental cooling in such a global case, using a carbon forcing well within the IPCC parameter envelope- 780 PPM C02 eq. , which approximates the RCP 6.0 projection for 2100.

In contrast, *The climate effects of increasing ocean albedo: An idealized representation of solar geoengineering* considers a more dystopic future.

As the authors candidly note:

> "The results obtained for G1ocean-albedo were to some extent by design. The objective of G1ocean-albedo was to achieve net top-of-atmosphere radiative flux balance, which resulted in warming.
> Conceivably, one could define an objective of no global temperature change, implying a net negative radiative flux at the top-of-atmosphere, or no global land temperature change, requiring adjustments over the oceans to make up the imbalance. It is unclear whether, unlike G1ocean-albedo, such alternate approaches would result in transient behavior that lasts longer than a few years. Such an experiment could be accomplished using feedback methods that have been introduced to geoengineering research in recent years (e.g., MacMartin et al., 2014b; Kravitz et al., 2016)."

It is natural to assume that model intercomparison experiments involve models with comparable forcings, use reasonably physical feedback parametrizations, and rely on the objective description of cited works. This is not evident in the following passage:

> "G1 ocean-albedo may be more apposite to the impact of geoengineering via "ocean microbubbles," whereby surfactants are added to the ocean surface, promoting the formation of microscopic, highly reflective bubbles (Seitz, 2011; Robock, 2011).

This does not represent the content of Seitz 2011, which speaks for itself -- neither its title: *Bright Water: Microbubbles, water conservation and climate change*, or its text contains the word 'geoengineering.'

It discusses the physics of reducing solar forcing in the hydrosphere, not the atmosphere, and while discussing the

relationship between microbubble lifetime and variable ocean biochemistry that gives rise to natural albedo effects like undershine, does not presume adding surfactants to promote their formation- none were used in the (physical) experiments in albedo modification it describes.

The authors continue:

> An area of investigation we did not undertake, yet one that repeatedly emerges in discussions of microbubbles is the resulting effects of surface albedo increase on the ocean mixed layer. By reflecting more solar radiation, microbubbles have the potential to inhibit vertical mixing and available light in the euphotic zone, which could have profound effects on marine biota. This implies that another useful future area of investigation for the G1 ocean-albedo simulation is an analysis of the marine carbon cycle.

This reflects Robock 2011, an Editorial Comment in *Climatic Change* entitled 'Bubble Bubble Toil and Trouble' and these issues are addressed at some length in in Seitz 2011, which called for their investigation by ecologists and systems biologists. Readers should also note that as modeled with CAM3.1, water brightening reduced peak water surface temperature, which could promote, rather than inhibit, diurnal mixing, by reducing thermal stratification.

I appreciate the utility of idealized simulations, but fear this article invites something best avoided—policy analysts may confuse idealizations with models of the real world. It would clearly be desirable to apply approximations of water reflectivity and temperature less naive that simple Mie theory, or unmixed slab models, to the complex evaporative response of both fresh water reservoirs and the sea surface, with a view to achieving less

idealized and more realistic representations of solar radiation management, especially on local scales.

Once again my thanks to Ken Caldeira for the CAM-1 modeling that informed Seitz 2011.